LIÈGE université
Gembloux
Agro-Bio Tech

COMMUNAUTÉ FRANÇAISE DE BELGIQUE
UNIVERSITÉ DE LIÈGE – GEMBLOUX AGRO-BIO TECH

Dynamics of water uptake and traits of wheat genotypes in mixture under water deficit

Samuel LE GALL

Dissertation originale présentée en vue de l'obtention du grade de doctorat en sciences agronomiques et ingénierie biologique

Promoteurs : Prof. Youri Rothfuss et Prof. Mathieu Javaux
Année civile : 2026

Abstract

The ability of agricultural systems to withstand rising climate variability is contingent, at least in part, on the capacity of crops to effectively utilize soil resources under stress conditions. Intraspecific varietal mixtures — the concurrent cultivation of two or more genotypes of the same species in the same field — have been demonstrated to stabilize yield under water deficit and low-nutrient soils. However, the belowground mechanisms underlying these agronomic benefits remain largely uncharacterized. The central question of this thesis is therefore: do wheat genotypes with contrasting root architectures develop complementary hydrological niches when cultivated in a shared soil profile, and does this complementarity translate into measurable agronomic advantages at the field scale?

We hypothesized that such genotypes growing in mixture would access water from distinct soil layers, thereby reducing inter-plant competition and enhancing collective soil resource exploitation. To test this hypothesis, three specific objectives were pursued: (i) to identify and validate a pair of wheat genotypes expressing sufficiently contrasting root traits under controlled conditions; (ii) to quantify individual root water uptake profiles of each genotype in monoculture and mixture at the booting stage –key in the yield constitution later - using water stable isotope tracing; and (iii) to assess whether the complementarity resulting from the mixture actually leads to improved yield components under field pedoclimatic variability across a full growing season.

Chapter 1 presents the theoretical framework underlying this work. This framework features the agronomic and ecological context for intraspecific wheat mixtures as a lever for agroecosystem resilience. The chapter also includes

1) a short overview on water stable isotope biogeochemistry and its application to root water uptake quantification and
2) a description of isotopic labeling strategies that can improve root water uptake estimation with Bayesian mixing models.

Finally, the detailed objectives and hypotheses of the doctoral project are detailed.

Chapter 2 focuses on the material and methods used to test the formulated hypotheses above, that is,

1) to characterize the traits differences of wheat varieties (two commercial wheat variety pairs (Treblir® and Milaneco®) and two near-isogenic experimental lines — UQR12 and UQR15). These experiments aimed at identifying a genotype pair expressing sufficiently contrasting root traits.
2) an in-house split-chamber system for the independent continuous measurement of the isotopic composition of transpiration of two plants grown in the same soil column,
3) a depth-specific isotopic labeling strategy to decorrelate the hydrogen and oxygen stable isotope profiles in soil water and decrease the uncertainty in

root water uptake location and relative amount calculated with the mixing model Stable Isotope Analysis in R (SIAR).

4) magnetic resonance imaging (MRI) tools to provide non-destructive three-dimensional root architecture mapping and generate biomass distribution of the two root systems growing in the same soil volume.

The conclusions of this chapter were as follows: first, the results indicated that the UQR12 (shallow root system—SRS) and UQR15 (deep root system—DRS) exhibited significant contrasting root traits (biomass distributions, root growth rate, rhizospheric enzymatic activity) at the booting stage under column conditions. Second, the multi-depth labeling protocol generated sufficient isotopic contrast to potentially improve the estimation of individual fractions of root water uptake (fRWU).

In Chapter 3, the ensemble of validated methods described in chapter 2 were used to address the central hypothesis of the study expressed above, under controlled and reproducible conditions. The conclusions of this chapter were as follows: first, the two genotypes maintain distinct fRWU in monoculture, consistent with their contrasting root traits; second, when grown together in mixture, both genotypes shift their uptake toward deeper soil layers relative to when grown as monocultures; and third, the differences between the monocultures and the mixture fRWU intensified under water deficit conditions. This mixture-induced root water uptake shift toward deeper soil layers cannot be predicted from the root biomass distributions of either genotype in monoculture and is inconsistent with purely competitive mechanisms. This study provides the first isotopic evidence of intraspecific hydrological niche complementarity in a wheat mixture at the individual plant level and suggests the existence of facilitative inter-genotype interactions whose mechanistic basis, potentially involving root exudate-mediated chemical signaling, remains to be directly demonstrated.

Chapter 4 reports on a complementary field study aiming at testing the previously documented wheat genotypes pairs and investigating possible non-additive mixture effects over an entire cycle until yield. The experiments took place at the TERENO Selhausen experimental platform (Jülich, Germany) during the 2022–2023 growing season, which was marked by a late cold wet phase (till middle of May), a spring drought (over May and June), and above-average rainfall during the grain filling stages (end of June to mid-Jully). In addition to soil water potential and content sensing, and regular UAS-based multispectral and LiDAR canopy observations, roots presence and content were respectively determined non-destructively from mini-rhizotron root imaging and destructively from soil core sampling. The conclusions of this chapter showed that the root traits of DRS and SRS exhibited a context-dependent phenotypic plasticity under field pedoclimatic conditions that attenuated the contrasts documented under controlled conditions. However as expected, the mixture plots outperformed both monocultures in yield, indicating that the non-additive yield advantage of mixture was confirmed at the field scale and community level, even

when the underlying root architectural contrasts are partially attenuated by environmental context.

Across its three experimental chapters, this thesis establishes that intraspecific root architectural complementarity in wheat mixtures can be confirmed through water isotope analysis. Furthermore, we demonstrates that these wheat mixtures enhance certain traits, such as tiller and primary root number, leading to higher yields in the face of spring drought. A significant direction for future research involves the mechanistic characterization of the inter-genotype facilitative interactions suggested by the non-additive uptake patterns documented here.

Résumé

La capacité des systèmes agricoles à résister à la variabilité climatique croissante dépend, au moins en partie, de la capacité des cultures à exploiter efficacement les ressources du sol dans des conditions de stress. Il a été démontré que les mélanges variétaux intra-spécifiques — c'est-à-dire la culture simultanée de deux génotypes ou plus d'une même espèce dans un même champ — permettent de stabiliser les rendements en cas de déficit hydrique et sur des sols pauvres en nutriments. Cependant, les mécanismes souterrains à l'origine de ces avantages agronomiques restent largement méconnus. La question centrale de cette thèse est donc la suivante : les génotypes de blé présentant des architectures racinaires contrastées développent-ils des niches hydrologiques complémentaires lorsqu'ils sont cultivés dans un profil de sol commun, et cette complémentarité se traduit-elle par des avantages agronomiques mesurables à l'échelle du champ ?

Nous avons émis l'hypothèse que de tels génotypes cultivés en mélange accéderaient à l'eau à partir de couches de sol distinctes, réduisant ainsi la concurrence inter-plantes et améliorant l'exploitation collective des ressources du sol. Pour tester cette hypothèse, trois objectifs spécifiques ont été poursuivis : (i) identifier et valider une paire de génotypes de blé exprimant des traits racinaires suffisamment contrastés dans des conditions contrôlées ; (ii) quantifier les profils individuels d'absorption d'eau par les racines de chaque génotype en monoculture et en mélange au stade du débourrement – déterminant pour la constitution du rendement ultérieur – à l'aide du traçage par isotopes stables de l'eau ; et (iii) évaluer si la complémentarité résultant du mélange conduit effectivement à une amélioration des composantes du rendement dans le contexte de la variabilité pédoclimatique en plein champ sur l'ensemble d'une saison de croissance.

Le chapitre 1 présente le cadre théorique sous-tendant ces travaux. Ce cadre met en avant le contexte agronomique et écologique des mélanges intra-spécifiques de blé comme levier de résilience des agroécosystèmes. Le chapitre comprend également

1) un bref aperçu de la biogéochimie des isotopes stables de l'eau et de son application à la quantification de l'absorption d'eau par les racines, et

2) une description des stratégies de marquage isotopique susceptibles d'améliorer l'estimation de l'absorption d'eau par les racines à l'aide de modèles de mélange bayésiens.

Enfin, les objectifs et hypothèses détaillés du projet de doctorat sont présentés.

Le chapitre 2 se concentre sur le matériel et les méthodes utilisés pour tester les hypothèses formulées ci-dessus, à savoir :

1) caractériser les différences de traits entre les variétés de blé (deux paires de variétés commerciales de blé (Treblir® et Milaneco®) et deux lignées expérimentales quasi-isogéniques — UQR12 et UQR15). Ces expériences visaient à identifier une paire de génotypes exprimant des traits racinaires suffisamment contrastés.

2) un système interne à chambre divisée pour la mesure continue et indépendante de la composition isotopique de la transpiration de deux plantes cultivées dans la même colonne de sol,

3) une stratégie de marquage isotopique spécifique à la profondeur pour décorréler les profils d'isotopes stables d'hydrogène et d'oxygène dans l'eau du sol et réduire l'incertitude quant à l'emplacement de l'absorption d'eau par les racines et à la quantité relative calculée à l'aide du modèle de mélange Stable Isotope Analysis in R (SIAR).

4) des outils d'imagerie par résonance magnétique (IRM) pour fournir une cartographie tridimensionnelle non destructive de l'architecture racinaire et générer la distribution de la biomasse des deux systèmes racinaires poussant dans le même volume de sol.

Les conclusions de ce chapitre étaient les suivantes : premièrement, les résultats indiquaient que les variétés UQR12 (système racinaire superficiel — SRS) et UQR15 (système racinaire profond — DRS) présentaient des caractéristiques racinaires significativement contrastées (distributions de la biomasse, taux de croissance racinaire, activité enzymatique rhizosphérique) au stade du débourrement dans des conditions en colonne. Deuxièmement, le protocole de marquage à plusieurs profondeurs a généré un contraste isotopique suffisant pour améliorer potentiellement l'estimation des fractions individuelles d'absorption d'eau par les racines (fRWU).

Au chapitre 3, l'ensemble des méthodes validées décrites au chapitre 2 a été utilisé pour tester l'hypothèse centrale de l'étude exprimée ci-dessus, dans des conditions contrôlées et reproductibles. Les conclusions de ce chapitre étaient les suivantes : premièrement, les deux génotypes conservent une fRWU distincte en monoculture, ce qui correspond à leurs caractéristiques racinaires contrastées ; deuxièmement, lorsqu'ils sont cultivés ensemble en mélange, les deux génotypes déplacent leur absorption vers des couches de sol plus profondes par rapport à leur culture en monoculture ; et troisièmement, les différences entre la fRWU des monocultures et celle du mélange s'intensifient dans des conditions de déficit hydrique. Ce déplacement de l'absorption d'eau par les racines vers des couches plus profondes du sol, induit par le mélange, ne peut être prédit à partir des distributions de biomasse racinaire de l'un ou l'autre génotype en monoculture et est incompatible avec des mécanismes purement compétitifs. Cette étude fournit la première preuve isotopique d'une complémentarité de niche hydrologique dans un mélange de blé au niveau de la plante individuelle et suggère l'existence d'interactions inter-génotypes facilitatrices dont la base mécanistique, impliquant potentiellement une signalisation chimique médiée par les exsudats racinaires, reste à démontrer directement.

Le chapitre 4 rend compte d'une étude de terrain complémentaire visant à tester les paires de génotypes de blé précédemment documentées et à étudier les effets non additifs possibles du mélange sur l'ensemble du cycle jusqu'au rendement. Les expériences se sont déroulées sur la plateforme expérimentale TERENO Selhausen (Jülich, Allemagne) pendant la saison de croissance 2022–2023, marquée par une

phase tardive froide et humide (jusqu'à la mi-mai), une sécheresse printanière (en mai et juin) et des précipitations supérieures à la moyenne pendant les stades de remplissage du grain (fin juin à mi-juillet). Outre la mesure du potentiel hydrique et de la teneur en eau du sol, ainsi que les observations régulières du couvert végétal par multispectrale et LiDAR à l'aide de drones, la présence et la teneur en racines ont été déterminées respectivement de manière non destructive par imagerie racinaire au mini-rhizotron et de manière destructive par échantillonnage de carottes de sol. Les conclusions de ce chapitre ont montré que les caractéristiques racinaires du DRS et du SRS présentaient une plasticité phénotypique dépendante du contexte dans les conditions pédoclimatiques de terrain, ce qui a atténué les contrastes observés en conditions contrôlées. Cependant, comme prévu, les parcelles de mélanges ont surpassé les deux monocultures en termes de rendement, indiquant que l'avantage de rendement non additif du mélange a été confirmé à l'échelle du champ et au niveau de la communauté, même lorsque les contrastes sous-jacents de l'architecture racinaire sont partiellement atténués par le contexte environnemental.

À travers ses trois chapitres expérimentaux, cette thèse établit que la complémentarité de l'architecture racinaire intra-spécifique dans les mélanges de blé peut être confirmée par l'analyse des isotopes de l'eau. De plus, nous démontrons que ces mélanges de blé renforcent certains traits, tels que le nombre de talles et de racines primaires, ce qui conduit à des rendements plus élevés face à la sécheresse printanière. Une orientation importante pour les recherches futures concerne la caractérisation mécanistique des interactions facilitatrices inter-génotypes suggérées par les schémas d'absorption non additifs documentés ici.

Acknowledgements

I would like to express my deep gratitude to my thesis advisors, Youri Rothfuss and Mathieu Javaux, who entrusted me in 2020 with the task of completing this doctoral thesis. I am grateful for their support over the years, and for their constructive comments, always delivered with elegance and kindness. I would particularly like to thank Youri Rothfuss, who was regularly available on site to guide and advise me, sharing his experience while giving me the freedom to achieve my objectives through the approaches I wanted to try. I thank Nicolas Brüggemann, Jan Vanderborght, and Harry Vereecken, who respectively lead my research team and the institute that welcomed me, advised me, and significantly enriched the ways I approached the topics covered in my thesis. My work on this thesis also greatly benefited from the relevant comments and insights observations of Bernard Heinesch and Pierre Delaplace, in their capacity as members of the thesis committee at the University of Gembloux. Their willingness to share their expertise significantly improved the manuscripts and experimental approaches, while challenging existing hypotheses and decisions. I would also like to thank Florence Volaire, Florian Fort, Pierre Delaplace, and Caroline De Clerck for their dedication and constructive feedback as members of the jury committee, as well as Haïssam Jijakli for his role as chair of the jury.

All the experiments described in this document, from their design to their implementation, were made possible thanks to Moritz Harings. I sincerely appreciated his expertise, the daily hours spent bringing our ideas to life, meticulously examining every detail, and methodically addressing every problem, despite the constraints imposed by the Covid-19 pandemic and the resulting delays. The success of the experiments, particularly those described in Chapter 3, was also possible with the technical support of Normen Hermes, whose assistance was essential in overcoming electrical engineering and programming obstacles that would otherwise have been insurmountable. I was fortunate to meet Paulina Deseano Diaz, who was nearing the completion of her PhD when I began mine. She demonstrated a strong commitment to sharing her knowledge with great kindness. The success of the second study described in Chapter 3 was facilitated by these exchanges and her active support. This doctoral research was also conducted in parallel and in collaboration with the PhD research projects of Mona Giraud, Adrian Lattacher, and Ahmed Sircan, with whom I began this work at the same time. I had the privilege of being part of this environment of cooperation, mutual respect, and support, which facilitated the completion of this work.

I would like to express my sincere gratitude to Dagmar van Dusschoten for his invaluable contribution to the control experiments described in Chapters 2 and 3. His expertise was instrumental in formulating and answering my scientific questions, and his kindness was deeply appreciated. The time spent working with him and his team was an enriching experience. I would also like to thank Johannes Kochs, whose ingenuity and expertise were crucial in overcoming numerous technical challenges and facilitating the execution of these experiments, as well as Daniel Pflugfelder for his invaluable assistance and flexibility, which played an essential role in the success

of the MRI measurements. I would like to express my gratitude to Ayhan Egmen and the entire workshop team at Forschungszentrum Jülich, who consistently provided high-quality solutions to meet all the technical requirements we had outlined. I also thank Lutz Weihermüller for the soil retention curve measurements and for his support with the experiments described in Chapters 2, 3, and 4. I would also like to express my gratitude to Jordan Bates, Xuerui Guo, and Carsten Monska for their contributions to the acquisition of drone measurements and the subsequent processing, as well as to Tim Spieker, Philipp Meulendick, and Yang Yu for their technical support and advice regarding the field measurements discussed in Chapter 4. I would like to express my sincere gratitude to all the co-authors of the published studies, who have significantly improved the manuscripts and this doctoral thesis. A big thank you to the successive interns who helped me conduct the experiments or analyze certain parts of the datasets produced, in particular Sandisiwe Moyo, Christoph Tempelmann, Esther Vogt, Humza Muhammad, Anna Hollweg, Akhil Kumar, Muhammad Ramish, Shayan Hassanpour, Ashley Malenfant, Sharmin Jahan, Annacleto Vunge, Meghana Koppadi, Bhavana Sitaphale, and Akib Ahmed. I wish them all the best in their future endeavors, whether in research or elsewhere. Furthermore, the invaluable support and contributions of Holger Wissel, Sirgit Kummer, Franz Leistner, Andreas Lücke, Tanja Ehrlich, Anna Galinski, and Beate Uhlig were also essential during my time at Forschungszentrum Jülich for learning measurement methods and procedures as well as their implementation. I would like to express my gratitude to them for their patience and willingness to guide me.

I would like to extend a special thank you to Nikos Kaloterakis, who began his PhD at the same as me. Together, we overcame the many obstacles of our PhDs. I enjoyed sharing our office—into which we tried to let more southern sunshine, though we would have liked to enjoy more. It was always a pleasure to get together from time to time to play rebetiko-jazz-fusion. I would also like to thank Khadija Boughazi for her valuable advice and expertise in plant physiology, which proved indispensable for the experiments described in Chapters 2 and 3 of this thesis. Her moral support and kindness were also very much appreciated. Thanks also to Heleni for teaching me backgammon and for the meals shared with Ousamma. Furthermore, I consider myself extraordinarily fortunate to have been part of an exceptional research group, composed of doctoral and postdoctoral students who were both friendly and cooperative in their approach. I would like to thank my colleagues Xinyue Cao, Daniel Schulz, Kerui Zhao, Katharina Neubert, Matthias Claß, Muhammad Islam, Adrian Hauperthal, Alexander Kelsch, Luidmila Kachalova, Otavio Leal, and Rüdiger Reichel for the sunny barbecues in the garden surrounded by chickens, the hikes in the region, and the relaxed lunch and coffee breaks. Thanks also to Xinyu Gan and Kerui Zhao for working together to improve living conditions for doctoral students. My thanks go to my successive roommates, Conny Breckheimer, Sebastian Soto Gaona, Astrid Muller, Elena Thul, Yulin Lu, and Sasha Kaspor, who supported me and sometimes helped me with German administrative tasks. I have fond memories of the time spent in the garden growing a few vegetables alongside the green grass and with the chickens Baguette, Pertelote, and Teresita, enjoying their red coop.

In 2017, Annette Bérard and Claude Doussan, of INRAE in Avignon, placed their trust in me and opened the doors to the world of agricultural research. This allowed me to devote three years of apprenticeship to learning and research alongside dedicated colleagues. It is to them that I owe the fundamental principles of the technical and scientific knowledge used in this thesis, as well as my deep interest in understanding the mechanisms that occur at the soil-root interface. My professor at the agricultural engineering school, Florian Celette, as well as my senior, Olivier Duchêne, also inspired me to pursue this path. I am truly grateful to them.

In conclusion, I must extend my deepest gratitude to my family, particularly my parents, Véronique and François, for their unconditional support and profound love. They did everything to ensure their children's success, whatever path they chose, which has allowed me to become the person I am today. I also thank my brothers Jonathan and Yannick for our close bond and their support, and my grandmother, Marie-José Muccio, whose strength is a source of inspiration. I am also fortunate to have shared wonderful experiences with exceptional friends who helped me grow - people I met in Gardanne, Lyon, Avignon, or Pinar del Río. Thank you Stan, Amadou, Jean Marie, Abdoulaye, Mamadou, David, Lopez, Jonathan, Hermann, Nicolas, Joseph, Stephan, Louise, and Gaëtan! Despite the distance and the different paths each of us has taken, these friendships have been extremely precious and indispensable in helping me persevere over the past six years, providing me with invaluable support and companionship during difficult times. Finally, Molly, thank you for your support and love, which played a decisive role in the success of this work, despite the geographical distance. The moments of shared joy, as well as the trust you placed in me and your sincere interest in my work, were invaluable in helping me complete it. I, too, am confident in the success of your PhD. I am happy to have gone through this period with you and to now embark on other adventures together.

Table of contents

Abstract 5

Résumé 9

Acknowledgements 13

Table of contents 17

List of figures 21

Liste of abreviations 29

Chapter 1 35

1. Intraspecific wheat mixtures as a lever for agroecosystem resilience.....37

1.1. A brief overview of the intertwined histories of humans and wheat, its root traits and the constitution of the grain yield.....37

1.2. Biodiversity as a buffer against climate variability 39

1.3. Development and interactions among the above-ground, below-ground, and reproductive traits of wheat in a mixture 42

1.4. Root water uptake strategies and below-ground interactions in intraspecific wheat mixtures.....44

2. Water stable isotopes – a useful tool for ecohydrological studies 45

2.1. Water stable isotope analysis for the study of root water uptake.....45

2.2. The isotopic labeling strategy—a lever for improving resolution and accuracy.....48

3. Main and specific objectives of the thesis.....49

4. Author contributions 53

Chapter 2 55

1. Introduction.....58

2. Root and shoot trait characterization of Milaneco and Treblir lines: screening for root traits and functions contrasts.....60

2.1. Material and Methods 60

2.2. Results.....64

3. Root and shoot trait characterization of UQR 12/ 15 lines: screening for root traits and functions contrasts 67

3.1. Material and Methods 67

3.2. Results 71

4. Experimental framework development: column design, multi-depth isotopic labeling, and non-destructive root imaging 74

4.1. Material and Methods 74

4.2. Results 76

5. Discussion 82

5.1. Selection of root contrasted wheat genotypes 82

5.2. Selection of the column size and the stage of interest for the genotype pair of interest 83

5.3. Coupling structural and functional root characterization: methodological considerations 85

6. Conclusion 86

Chapter 3 89

1. Introduction 92

2. Materials and methods 93

2.1. Experimental setup 93

2.2. Labeling strategy, water stable isotopic monitoring, and RWU determination 98

2.3. Aboveground physiological measurement and root traits 101

2.4. Statistics and data representation 102

3. Results 104

3.1. Root and shoot traits 104

3.2. Soil water status 110

3.3. Root water uptake 113

4. Discussion 118

4.1. Root traits and water uptake 118

4.2. Genotypes strategies facing water deficit 119

4.3. A niche complementarity in the wheat genotype mixture? 121

5. Conclusion 125

Chapter 4 127

1. Introduction 130

2. Materials and methods 131
2.1. Pedoclimatic conditions, agricultural practices and experimental design. 131
2.2. Soil and plant measurements 134
2.3. Aboveground plant measurements.....134
2.4. Mini-rhizotron measurements.....136
2.5. Statistics and Data Representation.....136
3. Results.....137
3.1. Plant aboveground measurements.....137
3.2. Roots development.....140
3.3. Soil water status 142
3.4. Yield and biomass.....146
4. Discussion 147
4.1. Genotype specific spatial niche occupation dynamic and water use ..147
4.2. Resource allocation strategies and adaptation to seasonal climate variability.....148
4.3. Non-additive effects of the wheat genotype mixture for better yield .149
5. Conclusions.....152
Chapter 5 153
1. General discussion 155
1.1. Originality and complementarity of the methods 155
1.2. Limitations 157
1.3. From controlled conditions to field variability 158
2. Conclusion and key messages.....160
3. Perspectives.....161
3.1. Technical improvements and simplification of the experimental framework 161
3.2. Towards more comprehensive semi-mechanistic modeling 162
3.3. Broadening the scope: nitrogen, genotype diversity, and field applicability 163
3.4. The root trait-function relationship and the plant-plant communication 164

References 166

List of figures

Fig. 1 Experimental and modelisation cluster repartition in CROP project.....50
Fig. 2 Schema of the general thesis architecture with the link between the chapters 51
Fig 3 Root length density (WLD, in cm cm^{-3}) profiles from 0 to 180cm, for the genotypes Milaneco (blue), Trebelir (green) and Capo (brown) at tillering stage under low (clear colors) of high (dark colors) nitrogen fertilization 62
Fig. 4 Root length density (WLD, in cm cm^{-3}) profiles from 0 to 180cm, for the genotypes Milaneco (blue), Trebelir (green) and Capo (brown) at flowering stage (anthesis) under low (clear colors) of high (dark colors) nitrogen fertilization.....63
Fig. 5: Schematic overview of the preliminary experiment comparing the winter wheat cultivars Treblir® and Milaneco® in rhizoboxes (45 cm high, 11 cm in diameter, n = 5). Plants were sown on November 23–27 and harvested at 45 DaS. Measurements included soil water and plant (SWaP) campaigns (December 15 and January 11), non-destructive root imaging, WinRHIZO™ root scanning, shoot traits (foliar surface area, dry matter), and soil profile analysis on five 9-cm segments (zymography, nitrogen, water content, root weight). 63
Fig. 6 Maximum root length (cm) of Treblir® (in blue) and Milaneco® (in red) of the days of growth, recorded with the rhizoboxes pictures every 1-2 days.....65
Fig. 7 Summary table of the total root length (cm), the mean and median inter-lateral distance (cm), the mean and median daily root growth rate (cm/day) and the root insertion angle (°), retrieved from rhizoboxes pictures. 65
Fig. 8 Total root length per rhizobox (m), according to the root order (basal roots, first and second order) for Treblir® and Milaneco® from the final rhizoboxes pictures 66
Fig. 9 a) Root fresh density profile over the five depth of 9cm of the soil column at 45 DaS; b) Shoot dry biomass average at 45 DaS and c) the average foliar surface evolution from 0 to 45 DaS; for Treblir® (in blue) and Milaneco® (in red). 66
Fig. 10 Zymographs of β-1,4-Glucosidase activity (degradation of cellulose and indicator for the activity of copiotrophic microorganisms) of Milaneco and Treblir, respectively. The following correspondence exists between the latin alphabet and enzymatic activity classes: A corresponds to 0 pM mm-2 h-1; B, 0-15 pM mm-2 h-1; C, 15-30 pM mm-2 h-1; D, 30-45 pM mm-2 h-1; E, 45-60 pM mm-2 h-1; F, 60-75pM mm-2 h-1; G, 75-90 pM mm-2 h-1; H, 90 pM mm-2 h-1 67
Fig. 11 Overview on rhizobox of the root system of the wheat genotype UQR12 (shallow root system) and UQR15 (deep root system). Angle of the seminal roots and the root biomass.....68
Fig. 12 Schema of the of the winter wheat UQR12 and UQR15 experiment, with the destructive sampling weeks 70
Fig. 13 Shoot and root fresh biomass (g) for UQR15 (in blue) and UQR12 (in orange) between 28 and 49 days after sowing.....71

Fig. 14 Root growth (g) by soil layers 9-18 cm (B, in green), 18-27 cm (C, in yellow) and 36-45 cm (E, in brown) between 15 and 45 days after sowing for UQR12 (on the left) and UQR15 (on the right) 72
Fig. 15 Temporal patterns of the mean β-glucosidase activity in topsoil and subsoil for the shallow root system (SRS) (yellow) and deep root system (DRS) (green) from day 28 to day 49 after sowing. Error bars represent the standard deviation of 3 replicates. The displayed p-values indicate significant effects ($p < 0.05$), determined using a linear mixed-effects model. In this model, the columns were treated as a random effect, while genotype, depth, and age were considered as fixed effects. From Lattacher et al. (2025)..... 72
Fig. 16 Leaf surface (cm^2) for UQR12 (on the left) and UQR15 (on the right) between 0 and 49 days after sowing 73
Fig. 17 Root fresh mass average (g) profile from 0 to 70cm for the 9cm and 12cm column (error bars for standard error), same variety UQR15, at 81 DaS 77
Fig. 18 Foliar surface evolution from 0 to 65 DaS of the UQR15 wheat genotype (DRS) in two pots of same high (70cm) but different outside diameters 12 vs 9cm (i.e. 11 vs 8 cm inner diameter) 77
Fig. 19 Theoretical profile of isotopic composition along the acrylic column for the acrylic column labelling pre-test. Left: labelling application on the bottom of a soil column. 78
Fig. 20 Soil column during the water stable isotopes labelling, 7/12/2021. On the left, ths acrylic soil column with the aboveground chamber without plants and the system for water stable isotopic meausremnets online is connected. On the top right, the manual valve to inject water in the soil dripping tubings. On the bottom right the labelled water to be injected 79
Fig. 21 Dual plot for delta 18O and 2H values between days 344,5 and 347,5 79
Fig. 22 Left side: MRI imaging of two wheats plants growing in the same column, 30 DaS. Middle: PVC column in the MRI scanner with the linear axis. Right side: picture of the linear axis robot built..... 81
Fig. 23 Experimental design: example of Run3 consisting of its columns (stable water isotopes (WSI), panel a) vs MRI columns, panel b)) and their specific underground and aerial measurements. In the lower panel c), randomly distributed composition of each experimental series (Run1-Run6) in terms of plant modality (two individuals with "shallow root systems ‘ – SRS or with 'deep root systems’ – DRS grown in monoculture, and their mixture – MIX) and water treatment (well-watered conditions – WW and water deficit – WD). The WSI columns (left side, A-C) included soil water potential sensors and gas-permeable membranes for online analysis of the stable isotopic composition of soil water (δ) and gas exchange chambers for non-destructive determination of transpiration flux and isotopic composition. The MRI columns (right side, D-I) did not include soil sensors, and the gas exchange chambers were used only to simulate the same atmospheric conditions that prevailed for the WSI columns. Each run of experiments included three WSI columns and six MRI columns 94

Fig. 24 Mean and standard deviation (sd) resulting of environmental parameters of the experiment in the afternoon between 1 and 3 pm at the booting stage (between 39 and 43 DaS) (air temperature in °C; air humidity in %, vapor pressure deficit (VPD) in kPa, pF matric potential and soil temperature in °C) for each culture type, genotype and water treatment (n=3). 95

Fig. 25 Evolution of soil water potential, expressed in pF, average (solid line) and standard deviation (transparent envelope) measured using Teros21 sensors, for well-watered treatments ("WW," panels a to g) and water deficit treatments ("WD," panels h to n) among seven soil depths displayed on the right-hand side (3, 8, 20, 42, 64, 74, 79 cm). The colors represent the three crop types: DRS monoculture, dark green; mixture – MIX, blue; and SRS monoculture, orange. 97

Fig. 26 (a) Experimental set-up with three acrylic columns for water stable isotope measurements, set on blue balances and under light panels. (b) Split plant chamber with an air inlet and outlet for each half, ventilators and an air temperature and humidity sensor. (c) Acrylic soil column with permeable tubes (for water stability measurements), Teros21 sensors (matric potential) and label drip tubes before filling the column with soil 98

Fig. 27 Schematic diagram of the air circuit in the experiment carried out to measure RWU profiles using stable isotope measurements of water. Each acrylic column is equipped with 13 permeable tubes opened and closed by valves (A1 to C13). The air inlet to the soil columns is controlled by the MFC1 and the pressure can be released by the A_PrRel valve. The sampled water vapor is then diluted with dry air by MFC2, and directed to the analyzer or flushed via the 3-way valves. A(B/C)_ACTO. The Std1 and Std2 calibration standards are measured the same way. Ambient air is pushed into the plant chambers, regulated by manual valves, and measured by the analyzer via the three-way valve A_CCTI. The outlet from each plant chamber is either flushed or directed to the analyzer via the 3-way valves A(B/C)_CCTI.....99

Fig. 28. Key root and shoot morphological traits (the total root system dry biomass (g) and surface (cm2), the crown root number per pot and the depth of 70% of the cumulated DRFW (D70, cm); as well as the shoot dry biomass (g), the total leaf surface (cm2) and tiller number per plant) recorded destructively at the elongation stage (43 DaS). The total amount of water transpired by soil column during the whole experiment till the botting stage (in mL) is also represented with their water use efficiency (WUE, g/L, calculated as the dry mass of whole plant per the total plant transpiration) among the culture type, the genotype and water treatment.....105

Fig. 29 Distributions of basal root angles for the well watered ("WW", line, panel a) and water deficit ("WD", dots, panel b) for the three plant modalities (DRS in monoculture, dark green color; DRS in mixture, dark blue color; SRS in mixture, light blue color; SRS in monoculture, orange color) measured on the in situ 3D MRI scans at the booting stage. Screenshot of a 3D MRI root scan analysis to measure the root angles of two wheat plants in a soil column (panel c). In blue the seminal roots are traced, in white to black the position of the root seminal at 2cm from the green the stem reference point to calculate the angles. 105

Fig. 30 Distributions of the percentage of digital root fresh weight (DRFW) per 10 cm soil layer, measured in situ by MRI at 43 DaS for the well-watered (WW, lines, panel a) and water deficit (WD, dots, panel b) treatments among the plant modalities (DRS in monoculture, dark green; Mixture – MIX, blue; and SRS in monoculture, orange) (n=6). 106

Fig. 31 Cumulated profiles of root tips amount per 2 cm soil layers, facet grid by plant modality DRS, MIX, and SRS, and for WW and WD treatments (n = 3)..... 106

Fig. 32 Distributions of the root surface density per soil volume (cm2 cm-3) as per root diameter class, measured for the destructive root sample scans at the booting stage, for the well-watered ("WW", lines, panel a, c, e) and water deficit ("WD", dots, panel b, d, f) treatments, in the topsoil (0-7cm depth, panel a, b), intermediate soil layers (7-73cm depth, panel c, d) and subsoil (73-80cm depth, panel e, f), among the plant modalities (DRS in monoculture, dark green color; Mixture – MIX, blue color; and SRS in monoculture, orange color) (n=3 in top- and subsoil, n=18). 107

Fig. 33 Total leaf area per plant (in cm^2, panels a, b, c, and d), and number of tiller per plant (panels e, f, g, and h) for the four plant modalities (DRS monoculture, dark green; DRS mixture, dark blue; SRS mixture, light blue; SRS monoculture, orange) under well-watered conditions (WW, lines, panels a, c, e and g) and water deficit (WD, dots, panels b, d, f and h), throughout growth, modelled by LOESS regression (Locally Estimated Scatterplot Smoothing, 95% confidence interval) (a, b, e and f) and at 43 DaS (c, d, g and h) (n = 18 for SRS and DRS in monoculture, n = 9 for SRS and DRS in mixture). 108

Fig. 34 Distributions of shoot-to-root ratio (S:R) for (a) the dry matter ($g\ g^{-1}$); (b) the water content ($\%\ \%^{-1}$); (c) the surface ratio ($cm^2\ cm^{-2}$); (d) the tiller number to seminal root number (–) measured at 43 DaS for three plant modalities (DRS in monoculture, dark green; MIX, blue; SRS in monoculture, orange) under well-watered (WW, solid lines) and water deficit (WD, dashed lines) conditions (n = 3) 109

Fig. 35 Soil depth profile distribution of water potential between 39 and 42 DaS in the afternoon during the plant transpiration measurements, expressed as pF, for the well-watered (WW, lines, panel a)) and water deficit (WD, dots, panel b) treatments among the plant modalities (DRS in monoculture, dark green, panel a; Mixture – MIX, blue, panel b; and SRS in monoculture, orange, panel c) (n=3). 111

Fig. 36 Soil matric potential difference, expressed as MPa, measured with the Teros21 sensors, between absolute values of matric potential in water deficit ("WD") and well watered ("WW") conditions for the three plant modalities (DRS in monoculture, dark green color, panel a; Mixture – MIX, blue color, panel b; SRS in monoculture, orange color, panel c), across ten soil layers (0-2; 2-4; 4-7; 7-14; 14-30; 30-52; 52-69; 69-76; 76-78; 78-80 cm). Standard deviations are indicated by black bars. 111

Fig. 37 Leaf Water Potential (in MPa) measured by leaf psychrometer from 37 to 43 DaS of a plant growing under well-watered conditions ("WW", line) and two plants under water deficit conditions ("WD", dots). (n=1) 112

Fig. 38 Measurement points modeled by LOESS (Locally Estimated Scatterplot Smoothing) regression with 95% confidence interval from 39 to 43 DaS of transpiration rate (in mL/min) monitored continuously by scale bellow the soil columns, for the three crop modalities (DRS in monoculture, dark green color; Mixture – MIX, blue color, and SRS in monoculture, orange color) under well watered ("WW", lines, panel a) and water deficit ("WD", dots, panel b) conditions. (n=3) 112

Fig. 39 Fraction of the Root Water Uptake (fRWU, % cm^{-1}) distributions (panels a and b) and mean values (panels c and d) estimated between 39 and 42 DaS , for the four plant modalities (DRS in monoculture, dark green; DRS in mixture, dark blue; SRS in mixture, light blue; SRS in monoculture, orange), across ten soil layers (0-2; 2-4; 4-7; 7-14; 14-30; 30-52; 52-69; 69-76; 76-78; 78-80 cm) under well-watered (WW, lines, panel a) and water deficit (WD, dots, panel b) conditions (n=7-12)...113

Fig. 40 Distributions of the Sink Term (mL min^{-1} cm^{-1}) estimated between 39 and 42 DaS, for the four plant modalities (DRS in monoculture, dark green; DRS in mixture, dark blue; SRS in mixture, light blue; SRS in monoculture, orange), across ten soil layers (0-2; 2-4; 4-7; 7-14; 14-30; 30-52; 52-69; 69-76; 76-78; 78-80 cm) under well-watered conditions (WW, lines, panels a and c) and water deficit (WD, dots, panels b and d) (n=7-12). 115

Fig. 41 Differences of fraction of the Root Water Uptake (fRWU, % cm^{-1}) estimated between 39 and 42 DaS between water deficit (WD) and well-watered (WW) conditions for the four plant modalities (DRS in monoculture, dark green, panel a; SRS in monoculture, orange, panel b, DRS in mixture, dark blue, panel c; SRS in mixture, light blue, panel d), across ten soil layers (0-2; 2-4; 4-7; 7-14; 14-30; 30-52; 52-69; 69-76; 76-78; 78-80 cm). Standard deviations are indicated by black bars (n=3). 116

Fig. 42 Density of the Digital Root Fresh Weight (dDRFW, % cm^{-1}, measured at 43 DaS) over the fraction of Root Water Uptake (fRWU, % cm^{-1}, estimated between 39 and 42 DaS). The points represent the average value of two plant modalities (DRS in monoculture, circle shape; SRS in monoculture, triangle shape), across ten soil layers (0-2; 2-4; 4-7; 7-14; 14-30; 30-52; 52-69; 69-76; 76-78; 78-80 cm) under well-watered conditions (WW, lines) and water deficit (WD, dots). Black bars indicate standard deviations..... 117

Fig. 43 Vertical distribution from 0 to 95 cm depth of the (a) bulk density (g cm^{-3}); (b) organic carbon content (%) ; (c) soil texture fractions showing sand (orange), silt (gray), and clay (dark gray) distribution..... 131

Fig. 44 Location of the destructive sampling on the plots (DRS in dark green, MIX in blue, SRS in orange) at the Elongation and Grain filling stage (aboveground biomass and belowground soil core) and the measure the compound of the yield at the harvesting time. The minirhizotron tubings are represented by dotted white lines. Drone picture credit Jordan Bates, 10/07/2023. 132

Fig. 45 Chronogram of the experiment with the labeling and destructive sampling campaigns, the manual, drone and mini-rhizotron measurements, the daily rain precipitation amount, the freezing days, the three main climatic periods and the plant stages. On the Zadoks scale, the numbers corresponds to: 0-Germinations; 1-Seedling

growth; 2-Tillering; 3-Stem elongation; 4-Booting; 5-Ear emergence; 6-Flowering (anthesis); 7-Milk development; 8-Doughy development; 9-Ripening..... 133

Fig 46 NDVI picture taken by drone on June 6, 2023, 77 DaS (end of the flowering stage). We see the heterogeneity inside each plot. On the plot, we see the photosynthetically active surface (green leaf surface) over the NDVI values, along the growing season. The data come from 36 plants measured manually and their NDVI corresponding pixels, over the growing season. 135

Fig. 47. (a–e) Foliar water potential at noon (bar), plant water content (frac.), dry biomass (g), leaf surface temperature relative variation (°C), and green leaf area (cm²/plant, calculated from NDVI data). (f–j) Canopy height (cm), number of tillers/ears, number of green leaves, leaf length (cm), and average SPAD index per plant. Climatic phases: wet/cold start (purple, 0–40 DaS), drought period with high evaporative demand (yellow, 40–100 DaS, peak stress ~92 DaS), return of precipitation (orange, >100 DaS). Flowering occurs between 75 and 80 DaS. Colors: DRS monoculture (green), MIX (blue, with dark blue for DRS components and light blue for SRS components), SRS monoculture (orange). Shading zone = ±1 standard deviation. 139

Fig. 48 Distribution of the plant root length density (pRLD, cm root per cm2 of soil) per soil depth (10 to 120cm) from 16 DaS (panel a) to 105 (panel i) for root diameters above 300µm. The evolution of the average (solid line) and the standard deviation (transparent envelope) from 16 to 105 DaS is displayed layer per layer pane j) to o). 141

Fig. 49. a) Evolution of the daily soil water content at the 6 soil depth during the growing season from 0 to 120 DaS, b) Soil Water Content (SWC, %, vol.) distribution among the plant modalities at the flowering stage between 77 and 79 DaS at 120, 80, 60, 40, 20 and 10 cm soil depth c) Water stock evolution in the soil during the growing season from 0 to 120 DaS. DRS was in green, MIX in blue and SRS in orange. .. 143

Fig. 50 Plane root length density (pRLD, cm cm^{-2}) over the daily absolute difference of SWC (volumetric fraction) recorded on the same dates (16, 22, 29, 36, 51, 65, 77, 92 and 105 DaS). The points represent the average value and the bars the standard deviations of three plant modalities (DRS in monoculture, dark green; MIX, blue; SRS in monoculture, orange), across six soil depths (10, 20, 40, 60, 80, 120 cm). Dashed lines represent the linear regression for each plant modality..... 144

Fig. 51 Plan root length density (pRLD, cm cm^{-2}) as a function of soil water content (SWC, volumetric fraction) recorded at the same dates (16, 22, 29, 36, 51, 65, 77, 92 and 105 DaS). Points represent mean values and bars indicate standard deviations for three plant modalities (DRS in monoculture, in dark green; MIX, in blue; SRS in monoculture, in orange) across six soil depths (10, 20, 40, 60, 80 and 120 cm), with point size increasing with DaS (from 20 to 100 DaS). Dashed curves represent second-order polynomial regressions fitted for each plant modality. 145

Fig. 52 The ear (a), aboveground plant organs (b) and grain (yield) (c) biomass after the harvest, as well the ear density per soil surface (d), the grain weight per ear (e), the weight of 100 grains (f) and the nitrogen content (g), for the three plant modalities

DRS (dark green), MIX (blue) and SRS (orange), evaluated over a surface of 40cmx40cm. (n = 18) 146

Liste of abreviations

Abreviation	Description	Units	Chap.
AMF	Arbuscular Mycorrhizal Fungi	—	5
ANOVA	Analysis of Variance	—	2,3,4
BMBF	Bundesministerium für Bildung und Forschung (German Federal Ministry of Education and Research)	—	1
CH	Canopy Height (derived from LiDAR digital surface model)	m	4
CNN	Convolutional Neural Network (RootPainter software for root segmentation in rhizotron images)	—	4
CPlantBox	Functional-structural plant and root architecture model (Giraud, Le Gall et al., 2023)	—	1
CRDS	Cavity Ring-Down Spectroscopy (Picarro L2130-i laser spectrometer)	—	1,2,3
CROP	Research project name (BMBF-funded) — Combining ROot contrasted Phenotypes for more resilient agro-ecosystems	—	1
CV	Coefficient of Variation	%	3,4
D70	Depth at which 70% of cumulative DRFW is reached (rooting depth indicator)	cm	3
DaS	Days after Sowing	d	2,3
DRFW	Digital Root Fresh Weight — MRI signal intensity integrated per depth interval, proxy of root biomass	a.u.	3
DRS	Deep Root System (UQR015 — seminal root angle narrow, predominantly deep extraction)	—	1,2,3,4,5
fRWU	Fraction of Root Water Uptake — relative contribution per soil layer, normalized by layer thickness	% cm^{-1}	1,3,5
FSPM	Functional-Structural Plant Model	—	2
FZJ	Forschungszentrum Jülich GmbH	—	1,3
GAI	Green Area Index (green leaf and stem area)	m^2 m^{-2}	4

GMWL	Global Meteoric Water Line ($\delta^2H = 8 \times \delta^{18}O + 10$, Craig 1961)	—	1,3
IBG-2	Institute of Bio- and Geosciences, division 2 — Plant Sciences, Forschungszentrum Jülich (MRI platform)	—	3
IBG-3	Institute of Bio- and Geosciences, division 3 — Agrosphere, Forschungszentrum Jülich	—	1
INRAE	Institut National de Recherche pour l'Agriculture, l'Alimentation et l'Environnement (France)	—	1
IRMS	Isotope Ratio Mass Spectrometry	—	1
LAI	Leaf Area Index	$m^2\ m^{-2}$	4,5
LER	Land Equivalent Ratio (mixture overyielding metric, sum of relative yields)	—	1
LiDAR	Light Detection And Ranging (laser canopy structure scanning)	—	4
LOESS / loess	LOcally Estimated Scatterplot Smoothing (local polynomial regression, R function)	—	3,4
MCMC	Markov Chain Monte Carlo (algorithm used in SIAR / siarmcmcdirichletv4)	—	1,3
MIX	Intraspecific mixture (50 : 50 of DRS + SRS in the same column or plot)	—	1,2,3,4,5
MRI	Magnetic Resonance Imaging (4.7 T magnet, Magnex; MR Solutions console)	—	1,2,3,5
NDVI	Normalized Difference Vegetation Index ((NIR−R)/(NIR+R))	—	1,4,5
NMR	Nuclear Magnetic Resonance (physics term for same technique as MRI)	—	1,2
NMRooting	Software for automated root angle and tip extraction from 3D MRI scans (van Dusschoten et al. 2016)	—	3
NPOC	Non-Purgeable Organic Carbon (dissolved organic C in soil extracts)	$mg\ L^{-1}$	2
NS	Not Significant ($p > 0.05$)	—	3,4
PCA	Principal Component Analysis	—	3,4

pF	$\log_{10}$ of the absolute soil matric potential in cm H_2O — measure of soil water availability	—	1,2,3,4
PGA	Plant Green Area	cm^2/plant	3
pRLD	plane Root Length Density (from mini-rhizotron image analysis)	cm cm^{-2}	1,4
PVC	PolyVinyl Chloride (material of WSI columns — NB: MRI columns are acrylic)	—	1,2,3
RHchamber	Relative Humidity in the gas exchange chamber	%	3
RLD	Root Length Density	cm cm^{-3}	2,4,5
RTD	Root Tip Density (number of root tips per soil layer)	tips cm^{-1}	2,3
RWC	Relative Water Content (leaf water status)	%	1
RWU	Root Water Uptake	mL min^{-1}	1,3,5
sd	Standard deviation	—	3,4
SIAR	Stable Isotope Analysis in R — Bayesian multi-source mixing model (Parnell et al. 2010)	—	1,3,5
Sink Term	Product of fRWU and transpiration rate — volumetric water extraction per unit depth	mL min^{-1} cm^{-1}	3
SMP	Soil Matric Potential (Teros 21 sensors in WSI columns, Ch3)	MPa	3
SPAD	Soil Plant Analysis Development (chlorophyll meter, Konica Minolta 502Plus)	SPAD units	2,3,4
SRS	Shallow Root System (UQR012 — seminal root angle wide, predominantly topsoil extraction)	—	1,2,3,4,5
SWC	Soil Water Content (volumetric)	m^3 m^{-3} or %	1,4
TERENO	TERrestrial ENvironmental Observatories — German long-term observatory network (Selhausen site used in Ch4)	—	1,4,5
Teros 21	Soil matric potential + temperature sensor (METER Group) in WSI columns	—	3

Tr	Transpiration rate (per plant or per gas exchange chamber)	mL min^{-1}	3
UAS	Unmanned Aerial System (drone platform)	—	1,4,5
UQR	University of Queensland Root lines (UQR12 = SRS; UQR15 = DRS)	—	1,2,3
VPD	Vapor Pressure Deficit	kPa	1,3,4
V-SMOW	Vienna Standard Mean Ocean Water (international isotope reference material)	—	1,3
WD	Water Deficit (chronic water deficit imposed from sowing; pF 3.5–4.5 in Ch3)	—	1,2,3,4
WD-DRS	Water-deficit monoculture of DRS	—	3
WD-MIX	Water-deficit mixture of SRS and DRS	—	3
WD-SRS	Water-deficit monoculture of SRS	—	3
WinRHIZO	Software for destructive root scanning and morphological analysis (Regent Instruments)	—	2,3
WSI	Water Stable Isotopes (general term for $\delta^{18}O$ and $\delta^{2}H$ measurements)	—	2,3
WUE	Water Use Efficiency (whole plant dry weight / cumulated transpired water in Ch3)	g L^{-1}	1,3
WW	Well-Watered (water treatment, no imposed stress; pF 2.0–3.0 in Ch3)	—	1,2,3,4
WW-DRS	Well-watered monoculture of DRS	—	3
WW-MIX	Well-watered mixture of SRS and DRS	—	3
WW-SRS	Well-watered monoculture of SRS	—	3
Zadoks scale	Decimal phenological staging scale for cereals (Zadoks et al. 1974)	—	3
$\delta^{18}O$	Delta oxygen-18: stable isotopic composition of ^{18}O in water (delta notation)	‰ vs V-SMOW	1,2,3,4
$\delta^{2}H$	Delta deuterium: stable isotopic composition of ^{2}H (deuterium) in water	‰ vs V-SMOW	1,2,3,4
δRWU	Isotopic composition of root water uptake (assumed = δTr at steady state)	‰	3

δsoil	Isotopic composition of soil liquid water (^{18}O or ^{2}H)	‰	3
δTr	Isotopic composition of transpired water vapor	‰	3
ψleaf	Leaf water potential (psi-leaf)	MPa	1,4
ψsoil	Soil matric potential (psi-soil, = SMP in Ch3)	MPa	1

Chapter 1

Introduction, state of the art and objectives

1. Intraspecific wheat mixtures as a lever for agroecosystem resilience

1.1. A brief overview of the intertwined histories of humans and wheat, its root traits and the constitution of the grain yield

Agricultural practices, particularly the domestication of soft wheat (*Triticum aestivum L.*), represent one of humanity's most transformative achievements. Yet, like the tool-making traditions that preceded it, the transition to agriculture was neither sudden nor inevitable, but rather the culmination of millennia of accumulated knowledge, refined tools, and the formation of social networks capable of preserving cultural innovations.

The growth of a cumulative culture—in which knowledge is transmitted from one generation to the next and from one population to another—depended fundamentally on two complementary forces: cognitive innovations enabling the faithful transmission of complex skills, and the demographic expansion of interconnected populations (Colagè and d'Errico, 2025; Henrich, 2004; Migliano and Vinicius, 2021). Without these conditions, even the most sophisticated technologies could disappear as small, isolated groups died out.

Archaeological evidences trace this accumulation over millions of years. The earliest known stone tools made by hominins, dating from the Lomekwian period (3.3 Ma), have been found; these were used by australopithecines for basic subsistence activities (Harmand et al., 2015). Around 2 Ma, Homo erectus is thought to have produced the first Acheulean bifaces, marking a qualitative leap in terms of technical complexity and, implicitly, the transmission of knowledge (Mussi et al., 2023). Our species, Homo sapiens, is also thought to have originated in Africa around 300,000 years ago (Hublin et al., 2017). Much later, during the Middle Pleistocene, wooden digging tools—potentially used for harvesting roots, but perhaps also for preparing seedbeds—were found in Neanderthal sites in Spain (approximately 90 ka; Rios-Garaizar et al., 2018). However, it was only recently, with Homo sapiens, that specialized stone sickles are thought to have appeared (approximately 23 ka), directly foreshadowing agricultural tools (Groman-Yaroslavski et al., 2016).

The transition to cereal agriculture itself took place through a process of gradual accumulation, trial and error, and evolving needs. Data from the Zagros Mountains (Iran) show that human populations were consuming cereals and possessed sophisticated knowledge of their growth cycles as early as at least 80,000 years ago (Riehl et al., 2024)—a finding that suggests centuries, if not millennia, of observation, experimentation, and the accumulation of knowledge. Between 13,000 and 11,000

years ago, in the Levant and Anatolia, cereals are believed to have played a prominent role in feasts, ceremonial practices, and settlement patterns within increasingly larger social groups, coinciding with favorable climatic conditions at the beginning of the Holocene) (Essell et al., 2023; Kabukcu et al., 2021; Liu et al., 2018). DNA analyses of Neolithic wheat further reveal that early farmers deliberately cultivated mixed genotypes, implying a sophisticated understanding of genetic diversity (Bilgic et al., 2016).

From these multiple centers of domestication, wheat subsequently spread and diversified across the globe (Fuks & Marom, 2021). This period diversification, spanning millennia, embodied the very essence of cumulative culture in action. However, this trajectory underwent a rupture in the late 19th and 20th centuries. Systematic breeding programs and pure-line selection introduced with the Industrial Revolution (Charmet, 2011), followed by the Green Revolution's emphasis on semi-dwarf cultivars, high-yielding genotypes, and intensive nitrogen responsiveness (Würschum et al., 2017), led to considerable genetic erosion in favor of uniform, high-yielding genotypes.

However, this last century of selection focused primarily on above-ground traits has resulted, over the past three decades, in a marked stagnation of wheat yields in most major European producing countries—France, the United Kingdom, Germany, and the Netherlands (Silva et al., 2026). This stagnation in yields can be attributed to 1) suboptimal agricultural practices (inadequate crop rotations, ineffective disease management, and inadequate soil conservation) as well as 2) the adverse effects of climate change (accelerated phenology, increased susceptibility to spring drought episodes, and the continued risk of late frosts) (Haslinger and Mayer, 2023b; Ortiz et al., 2008; Silva et al., 2026; Wilcox and Makowski, 2014; Zohner et al., 2020). This yield plateau prompts the question of integrating novel traits, particularly belowground ones, into future breeding objectives, given the current lack of descriptions of root traits for commercial genotypes (Baca Cabrera et al., 2025; Huang and Zhang, 2025; Ober et al., 2021).

The wheat root system of is characterized by its fasciculate structure, which consists of two types of roots of first order. The seminal roots emerge from the embryo and are predominantly responsible for water uptake during the early stages of establishment. The nodal (or crown) roots emerge progressively from the basal nodes during tillering and become the predominant contributors to water and nutrient uptake from stem elongation onwards (Pflugfelder et al., 2022a). Under non-limiting conditions, wheat extracts the majority of its water from the top 60 centimeters of the soil profile but functional rooting depth can extend to reach 2 m in deep loamy soils (Guo et al., 2020). The total seasonal water requirement of a wheat crop ranges from 350 to 600 millimeters, contingent upon the cultivar, the prevailing climatic context, and the management practices employed. The period of peak transpiration demand

corresponds to the stages of stem elongation, booting, and flowering. A moderate water deficit during these reproductive stages has been shown to reduce final grain yield by 20–50%, likely due to a reduction in ear density and grain number per ear (Senapati et al., 2019). The final grain yield of wheat results from the sequential establishment of three main components: 1) the number of ears per unit area, set during tillering and shaped by the early competition for light and resources; 2) the number of grains per ear, fixed between booting and flowering through floret survival; 3) and the individual grain weight, which depends on the post-anthesis assimilate supply during grain filling (Slafer et al., 2014).

Beyond grain quantity, wheat grain quality is a critical attribute for end-use and is directly modulated by the timing and intensity of stress events during grain filling. The two main quality-related elements are nitrogen, accumulated mainly as storage proteins (gluten), and carbon, allocated principally to starch in the endosperm. Nitrogen (N) is a highly mobile element within the plant: a large fraction (50 to 95%) of grain N originates from the remobilization of stem and leaf N reserves accumulated before anthesis, with a complementary contribution from post-anthesis root N uptake when soil water and nitrogen remain available. Conversely, grain carbon is provided almost exclusively (about 85%) by post-anthesis assimilation and is consequently more sensitive to canopy senescence, stomatal closure and water deficit during grain filling (Sharma et al., 2023). Under water deficit imposed during grain filling, grain nitrogen concentration typically increases while grain weight and starch content decrease, because the dilution effect of starch deposition is reduced more strongly than the supply of remobilized nitrogen. The agronomic impact of this trade-off depends critically on the timing of the stress: a recent meta-analysis showed that terminal drought reduced grain yield by 26 %, while continuous drought from emergence reduced grain yield by 84 %, with comparable 9 % increases in grain protein concentration in both cases (Wan et al., 2022).

1.2. Biodiversity as a buffer against climate variability

Over the past three decades, Europe has seen its average temperatures rise faster than the rest of the globe and this has also been accompanied by increased variability in hydrological regime and thermal conditions (Copernicus Climate Change Service (C3S), 2025). Summer droughts have been recurring for several consecutive years since the early 2000s, occurring earlier and earlier in the spring, becoming more regular and intense in recent decades, and could be amplified in the future (Haslinger and Mayer, 2023a; Ionita et al., 2020; van der Wiel et al., 2023). In addition, while the average number of frost days has declined steadily in recent decades, the frequency and severity of late frosts increased (Chamberlain et al., 2021; Lamichhane, 2021). These climate changes are among the factors contributing to the observed stagnation in agricultural yields and may lead to substantial declines, particularly for wheat (Rezaei et al., 2023; Schmidt and Felsche, 2024). These changes raise questions about

the effectiveness of current breeding programs and the traits that should be prioritized to ensure adaptation and yield stabilization, or even increase (Prado et al., 2025).

In this context, certain root traits, such as maximum depth or root insertion angles, are receiving increasing attention. However, these traits responses to environmental stress are often evaluated on root and shoot separately rather than belonging to the same plant system, at an early stage and under homogeneous laboratory conditions (Bagale et al., 2025; Chen et al., 2025; Zhili Wang et al., 2024; Weigel et al., 2025). Furthermore, the dynamic nature of these characteristics during the growth process and under varying climatic conditions has received little attention in research (Asadullah et al., 2024; Holz et al., 2024a).

The ability of cultivated plants to adapt to variable environmental conditions depends in particular on how they allocate resources between their shoots, roots and reproductive organs (Calleja-Cabrera et al., 2020; Mason et al., 2017). This allocation is initiated during early developmental stages but remains responsive to developmental stage progression and stress events throughout the growing season. The localized abundance of resources may also alter these traits within the limits of genotype plasticity (Lopez et al., 2025; Ren et al., 2024). Therefore, it is difficult for a single ideotype - defined here as a plant type combining an optimal combination of traits for a given target environment and production system (Donald, 1968) - to have the appropriate traits and optimal plasticity to cope with increasing environmental variability throughout the growing period.

Faced with these limitations, one strategy for agriculture to maintain high yields and favor soil health involves the (re)introduction of greater biodiversity to agroecosystems (Altieri et al., 2017; Messéan et al., 2021). At the landscape scale, this can be achieved through the implementation of hedges, patchwork cultivation, or grass strips (Vanneste et al., 2020). At the field scale, biodiversity enhancement can be achieved through the implementation of diverse crop rotations. These rotations may include various cultivation cycles of different durations. Examples include perennial grains (Duchene et al., 2020) and, more commonly, pluriannual forages (Martani et al., 2022). Between cycles of the crop of interest, the introduction of a catch or a cover crop can be a complementary practice (Moreau et al., 2012; Vincent-Caboud et al., 2019). Biodiversity can also be cultivated within the same time and space, for example through the implementation of agroforestry systems, which combine large perennial and small annual plants (Mettauer et al., 2023; Nerlich et al., 2013). Alternatively, different annual crops can be grown in the same field, a practice known as intercropping, co-culture, blending or maslins (Blanc et al., 2024; Brooker et al., 2015; Duchene et al., 2017; Hawes et al., 2021). It has been demonstrated that these different agricultural practices have beneficial effects linked to the mixing of genetically different individuals interacting in the same environment. On the one hand, the combined effects of physiological diversity and plastic adjustment of

genotypic traits ultimately lead to improved yield stability and pest resistance (Angeletti et al., 2022; Gaba et al., 2015; McAlvay et al., 2022; Schöb et al., 2023). Genetic mixture cross-pollination has been demonstrated to enhance the number of fertile flowers and the quality of their fruits in the case of large-scale cereal crops (Chabert et al., 2024). When genotypes differ in root morphology or physiology — through contrasting rooting depths or shifted phenological timing — their patterns of resource extraction can be spatially or temporally offset, enabling niche complementarity for a given resource. This has been documented in particular for water uptake, where genotypic differences in rooting depth allow co-occurring plants to access distinct soil horizons (Durodola et al., 2025; Schmutz and Schöb, 2023).

However, the necessity for specific technical itineraries, inputs (fertilizer, pesticides, etc.) and adapted machinery to account for differences in physiological development of the associated species are significant obstacles to the implementation of co-cropping, especially in Europe (Brannan et al., 2023; Bybee-Finley and Ryan, 2018; Wezel et al., 2014). A promising yet less well-studied alternative to adding more plant diversity to agroecosystems was to take advantage of the existing intra-specific crop biodiversity with crop mixtures (Albert et al., 2011; Bruelheide et al., 2018; Jung et al., 2010; Litrico and Violle, 2015).

In this context, several agronomic concepts are commonly mobilized to quantify the performance of crop mixtures (intraspecific) or association (inter-specific) and their response to water-limited conditions. Water Use Efficiency (WUE) is typically defined as the ratio of biomass or grain yield produced per unit of water transpired (e.g. in kg of dry mass mm^{-1} ha^{-1}) and integrates the combined effects of stomatal regulation, root water uptake efficiency, and harvest index. A water deficit is generally diagnosed when the soil matric potential becomes more negative than the threshold at which stomatal closure begins and is approached by complementary markers including leaf relative plant water content (RWC), leaf water potential, stomatal conductance, and canopy temperature relative to air (Carminati and Javaux, 2020).

The benefit of mixtures is itself classically expressed through two distinct concepts: over-yielding, when the mixture yield exceeds the weighted average of the component monocultures, and transgressive over-yielding, when the mixture yield exceeds the yield of the best-performing monoculture (Schmid et al., 2008). A complementary indicator, the Land Equivalent Ratio (LER) (Mead and Willey, 1980), corresponds to the relative land area that would be required under monoculture to achieve the same total production as the mixture; LER > 1 indicates that the mixture is more land-efficient than the corresponding monocultures.

1.3. Development and interactions among the above-ground, below-ground, and reproductive traits of wheat in a mixture

The introduction of genotypic diversity into a cropping system, where varieties have been bred individually for monoculture performance, carries with it the potential risk of unintended competition. Modern wheat cultivars are selected to maximize their own resource capture under uniform, high-input conditions, which favor genotypes with traits associated with vigorous early shoot growth, tall canopies and high tillering — features that may give them a competitive advantage over a less aggressive neighbor in a mixture. It is important to note that several mechanisms of competition can operate in parallel: above-ground, asymmetric competition for light through canopy overtopping; below-ground, competition for water and nutrients through root systems in shared soil volumes. When two plant individuals are combined without consideration of their relative competitive ability, the more competitive genotype may dominate the mixture, resulting in the suppression of its neighbor and the erasure of the expected complementarity benefit.

However, it should be noted that competition between genotypes does not invariably evolve towards a hierarchical exclusion of one partner by the other. Recent findings demonstrated that, within diverse plant communities, water deficits amplified intransitivity — that is to say, competitive relationships in which dominance between individuals is circular rather than linear (A outcompetes B, B outcompetes C, but C outcompetes A), thus preventing any single genotype from excluding the others — in plant networks, thereby enhancing ecosystem hydraulic functioning (Bittlingmaier et al., 2026). The authors of this study hypothesized that the spatial diversification of root exudate chemistry between neighboring genotypes could generate structural heterogeneity in rhizosphere aggregate organization and increase pore connectivity and hydraulic conductance at the profile scale. From an agronomic standpoint, this means that the introduction of architectural and metabolic diversity in a wheat stand may, especially under stress, generate emergent stabilizing mechanisms that are not predictable from monoculture-based ideotype evaluation. This result is consistent with the empirical observation of yield stabilization in cultivar mixtures across European wheat-producing regions.

Functional complementarity between genotypes is not static, rather, it varies according to the stage of development, the climatic conditions, and the history of previous interactions (Bongers et al., 2025; Kaisermann et al., 2017; Zheng et al., 2024). During the early vegetative stages of wheat, competition for light and shallow underground space may plays a decisive role in early stages of development (Kong et al., 2023a). Mixing varieties showed mitigation of early root competition in wheat under water and nutrient limitation (Montazeaud et al., 2025a). Then an increase in tillering rate is consistently reported in the recent literature for the wheat mixture compared to the respective monocultures, although the underlying mechanisms are

not yet fully understood (Gawinowski et al., 2024; Schmidt et al., 2026; Stefan et al., 2025a; Wang et al., 2026). During stem elongation and booting, water and nitrogen demand peaks and underground hydraulic interactions become critical, tend to happen a bit earlier than in monocultures and tend to buffer the risk of flowering too early or too late (Engbersen et al., 2021; Fletcher et al., 2019). During the grain filling phase, the reallocation of assimilates from the stems and leaves to the ears is essentially an intra-individual process (Fang et al., 2024). While achieving synchrony in the final maturation of the grain is necessary to enable a collective harvest, the asynchrony among the associated genotypes has been shown to exceed the genetic distance between the mixed varieties (Stefan et al., 2024). The genotypic mixture even exhibited an enhancement in the final grain quality according to several studies when compared to monoculture (Stefan et al., 2025b). In addition to these issues of competition for access to resources, wheat plants can be affected by various diseases during their growth, which the mixture helps to reduce, leading to diminish the dependency on pesticides (Akanda and Mundt, 1997; Dubin and Wolfe, 1994; Kristoffersen et al., 2020; Orellana-Torrejon et al., 2022; Vidal et al., 2020b). Ultimately, the vast majority of studies conducted over the past 30 years on wheat mixtures across different continents and environmental conditions have reported over-yielding or even transgressive over-yielding (Borg et al., 2018; Chen et al., 2020; Kiær et al., 2009; Kong et al., 2023b; Mille et al., 2006; Sarandon and Sarandon, 1995; Sharma and Dubin, 1996; Vestergaard and Jørgensen, 2024).

At each of these development stages, the benefits and costs of mixing may therefore differ, and a genotypic pair complementary at one stage may prove competitive at another. For these reasons, a dynamic monitoring of both aboveground and belowground traits throughout the season is necessary to better understand the mechanisms of non-additive effects in wheat mixture, leading to higher yield than monocultures (Chung, 2023).

The combination of these advantages, as well as the relative ease with which they can be adapted to different agricultural techniques, compared to interspecific mixtures (i.e., intercropping), has sparked growing interest among farmers, often in random mixtures of genotypic diversity (Perrone et al. 2017). The beneficial effects of this type of “random mixture” could be enhanced by reconsidering the selection criteria for mixed varieties for specific environmental conditions (Lamichhane et al. 2018, Barot et al. 2017). Although wheat genotype mixtures have shown consistent benefits in terms of epidemiological resistance and water use efficiency, the underlying mechanisms at the individual plant level remain poorly understood (Giunta et al., 2020; Huang et al., 2023; Wang et al., 2016). Especially since a significant proportion of plant-plant interactions occurs beneath the soil, these interactions have often been overlooked in research (Homulle et al. 2022).

1.4. Root water uptake strategies and below-ground interactions in intraspecific wheat mixtures

As demonstrated in the previous section, complementarity, competition or non-additive emerging effect between genotypes shifts across developmental stages. Dynamic monitoring over space and time (or at least focusing on key developmental stages) is therefore necessary to identify the underlying mechanisms.

Within these mechanisms, the strategies and patterns of root water uptake (RWU), in addition to the nutrient uptake, are of critical importance to the plant's adaptation to water deficit. RWU is determined by the soil-plant-atmosphere hydraulic gradient, further regulated by root hydraulic resistance (itself governed by root traits such as root tip density, root hair development, and root biomass distribution, which collectively determine the radial and axial conductance of the root system) as well as by root and microbial exudation which modifies rhizosphere hydraulic properties (Doussan et al., 2024; Freschet et al., 2021a; Giraud et al., 2023). Research has demonstrated that deep-rooting wheat genotypes enhance grain yield under water deficit conditions (El Hassouni et al., 2018; Nakhforoosh et al., 2014; Wasson et al., 2012) and water use efficiency (Feng et al., 2017; Hafeez et al., 2024). Root plasticity also enables plants to adapt their root traits and their water uptake to optimize RWU under water-deficit conditions, shifting it either more toward the subsoil (Ziqian Wang et al., 2024; Xu et al., 2016) or the topsoil (Shazadi et al., 2024).

While above-ground complementarity has been widely documented (phenology, stem height, canopy architecture), the specific contribution of contrasting root architectures to niche partitioning in wheat mixtures remains largely uncharacterized at the individual level. However, roots are the main organ for acquiring the limiting resources of water and nitrogen, and their architecture directly determines the portion of the soil profile explored. The idea that two genotypes with contrasting root systems—one oriented toward the topsoil, the other toward the subsoil—can tap into complementary vertical niches in the soil is conceptually founded and supported by observations in interspecific mixtures. However, direct demonstration of this in intraspecific wheat mixtures, at the individual level, remains very limited in the literature to date.

The vast majority of available studies considers the population (or canopy) level as a whole and not the contribution of each genotype to the total uptake. Under intraspecific mixture, one unresolved question is whether the genetic and physical proximity of a given genotype to another with contrasting root traits modifies its RWU plasticity —and, if so, through what mechanisms. Furthermore, plants interact with each other through various chemical communication channels (soluble exudates in the soil solution or VOCs diffusing into the soil gas phase) (Mathieu et al., 2025; Stirling et al., 2024). It has been demonstrated that this communication can also be mediated by microbial modulations (under the effect of rhizo-depositions), which influence the

growth, nutrient mineralization activity, or microbial recruitment of neighboring plants (Ghatak et al., 2025; Zhou et al., 2024). These interactions have the capacity to amplify the positive effects of mixtures, for example by modifying soil microbiome dynamics or pathogen tolerance (Feng et al., 2024; Mathieu et al., 2025).

2. Water stable isotopes – a useful tool for ecohydrological studies

2.1. Water stable isotope analysis for the study of root water uptake

The two heavier stable isotopes of hydrogen and oxygen, namely deuterium (^{2}H) and oxygen-18 (^{18}O), occur at low but measurable abundances in water in nature. Their atom ratios ($^{2}H/^{1}H$ and $^{18}O/^{16}O$) are typically expressed on the so-called *δ-scale*, in permil (‰) relative to the atom ratios of the Vienna Standard Mean Ocean Water (V-SMOW), the internationally accepted isotopic reference standard for water (Harmon Craig, 1961; H. Craig, 1961; Gonfiantini, 1978), calculated as follows:

Equation 1.

$$\delta = \frac{R_{sample} - R_{standard}}{R_{standard}} = \frac{R_{sample}}{R_{standard}} - 1$$

where R is the isotope ratio ($^{2}H/^{1}H$ or $^{18}O/^{16}O$) of the sample and the V-SMOW standard, respectively.

The isotopic composition ($\delta^{2}H$ and $\delta^{18}O$) of natural water pools — including precipitation, surface waters, groundwater, soil water at various depths, and plant water (xylem sap, leaf water, and transpiration flux) — is not uniformly distributed, but it varies as a function of the hydrological history and driving processes. Precipitation exhibits, for instance, a progressive δ-decrease with increasing altitude, latitude, and distance from the evaporating source (known as the continentality effect). In between precipitation events, soil evaporation discriminates against heavier stable isotopes, leading to a progressive enrichment in surface water and diffusion of the isotopic excess to deeper layers, generating a heterogeneous soil water δ-depth profiles. Precipitation, which is generally isotopically more depleted than surface water, strongly influences the setting of the δ-profile by mixing with the antecedent, isotopically heavier water.

In a dual $\delta^{2}H$ *vs* $\delta^{18}O$ space, meteoric waters (i.e., precipitation and groundwater) fall globally onto a line, the Global Meteoric Water Line (GMWL: $\delta^{2}H = 8\times\delta^{18}O + 10$) Craig (1961a). Deviations from this relationship reflects on the other hand the prevalence of the evaporation process in other natural water bodies (e.g., soil water,

open water bodies). Distinct and often well-separated positions in the δ^2H–$\delta^{18}O$ isotopic space are occupied by groundwater, stream water, and precipitation, respectively. This spatial separation in the isotopic space is what makes stable isotope tracing a powerful tool for identifying plant water sources, as each potential source carries a distinct isotopic composition.

The isotopic composition of plant root water uptake (δ_{RWU}) is generally assumed to be the average of those of the soil water sources (i.e., the water contained in the rooted zone across the soil profile) and weighed by the relative contributions to RWU.

Equation 2.

$$\delta_{RWU} = \sum_{n=1}^{n} f_i * \delta_i$$

where f_i is the contribution fraction of layer i and δ_i is the isotopic composition of the soil water at depth i, with sum of f_i equal to 1.

Estimating the f_i values from measured δ_{RWU} and δ_i constitutes an underdetermined mixing problem when the number of potential sources exceeds two. The earliest multi-source mixing models employed in the field of ecohydrology (IsoSource, Phillips and Gregg, 2003) addressed the issue in a deterministic manner by seeking all combinations of source proportions that aligned with the isotopic mass balance equations. In scenarios involving more than two sources, such as a soil profile discretized into several horizons, the system becomes underdetermined, resulting in a number of infinite solutions. The transition to a Bayesian framework was pioneered by Moore and Semmens (2008) and achieved widespread application with the Stable Isotope Analysis in R (SIAR) multisource mixing model (Parnell et al. (2010). This framework represented a significant advancement, enabling the incorporation of a priori information on the contributions of each source (e.g., root biomass distribution per horizon) to the analysis. The Markov Chain Monte Carlo (MCMC) algorithm implemented in SIAR allows the space of possible solutions to be explored robustly, with a sufficient number of iterations to ensure chain convergence.

δ_{RWU} is determined either destructively, by extracting soil water and stem/root xylem water through cryogenic vacuum distillation (CVD) and measuring their isotopic composition directly (Ceperley et al., 2024a). Under the assumption that roots take up water without fractionation, the isotopic composition of xylem water equals that of the water absorbed at the root surface, yielding:

Equation 3.

$$\delta_{RWU} = \delta_{xylem}$$

Dawson and Ehleringer's seminal study (1991), "Streamside trees that do not use stream water," pioneered the application of this principle at the individual plant scale in a field setting. By comparing the δ^2H values of stem xylem water against those of streamwater, soil water at multiple depths, and groundwater across several riparian tree species, they demonstrated that these tree water uptake depth was decoupled from their root distribution, demonstrating that the presence of roots at a given depth does not imply active water extraction at that depth. The methodological approach employed — namely, cryogenic vacuum distillation (CVD) of stem water, multi-depth soil water sampling — provided the template that was adopted by the ecohydrological community for the following decades. Typically for this method, plant or soil frozen samples were placed at one end of a sealed line under low pressure (~0.01 to 0.1 mbar) and heated to a temperature of 60 to 90°C (Koeniger et al., 2011; Orlowski et al., 2013). The solid water contained in the sample sublimates and is collected (by inverse sublimation) in a trap immersed in liquid Nitrogen (temperature of ~-180°C) located at the other end of the line. Subsequent analyses of the extracted water is conducted using isotope ratio mass spectrometry (IRMS) or infrared laser spectroscopy (IRIS).

This combination of these two steps generally yield accurate measurements however is limited in terms of temporal resolution (typically daily) and spatial coverage by its destructive nature. Additionally, it had the potential to introduce biases during the extraction of water from the presence of volatile organic compounds that can be co-extracted affecting IRIS measurements by mimicking water in the near-infrared region. However, IRMS measurements are not affected by these potential artifacts. The recent recommendations by Ceperley et al. (2024) to standardize these protocols illustrates the importance of these methodological artifacts.

These limitations motivated the development of non-destructive, online isotopic monitoring methods. The development of IRIS in the 2000s and 2010s, particularly Cavity Ring-Down Spectroscopy (CRDS) and Off-Axis Integrated Cavity Output Spectroscopy (OA-ICOS), signified a substantial technological advancement. These instruments have the capacity to measure the isotopic composition of water vapor online and continuously at high frequency (typically 1 Hz) with an accuracy comparable to that of IRMS. Building on this capability, Rothfuss et al., (2013) developed and validated a methodology for in situ soil water vapor sampling using probes inserted at varying depths, providing soil water isotopic profiles at centimeter-scale spatial resolution and minute-scale temporal resolution — overcoming the limitations of destructive cryogenic vacuum extraction. The measurement of plant transpiration isotopic composition (δT) was subsequently achieved by Deseano Diaz et al., (2023) and Kühnhammer et al. (2020), who coupled an open gas exchange chamber enclosing the plant with the same laser spectrometer, yielding :

Equation 4.

$$\delta_{RWU} = \delta_T$$

δ_T was retrieved from the difference between inlet and outlet vapor isotopic compositions and corrected for ambient vapor contributions. The isotopic composition of plant transpiration (δ_{Tr}) was calculated using the following equation (Dubbert et al., 2014):

Equation 5.

$$\delta_{Tr} = \frac{w_{out}\delta_{out} - w_{in}\delta_{in}}{w_{out} - w_{in}} - \frac{w_{in}w_{out}(\delta_{out} - \delta_{in})}{w_{out} - w_{in}}$$

where δ_{in} and δ_{out} are the isotopic composition of the water vapor in the inlet and outlet airstream of the plant chamber, respectively and w_{in} (-) and w_{out} (-) are the mixing ratio of the water vapor in the inlet and outlet airstream of the plant chamber.

For woody species and trees, an alternative approach consists of drilling a borehole in the stem and monitoring the isotopic composition of the water vapor equilibrating inside, which reflects — under steady-state conditions — that of the water absorbed by the roots (Marshall et al., 2020). The combined deployment of soil and plant transpiration isotopic monitoring has thus enabled eco-hydrological studies at an unprecedented combination of temporal and spatial resolution.

It should be noted that transpiration, like soil evaporation, does involve isotopic fractionation: leaf water is enriched in heavy isotopes relative to source water due to both equilibrium and kinetic fractionation during evaporation at the leaf surface (Craig-Gordon model). However, under steady-state conditions — when the isotopic composition of leaf water is constant through time, i.e., when water input equals water loss — the flux-weighted isotopic composition of transpired water vapor equals that of the water taken up at the roots, with no net fractionation at the whole-plant level (Farquhar & Lloyd, 1993; Yakir & Sternberg, 2000). The Equation 4. therefore holds only under this steady-state assumption, which may be violated in the early morning, during rapid changes in evaporative demand, or under severe water stress — conditions that must be carefully identified and excluded from the analysis (Kühnhammer et al., 2022; Rothfuss and Javaux, 2017).

2.2. The isotopic labeling strategy—a lever for improving resolution and accuracy

As we have seen in the previous section, natural soil isotope profiles may not be monotonic with depth — exhibiting inversions or plateaus — or may display isotopic depth gradients that are too small to reliably constrain mixing model outputs. Indeed, neighboring horizons may carry similar isotopic compositions, rendering them

statistically indistinguishable, which results in wide and poorly resolved posterior distributions of RWU depth contributions.

To address this limitation, the majority of published isotopic labeling protocols involve the targeted enrichment or depletion of a specific defined horizon within the soil profile e.g. (Beyer et al., 2016; Kaloterakis et al., 2025; Kübert et al., 2020; Sprenger et al., 2016). This approach has also been employed to monitor the trajectory of a specific water source within the soil-plant continuum. However, even this approach is subject to limitations, as it can, at best, amplify or invert an existing natural gradient or create a very strong signal that is only localized in a discrete manner. In the dual isotope space, these profiles therefore plot along a line rather than occupying a two-dimensional area. Consequently, the $\delta^{18}O$ and $\delta^{2}H$ values are often redundant information for the mixing models. On the other hand, the strategy developed by Deseano Diaz et al. (2023) sought to proactively decouple $\delta^{2}H$ and $\delta^{18}O$, with top-and-bottom column labeling, generating two orthogonal soil isotope profiles through soil depth-specific injections of small volumes of isotopically distinct water. To the best of our knowledge, this was the only attempt of dual water isotopic composition labelling at multiples depth in the same soil profile.

However, this strategy resulted in a persistent negative $\delta^{2}H$ - $\delta^{18}O$ correlation. The development of an appropriate labeling strategy to reliably decorrelate both isotopic information thus remains an unresolved methodological challenge — and a prerequisite for individual root water uptake estimation in systems where the natural isotopic heterogeneity is not enough pronounced across depths.

The implementation of multi-depth isotopic labeling in a soil column presents several additional technical challenges. The volumes of water injected must be sufficiently small so as not to disturb the soil water content—and therefore affect plant RWU—while providing sufficient isotopic contrast. Furthermore, diffusion effects can progressively "tone down" the isotopic contrasts among soil layers over time, requiring careful timing between labeling and measurement campaigns.

3. Main and specific objectives of the thesis

This doctoral thesis was conducted in the framework of the CROP (Combining ROot contrasted Phenotypes for more resilient agro-ecosystem) research project, which was funded by the German Federal Ministry of Education and Research (BMBF). The project centered on the winter wheat species *Triticum aestivum* due to its economic importance and sensitivity to climate change. The objective of the project was to assess the benefits of integrating two wheat cultivars with contrasting root traits on parameters such as water, carbon, and nitrogen fluxes, microbial communities, and yield.

The objectives of the program were to estimate the beneficial impacts of combining contrasted root phenotypes within a single field. We hypothesized that the roots of the two cultivars would partly explore distinct soil layers (ecological niches), mobilizing different sources of water and nitrogen, exudation different carbon pools in the soil profile driving different microbial community structures and leading to positive effects on the final yield.

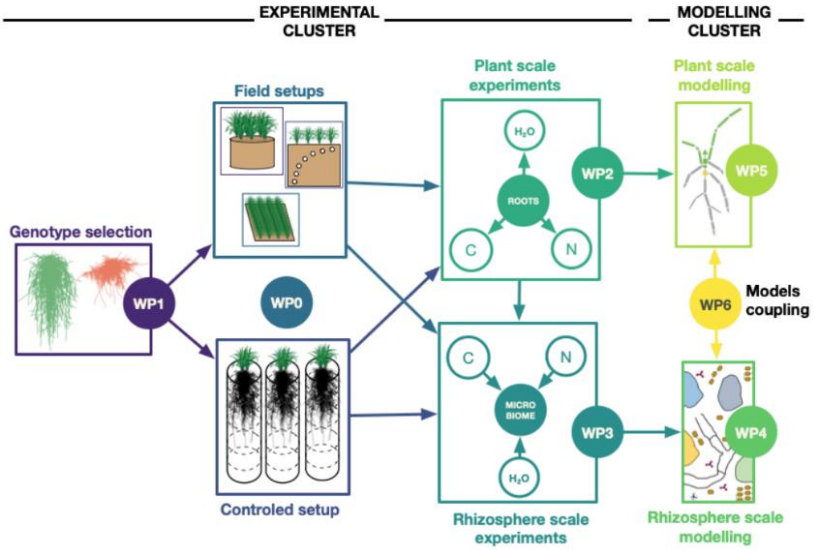

Fig. 1 Experimental and modelisation cluster repartition in CROP project

The project was organized into two complementary clusters — experimental and modeling — each corresponding to a distinct doctoral thesis (Fig. 1). The experimental cluster comprised three work packages: WP1 identified the genotypes of interest, WP2 quantified the effect of genotype mixture on water, carbon, and nitrogen fluxes in the soil-plant system, and WP3 characterized mixture effects at the rhizosphere scale. The modeling cluster integrated these findings across three scales: WP4 incorporated microbial processes into a rhizosphere-microbiome model (PECCAD), WP5 embedded genotype mixing effects into a soil-plant model (CPlantBox), and WP6 coupled both models into a unified framework.

My own work objectives where concentrated on the two first work packages at both the field and soil column scale, with a particular emphasis on the interconnected nature of these packages, particularly in relation to the work packages 3, led by Adrian Lattacher, and 5, led by Mona Giraud. Indeed, the development of the two articles published as first author as part of my thesis was accomplished in particular in collaboration with them. The primary objective of my doctoral work was to:

Understand how the combination of two wheat genotypes with contrasting root architectures modifies their individual strategies for water uptake from the soil under conditions of water deficit, and what the consequences are for the agronomic performance of the system.

The present thesis was structured around three specific objectives, which correspond to chapters 2-4 (Fig. 2).

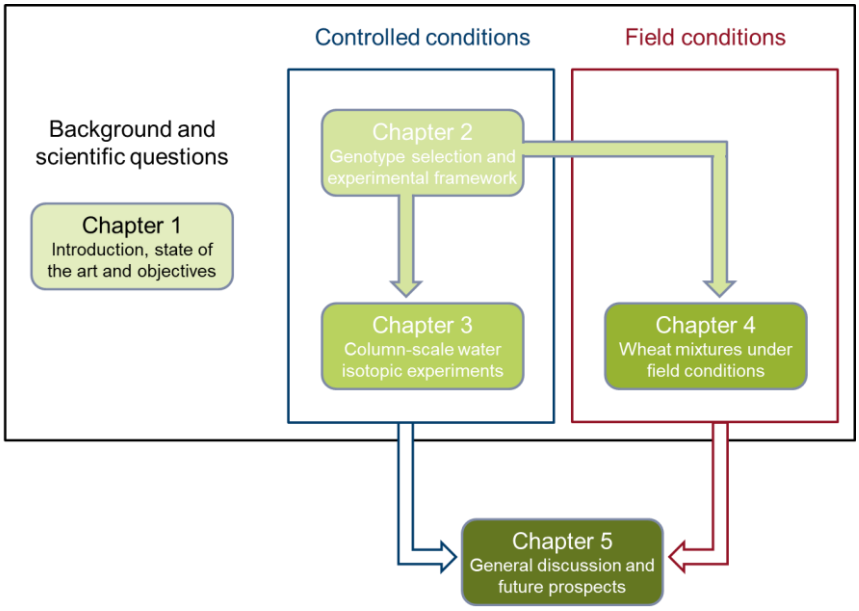

Fig. 2 Schema of the general thesis architecture with the link between the chapters

My first specific objective (O1) (Chapter 2) was to:

Select a pair of wheat genotypes with significantly contrasting root traits and similar aboveground development under controlled conditions, and develop a suitable experimental framework (i.e., relating to the soil column geometry, water isotope labeling protocol, and coupling with MRI imaging) to enable the simultaneous and non-destructive estimation of the water uptake profile of each genotype grown in mixture.

The corresponding research questions were:

1- among the available and known genotypes, which ones expresses the most pronounced contrast in functional root traits over different growth stages under controlled conditions, and

2- which experimental design — pot size, column depth, labeling protocol — allows this contrast in functional root traits to be expressed while meeting the constraints of isotopic tracing?

To address this objective, a systematic comparison of two genotype pairs, two column geometries, and two isotopic labeling protocols was conducted. Root architecture was characterized non-destructively by MRI and destructively by WinRHIZO root scanning at multiple developmental stages. A split-gas-exchange chamber to monitor separately the transpiration flux and isotopic composition of two plants sharing the same soil column was designed and its practicability validated.

The second specific objective (O2) (Chapter 3) was to:

Quantify and compare the root water uptake profiles of two selected genotypes at the booting stage grown in monoculture and in mixture, under well-irrigated and chronic water deficit conditions, and identify the root and physiological mechanisms underlying the observed differences.

Three research questions guided this objective.

1- Do the contrasting root traits selected in our varieties also induce contrasting root water uptake at the booting stage, a key stage for yield formation?

2- Do the two genotypes maintain their preferred water uptake niches when grown in mixture, and does water deficit reinforce or attenuate this niche segregation?

3- Beyond niche segregation, does varietal mixing induce a collective shift in water uptake toward soil layers different from those observed in monoculture — and if so, can this phenomenon be explained solely by mechanisms of hydraulic competition, or does it involve other physiological interactions between genotypes?

To address this objective, plant physiological parameters — including root biomass distribution by MRI and destructive sampling, leaf water potential, canopy conductance, water use efficiency, and tiller number — as well as above- and below-ground environmental conditions were monitored under two contrasting water regimes. Daily root water uptake profiles were estimated from soil water and plant transpiration isotopic measurements using the multi-source Bayesian mixing model SIAR (Parnell et al., 2010), with root biomass profiles derived from MRI as prior information. Six experimental treatments were implemented across three plant modalities and two water regimes, with nine replicates per treatment.

The third specific objective (O3) (Chapter 4) was to:

Test the robustness of the contrasting root traits and the effects of mixing observed under controlled conditions in a field context over a complete growth cycle characterized by pedoclimatic variability (i.e., late frost, spring drought, and extreme rainfall events) and discuss the root and above-ground dynamics observed to the yield components — ear density, grain number per ear, and grain weight. Two research questions were formulated.

1- Are the root traits identified under controlled conditions expressed in field conditions, and to what extent does seasonal pedoclimatic variability modify the resource allocation strategies of each genotype?

2- Are the non-additive effects of mixing on yield reported in the literature confirmed, and can their main agronomic and physiological components be identified?

To address this objective, root dynamics were monitored non-destructively by mini-rhizotron imaging at six depths over a full growing season in 18 microplots at the TERENO Selhausen experimental site. Canopy dynamics were assessed by repeated UAS flights combining multispectral and LiDAR sensors. Soil water dynamics were monitored continuously by matric potential sensors and by cryogenic extraction of soil water for isotopic analysis. A comprehensive set of manual aboveground measurements was conducted at weekly intervals, and yield components were determined at harvest.

4. Author contributions

Youri Rothfuss (YR) and Mathieu Javaux (MD) acquired the funding for and administrated the research program, in which this doctoral project was embedded. YR, and MJ provided continuous supervision and support to the doctoral candidate, author of this thesis (SLG) in all research and administrative tasks. Additionally, Bernard Heinesch (BH) and Delaplace Pierre Delaplace (PD), in their role as members of the thesis committee and Harry Vereecken (HV) and Jan Vanderborght (JV) in their role as institute directors in the research center where the project was done supervised yearly the progress of the doctoral project. They provided written and verbal feedback on the reports and presentations prepared by SLG.

For the study described in chapter 2, SLG, YR, Adrian Lattacher (AL) and MG conceived the experiments. Samir Alahmad (SA) and Lee Hickey (LH) developed and provided the required wheat genotypes. SLG, Moritz Harings (MH), (AL) ran the experiments under the supervision of YR and Dagmar van Dusschoten (DvD). SLG wrote the original manuscript.

For the study described in chapter 3, SLG, Adrian Lattacher (AL), Mona Giraud (MG), Holger Pagel (HP), Andrea Schnepf (AS), Guillaume Lobet (GL), Ellen Kandeler (EK), Christian Poll (CP), MJ and YR developed the study concept. SLG, Dagmar van Dusschoten (DvD), AL, MG, Moritz Harings (MH), (PDD), GL, PC, MJ and YR contributed to build the experimental design and conduct the study. SA and LH developed and provided the required wheat genotypes. SLG and MH constructed, automated and adjusted the entire experimental platform, according to the recommendations of PDD, DvD and YR. SLG, DvD AL, MG, MH, AS, and YR conducted the column experiment in the climate chamber and collected the data. Daniel Pflugfelder (DP) and DvD assisted SLG in performing and analyzing the MRI scans. SLG analyzed the samples, evaluated the data and performed statistics with the contribution of CP, MJ, and YR. SLG wrote the first draft of the manuscript under the

supervision of MJ and YR. All authors critically revised previous versions of the manuscript.

For the study described in chapter 4, SLG, AL, MG, HP, AS, GL, EK, CP, MJ and YR developed the study concept. SLG, MH, AL, Yang Yu (YY) ran the experiments under the supervision of YR and MJ. Jordan Bates (JB) monitored the UAS imaging. SLG analyzed the samples, evaluated the data and performed statistics with the contribution of MJ, and YR. SLG wrote the first draft of the manuscript under the supervision of MJ and YR.

Chapter 2

Genotype selection and experimental framework for isotope-based root water uptake analysis

As delineated in Chapter 1, Section 3, the first objective of the thesis was to select a pair of wheat genotypes that exhibited sufficiently contrasting and quantifiable root and aerial traits under controlled conditions. In order to address this objective, the development of the experimental design and methods is described in this chapter, with the aim of enabling the simultaneous and non-destructive estimation of the water uptake profile of each genotype grown in mixture.

Some methodological developments and genotype screening described in this chapter have been integrated into two peer-reviewed publications co-authored with PhD colleagues working on the same wheat genotypes within the CROP project. The first one was entitled "*Development and calibration of the FSPM CPlantBox to represent the interactions between water and carbon fluxes in the soil-plant-atmosphere continuum*" (in silico Plants, 2023), in which Mona Giraud and me were both co-first authors, parameterizating the functional-structural plant model CPlantBox based on the UQR15 phenotyping dataset described in the third section of this chapter. The second paper from Lattacher, Le Gall et al. (*Rooting for microbes: impact of root architecture on the microbial community and function in top- and subsoil*, 2025, Plant and Soil) was focusing on the microbial and enzymatic characterization of the rhizosphere of UQR12 and UQR15 across developmental stages.

.

1. Introduction

Root systems play a pivotal role in the functioning of agroecosystems by influencing water and nutrient uptake, plant-microorganism interactions, and soil physical structure (Holz et al., 2024b). Beyond their anchoring function, roots determine the ability of crops to exploit heterogeneous resources in the soil profile and cope with increasing environmental constraints, such as drought or nitrogen limitation (Shoaib et al., 2022; Zhang et al., 2025). These processes collectively enhance the resilience of cultivated systems. In this context, elucidating the mechanisms through which root architecture modulates both resource fluxes and microbial functioning represents a challenge for the development of sustainable agricultural systems. The efficiency of a root system is contingent upon a balance between the benefits of resource acquisition and the costs associated with root construction and maintenance (Matthus et al., 2025; Scheifes et al., 2024). Excessive carbon allocation to roots is known to limit aboveground growth, while shallow rooting has been shown to restrict access to deep resources (B. Li et al., 2022; H. Li et al., 2022). However, the findings of Deseano Diaz et al. (2023) underscored that the presence of deep roots does not reliably ensure a corresponding shift in water uptake toward deeper soil layers — revealing a structural-functional decoupling that purely morphological assessments of root systems cannot resolve. Characterizing the functional behavior of root systems therefore requires integrated approaches that account simultaneously for root traits, soil water dynamics, and the environmental conditions under which uptake occurs. Rather than selecting a single root genotype, an alternative approach is to exploit the complementarity of contrasting root traits through species associations or mixtures of genotypes. Ecosystems incorporating both shallow and deep roots systems therefore facilitate more homogeneous soil exploration, enhance water and nutrient use efficiency, and mitigate losses through leaching (Montazeaud et al., 2025b; Wu et al., 2026). In this context, the selection of a pair of wheat genotypes with contrasting root architectures growing in mixture would enable us examining the relationships between root traits, water uptake function, and rhizospheric interactions.

In this chapter, the focus was on the experiments conducted to determine the root and aerial traits of a pair of contrasting root traits wheat genotypes. The initial pair of plants evaluated were two commercial varieties, Treblir® and Milaneco®, which were selected based on the assumption that their root profiles exhibited contrasting characteristics. Specifically, it was hypothesized that Treblir® would manifest a genotype with shallow roots, while Milaneco® would display a genotype with roots more oriented towards subsoil.

We then assed the two other lines traits, designated UQR12 and UQR15, which were developed in the laboratory at the University of Queensland (Lee Hickey Lab). These lines were selected based on differences in the angle of their roots during the early stages of development, which are likely to result in contrasting patterns of water uptake and drought resistance (Siddiqui et al., 2025). Concurrently, with regard to the

aboveground parts, these two lines, which are descended from the same parent, have the advantage of, in principle, exhibiting similar and synchronized aboveground phenological development under optimal conditions, allowing for simultaneous harvesting of the mixed crop in the field.

The hypothesis was that the genotype with large root insertion angles (UQR12) at the early stage will condition the root system towards the topsoil. Conversely, UQR15 with low root insertion angles would condition a more deep-rooted system. In the event that one of these pairs manifests sufficiently contrasting quantifiable root traits and associated microbial activity functions, it would provide a robust model for testing the hypothesis of functional complementarity between mixed surface and deep roots. In parallel, we tested the material base (water stable labelling, split plant chamber, MRI root measurements…) of the experiment detailed in Chapter 3 to investigate the root trait-function relationship of the contrasting root pair of genotype in monoculture and in mixture facing water deficit.

2. Root and shoot trait characterization of Milaneco and Treblir lines: screening for root traits and functions contrasts

2.1. Material and Methods

2.1.1. Plant growth conditions

Two winter wheat cultivars (*Triticum aestivum L.)*, which were widely cultivated in Germany, were selected based on their contrasting root density profiles (Fig. 3 and 4). Another experiment conducted in field conditions in Selhausen, Germany (50°52'07.8" N, 6°26'59.7" E), with these two varieties and recording with a mini-rhizotron the evolution of root density distribution, showed contrasting root distribution between them (Bauer et al., 2022a).

Both cultivars were cultivated under controlled conditions in a climate chamber set at 20°C and 50% relative humidity for a period of 45 days after sowing (DaS) from the 23/11/2020 to the 7/01/2021. The plants were cultivated in two distinct experimental systems: rhizoboxes and PVC columns. The rhizoboxes measured 2.5 centimeters in width, 35 centimeters in length, and 55 centimeters in height, with a volume of 7 liters. Each rhizobox was assigned to one plant, with five replicates per genotype (Fig. 5).

Concurrently, the genotypes were cultivated in PVC columns with an internal diameter of 8 centimeters, a height of 45 centimeters, and a volume of 2.3 liters. Each PVC column was assigned to two plants, with two columns replicated per genotype.

Both rhizoboxes and columns contained air-dried soil of a silt-clay texture, composed of 22% clay, 66% silt, and 12% sand (Weihermüller et al., 2007). The soil had been sieved to a mesh size of 2 mm and taken from the top 30 cm of an agricultural field (haplic luvisol) in Selhausen, Germany (50°52'07.8" N, 6°26'59.7" E), which has a temperate oceanic climate. The soil within the columns was subjected to compaction through the application of pressure, thereby attaining a uniform bulk density of 1.4 g/cm³ across the entire soil column. This density was indicative of the average field conditions measured in the original agricultural field. Subsequently, the soil in all columns was saturated with water from below via a series of holes. Four pre-germinated shoots were placed in each column, the two stronger were kept. Subsequent to a designated interval, the two shoots exhibiting the least vitality were excised. The total water content of the soil was assessed using a weighing technique involving a column. The water content was maintained at 25% (g/g) of the soil water content by supplying water on the topsoil.

2.1.2. Non destructive measurements

For the rhizoboxes, root pictures were taken daily on the transparent plexiglas cover on working days from a distance of 60 cm using a tripod and a camera. These images were then processed with Image J to extract the total lengths, inter-lateral root distances, root angles, and root growth rates.

In the PVC columns, the progression of the plants was evaluated at three time points, at 17 (10/12/2020), 22 (15/12/2020) and 45 DaS (07/01/2021). The following metrics were utilized to assess this progression: the quantity of shoots and leaves, the stage of development (on the Zadok scale), and the dimensions of the leaf blade (length and width) to calculate the leaf surface. The mean water content value for each column was assessed gravimetrically.

It was planned to use of the Soil Water Profiler (SWaP) device, which was developed by Dusschoten et al. (2020), to assess the root water uptake profile. But we will not show there the results of this part of the experiment. Subsequently, at 22 and 45, the 4 soil columns were analysis. The measurements were recorded over a period of 36 hours, covering two consecutive days and one night. The temporal and spatial (vertical) resolutions of the sensor were 15 minutes and 1 centimeter, respectively. The soil surface was covered, and therefore, evaporation was considered negligible.

2.1.3. Destructive measurements

Subsequent to the SWaP measurement at 45 DaS, aboveground plant biomass was removed and the soil was taken out of the columns. The soil column was cut into horizontal segments of 9 cm thickness. To obtain the plane surfaces required for soil zymography the 9 cm thick soil cores were cut orthogonally in half using a sharp knife.

Soil zymography is a two-dimensional in situ imaging technique that visualises the spatial distribution of extracellular enzyme activity at the soil-root interface (Spohn and Kuzyakov, 2014). The method utilises fluorogenic substrates, which are immobilised on a membrane. The membrane is briefly placed in contact with a freshly cut soil surface, where the targeted enzyme is active. Substrate hydrolysis occurs, resulting in the accumulation of a fluorescent product (methyl-umbelliferone, MUF) in the localised area. Subsequent imaging of this area under UV light allows for the quantification of the fluorescent product by image analysis. Two enzymes were selected for investigation: β-glucosidase (BG), which catalyses the hydrolysis of cellobiose into glucose during the final step of cellulose degradation and serves as a well-established marker of copiotrophic microbial activity, and β-N-acetyl-glucosaminidase (NAG), which catalyses the hydrolysis of chitin oligomers and functions as a proxy for the microbial turnover of fungal cell-wall residues and microbial necromass. Both activities are stimulated locally by labile carbon and nitrogen inputs derived from root exudation and from the microbial community recruited around active roots. Consequently, the spatial pattern around individual roots is widely used as a functional fingerprint of the rhizosphere. In the present study, zymography was utilised to ascertain whether the two genotype pairs of interest

induce significantly different patterns of rhizospheric activity along the soil profile, complementary to the root biomass distribution. This component of the research, in which the candidate participated as co-author, forms the foundation for the publication of Lattacher, Le Gall et al. (2025, Plant and Soil). Enzyme activity was quantified from fluorescence intensity using ImageJ after background correction and calibration with known MUF concentrations. Eight levels of BG and NAG activity were calculated as proportions of the soil surface.

Microbial biomass carbon were determined by chloroform fumigation-extraction (CFE) following the method of (Vance et al., 1987) described in detail in Lattacher, Le Gall et al. (2025, Plant and Soil).

Subsequently, the roots were washed out of the soil segment and preserved in 30% ethanol solutions. The fresh weight of the roots, stems, and leaves was measured using an electronic balance (accuracy 1 mg; Kern 572-30, Kern & Sohn GmbH, Balingen, Germany). The stems and leaves were stored in a freezer at -20 °C.

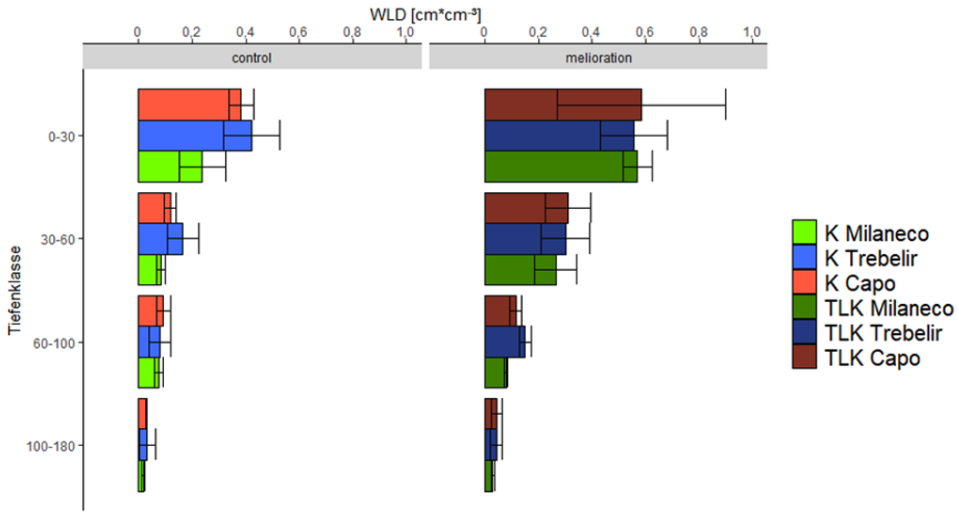

Fig 3 Root length density (WLD, in cm cm^{-3}) profiles from 0 to 180cm, for the genotypes Milaneco (blue), Trebelir (green) and Capo (brown) at tillering stage under low (clear colors) of high (dark colors) nitrogen fertilization

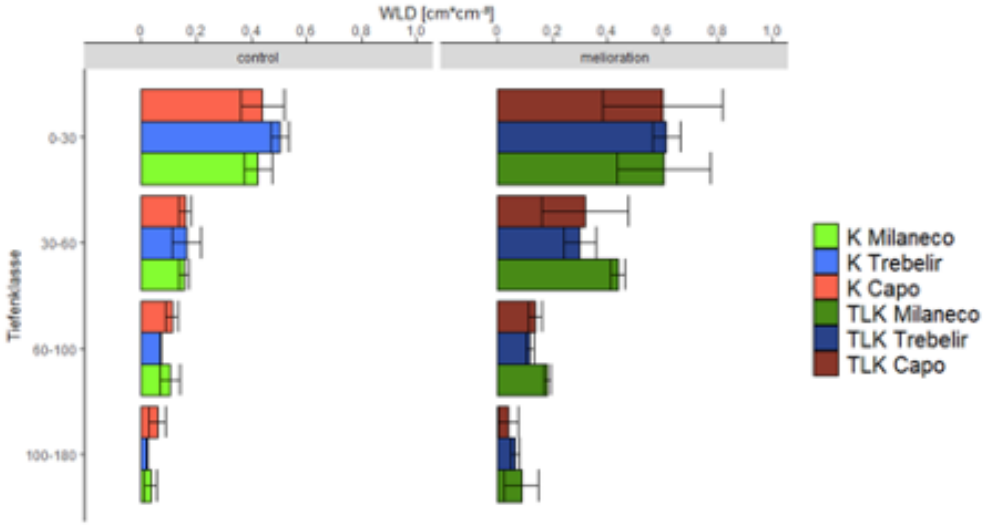

Fig. 4 Root length density (WLD, in cm cm^{-3}) profiles from 0 to 180cm, for the genotypes Milaneco (blue), Trebelir (green) and Capo (brown) at flowering stage (anthesis) under low (clear colors) of high (dark colors) nitrogen fertilization

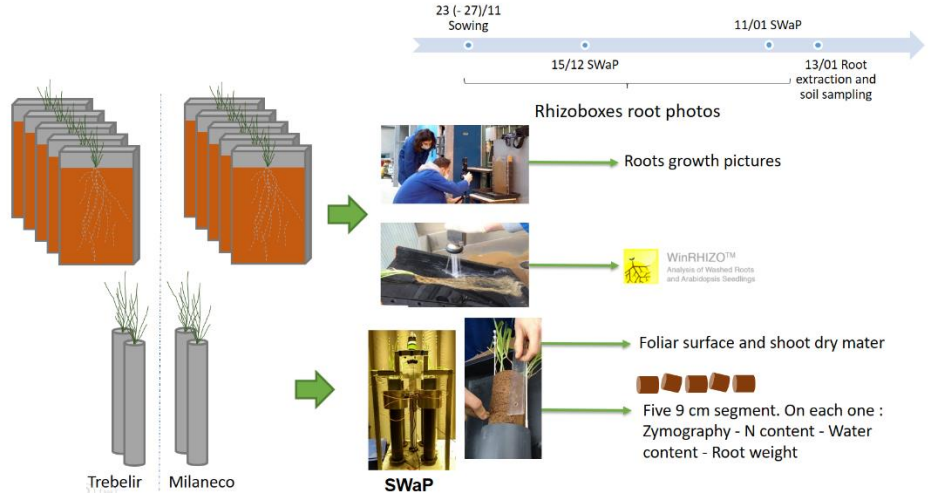

Fig. 5: Schematic overview of the preliminary experiment comparing the winter wheat cultivars Treblir® and Milaneco® in rhizoboxes (45 cm high, 11 cm in diameter, n = 5). Plants were sown on November 23–27 and harvested at 45 DaS. Measurements included soil water and plant (SWaP) campaigns (December 15 and January 11), non-destructive root imaging, WinRHIZO™ root scanning, shoot traits (foliar surface area, dry matter), and soil profile analysis on five 9-cm segments (zymography, nitrogen, water content, root weight).

2.2. Results

During the initial 10 days following sowing (DaS), the root growth rate along the rhizobox glass exhibited a slight increase for Milaneco® (3.8 cm/day) in comparison to Treblir® (2.9 cm/day) (Fig. 6). However, this difference did not attain statistical significance. Milaneco® exhibited a significantly larger mean interlateral distance (5.5 millimeters vs. 4.3 millimeters) and a slightly higher seminal root angle (37° vs. 35°), although the latter was not significant (Fig. 7). The total root length, as well as those from basal, first-order, and second-order roots, did not differ significantly between the two cultivars (Fig. 8). However, the growth of second-order lateral roots exhibited a significantly faster rate for Milaneco®, which also demonstrated a higher basal root interlateral distance (Fig. 9).

The analysis of soil section enzymatic activity revealed no significant differences between Milaneco® and Treblir® across the majority of soil depths, with the exception of elevated β-1,4-N-acetyl-glucosaminidase activity at the 4-centimeter depth for Treblir® (Fig. 10). This finding suggests that, during at the stem elongation stage at 45 DaS under these controlled conditions, the two cultivars elicit comparable microbial responses in the topsoil, exhibiting only minor variations in enzymatic activity. Treblir® exhibited a marginally higher foliar surface growth rate during the experiment (6.9 cm^2/day vs. 5.6 cm^2/day) (Fig. 9). However, at the 45-day stage, the aboveground dry biomass of Treblir® and Milaneco® was found to be similar (1.35 g for Treblir® vs. 1.30 g for Milaneco®) (Fig. 9).

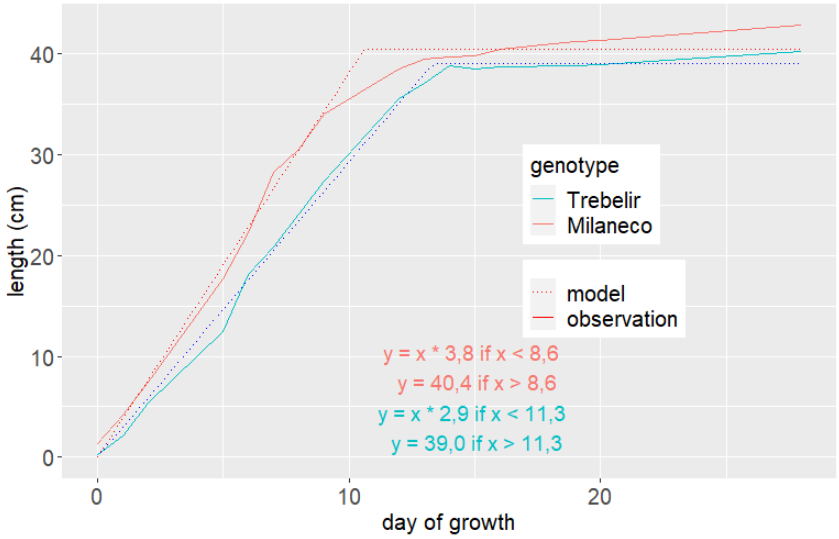

Fig. 6 Maximum root length (cm) of Treblir® (in blue) and Milaneco® (in red) of the days of growth, recorded with the rhizoboxes pictures every 1-2 days

		Total length ± sd (m)	Mean | median inter-lateral distance (cm)	Mean | median growth rate (cm/day)	Root angle ± sd (°)
Trebelir	Basal roots	19.82 ± 8.82	0.43* | 0.44	2.91 ± 0.04	**34.8** ± 7,5
	1st order laterals	72.22 ± 36.38	0.44* | 0.44	1.34* | 1.29	NA
	2nd order laterals	104.13 ± 52.45	NA	0.10* | 0.10	NA
Milaneco	Basal roots	12.83 ± 1.94	0.55* | 0.53	3.81 ± 0.07	**37.1**± 2,8
	1st order laterals	47.00 ± 13.32	0.39* | 0.41	1.80* | 1.83	NA
	2nd order laterals	65.42 ± 15.87	NA	0.26* | 0.28	NA

Fig. 7 Summary table of the total root length (cm), the mean and median inter-lateral distance (cm), the mean and median daily root growth rate (cm/day) and the root insertion angle (°), retrieved from rhizoboxes pictures.

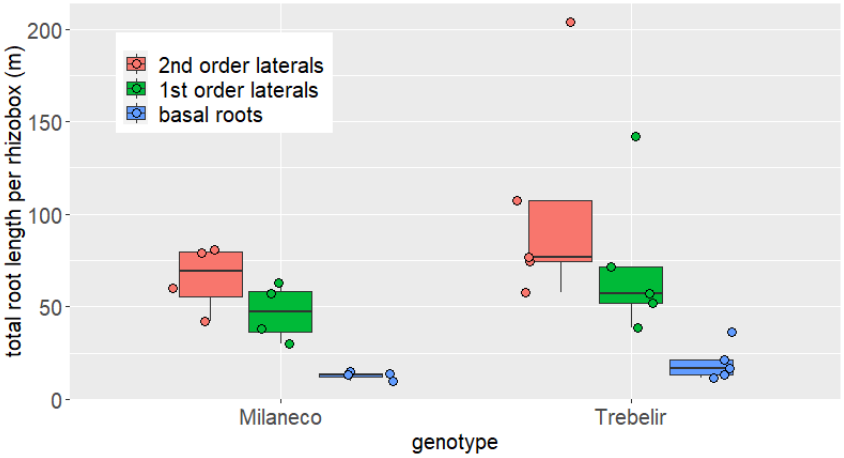

Fig. 8 Total root length per rhizobox (m), according to the root order (basal roots, first and second order) for Treblir® and Milaneco® from the final rhizoboxes pictures

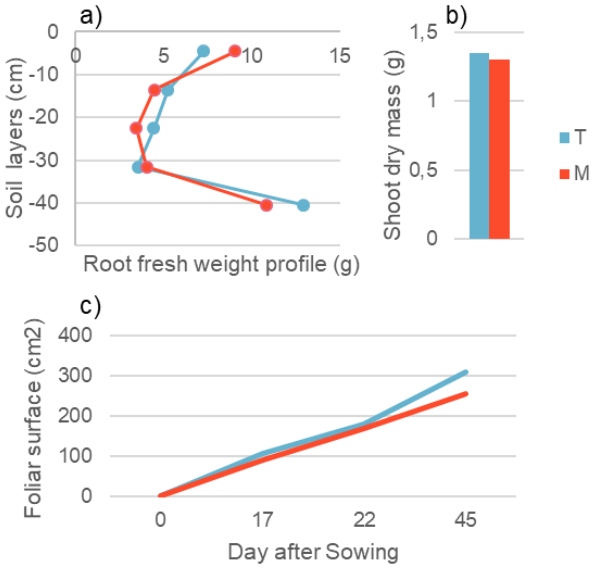

Fig. 9 a) Root fresh density profile over the five depth of 9cm of the soil column at 45 DaS; b) Shoot dry biomass average at 45 DaS and c) the average foliar surface evolution from 0 to 45 DaS; for Treblir® (in blue) and Milaneco® (in red).

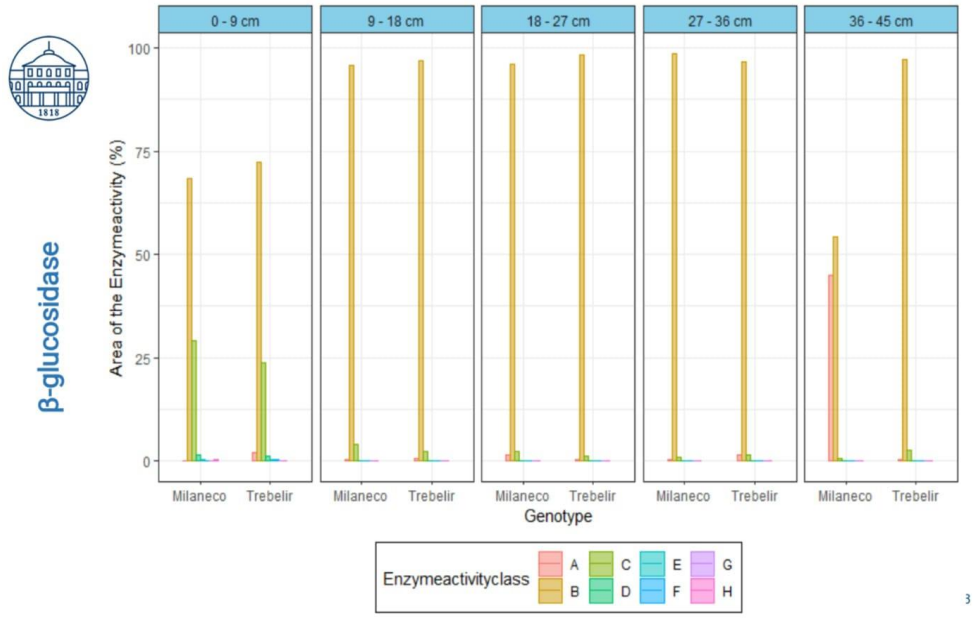

Fig. 10 Zymographs of β-1,4-Glucosidase activity (degradation of cellulose and indicator for the activity of copiotrophic microorganisms) of Milaneco and Treblir, respectively. The following correspondence exists between the latin alphabet and enzymatic activity classes: A corresponds to 0 pM mm-2 h-1; B, 0-15 pM mm-2 h-1; C, 15-30 pM mm-2 h-1; D, 30-45 pM mm-2 h-1; E, 45-60 pM mm-2 h-1; F, 60-75pM mm-2 h-1; G, 75-90 pM mm-2 h-1; H, 90 pM mm-2 h-1

3. Root and shoot trait characterization of UQR 12/ 15 lines: screening for root traits and functions contrasts

3.1. Material and Methods

3.1.1. Plant growth conditions

Two experimental spring wheat (*Triticum aestivum* L.) lines, UQR012 (shallow-rooted system: SRS) and UQR015 (deep-rooted system: DRS) with strongly contrasting seminal root angles, determined at early growing stage, were choosed, developed by backcrossing a donor source for narrow root angle to the high-yielding spring wheat genotype Borlaug100 (Rambla et al. 2022) (Fig. 11).

The two genotypes were cultivated independently in PVC columns (8 cm inner diameter, 45 cm height, and 2.3 L volume) within a climate chamber set at 20°C and 50% relative humidity. The cultivation period for UQR15 spanned from May 19, 2021, to July 5, 2021, while for UQR12, it extended from June 13, 2021, to August 3, 2021. For each genotype, thirteen PVC columns (8 cm diameter, 45 cm height) were

filled with loamy soil (sieved to 2 mm) from a test site at the Jülich Research Center in Selhausen (50.8659° N, 6.4471° E). As in the preceding experiment, a bulk density of 1.4 was achieved by means of tamping the column.

The columns were each planted with two seeds (equivalent to a seeding density of 400 seeds/m²) and then placed in a climate chamber (20°C during the day, 18°C at night, 50% relative humidity, 1,000 mol m^{-1} from 6 a.m. to 8 p.m.). The initial average gravimetric water content of the soil was determined to be 0.40 cm cm-2. Water was added to the system twice weekly to maintain the value between 0.30 and 0.44 centimeters of mercury.

The fertilization experiment involved the application of a liquid solution containing 7% nitrate and 19% ammonium at rates of 3 kilograms per square meter. This solution was administered at specific stages of the Zadok growth scale, specifically Z11 (6 days after sowing) and Z25 (34 days after sowing).

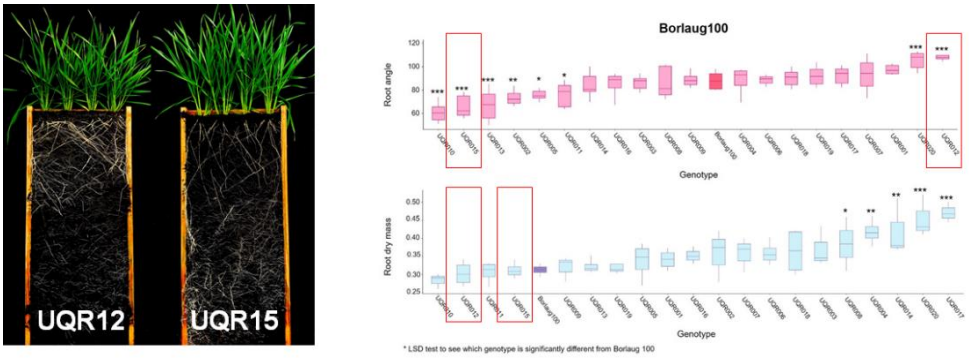

Fig. 11 Overview on rhizobox of the root system of the wheat genotype UQR12 (shallow root system) and UQR15 (deep root system). Angle of the seminal roots and the root biomass. panel communicated by Lee Hickey on wheat genotypes from the same parent Borlaug100.

3.1.2. Non destructive measurements

Above- and belowground plant physiology observations were made, at least once a week, namely the tiller and leaf number, the stage of development (on the Zadok scale), the chlorophyll content with SPAD 502Plus (Konica Minolta, Munich, Germany) and the dimensions of the leaf blade (length and width) to calculate the leaf surface. The mean water content value for each column was assessed gravimetrically. As for the previous experiment, the Soil Water Profiler (SWaP) results will not be shown or discussed.

3.1.3. Destructive measurements

Of the 13 columns used for each genotypes, three were harvested destructively, after the SWaP measurement, 28, 35, and 42 days after sowing (DaS), and the remaining four were harvested 49 DaS (Fig. 12). On each pf theses designated days, the above-ground plant biomass was sampled, and soil samples were collected from the columns and divided into horizontal segments measuring 9 centimeters in thickness. These segments represented soil depths ranging from 0 to 9 centimeters, herein designated as "topsoil" to 45cm (layer A). The segment from 27 to 36 centimeters was designated as "subsoil" to avoid the root accumulation effect of the bottom of the column (layer D). These soil segments were stored at -20°C until microbial biomass and zymography measurements were performed (see the description of this method in the previous experiment).

For the three additional soil segment depths (i.e., B: 9-18; C: 18-27, and E: 36-45 cm at 28, 35, 42, and 49 DaS), soil samples were collected to ascertain their water content, total nitrogen (TN) content, and non-purgeable organic carbon (NPOC) content. Subsequently, the root systems were extracted from the soil by washing the soil segments with water. The roots were then preserved in 30% ethanol solutions in order to scan them with WinRhizo™ (Regent Instruments Inc., Quebec, Canada). Subsequent to each SWaP measurement at 45 DaS, the above-ground plant biomass was harvested, and the soil was also extracted from the columns. The fresh weight of the roots, stems, and leaves was measured using an electronic balance (Kern 572-30, Kern & Sohn GmbH, Balingen, Germany). The stems and leaves were stored in a -20°C freezer.

The leaves were then scanned (Canon, 4 Krefeld, Germany) for analysis with ImageJ to measure the surface area of the leaf blade and sheath, as well as the position and number of nodes along the stems. The volume of the leaves and stems was obtained by immersing them in a graduated cylinder containing water and measuring the change in water level. Lateral sections of the leaf blades (5 centimeters from the leaf sheath, on the second leaf of the tillering stage), stems (1 centimeter above the ground, when stems were present), and roots (at a depth of 9 to 18 centimeters) were made using a cryomicrotome (CM 3050S; Leica Microsystems GmbH, Wetzlar, Germany). The images were then subjected to analysis using ImageJ, a software program designed for biological imaging, to determine the number of vascular bundles and the mean morphology of the xylem and phloem tissues within each bundle. These detailed leaves and root cut results will not be detailed in this document.

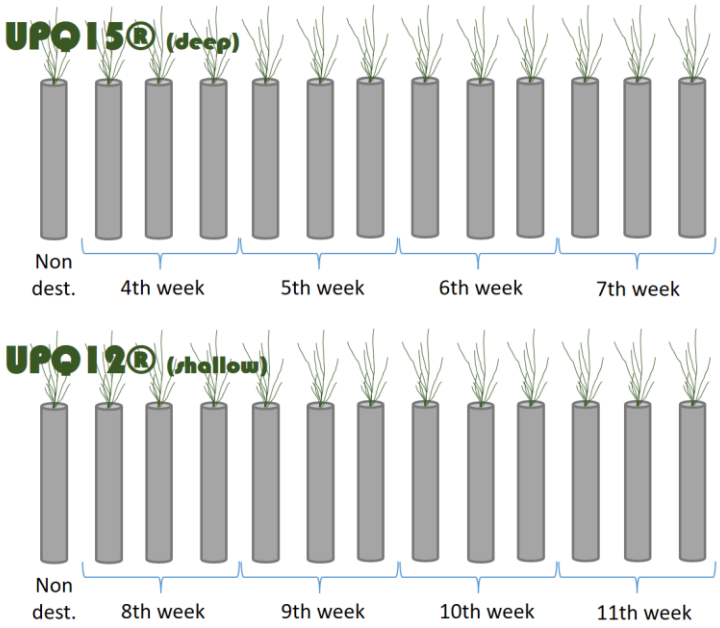

Fig. 12 Schema of the of the winter wheat UQR12 and UQR15 experiment, with the destructive sampling weeks

3.2. Results

The total fresh biomass of the roots exhibited a nearly linear increase between 28 and 43 days after sowing (DaS) for both genotypes, subsequently entering a stabilization phase. It was important to note that the root biomass measured represented only three of the five soil layers. This was because two layers were reserved for zymographic analyses as described previously. The total root system of these three segments exhibited an overall growth rate of 0.3 g of fresh root per day (Fig. 13). While the growth rates were comparable over time, the root biomass of UQR15 remained consistently close to double that of UQR12. Therefore, for UQR12, root growth rates exhibited relative homogeneity, with approximately 0.10 g day-1 observed in the 9-18 cm and 36-45 cm layers, and a marginally higher rate (0.14 g day-1) recorded in the intermediate layer (18-27 cm). In contrast, UQR15 exhibited low and highly variable root growth in the 9-18 cm layer (approximately 0.02 g day-1), moderate growth in the 18-27 cm layer (0.11 g day-1), and the highest growth rate in the deepest layer (36 to 45 cm; 0.18 g day-1), thereby confirming its deep-rooted phenotype (Fig. 14). The results indicated that UQR15 exhibited accelerated and more substantial root system development compared to UQR12, particularly in the deeper soil layers.

The dynamics of β-glucosidase activity measured at depths of 4.5 and 31.5 centimeters differed significantly between genotypes, depending on both soil depth and plant development stage. UQR12 demonstrated an increase in activity, ranging from 28 to 49 DaS, in the topsoil (Fig. 15, published in (Lattacher et al., 2025a)). Conversely, it exhibited stagnation or even a decline in the subsoil during the same period. Conversely, enzyme activity exhibited stability throughout growth at levels lower than those observed for UQR12 in topsoil. However, in subsoil, there was a tendency for enzyme activity to increase over time (Genotype x Depth x Age: $p<0.001$) (Fig. 15). Furthermore, microbial biomass was found to be significantly higher for UQR15 than for UQR12 in subsoil (genotype x depth: $p < 0.05$).

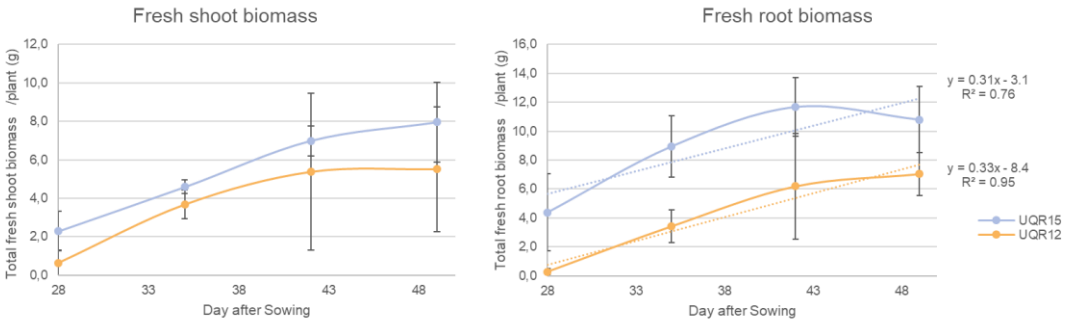

Fig. 13 Shoot and root fresh biomass (g) for UQR15 (in blue) and UQR12 (in orange) between 28 and 49 days after sowing

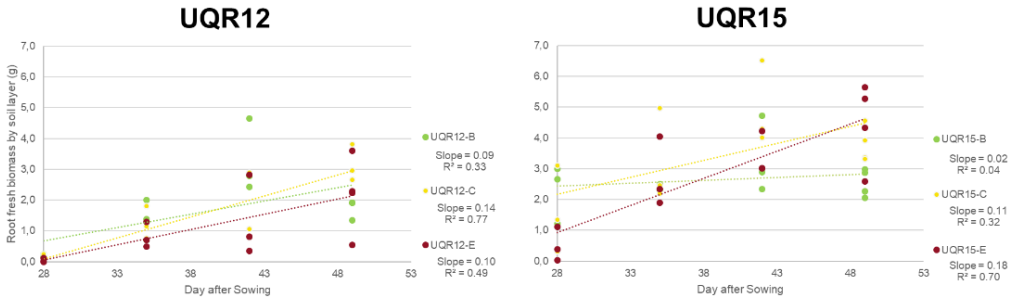

Fig. 14 Root growth (g) by soil layers 9-18 cm (B, in green), 18-27 cm (C, in yellow) and 36-45 cm (E, in brown) between 15 and 45 days after sowing for UQR12 (on the left) and UQR15 (on the right)

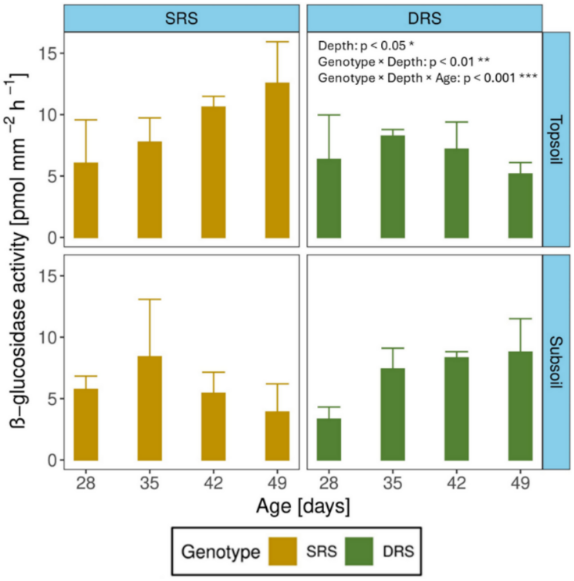

Fig. 15 Temporal patterns of the mean β-glucosidase activity in topsoil and subsoil for the shallow root system (SRS) (yellow) and deep root system (DRS) (green) from day 28 to day 49 after sowing. Error bars represent the standard deviation of 3 replicates. The displayed p-values indicate significant effects ($p < 0.05$), determined using a linear mixed-effects model. In this model, the columns were treated as a random effect, while genotype, depth, and age were considered as fixed effects. From Lattacher et al. (2025).

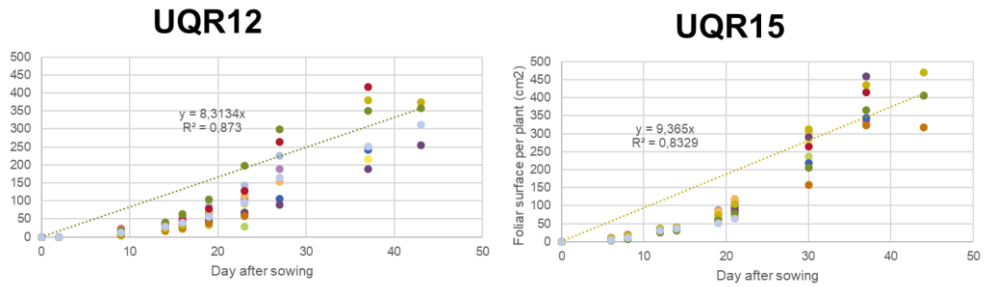

Fig. 16 Leaf surface (cm^2) for UQR12 (on the left) and UQR15 (on the right) between 0 and 49 days after sowing

Non-destructive measurements showed a progressive increase in leaf blade length and leaf surface area during the first 40 DaS for both genotypes. UQR12 displayed higher variability in leaf surface measurements. At 45 DaS, the average foliar surface reached approximately 400 cm^2 for UQR15 and 350 cm^2 for UQR12, while maintaining similar growth dynamics, as also observe on the shoot fresh biomass evolution (Fig. 13 and 16).

Similar trends in leaf number and leaf blade length were observed over time in both genotypes. After 15 DaS, tiller number increased linearly at a rate of approximately one new tiller every five days, regardless of genotype. Aboveground fresh biomass increased almost linearly between 28 and 43 DaS before stabilizing, with similar growth rates for both genotypes, although UQR15 tended to reach slightly higher values. Chlorophyll content, measured using a SPAD meter, remained stable around 45 units between 15 and 25 DaS for both genotypes. Thereafter, chlorophyll values gradually declined, reaching approximately 38 for UQR15 and 30 for UQR12 by the end of the observation period, indicating a stronger sensitivity of UQR12 to nitrogen limitation after 40 DaS.

4. Experimental framework development: column design, multi-depth isotopic labeling, and non-destructive root imaging

4.1. Material and Methods

4.1.1. Pot size

In consideration of the substantial impact of rooting volume and pot geometry on plant growth, as evidenced by (Poorter et al., 2012, "Pot size matters"), a preliminary experiment was organized to assess the influence of pot diameter and depth on one of our wheat genotype development and to circumvent the growth restriction imposed by root confinement. Two pot configurations were tested using the genotype UQR15: three pots with an inner diameter of 8 cm and 11 cm, and deep columns with a height of 80 cm. The plants were cultivated for a period of 81 days after sowing (DaS) in controlled conditions in a climate chamber set at 20°C and 50% relative humidity.

The cultivation period was from May 14, 2021, to August 3, 2021, spanning a duration of 81 DaS. The soil columns were filled with the same loamy soil (sieved to 2 mm) from a test site at the Jülich Research Center in Selhausen (50.8659° N, 6.4471° E). As in the preceding experiment, a bulk density of 1.4 was achieved by means of tamping the column.

The columns were each planted with two seeds, which was equivalent to a seeding density of about 400 seeds/m² for 8-centimeter diameter and 200 seeds/m² for 11-centimeter diameter. The initial average gravimetric water content of the soil was ascertained to be 0.40 cm^{-2}, and it was subsequently maintained by irrigation between 0.30 and 0.44 cm^{-2}. The fertilization process was executed in a manner consistent with the protocol employed in the preceding experiment.

A series of observations were conducted on the above- and below-ground plant physiology of the subject at a minimum frequency of once per week. The following parameters were observed: the tiller and leaf number, the stage of development (on the Zadok scale), the chlorophyll content with SPAD 502Plus (Konica Minolta, Munich, Germany), and the dimensions of the leaf blade (length and width) to calculate the leaf surface. The mean water content value for each column was assessed gravimetrically.

Subsequent to the conclusion of the 81-day growth period, the above-ground plant biomass was extracted, and soil samples were collected from the columns and divided into horizontal segments measuring 9 centimeters in thickness. A series of soil samples were collected for the purpose of determining their water content, total nitrogen (TN) content, and non-purgeable organic carbon (NPOC) content.

Subsequently, the root systems were extracted from the soil by washing the soil segments with water. Subsequently, the roots were preserved in 30% ethanol solutions to facilitate scanning with WinRhizo™ (Regent Instruments Inc., Quebec, Canada). The fresh and dry weight of the roots, stems, and leaves was measured.

The objective of this experiment was to ascertain the optimal rooting volume necessary to facilitate the mixture cultivation of two plants per pot without inducing early shoot growth limitation. A comparison of the results with those of previous experiments conducted on the same genotype grown for 49 DaS was used to determine the pot dimensions most suitable to sustain normal shoot and root development. The study also sought to define the developmental stage up to which phenotypic differences between contrasting root architectures (UQR15 vs. UQR12) can be reliably observed.

4.1.2. Labelling

To facilitate the online isotopic measurement of soil water vapor in soil columns, and learning from (Deseano Diaz et al., 2023) recommendations to de-correlate the vertical profiles of hydrogen and oxygen stable isotopes (δ^2H and $\delta^{18}O$) in soil water, we tested the new labelling set-up. Soil columns were isotopically labeled at five depths (0, 20, 40, 60, and 80 centimeters from the bottom porous plate). At depths of 20, 40, and 60 centimeters, the experiment involved the introduction of labeled water via micro-perforated dripping tubes (Synflex "1300" with 1/4-inch perforations at 5-millimeter intervals). The labeling at the soil surface was achieved through direct water input and at the bottom via a porous plate.

Initial labeling tests were conducted on November 22th 2021 using syringe injection of 20 milliliters of isotopically labeled water at selected depths. However, the injected volumes and isotopic enrichments proved to be inadequate in relation to the substantial water content of the saturated soil, consequently yielding a limited isotopic contrast in soil water vapor measurements. Consequently, a second labeling experiment was conducted on December 7th 2021, employing 20 milliliters of labeled water with doubled delta-18O and delta-2H values. In this case, the introduction of the labeled water occurred through diffusion via tubing connecting the water reservoirs to the soil surface and to the micro-perforated tubes installed at depths of 20, 40, and 60 centimeters.

The measurement of soil water vapor mixing ratios and isotopic compositions was conducted using a cavity ring-down spectroscopy (CRDS) analyzer (L2130-i, Picarro Inc., Santa Clara, CA, USA). The isotopic composition of soil liquid water was inferred from soil water vapor isotopic values using temperature-dependent empirical calibration equations (Rothfuss et al., 2013). The calibration process entailed the utilization of two soil vessels, each possessing a known and constant soil water isotopic composition, which were positioned within the climate chamber in close proximity to the experimental columns.

4.1.3. MRI

Preliminary magnetic resonance imaging (MRI) tests were conducted in autumn 2021. This MRI measurement evaluation was conducted to ascertain whether the loamy soil (sieved to 2 mm) from a test site at the Jülich Research Center in Selhausen (50.8659° N, 6.4471° E), utilized in our experimental experiment necessitated pre-demagnetization or if its inherent low ferromagnetic particles exhibited minimal interference with the MRI coil. The selection of two scanning time points was informed by the plant growth dynamics observed in earlier experiments, which identified 30 and 40 days after sowing (DaS) as optimal. Two columns were filled with the soil, one of which was demagnetized, while the other remained magnetized. Two UQR15 genotypes per pots were scanned. Subsequent to the scanning process, the soil was extracted, and the smaller root diameter was measured using a caliper gauge.

Additionally, to allow the MRI measurements of the 80-centimeter-high, 11-inch-diameter and 15 kg soil columns, a specialized robotic arm was designed, based on a linear axis (Dold Mechatronics, Haslach im Kinzigtal, Germany). The 1,200-mm-long linear axis could support up to 40 kg over an 880-mm span. The self-braking spindle was fail-safe, and additional bumpers were added to reduce the risk of pinching. The controller was based on an Arduino Nano V3 (Arduino S.r.l., Monza, Italy), and we wrote a C program to operate it via a serial interface. After purchasing, assembling, and programming the components, we performed a series of tests on columns with the specified dimensions and mass.

4.2. Results

4.2.1. Pot size

It was observed on each soil layer that the roots growing in the columns of 8cm inner diameter (9cm external diameter, 50cm2 of inner soil surface) had a biomass almost two times lower than those of the columns of 11cm inner diameter (12cm of external diameter, 100cm2 of inner soil surface). Therefore, the average total fresh root biomass for 50cm2 was 15g/plant, and 25g/plant in 100cm2 soil surface. Concerning the aboveground, the two UQR15 plant growing in 100cm2 soil surface showed a fresh shoot biomass of about 20 g/plant, instead of 10g/plant for two plants in 50cm2 (Fig. 17).

We observed any foliar surface differences between the two soil surfaces before 35 days after sowing. After this, the 100cm2 soil surface plant showed a higher foliar surface (for example 650cm2 against 300cm2 in the 45th day after sowing). Even with the plant senescence and the leaf and tiller drying, the foliar surface of the 100cm2 soil surface wheat stay significantly higher. The 100cm2 soil surface plants show also higher tiller number, more than 4 tillers per plant at 65 days against 2 tillers per plant for the 50cm2 soil surface (Fig. 18).

The difference between the two pot size was also observed on the late phenological stages. For example the 50cm2 reach the inflorescence emerging (index 59 on Zadock scale) 5 days before the 100cm2. This advanced was conserved for all the following stages.

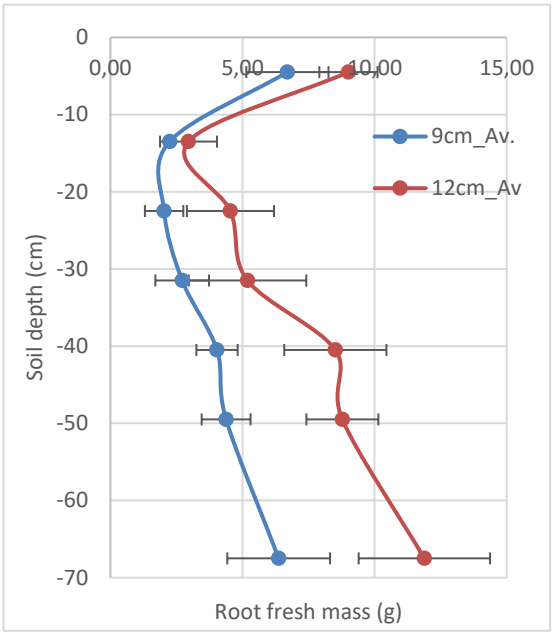

Fig. 17 Root fresh mass average (g) profile from 0 to 70cm for the 9cm and 12cm column (error bars for standard error), same variety UQR15, at 81 DaS

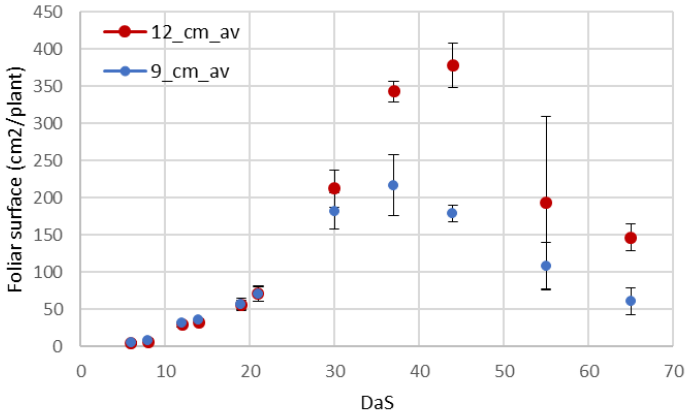

Fig. 18 Foliar surface evolution from 0 to 65 DaS of the UQR15 wheat genotype (DRS) in two pots of same high (70cm) but different outside diameters 12 vs 9cm (i.e. 11 vs 8 cm inner diameter)

The indexed chlorophyll content (or “greenness” of your plants on a scale of -9.9 to 199.9) measured by the SPAD 502 Plus Chlorophyll Meter oscillated between 40 and 50. We observed that the leaf chlorophyll content were significantly smaller for the 50cm2 columns between 15 and 40 DaS. This difference between the two soil surface column type were no longer significant after 40 DaS (data not shown).

4.2.2. Labelling

Subsequent to the second labeling experiment, a reorganization of the vertical $\delta^{18}O$ and $\delta^{2}H$ profiles was observed (Fig. 19 and 20). This reorganization exhibited a high degree of stability over the subsequent week. During this interval, the $\delta^{18}O$ and $\delta^{2}H$ values represented in the double isotopic space manifested as a triangle-shaped space, rather than a linear correlation (Fig. 21).

Subsequent examination of the stable isotopes oxygen-18 ($\delta^{18}O$) and hydrogen ($\delta^{2}H$) indicated substantial evaporative enrichment in the upper soil layers, particularly within the top 5 centimeters. At greater depths, the effects of evaporation were less pronounced, and the isotopic composition reflected a mixture of initially saturated water and injected labeled water. The delta-18O and delta-2H profiles exhibited approximate monotonicity within the depth range of 10 to 60 centimeters, with values ranging from approximately -7‰ to -60‰, respectively. The most depleted δ18O values were observed at a depth of 60 centimeters, while the most enriched values were observed at a depth of 40 centimeters.

In the 60-centimeter range, the $\delta^{18}O$ values increased from approximately −8‰ to −6‰, while the $\delta^{2}H$ values decreased from −60‰ to −70‰. A comparison of the observed isotopic profiles as a function of depth with the theoretical profiles expected according to the applied labeling scheme revealed a discrepancy, suggesting the need to further optimize the volume and isotopic enrichment of the injected labeled water.

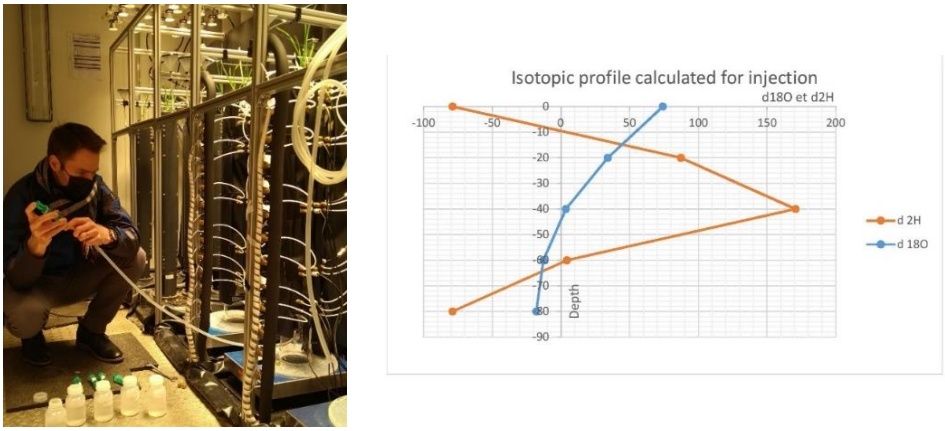

Fig. 19 Theoretical profile of isotopic composition along the acrylic column for the acrylic column labelling pre-test. Left: labelling application on the bottom of a soil column.

Fig. 20 Soil column during the water stable isotopes labelling, 7/12/2021. On the left, ths acrylic soil column with the aboveground chamber without plants and the system for water stable isotopic meausremnets online is connected. On the top right, the manual valve to inject water in the soil dripping tubings. On the bottom right the labelled water to be injected

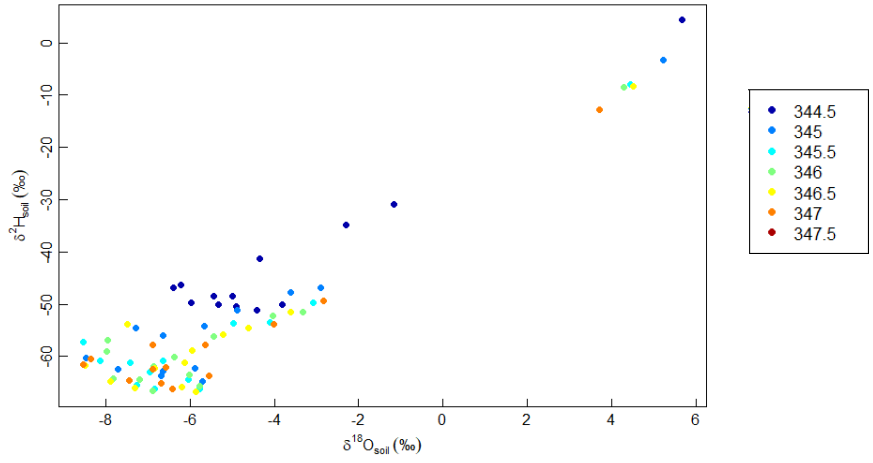

Fig. 21 Dual plot for delta 18O and 2H values between days 344,5 and 347,5

4.2.3. MRI

In both soil columns diameters, roots with a diameter greater than approximately 300 µm were clearly detectable, allowing for the visualization of the seminal and basal root systems of the wheat (Fig. 22). Three-dimensional reconstruction of the MRI images revealed two spatially distinct root populations within the columns. The initial population developed in the central region of the soil volume, following trajectories that were largely consistent with the natural insertion angles of the roots of each genotype. A secondary population of roots was observed to deviate from the main population upon reaching the column wall. These roots continued to grow downward, maintaining their angle along the wall, following what eventually became the equivalent of a crack caused by the swelling and shrinkage of the clay—a path through which water and nutrients flows preferentially. In some cases, these deviated roots converged with adjacent deviated roots to form dense longitudinal root bundles. This phenomenon has been described in the literature as root "channeling", “clumping” or the formation of preferential root pathways in constrained geometries (White and Kirkegaard, 2010).

The distribution of these wall-associated root bundles was particularly pronounced in the lower half of the column, where the reduced soil volume relative to root length increased the likelihood of contact with the wall. This boundary artifact is an inherent limitation of column-based root phenotyping and is expected to be more pronounced in narrower columns. This provides an additional methodological argument in favor of using the 11-cm internal diameter chosen in the present study rather than smaller formats.

A comparison of image quality revealed no significant differences between the demagnetized and non-demagnetized soil treatments, suggesting that demagnetization may not be necessary for future experiments with this type of soil.

Finally, the evaluation of the specialized robotic arm to lift the column was also met with positive outcomes (Fig. 22).

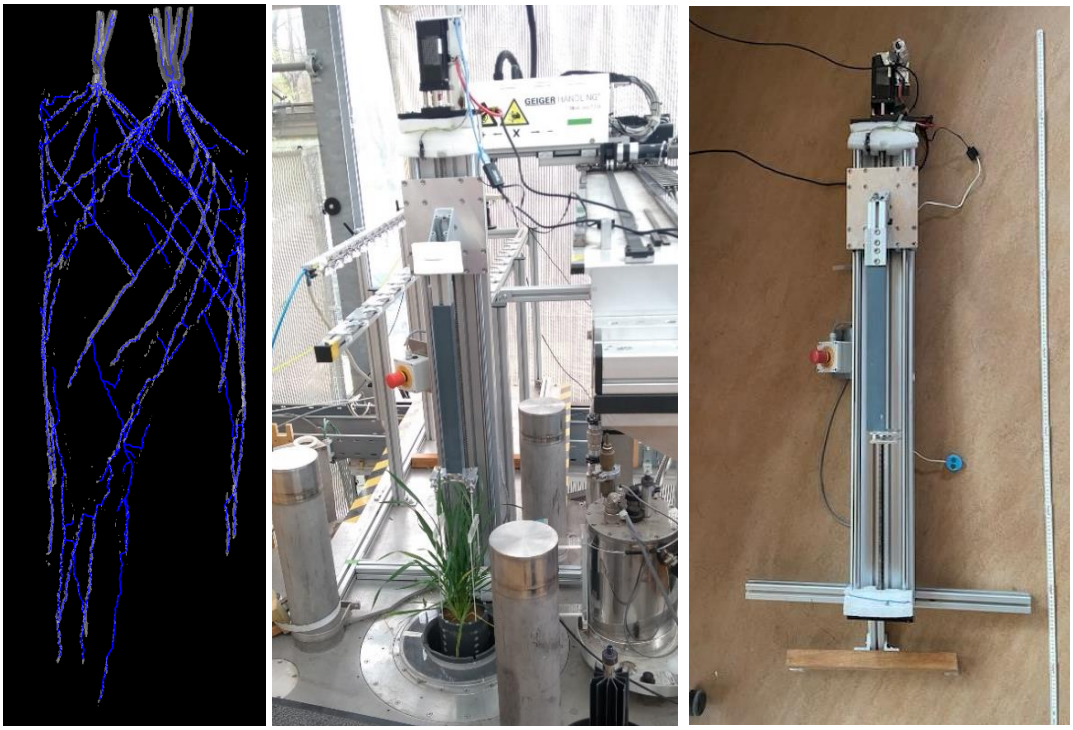

Fig. 22 Left side: MRI imaging of two wheats plants growing in the same column, 30 DaS. Middle: PVC column in the MRI scanner with the linear axis. Right side: picture of the linear axis robot built.

5. Discussion

5.1. Selection of root contrasted wheat genotypes

These two preliminary comparative experiments on two wheat genotypes demonstrated that the UQR12-UQR15 pair showed greater contrast in root growth under the optimal conditions tested in the laboratory compared to the Treblir-Milaneco pair.

While Milaneco® and Treblir® exhibited comparable total root biomass, some disparities in secondary root growth and lateral root density were discerned. For basal roots, these inter-lateral distances were greater for Milaneco® than Treblir®, and for first-order roots, they were longer for Treblir® than Milaneco®.

However, no significant disparities were detected at 45 DaS with respect to root density profile, root insertion angle, or even β-glucosidase and β-N-acetyl-glucosaminidase activity. However, Milaneco® exhibits accelerated growth patterns, particularly in the belowground environment. At 45 DaS, we observed for Milaneco® a higher mean root biomass than Treblir® in the superficial layers. This finding stands in contrast to the field experimental data that served as the basis for their selection, which indicated that Treblir® exhibited characteristics of a shallow-rooted type, while Milaneco® displayed characteristics of a deep-rooted type.

The aboveground growth trends were similar in the aerial environment, although Treblir® showed accelerated growth compared to Milaneco®, which was characteristic of underground traits. Our observations revealed no substantial disparity in total nitrogen or organic matter content in the soil profile of the two genotypes, suggesting that these differences are not attributable to divergent nutrient uptake or divergent carbon release by their root activity.

Conversely, the data demonstrate that UQR15 grew a root system more oriented toward deeper horizons compared to UQR12, particularly within the subsoil layer (36–45 cm), while UQR12 exhibits a distribution that was more oriented towards the topsoil. Furthermore, UQR15 exhibited accelerated development of its deep roots in comparison to UQR12. This phenomenon may be partially attributed to the contrasting root angles on which these varieties were selected. This discrepancy validated the anticipated divergence between "deep-rooted" and "shallow-rooted" genotypes. It should be noted that around 40 DaS, at the booting stages, their root and shoot traits showed the higher disparities for UQR15 and UQR12.

Furthermore, the measurements of β-glucosidase activity provided insights into the enzyme profiles, which in turn serve as proxies for microbial and root activity. These profiles were found to be contingent upon both depth and genotype, with UQR15 exhibiting a propensity to stimulate heightened microbial activity within the subsoil and UQR12 demonstrating a greater degree of activity within the topsoil. This enzymatic gradient was consistent with the measured microbial biomass and respective root distribution, suggesting that root architecture modulates the

rhizosphere and microbial functioning, and potentially influences organic nutrient availability (Lattacher et al., 2025a).

The growth trends observed above ground were analogous to those observed underground, with UQR15 exhibiting a faster growth rate compared to UQR12. However, after 40 days of submergence (DaS), UQR12 exhibited heightened sensitivity compared to UQR15, manifesting as a more pronounced decline in leaf chlorophyll content. This observation suggests the potential for UQR15 to better compensate for nitrogen uptake deficits at depth, a capacity attributable to its more dynamic root system compared to that of UQR12.

It is worth noting that this homogeneous bulk density of 1.4 g cm^{-3} across the entire column profile constitutes a methodological simplification with respect to in situ conditions, where bulk density typically increases with depth — from about 0.9 g cm^{-3} in the loose topsoil to 1.6 g cm^{-3} in compacted subsoil horizons of the same agricultural Luvisol (Weihermüller et al., 2007). Adopting an artificially homogeneous profile was a deliberate choice to (i) avoid introducing additional inter-replicate variability, (ii) ensure that any genotypic differences in root distribution and water uptake could be attributed unambiguously to plant traits rather than to differences in mechanical impedance, and (iii) facilitate the comparison with the soil-plant model parameterization in Giraud, Le Gall et al. (2023). The trade-off is that the deeper soil layers in our columns are mechanically more permissive than in the field, which may partly explain the more pronounced deep-rooting expression of UQR15 in the columns compared with the field experiment of Chapter 4.

5.2. Selection of the column size and the stage of interest for the genotype pair of interest

The results demonstrate a significant impact of soil surface area (50 vs. 100 cm^2, c.a.d. 400 vs 200 plants per m^2) on root biomass, above-ground biomass, leaf area, tillering, and phenology. The observed decrease in root and aboveground biomass in the 8-centimeter-diameter columns was consistent with the concept of root confinement, as described by Poorter et al. (2012). According to this concept, a restriction in root volume induces an early limitation of aboveground growth, regardless of resource availability. The reduction in root biomass, tillering, and leaf area in the 50 cm^2 columns could limit the ability to detect specific differences between UQR15 (deep root system) and UQR12 (shallow root system), particularly in the later stages.

In order to draw meaningful discussion about root and shoot expression in the 50 and 100 cm^2 columns, it is also necessary to consider factors beyond the effects of soil volume. Firstly, the increased surface area relaxed the spatial constraints on root proliferation. In addition, this also increased the absolute amount of stored water and

mineral nutrients available per plant. Secondly, the surface-to-volume ratio of the column also affects its thermal regulation: smaller columns equilibrate faster with the chamber air temperature, which can induce a slightly higher mean root-zone temperature and thereby alter both root elongation rate and microbial activity (Schenk and Jackson, 2002). Thirdly, although the soil inoculum carries indigenous arbuscular mycorrhizal fungi (AMF) propagules, the conditions of growth in homogeneously repacked sieved soil with intensive root proliferation are likely to favor a relatively low and homogeneous mycorrhizal colonisation across treatments. This is distinct from the heterogeneous AMF networks that develop in undisturbed field soils. Therefore, the observed variations in tillering, leaf area and root biomass profile between the two column sizes cannot therefore be unambiguously attributed to a single mechanism and are more likely to reflect a combination of these.

The height of 80 centimeters appears to be necessary, rather than the 45 centimeters used in preliminary tests, or even the 60 centimeters used by Deseano et al. (2024). Indeed, an accumulation of 80 centimeters has already been observed for one species, ble, which, at its peak, easily reaches a depth of 100 centimeters. In some cases, this accumulation can reach even greater depths (White and Kirkegaard, 2010), which would be even more biased for smaller column sizes. Moreover, to discern variations in root profiles oriented towards the surface versus depth, the size of the column was of paramount importance.

The absence of differences in leaf area before 35 DaS, followed by a marked divergence, suggests a late but lasting perception of spatial constraint, leading to phenological acceleration (advancement of Zadoks stage 59) and a reduction in tillering potential in pots with smaller surface areas. These observations indicate that the diameter of the pot was a critical parameter for the full expression of the root and aerial phenotype. The use of 11-centimeter diameter columns for comparative experiments between genotypes was therefore justified.

The booting stage that occurs under our controlled conditions at approximately 40 DaS appears to be the most suitable for conducting our experiment. Subsequent to 50 days after sowing (DaS) and the onset of flowering, a decline in leaf area and chlorophyll content becomes evident. This decline may be attributable to the advanced stage of development. However, it was also plausible that the restriction of column volume exerts a more substantial influence than in earlier stages. Moreover, the initial stage was pivotal for the development of various yield components.

Finally, it should be noted that root architecture alone does not fully account for the between-genotype and between-treatment differences documented in this chapter. Several non-architectural mechanisms may contribute to the observed patterns. Root hydraulic conductance — which varies independently of root length and angle — determines the rate at which a given root volume can transport water toward the xylem, and has been shown to decline under both water deficit and high mechanical

impedance (Carminati and Javaux, 2020). Phytohormone signaling, in particular abscisic acid (ABA) produced in drying root zones and transported to the shoot, can trigger stomatal closure and modify above-ground carbon allocation before any measurable reduction in soil water content occurs (Tardieu and Simonneau, 1998). The enzymatic activity profiles observed in the rhizosphere — including the β-glucosidase and NAG gradients differentiated between UQR12 and UQR15 — reflect not only root distribution but also root exudate chemistry, which differs between genotypes and modulates the local microbial community independently of root biomass (Lattacher et al., 2025a). In the two-plant column, these chemical signals may propagate through the shared soil solution and influence the physiology of the neighbouring genotype, an interaction that cannot be disentangled from the hydraulic competition effects with the current measurement framework. The results presented in this chapter should therefore be read as documenting the net outcome of architectural, hydraulic, hormonal and microbial mechanisms operating simultaneously, rather than as a direct demonstration of a root-architecture causal pathway.

5.3. Coupling structural and functional root characterization: methodological considerations

Magnetic resonance imaging (MRI) scans have been demonstrated to be feasible for non-destructive visualization of roots in the columns used, thereby eliminating the need for prior soil demagnetization. The reliable detection of roots with a diameter greater than 300 µm facilitates analysis of the architecture of seminal and basal roots. This, in turn, complements destructive and indirect approaches (e.g., biomass, zymography, isotopes). Furthermore, the design and implementation of the new technical system now allows for the utilization of columns with a weight exceeding 15 kilograms, a length of 80 centimeters, and an outer diameter of 12 centimeters.

The integration of MRI with isotopic and microbiological measurements allow then a multi-scale approach that combines root growth dynamics, water uptake, and rhizospheric interactions into a single experimental system.

To overcome this scientific constraint and measure the water uptake profiles of each modality, stable water isotopes can be used, as demonstrated in the work of Paulin Deseano et al. (2024). In order to enhance the precision of our multi-source Bayesian model in estimating the relative contributions of each depth, we have conducted a series of tests to decouple the $\delta^{18}O$ and $\delta^{2}H$ profiles. The results of the isotopic labeling pre-test confirm the feasibility of online monitoring of the isotopic composition of soil water, with temporal stabilization of the $\delta^{18}O$ and $\delta^{2}H$ profiles after the second labeling. The formation of a triangular space in the $\delta^{2}H$–$\delta^{18}O$ diagram was indicative of successful vertical decorrelation of the isotopes. However, the observed discrepancy between the isotopic profiles and the anticipated theoretical profiles underscores the necessity to optimize the volume and isotopic enrichment of the injected water. The marked influence of evaporation in the surface layers also

highlights the difficulty of maintaining a stable isotopic signal in the first few centimeters of soil, which will need to be taken into account in future experiments with plants.

During the system development process, a number of technical challenges were identified, including issues related to software communication between the control computer and valve/sensor modules (LabVIEW) and the condensation of water vapor in the sampling lines connected to the isotope analyzer. The resolution of these issues was achieved through a combination of hardware adjustments, optimization of the control software, increased dry air dilution at the column outlet, and thermostating of the water bath to maintain the temperature of the air flushed through the semi-permeable tubes slightly below that of the soil column.

6. Conclusion

The present study demonstrates that, under controlled laboratory conditions, the UQR12-UQR15 genotype pair exhibits a significantly greater contrast in root system architecture and function than the Treblir®-Milaneco® pair. While the latter exhibited only subtle disparities in lateral root characteristics and early growth dynamics, these discrepancies were not consistently reflected in root biomass distribution, enzyme activity, or microbial indicators at later stages of development. In contrast, UQR15 exhibited a distinctly developed root system, characterized by greater depth and vigor, particularly in the subsoil. This observation aligns with the contrasting primary root angles that led to their designation as deep-rooted and shallow-rooted genotypes, respectively. These architectural differences were associated with depth-dependent microbial activity patterns and enzyme profiles, thereby confirming the hypothesis that root system architecture exerts a significant influence on rhizosphere functioning along the soil profile. This aspect was the subject of a publication with Adrian Lattacher et al. (Plant and Soil, 2025) entitled "*Rooting for microbes: impact of root architecture on the microbial community and function in top- and subsoil*". The detailed description of root and aerial traits at several stages of development of the UQR15 genotype was used to parameterize the CPlantBox model. This work was also the subject of a publication in which Mona Giraud and me were both co-first authors, entitled "*Development and calibration of the FSPM CPlantBox to represent the interactions between water and carbon fluxes in the soil-plant-atmosphere continuum*" (in silico Plants, 2023).

The experiments underscore the pivotal role of experimental design, particularly pot diameter, soil volume, and column depth, in accurately expressing genotypic differences in root characteristics. The reduction in soil surface area (50 cm^2) induced root confinement effects, leading to a decrease in root and vegetative biomass, reduced tillering, and accelerated phenological development. Consequently, this limited the ability to distinguish contrasting root phenotypes. The columns, with a diameter of 11

centimeters and a depth of 80 centimeters, provided an adequate volume of soil and vertical space to facilitate the full expression of root and shoot characteristics, particularly up to at least 50 days after sowing. The emergence phase (approximately 40 DaS) proved to be a pivotal development stage, during which root architecture, microbial activity, and the nutritional status of plants could diverge most significantly between genotypes, allowing them potentially to express their plastic and functional adaptation to contrasting water treatments.

In conclusion, the present study proposes a comprehensive methodological framework for conducting an integrative, multi-scale investigation of root characteristics and root-soil interactions. The integration of destructive measurements and non-destructive techniques, such as MRI for root architecture and online monitoring of stable isotopes for depth-specific water source, provides complementary information on the relationships between root structure and function. Despite the some identified technical limitations, particularly those associated with isotopic labeling near the soil surface and the differentiation of water uptake by individual plants within a column, the feasibility of these approaches has been demonstrated. These results lay the foundation for future studies that will integrate root system architecture, rhizosphere processes, and water and nutrient acquisition to enhance our understanding of the genotypic strategies underlying crop adaptation to soil resource heterogeneity.

Chapter 3

Combining spring wheat genotypes with contrasting root traits for a better use of water resources in soil? Evidence from column-scale water stable isotopic experiments

In this chapter, the slightly modified version of the study Le Gall et al. (2026) is presented describing the column design, the split-chamber transpiration monitoring system, the multi-depth isotopic labeling strategy, the MRI-based root architecture monitoring as well as the two water treatment applied to each genotype cultivated in monoculture and mixture. As hypothesized, UQR12 and UQR15 displayed distinct fRWU profiles in monoculture, consistent with their contrasting root biomass distributions. In mixture, both genotypes shifted their uptake toward deeper horizons relative to their monoculture profiles — a non-additive collective response that intensified under water deficit and cannot be explained by root biomass distributions alone. This article will be discussed, in particular, in light of the companion article addressing microbiological aspects, nitrogen dynamics, and rhizosphere exudates, published by Lattacher et al. (2025).

1. Introduction

The objective of this study was to evaluate whether combining wheat genotypes with contrasting root traits could improve water supply to the plant population. We focused on the booting stage because it was crucial for yield determination, involving the stabilization of the number of fertile spikes and flower formation, as well as the development of grain filling potential (Fischer, 1985; Wu et al., 2022; Xu et al., 2022). First, we hypothesized that the two genotypes, which were selected for their contrasting root traits - shallow vs. deep root systems - would exhibit significantly different root water uptake (RWU) profiles at this key stage of development. Secondly, water deficit should result in the RWU shifting to the subsoil and wetter soil layers, affecting all the genotypes. Thirdly, when the two genotypes are cultivated in mixture, it was hypothesized that each genotype will keep its specific water extraction niche, thereby enabling both plants to cope better with water deficit conditions.

Our study uses a controlled plant-soil column experiment to analyze the water use of two wheat genotypes with similar root biomass and contrasting root angle of insertion in the early stages of development (Rambla et al., 2022). Root traits of these genotypes also exhibit contrasting traits in later stages of development (Lattacher et al., 2025a). The experimental system enabled the quantification of the daily vertical profiles of RWU for wheat genotypes cultivated under adequate irrigation (WW) and water deficit (WD) conditions in monoculture and mixture, based on stable isotope measurements of soil water and transpiration flux after isotopic labeling. For this, a set of non-destructive methods and Bayesian modeling were employed, building upon the earlier work of Deseano Diaz et al. (2023). This approach enabled us to estimate for the first time to the best of our knowledge, the individual RWU profile of each genotype growing in mixture in the same soil column, at the same time of day, non-destructively, with a spatial resolution more detailed than what was currently done in the literature. These results were then compared with continuous non-destructive monitoring of soil water status, plant physiology (leaf area, tillering, biomass, stomatal density, etc) and root system (3D MRI scans), verified *a posteriori* by destructive observation (root scans and biomass). Based on these experimental evidences, we then discuss the inter-genotype plasticity of root water uptake patterns and potential benefits of cropping wheat genotype mixtures to cope with water deficit.

2. Materials and methods

2.1. Experimental setup

For the study, soil columns with an internal diameter of 11 cm and a height of 80 cm were used. These columns contained air-dried soil with a silt loam texture containing 22% clay, 66% silt, and 12% sand (Weihermüller et al., 2007) that had been sieved to a mesh size of 2 mm, collected from the upper 30 cm an agricultural field (Haplic luvisol) in Selhausen, Germany (50°52'07.8" N, 6°26'59.7" E), with temperate oceanic climate. The soil within the columns was compacted using a vibrating plate (Haver EML 450 Digital Plus N, Haver & Boecker, Oelde, Germany) to attain a homogeneous dry bulk density of 1.4 g cm^{-3} across the entire soil column. This density was representative of field conditions measured on average in the origin agricultural field. Subsequently, the soil of all columns was saturated with water from below via a porous plate. Then the soil columns were covered for a period of two weeks to prevent evaporation and to establish a stable level of homogeneous hydraulic status and microbial activity within the entire column. Thereafter, four pre-germinated sprouts were placed within each column and some days later, the two less vigorous were removed.

Two experimental spring wheat (*Triticum aestivum* L.) lines, UQR012 (shallow-rooted system: SRS) and UQR015 (deep-rooted system: DRS) with strongly contrasting seminal root angles, determined at early growing stage, were used (Rambla et al., 2022). The genotypes were developed by backcrossing a donor source for narrow root angle to the high-yielding spring wheat genotype Borlaug100 (Rambla et al. 2022).

We tested six 'plant modality x water treatment' combination composed of three plant modalities - monoculture of SRS, of DRS and the mixture (MIX) of both – and two water treatments - well-watered (WW) vs. water deficit (WD) conditions during four successive days at the booting stage. This resulted in the following plant modalities and water treatments combinations: WW-SRS, WW-DRS, WW-MIX, WD-SRS, WD-DRS and WD-MIX. Each combination was replicated over nine soil columns replicates, which were generated in six separate runs due to the spatial limitation of the climate chamber (Fig. 23 c). Each of the nine replicates include three soil columns for the water stable isotopic measurements (WSI columns) and six soil columns for magnetic resonance imaging measurements (MRI columns) (Fig. 23 a, b).

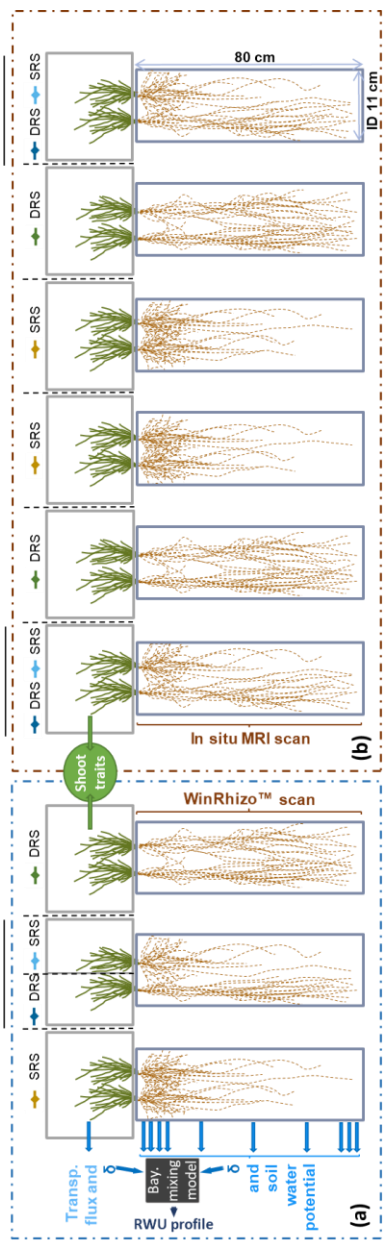

(c)

Col.	WSI column A	B	C	MRI column D	E	F	G	H	I
Run1	DRS WD	SRS WD	SRS WW	SRS WD	MIX WD	SRS WW	DRS WW	DRS WD	MIX WW
Run2	DRS WD	DRS WW	SRS WD	DRS WD	SRS WW	MIX WD	MIX WW	SRS WD	DRS WW
Run3	SRS WW	MIX WD	DRS WD	MIX WW	DRS WD	SRS WD	SRS WW	DRS WW	MIX WD
Run4	MIX WD	SRS WW	DRS WW	DRS WW	MIX WW	DRS WD	SRS WD	SRS WW	MIX WD
Run5	DRS WW	MIX WW	MIX WD	SRS WW	MIX WD	DRS WW	MIX WW	DRS WD	SRS WD
Run6	MIX WW	SRS WD	MIX WW	SRS WD	DRS WW	SRS WW	MIX WD	MIX WW	DRS WD

Fig. 23 Experimental design: example of Run3 consisting of its columns (stable water isotopes (WSI), panel a) vs MRI columns, panel b)) and their specific underground and aerial measurements. In the lower panel c), randomly distributed composition of each experimental series (Run1-Run6) in terms of plant modality (two individuals with "shallow root systems ' – SRS or with 'deep root systems' – DRS grown in monoculture, and their mixture – MIX) and water treatment (well-watered conditions – WW and water deficit – WD). The WSI columns (left side, A-C) included soil water potential sensors and gas-permeable membranes for online analysis of the stable isotopic composition of soil water (δ) and gas exchange chambers for non-destructive determination of transpiration flux and isotopic composition. The MRI columns (right side, D-I) did not include soil sensors, and the gas exchange chambers were used only to simulate the same atmospheric conditions that prevailed for the WSI columns. Each run of experiments included three WSI columns and six MRI columns

			Air temperature (°C)		Air humidity (%)		VPD (kPa)		pF		Soil temperature (°C)	
Culture type	Genotype	Water treatment	mean	sd	mean	sd	mean	sd	mean	sd	mean	sd
Monoculture	DRS	WD	24.3	0.9	68	10	0.92	0.31	3.6	0.3	20.9	0.7
Mixture	DRS	WD	24.2	0.4	71	12	0.88	0.33	3.7	0.3	21.1	0.6
	SRS	WD	24.4	0.2	76	11	0.72	0.32				
Monoculture	SRS	WD	24.3	0.7	69	8	0.91	0.27	3.6	0.5	21.1	0.7
Monoculture	DRS	WW	23.4	0.6	79	4	0.65	0.13	2.8	0.4	21.1	0.9
Mixture	DRS	WW	24.4	0.8	73	7	0.82	0.23	2.9	0.8	21.4	0.5
	SRS	WW	24.5	0.7	76	5	0.73	0.15				
Monoculture	SRS	WW	23.8	0.6	78	5	0.68	0.14	2.6	0.6	21.0	0.7

Fig. 24 Mean and standard deviation (sd) resulting of environmental parameters of the experiment in the afternoon between 1 and 3 pm at the booting stage (between 39 and 43 DaS) (air temperature in °C; air humidity in %, vapor pressure deficit (VPD) in kPa, pF matric potential and soil temperature in °C) for each culture type, genotype and water treatment (n=3).

We conducted this experiment in a climate chamber under controlled conditions, with air temperature set to 20 ± 0.22°C, relative humidity was set to 50.0 ± 2%. Light was provided with homemade LED panels (LEDs: CXA2520-0000-000N0YN430H, Lighting Solutions, Ludenscheid, Germany) cooled with a water bath (RP1845, LAUDA, Germany). The light intensity followed a sinusoidal-like 24-hour cycle from 0 µmol m^{-2} s^{-1} at "night" (from 8 pm to 6 am) to 1200 µmol m^{-2} s^{-1} at "midday" (1 pm).

From the sowing time on, water was applied to the topsoil using two different watering treatments. Watering regimes were adjusted to varying intensities, targeting for the 6th week of growth a matric potential corresponding to a pF value of 2.0-3.0 for the WW treatment and a pF value of 3.5-4.5 for the WD treatment. The pF value corresponds to the $\log_{10}$ of the absolute soil water matric potential (in kPa), and reflects soil water availability. The WW treatment therefore corresponds to wet soil condition, close to field capacity (pF ~2.0–2.5), where water was easily available to plants. The WD treatment corresponds to drier soil conditions where water was highly retained, requiring the roots to exert strong suction to extract water (pF 4.2 corresponds generally to the permanent wilting point) (Fig. 24). The watering for the WW treatment represented a total quantity of about 1300 mL of water over 6 weeks of growth, equivalent to 137 mm of rainfall, approaching the 10-year average of rainfall accumulated over 6 weeks between March and May in Selhausen (Zoomash, n.d.). For the WD treatment, only 200 ml of water was applied over the same growth period, equivalent to 21 mm of rainfall, similar to two of the dry spring months in 2021 or 2022, to achieve chronic and progressive water deficit (Lynch, 2018). Evaporation from the topsoil was minimized by covering it with a plastic film during the experiment.

The WSI columns were specifically designed to include gas probes (KM-PPMF-055-00-000-0000-0, 0.155 cm wall thickness, 0.55 cm i.d., 0.86 cm o.d., 0.2 µm pore size; Katmaj Filtration®, Poland) for the online and non-destructive determination of the soil water vapor δ^2H and $\delta^{18}O$ (Rothfuss et al., 2013). We also installed soil matric

potential (SMP, MPa) and temperature (T, °C) sensors (Teros 21, Meter, München, Germany) (Fig. 25). The WSI columns were complemented by six polyvinyl chloride (PVC)-made columns of the exact same dimensions for magnetic resonance imaging (MRI) measurements. These MRI columns did not include any metal parts or metal-built sensors, which allowed for the visualization of the 3D root architecture with (MRI) at the 6th week of plant growth. Each WSI column was equipped with a gas exchange chamber containing the two plants from their shoot collars from 39 DaS. In the context of MIX conditions, the WSI columns were divided into two impermeable half-chambers (see section 2.2). The MRI columns were also equipped with gas exchange chambers from 39 DaS to maintain consistent humidity and temperature conditions during the final four days of the experiment. However, the plants in the MRI columns were grouped into sets of three columns in a single gas exchange chamber (79 L in volume, 33 cm in width, 40 cm in height and 60 cm in length).

The thermal insulation of the soil column sides allowed the establishment of a soil temperature gradient as would be observed in field conditions, with 2°C higher values in the topsoil layers than lower values in the subsoil layers. In the transpiration chambers, no significant differences were observed between the cultivation modalities and the water treatment in terms of air humidity (74 ± 9%), air temperature (24.0 ± 0.8°C) and vapor pressure deficit (VPD) (0.78 ± 0.27) (Fig. 24).

A mineral fertilization, equivalent to 60 kg N ha^{-1}, was applied in each soil column at the three leaves-stage. The growth period was restricted to 6 weeks (until 43 days after seeding – DaS) when the plants reached ear emergence from boot, equivalent to Z51-59 on the Zadoks scale (Zadoks et al., 1974).

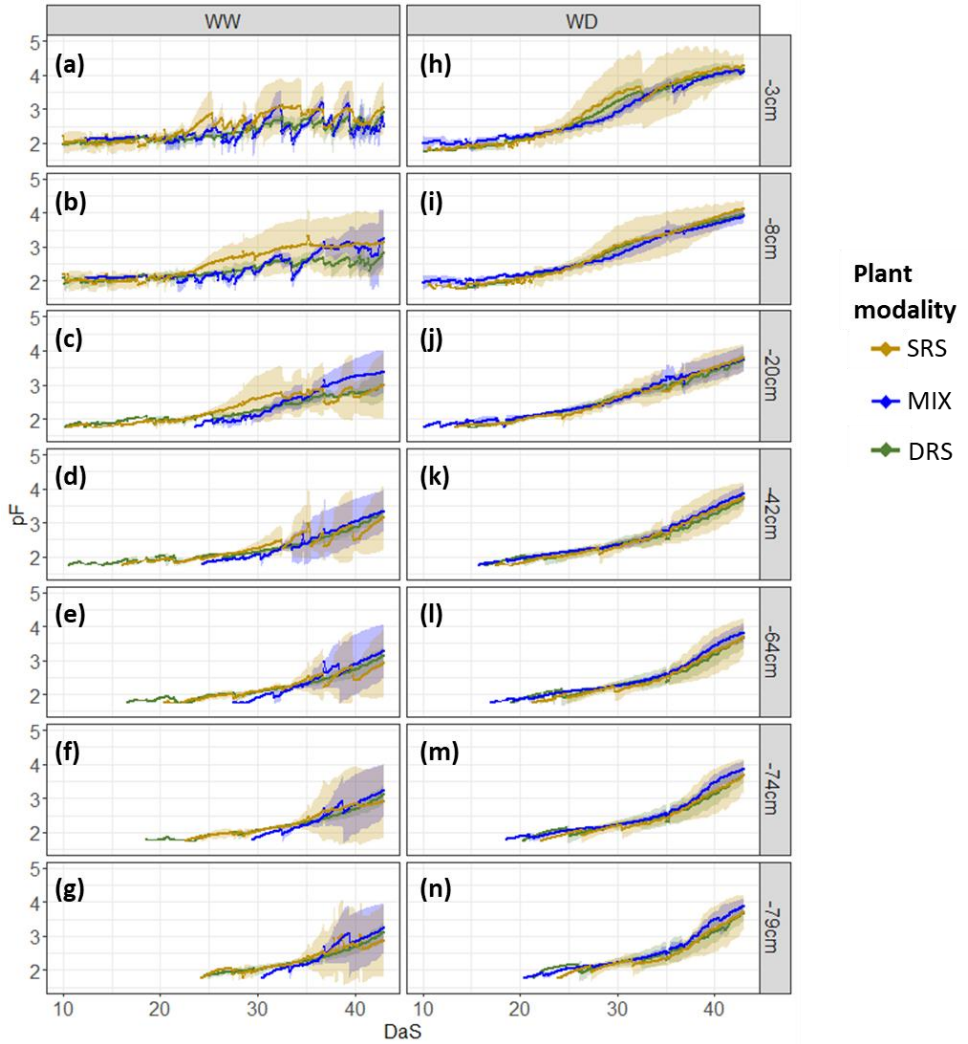

Fig. 25 Evolution of soil water potential, expressed in pF, average (solid line) and standard deviation (transparent envelope) measured using Teros21 sensors, for well-watered treatments ("WW," panels a to g) and water deficit treatments ("WD," panels h to n) among seven soil depths displayed on the right-hand side (3, 8, 20, 42, 64, 74, 79 cm). The colors represent the three crop types: DRS monoculture, dark green; mixture – MIX, blue; and SRS monoculture, orange.

2.2. Labeling strategy, water stable isotopic monitoring, and RWU determination

Labeling was conducted to increase the precision of the RWU estimates of the WSI columns. The labeling approach was designed to lead to 1) diverging vertical profiles in soil water δ^2H and $\delta^{18}O$; 2) the increase in soil water δ^2H and $\delta^{18}O$ gradients across depth and 3) to a non-significant rise in soil water content value. This was done by adding small amounts (10 ml) of isotopically labeled water ($-149.0‰ < \delta^2H < 1026.0‰$, $-302.0‰ < \delta^{18}O < 96.0‰$) at 0, 20, 40, 60, and 80 cm depth via perforated tubing (Synflex "1300" 1/4", Eaton, Dublin, Ireland) at 28 and 34 DaS, in order to achieve contrasting isotopic composition profiles later between 39 and 42 DaS for estimating the fRWU (Fig 26 a, c). We targeted a monotonic $\delta^{18}O$ profile on the one hand, and a non-monotonic δ^2H profile in the shape of a V with a maximum in the middle of the column on the other. We aimed the following labelling $\delta^{18}O$ and δ^2H values: 0 cm: +70‰/–70‰; -20 cm: +30‰/+90‰; -40 cm: +5‰/+170‰; -60 cm: -15‰/+4‰; -80 cm: -20‰/-70‰.

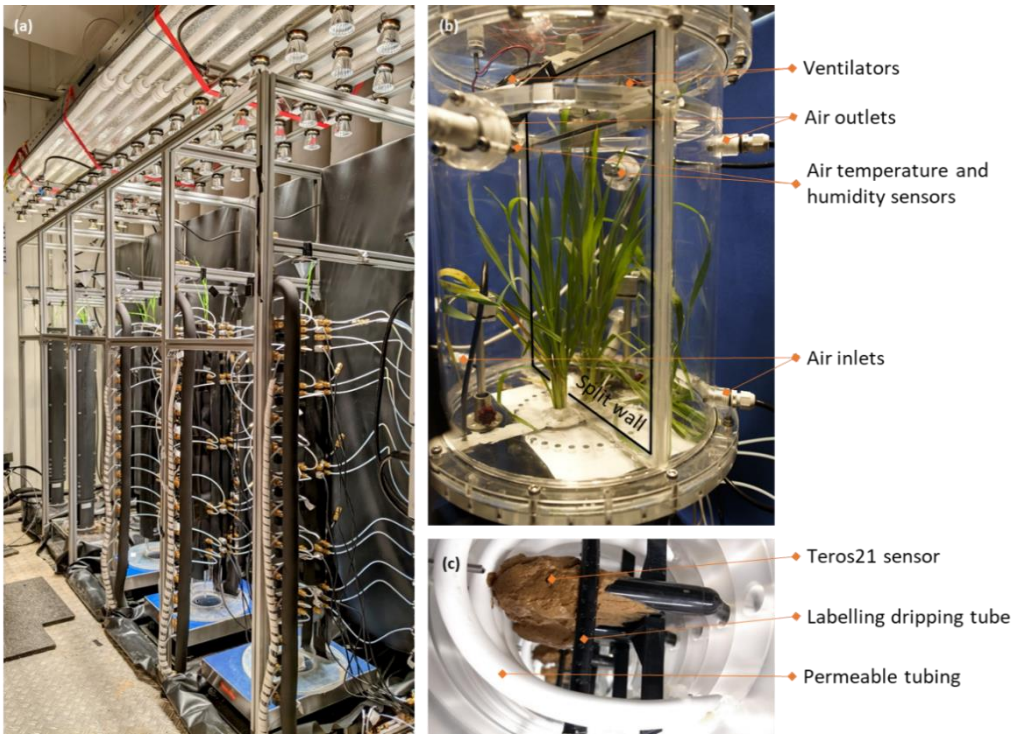

Fig. 26 (a) Experimental set-up with three acrylic columns for water stable isotope measurements, set on blue balances and under light panels. (b) Split plant chamber with an air inlet and outlet for each half, ventilators and an air temperature and humidity sensor. (c) Acrylic soil column with permeable tubes (for water stability measurements), Teros21 sensors (matric potential) and label drip tubes before filling the column with soil

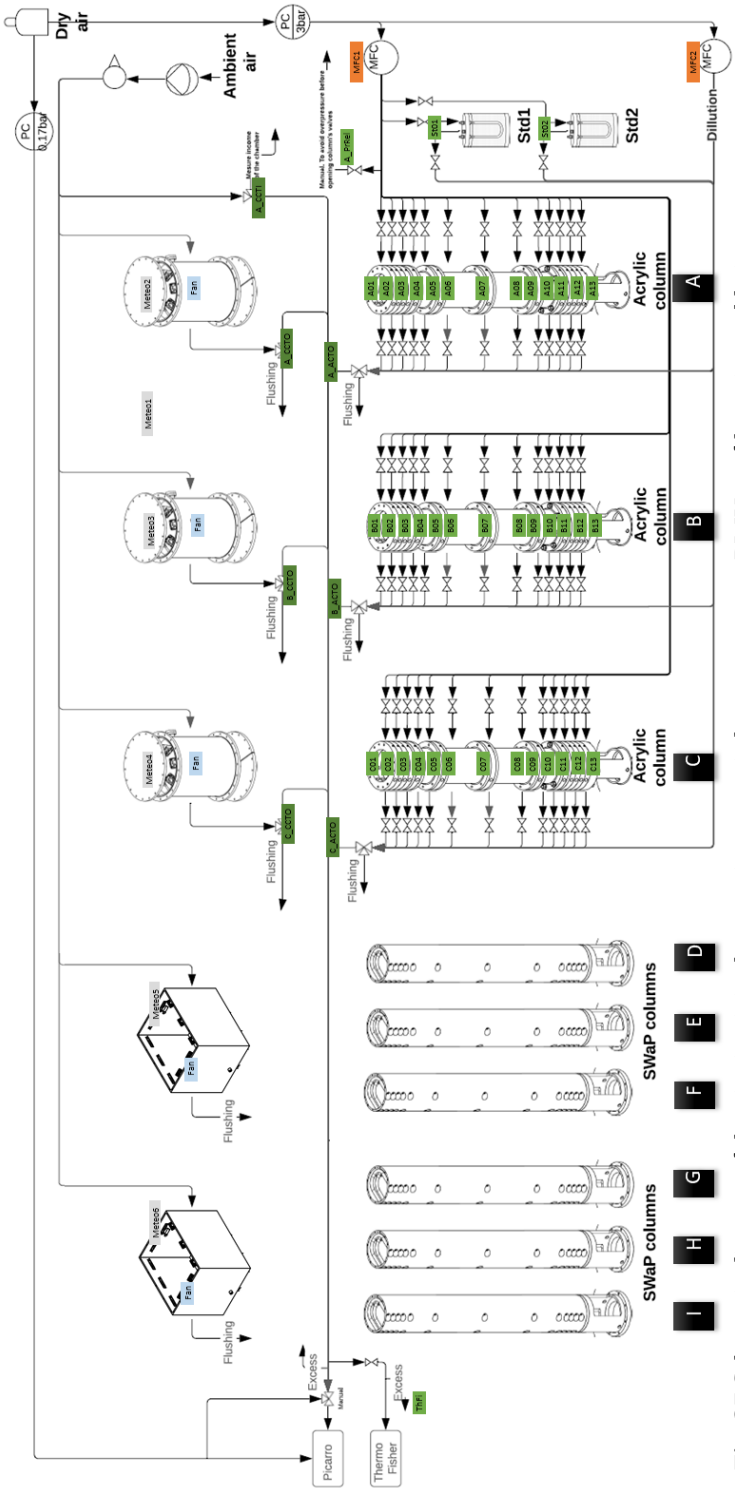

Fig. 27 Schematic diagram of the air circuit in the experiment carried out to measure RWU profiles using stable isotope measurements of water. Each acrylic column is equipped with 13 permeable tubes opened and closed by valves (A1 to C13). The air inlet to the soil columns is controlled by the MFC1 and the pressure can be released by the A_PrRel valve. The sampled water vapor is then diluted with dry air by MFC2, and directed to the analyzer or flushed via the 3-way valves. A(B/C)_ACTO. The Std1 and Std2 calibration standards are measured the same way. Ambient air is pushed into the plant chambers, regulated by manual valves, and measured by the analyzer via the three-way valve A_CCTI. The outlet from each plant chamber is either flushed or directed to the analyzer via the 3-way valves A(B/C)_CCTI

The weight loss in the WSI columns was recorded (IFS60K0.5D, Kern, Balingen, Germany) throughout the experiment to calculate the transpiration rate gravimetrically. In the sixth and final week of each experimental series, plant transpiration rate (Tr, mL/min) and transpiration isotopic composition values δ^2H_{Tr} and $\delta^{18}O_{Tr}$ (δ_{Tr}) were measured on the WSI column plants, following the method described in Deseano Diaz et al. (2023). For this we used a gas exchange chamber (29 cm diameter, 40 cm length, 27 L volume) that was connected to a laser spectrometer (L2130-i, Picarro Inc. Santa Clara, USA) (Fig. 26b) for 20 minutes per plant during the afternoon between 12 and 3 pm to measure maximum water flux (due to maximum light radiation at 1 pm).

The gas exchange chamber was equipped with an air inlet and outlet, a fan and temperature and humidity sensor humidity and air temperature sensors (RFT-2, precision for RHchamber and Tchamber = 2% and 0.1°C, respectively; METER Group, Munich, Germany) and fans (500F, DC-Axiallüfter, ebm-papst, Mulfingen, Germany). Under mixture (MIX), each gas exchange chamber was divided into two air-tight chambers, each of which was equipped with the features described above. The WSI column plant chambers were constantly supplied with 6 to 12 l min^{-1} of air taken from the climatic chamber (T_{cc} = 20 ± 0.22 °C, RH_{cc} = 50.0 ± 2%) (Fig. 26b; Fig. 27). Measurements of relative air humidity ($RH_{chamber}$, %) and air temperature ($T_{chamber}$, °C) in the gas exchange chambers were used to calculate the vapor pressure deficit (VPD, kPa).

We sampled soil water vapor (swv) for 13 minutes at 13 depths (1, 3, 5, 8, 18, 20, 40, 42, 62, 64, 74, 77 and 79 cm depth) in the WSI columns with gas-permeable probes (Fig. 26c; Fig 27). The probes were flushed, further diluted with dry synthetic air (at 70 and 30 ml min^{-1}, respectively; GF40 mass flow controller, Brooks Instruments, Hatfield, USA), and analyzed online with a laser spectrometer (L2130-i, Picarro Inc., Santa Clara, USA) for isotopic analysis (δ^2H_{swv} and $\delta^{18}O_{swv}$). δ^2H_{soil} and $\delta^{18}O_{soil}$ (δ_{soil}) were assessed from δ^2H_{swv} and $\delta^{18}O_{swv}$ readings considering thermodynamic equilibrium between soil water vapor and liquid phases according to (Rothfuss et al., 2013) (Fig. 27). Data acquisition at a 30-s time resolution as well as the flushing and dilution of the soil gas probes and gas-exchange chambers were automatized in LabView® (NI™, Austin, USA). The raw isotopic data was calibrated following Deseano Diaz et al. (2023) and Kühnhammer et al. (2020) against two soil water vapor standards (δ^2H_{st1} = 102.4 ± 1.4‰ and $\delta^{18}O_{st1}$ = 30 ± 0.3‰, δ^2H_{st2} = –78.4 ± 0.6‰ and $\delta^{18}O_{st2}$ = –18.8 ± 0.1‰).

2.3. Aboveground physiological measurement and root traits

The number of leaves and tillers, the dimensions of the blades (length and width) and sheaths (diameter and length) as well as leaf blade chlorophyll content (SPAD 502Plus, Konica Minolta, Munich, Germany) were manually and non-destructively measured twice a week during growth. We related the transpiration to the total leaf area by adding the area of both sides of the leaves' blades and sheaths, although the latter was close to negligible compared to the former. The leaf blade surface area was calculated considering the measured length of each leaf blade, a constant increasing leaf width over times inferred from regular measurements points, and a coefficient of 0.75 to take into account the oblong wheat leaf shape (Chanda and Singh, 2002). The leaf sheath surface was calculated considering it as a cylinder with an average diameter of 5 mm and a length equal to the maximum leaf sheath-distance of each tiller. The stomata density was obtained by destructively sampling the flag leaf, applying a nail polish to the bottom part and counting the number of stomata on the nail polish impression with a stereo microscope (Axiophot 2, Zeiss, Germany) (Pathoumthong et al., 2023).

During the 4^{th} and 6^{th} week of plant growth, the root traits of the plants in the six MRI columns were monitored non-destructively using a 4.7 T MRI magnet (Magnex, Oxford, UK) and a MR Solutions console (Guildford, UK). We constructed a linear axis on top of the magnet to handle these long and heavy soil columns (16 kg) and integrated this axis into the scanning software. 3D root scans at different soil column depths were realized to fully measure the root traits, which were concatenated afterwards. Signal to noise ratio allowed the detection of roots with a diameter > ~ 350 µm, which was sufficient to visualize the crown, the seminal and part of the lateral wheat root structure. Digital root fresh weight (DRFW, a.u) was obtained at 7 mm-vertical resolution by integrating over each depth interval the intensity of the horizontal MRI signal, following Deseano Diaz et al. (2023) and Ceolin et al. (2025) working with contrasted soil water conditions as well. The MRI signal intensity, which was proportional to the water content of the roots, was used as proxy of the root biomass. Comparison with the destructive analysis showed (WinRhizo™, see next paragraph), that these roots greater than 350 µm for our wheat lines at the booting stage represented 20% of the total root surface area on average across soil layers. Root angles and tips were also automatically extracted by processing the 3D MRI scans at the start-up stage using NMRooting software, and manually verified according to van Dusschoten et al. (2016). Then, the number of root tips was aggregated by layers of 2cm soil depths.

At the end of the experiment (43 DaS), the roots in the WSI columns were destructively sampled from the soil layers 0-6, 6-17, 17-28, 28-39, 39-50, 50-61, 61-

73, 73-80 cm, weighted and scanned (Expression 10000XL Model J181A; EPSON, Japan). The images were analyzed with WinRhizo™ (Regent Instruments Inc., Quebec, Canada) for determination of the root surface per root diameter classes in each of the aforementioned soil layers. The number of basal roots was assessed by counting them manually on the topsoil root scans and the total root biomass after scanning by drying and weighting them. Aboveground biomass was assessed by sampling the leaves, stems and ears, and drying and weighing them. The water use efficiency (WUE, g/L) was calculated as the ratio of whole plant (above- and below-ground) weight to the amount of cumulated transpired water between the sowing and the booting stage.

2.4. Statistics and data representation

Statistical analyses were performed in R (Version 4.2.0; R Core Team 2020). Assumptions of normality and homoscedasticity of model residuals were evaluated using qqplots and Levene tests (Fox et al. 2001). When residuals showed substantial deviations from these assumptions, logarithmic or square-root transformations were applied to stabilize variance and improve residual distributions. The significance of differences was assessed with a linear mixed-effects model using the lme function from the nlme package (Pinheiro and Bates, 2000). Genotype, depth, and water regime were considered as fixed effects, while columns and runs were treated as random effects. We used the following symbols to indicate statistical significance: " ": $p > 0.05$; "*": $p <= 0.05$; "**": $p <= 0.01$; "***": $p <= 0.001$; "****": $p <= 0.0001$. The comparison among treatments were carried out via the emmeans test adjusted with the bonferroni method with the package stat_pwc {ggpubr}. Differences in root tips count depth-related slopes among plant modalities were assessed using estimated marginal trends (emtrends) with post hoc pairwise comparisons adjusted using the Bonferroni correction. To interpolate the plant aboveground parameter evolution (e.g., leaf number) over the time, the local polynomial regression fitting function "loess" was used.

Daily-resolved depth profiles of the relative contribution of RWU to plant transpiration, normalized by the thickness of each layer (fraction of Root Water Uptake; fRWU), were computed from 39 to 42 DaS using the multi-source mixing model Stable Isotope Analysis in R (SIAR) (Parnell et al., 2010) following the method of Couvreur et al. (2020) and Deseano Diaz et al. (2023). The parameters (prior, number of iterations, and values for burn-in and thinning) of the function siarmcmcdirichletv4 of the R package "siar" used are the same as those described in Deseano Diaz et al. (2023). The function uses a Markov chain Monte Carlo algorithm to produce estimated source proportions (water at different soil layers) in the observed product (the plant transpiration). These estimates on soil liquid water (δ_{soil}) and transpired water vapor (δ_{Tr}) isotopic compositions, assumed steady state transpiration yielding to $\delta_{Tr} = \delta_{RWU}$. For each 'plant modality x water treatment' combination, we

had three repetitions of columns measured over four successive days, giving a maximum of twelve fRWU profiles per combination, except when a technical problem during the measurement hindered us from obtaining either the soil profile or the plant transpiration data. The fRWU contribution from 18 and 20; 40 and 42, 62 and 64 cm depth were grouped together to better represent respectively the soil layers 14-30, 30-52, 52-69 cm. The Sink Term (mL min^{-1} cm^{-1}) was calculated as the product of the fRWU (cm^{-1}) and the transpiration rate (mL min^{-1}) calculated from the water vapor mixing ratio measured with the Picarro laser spectrometer, according to the plant transpiration rate formula in Deseano Diaz et al. (2023).

3. Results

3.1. Root and shoot traits

Across plant modalities and water treatments, the total dry biomass (1.7±0.4 g) and root surface area (32±6 dm2) was very similar (Fig. 28). Although the differences were not significant, we note that the MIX led to higher biomass than both DRS and SRS monocultures in WW (respectively 56% and 26% more) but was intermediate under WD (resp. 2% more and 7% less). The root crown number was significantly higher under WW treatment than under WD (water: $p<0.001$). Under both WD and WW treatment, the mixture MIX showed on average higher root crown numbers than both monocultures (12% and 15% less respectively under WW; 5% and 15% less under WD; non-significant (NS)) (Fig. 28). The average root crown angles were similar among the plant modality and the water treatments (Fig. 29).

The digital root fresh weight (DRFW), root tips density and the root surface densities calculated from scanned roots were significantly higher in the topsoil than in the other soil layers (depth: $p<0.001$) (Fig. 28; 30; 31). Thus, the depth of 70% of the cumulative DRFW (D70, cm) deepened with WD from an average depth of 30 cm to a depth of 48 cm (water: $p<0.01$, Fig. 28). Root distribution was greater in the topsoil under the WW treatment than under the WD treatment (10% difference at this soil layer) and the opposite was observed in subsoil layers (depth x water: $p<0.001$), i.e. from 6 to 12% in average at 70-80 cm (Fig. 30). The root surface area of SRS was greater than that of DRS for root diameters between 150 and 300 μm. The opposite was observed in the subsoil (Fig. 32).

The DRFW was greater for SRS than for DRS in the topsoil from 0 to 10 cm, whereas DRS showed higher DRFW at soil depths below 40 cm (Fig. 30) and SRS D70 was shallower than DRS whatever the water treatment (Fig. 28, NS). The root surface densities generally showed the same patterns in some root diameter classes (Fig. 32). Root distribution across the profile in the MIX treatment was generally between SRS and DRS or on the same level with the exception of the 20- to 40-cm layers (Fig. 30). SRS showed a steeper reduction in root tip density with depth, whereas DRS plants maintained higher root tip numbers in subsoil layers and MIX displayed an intermediate response (plant × depth : $p < 0.001$; Fig. 31).

		Root dry biomass (g)		Root total surface (cm^2)		Root crown number		D70 of DRFW (cm)		Stomata density (mm^{-2})		Tiller/Crown root number ratio		Total plant transp. (mL)		WUE (g/L)	
Plant mod.	Water treat.	av	sd	av	sd	av	sd	av	sd	av	sd	av	sd	av	sd	av	sd
DRS	WD	1,55	0,22	2976	220	34	5	-52	13	49.5	17.6	0,29	0,02	2349	148	2,63	0,59
MIX	WD	1,57	0,38	2861	143	40	2	-44	18	46.9	15.8	0,29	0,07	2451	155	2,19	0,31
SRS	WD	1,69	0,51	3281	896	38	7	-47	13	47.1	17.2	0,49	0,09	2517	375	2,65	0,80
DRS	WW	1,38	0,36	2717	671	62	11	-36	14	50.9	17.7	0,18	0,05	2610	580	2,38	0,78
MIX	WW	2,15	0,75	3869	834	73	5	-36	14	46.4	14.2	0,18	0,02	3595	899	1,88	0,27
SRS	WW	1,70	0,39	3394	771	64	16	-21	21	43.8	13.2	0,25	0,12	2831	647	2,52	0,37

Fig. 28. Key root and shoot morphological traits (the total root system dry biomass (g) and surface (cm2), the crown root number per pot and the depth of 70% of the cumulated DRFW (D70, cm); as well as the shoot dry biomass (g), the total leaf surface (cm2) and tiller number per plant) recorded destructively at the elongation stage (43 DaS). The total amount of water transpired by soil column during the whole experiment till the botting stage (in mL) is also represented with their water use efficiency (WUE, g/L, calculated as the dry mass of whole plant per the total plant transpiration) among the culture type, the genotype and water treatment

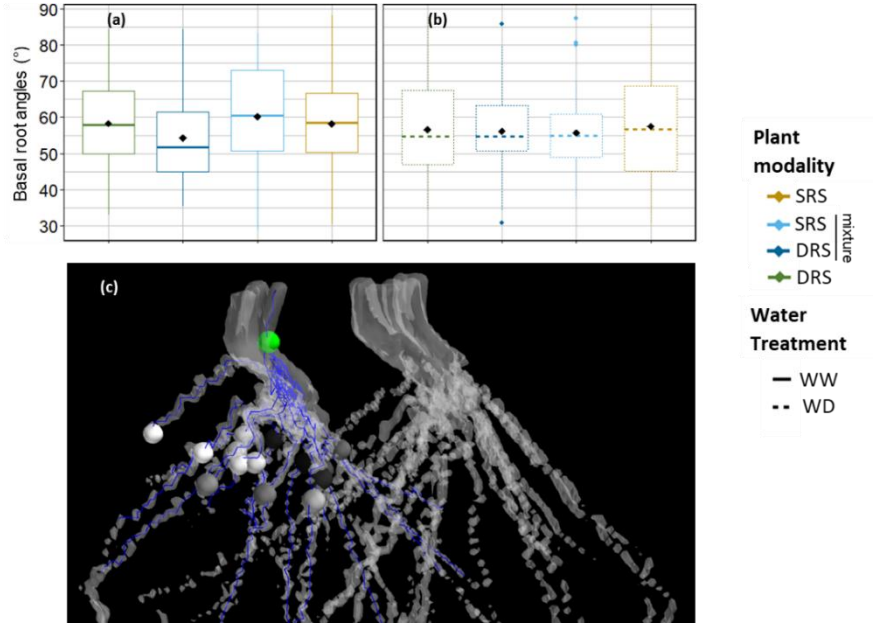

Fig. 29 Distributions of basal root angles for the well watered ("WW", line, panel a) and water deficit ("WD", dots, panel b) for the three plant modalities (DRS in monoculture, dark green color; DRS in mixture, dark blue color; SRS in mixture, light blue color; SRS in monoculture, orange color) measured on the in situ 3D MRI scans at the booting stage. Screenshot of a 3D MRI root scan analysis to measure the root angles of two wheat plants in a soil column (panel c). In blue the seminal roots are traced, in white to black the position of the root seminal at 2cm from the green the stem reference point to calculate the angles.

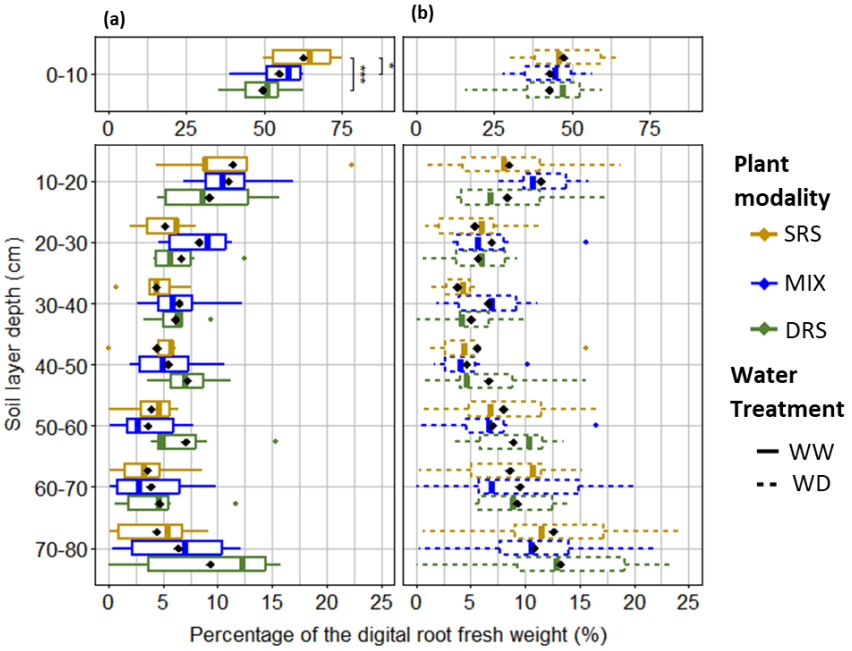

Fig. 30 Distributions of the percentage of digital root fresh weight (DRFW) per 10 cm soil layer, measured in situ by MRI at 43 DaS for the well-watered (WW, lines, panel a) and water deficit (WD, dots, panel b) treatments among the plant modalities (DRS in monoculture, dark green; Mixture – MIX, blue; and SRS in monoculture, orange) (n=6).

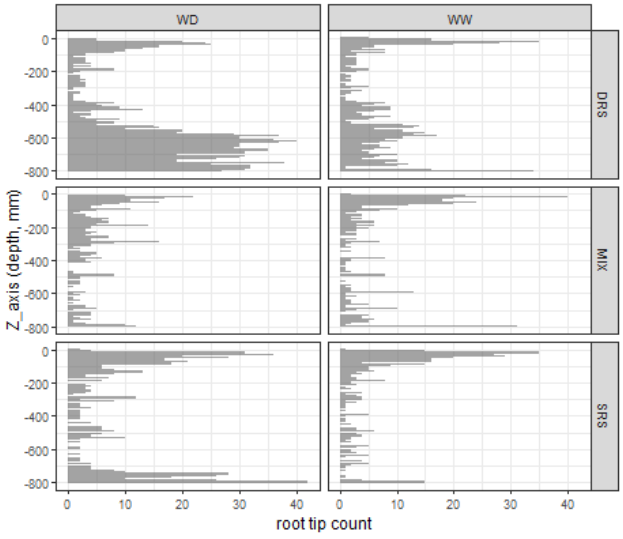

Fig. 31 Cumulated profiles of root tips amount per 2 cm soil layers, facet grid by plant modality DRS, MIX, and SRS, and for WW and WD treatments (n = 3)

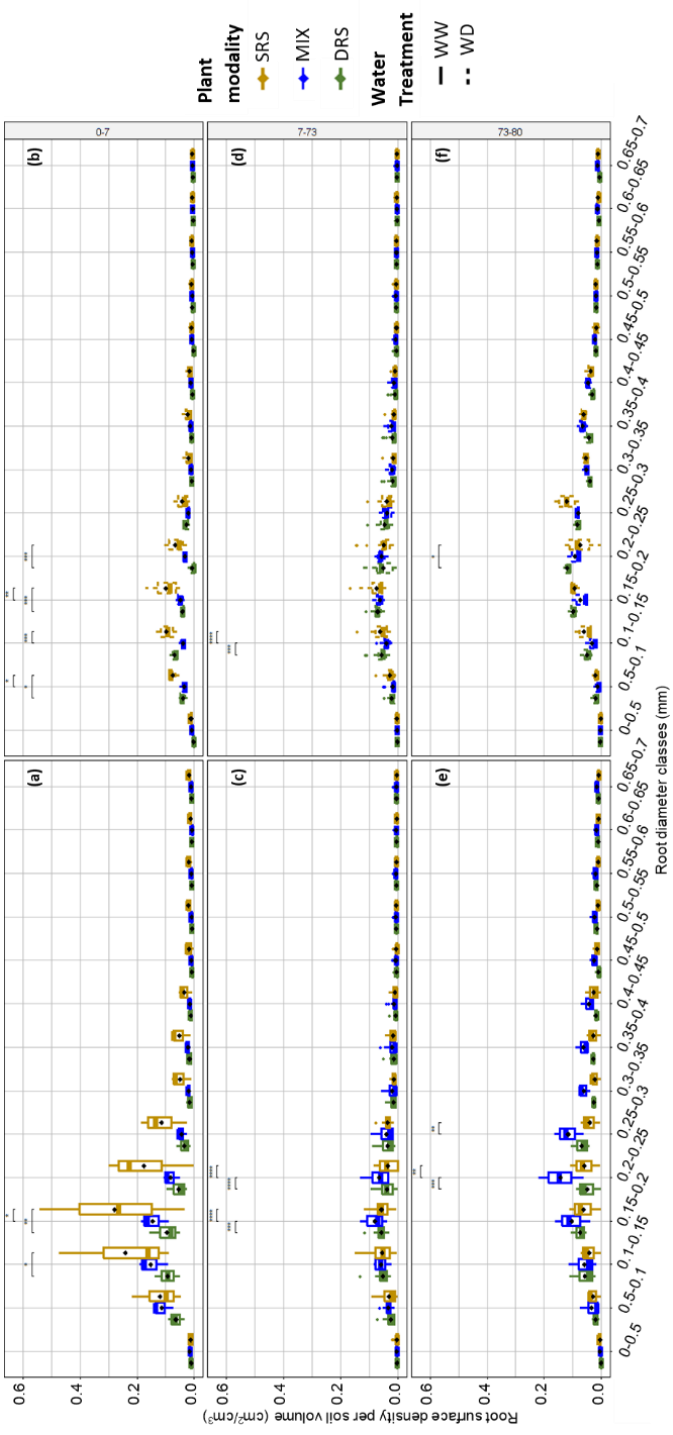

Fig. 32 Distributions of the root surface density per soil volume (cm2 cm-3) as per root diameter class, measured for the destructive root sample scans at the booting stage, for the well-watered ("WW", lines, panel a, c, e) and water deficit ("WD", dots, panel b, d, f) treatments, in the topsoil (0-7cm depth, panel a, b), intermediate soil layers (7-73cm depth, panel c, d) and subsoil (73-80cm depth, panel e, f), among the plant modalities (DRS in monoculture, dark green color; Mixture – MIX, blue color; and SRS in monoculture, orange color) (n=3 in top- and subsoil, n=18).

The plant shoot dry biomass at the elongation stage was not significantly different among the treatments and modalities (2.6 ± 1.1 g). Differences between water treatments began to appear on the surface at 35 DaS (stem elongation) and were significant at the booting stage (43 DaS). At this stage, the water deficit treatment significantly decreased the plant shoot surface able to transpire (water: $p<0.05$) (Fig 33 a-d) and the tiller number per plant became significantly lower for DRS as compared to SRS (plant: $p<0.05$), which was pronounced for the WD treatment (water x plant: $p<0.01$) (Fig 33 e-h). However, we noted no significant differences for the leaf stomatal density between the two genotypes (Fig. 28).

The biomass and surface area ratios of aboveground and belowground organs remained stable regardless of water treatment and plant modality (resp. 2.92 ± 0.72 and 0.75 ± 0.29, NS, Fig. 34a, c). The shoot-root water content ratio disparities were minimal indicating that the relative shoot/root water status could have been homeostatically regulated, independent of genotype and irrigation treatment (from 0.87 to 0.95, NS, Fig. 34b). The tiller/crown root ratio, however, was significantly higher under WD than WW (water: $p<0.01$), and SRS showed higher values than MIX and DRS (plant: $p<0.05$, 34d).

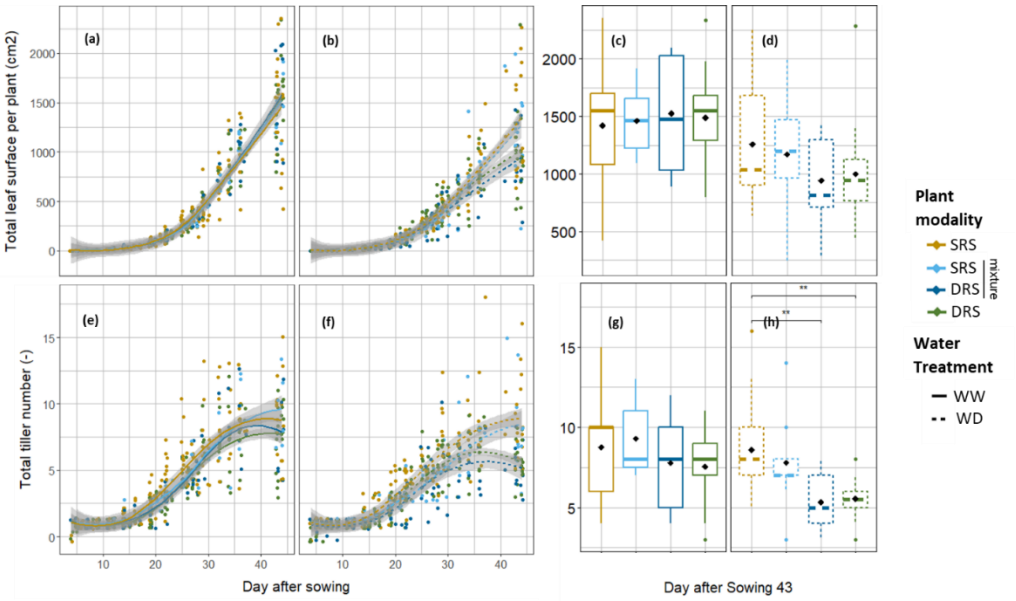

Fig. 33 Total leaf area per plant (in cm^2, panels a, b, c, and d), and number of tiller per plant (panels e, f, g, and h) for the four plant modalities (DRS monoculture, dark green; DRS mixture, dark blue; SRS mixture, light blue; SRS monoculture, orange) under well-watered conditions (WW, lines, panels a, c, e and g) and water deficit (WD, dots, panels b, d, f and h), throughout growth, modelled by LOESS regression (Locally Estimated Scatterplot Smoothing, 95% confidence interval) (a, b, e and f) and at 43 DaS (c, d, g and h) (n = 18 for SRS and DRS in monoculture, n = 9 for SRS and DRS in mixture).

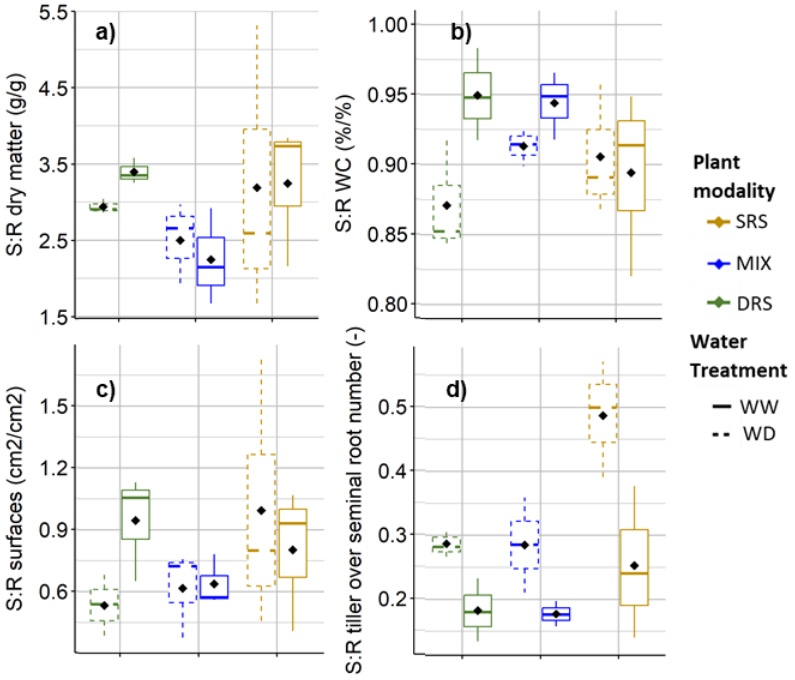

Fig. 34 Distributions of shoot-to-root ratio (S:R) for (a) the dry matter (g g^{-1}); (b) the water content (% $\%^{-1}$); (c) the surface ratio (cm^2 cm^{-2}); (d) the tiller number to seminal root number (–) measured at 43 DaS for three plant modalities (DRS in monoculture, dark green; MIX, blue; SRS in monoculture, orange) under well-watered (WW, solid lines) and water deficit (WD, dashed lines) conditions (n = 3)

3.2.

3.2. Soil water status

With regard to soil water status, a gradual increase in average pF was observed in the different soil horizons as the plants developed during the 43 days after sowing (Fig. 35). The average value in pF was lower than 3 in WW due to the regular addition of water to the top of the column, but exceeded this value in WD for the topsoil from 30 DaS onwards. During the early stages of plant development, soil water availability was fairly similar across the three treatments, and even higher in the mixture than in the monoculture (which could reflect less intense water uptake). From 35 days after sowing, which corresponds to the transition between the elongation and tillering stages, the trend in the subsoil (-42, -64, -74, and -79 cm depth) changed in both WD and WW, with MIX decreasing soil water availability quicker than the two monocultures (Fig. 25).

More precisely at the booting stage (between 39 and 42 DaS), the matric potential was significantly higher in water-deficit (WD) conditions (pF 3.7 ± 0.4 on average) than in well-watered (WW) conditions (pF 2.8 ± 0.6) (water: $p < 0.01$, Fig. 35; 36). The Leaf Water Potential (LWP) was also recorded to be lower under water deficit conditions than under well-watered conditions (resp. 0 to-0.25 MPa vs -0.25 to -1.7 MPa; Fig. 37) and this difference increased with each passing day. The total transpiration throughout the entire experiment (water: $p<0.05$, Fig. 28) as well as the hourly transpiration rate between 39 and 43 DaS (water: $p<0.001$, Fig. 38) were significantly lower under WD. However, the WUE was similar across water treatments and plant modalities (NS, 2.38 ± 0.52 mL g^{-1}, Fig. 28).

The SMP for the different plant modalities showed significant differences at each depth (plant x depth: $p<0.0001$). In the interactions with water treatment, we observed under WD that SMP profiles all decreased from the topsoil to the subsoil layers for all three plant modalities. Under optimal WW conditions, the SMP profiles of SRS and DRS were contrasting (Fig. 35). For SRS, SMP profile decreases from dry topsoil (2.62 ± 0.42) to moister subsoil (2.43 ± 0.73). For DRS, the SMP increased from the moist topsoil (2.42 ± 0.35) to the drier subsoil (2.98 ± 0.39), with a local maximum in the middle at 42 cm (3.16 ± 0.34). MIX behaved intermediately, similar to DRS (from moist topsoil to drier subsoil) but with more variability and a shallower local maximum than the DRS one, at 20 cm (3.28 ± 0.49) (Fig. 35).

Thus, this effect of water treatment differed between plant modalities and between profiles, with SRS showing an almost constant difference at all depths, while DRS showed pronounced differences in the upper soil layers and the MIX treatment showed the smallest difference at a depth of 20 cm (plant x water x depth: $p<0.001$, Fig. 28). When we compared the matric potential "WW-WD" in MPa and not on a logarithmic scale, we found that the largest absolute difference in SMP was in the topsoil and was the most pronounced for SRS (Fig. 36).

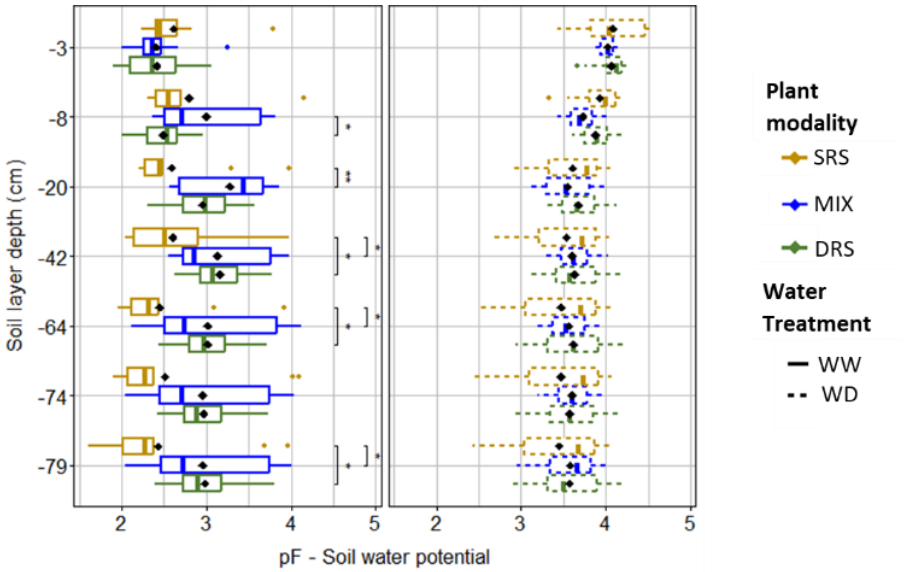

Fig. 35 Soil depth profile distribution of water potential between 39 and 42 DaS in the afternoon during the plant transpiration measurements, expressed as pF, for the well-watered (WW, lines, panel a)) and water deficit (WD, dots, panel b) treatments among the plant modalities (DRS in monoculture, dark green, panel a; Mixture – MIX, blue, panel b; and SRS in monoculture, orange, panel c) (n=3).

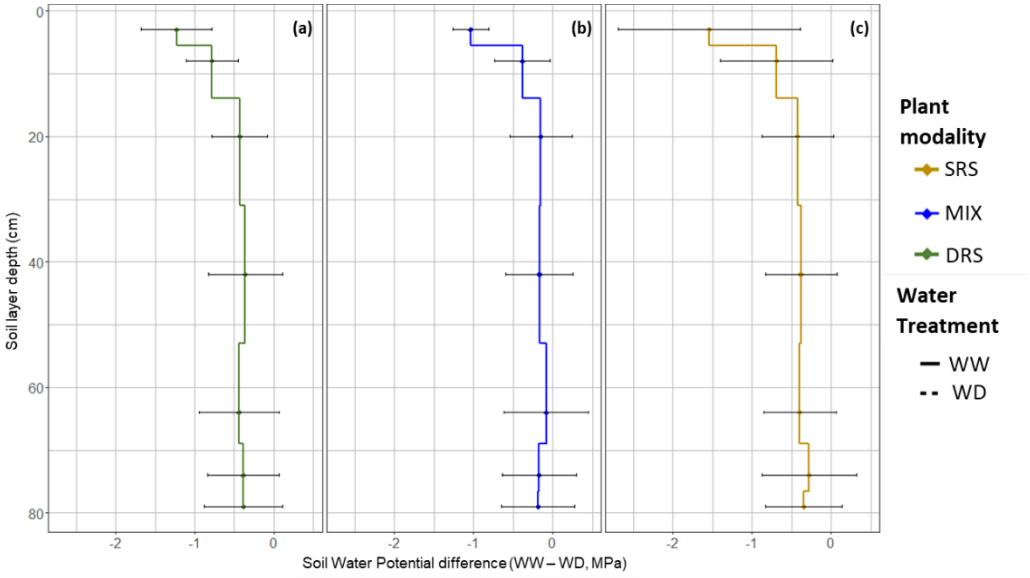

Fig. 36 Soil matric potential difference, expressed as MPa, measured with the Teros21 sensors, between absolute values of matric potential in water deficit ("WD") and well watered ("WW") conditions for the three plant modalities (DRS in monoculture, dark green color, panel a; Mixture – MIX, blue color, panel b; SRS in monoculture, orange color, panel

c), across ten soil layers (0-2; 2-4; 4-7; 7-14; 14-30; 30-52; 52-69; 69-76; 76-78; 78-80 cm). Standard deviations are indicated by black bars.

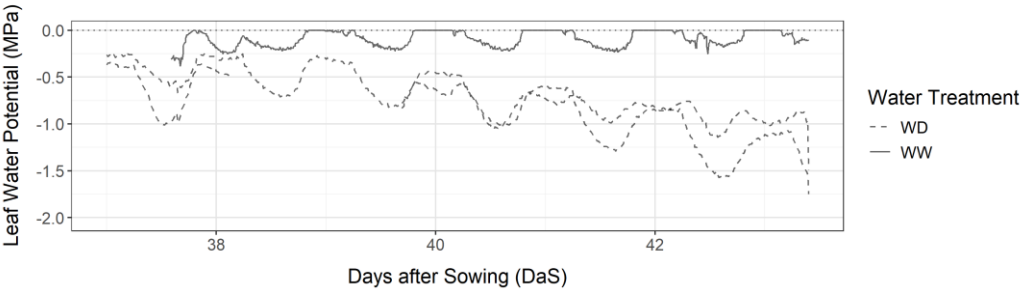

Fig. 37 Leaf Water Potential (in MPa) measured by leaf psychrometer from 37 to 43 DaS of a plant growing under well-watered conditions ("WW", line) and two plants under water deficit conditions ("WD", dots). (n=1)

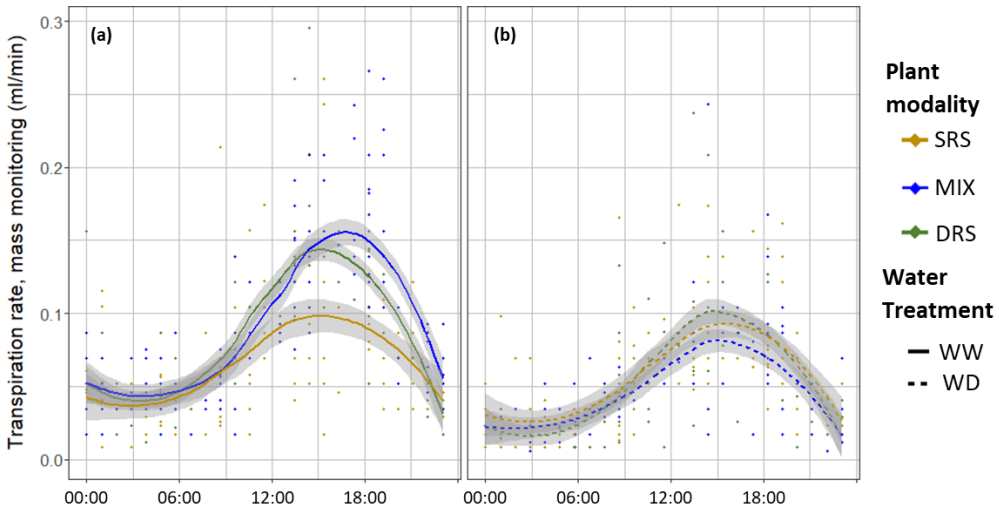

Fig. 38 Measurement points modeled by LOESS (Locally Estimated Scatterplot Smoothing) regression with 95% confidence interval from 39 to 43 DaS of transpiration rate (in mL/min) monitored continuously by scale bellow the soil columns, for the three crop modalities (DRS in monoculture, dark green color; Mixture – MIX, blue color, and SRS in monoculture, orange color) under well watered ("WW", lines, panel a) and water deficit ("WD", dots, panel b) conditions. (n=3)

3.3. Root water uptake

At the booting stage between 39 and 42 DaS, the wheat roots extracted water more intensively from the topsoil layer (the top 7 cm; 4.04 ± 0.75 % cm^{-1} in WW; 4.33 ± 1.4% cm^{-1} in WD), less intensively from subsoil (69 to 80 cm; 1.46 ± 0.65 % cm^{-1} in WW; 1.96 ± 1.03% cm^{-1} in WD). The least of the fRWU contributions came from intermediate soil layers (0.67 ± 0.34% cm^{-1} WW; 0.57±0.30% cm^{-1} WD) (Fig. 39). However, this pattern changed with the reduction in water availability with the root water uptake intensifying mainly in the subsoil (also to a lesser extent in the topsoil) and decreasing in the intermediate soil layers (depth x water: $p<0.001$).

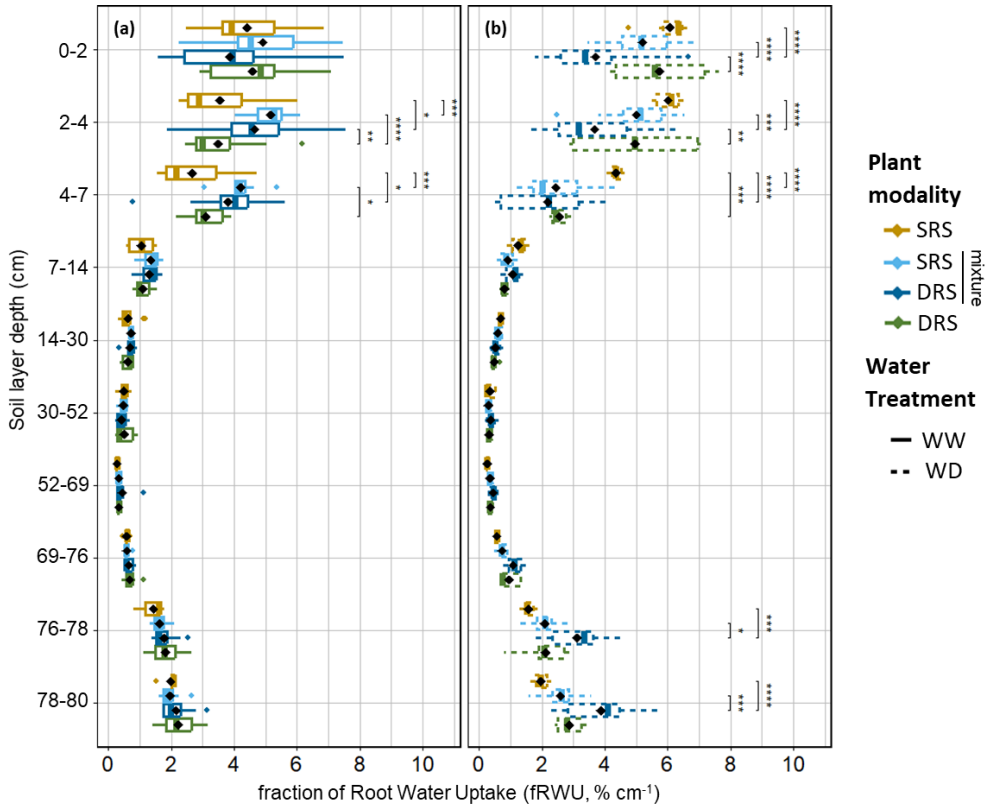

Fig. 39 Fraction of the Root Water Uptake (fRWU, % cm^{-1}) distributions (panels a and b) and mean values (panels c and d) estimated between 39 and 42 DaS , for the four plant modalities (DRS in monoculture, dark green; DRS in mixture, dark blue; SRS in mixture, light blue; SRS in monoculture, orange), across ten soil layers (0-2; 2-4; 4-7; 7-14; 14-30; 30-52; 52-69; 69-76; 76-78; 78-80 cm) under well-watered (WW, lines, panel a) and water deficit (WD, dots, panel b) conditions (n=7-12).

The fRWU profiles were also affected by the genotypes with SRS having extracted more water from the topsoil layer than DRS while the opposite was observed in the subsoil layer (depth x plant: $p<0.001$) (Fig. 39). These differences between DRS and

SRS were more prominent for WD compared to WW (water x depth x plant: $p<0.001$). We observed this same trend within the mixtures under WD, where SRS in mixture ($4.23 \pm 1.54\%$ cm^{-1}) extracted more water than DRS in mixture in the first 7 cm soil layer (3.19 ± 0.87 cm^{-1}) and less in the 76-80 cm subsoil layer ($2.34 \pm 0.35\%$ cm^{-1} SRS in mixture; $3.50 \pm 0.54\%$ cm^{-1} DRS in mixture). Thus, under WD we noted a constant absolute difference between DRS and SRS (both in monoculture and mixture) of $1.09 \pm 0.46\%$ cm^{-1} from 0 to 7 cm and from 76 to 80 cm (Fig. 39b).

In a similar vein, it was observed that in mixtures, the absolute root water uptake (Sink Term; mL min^{-1} cm^{-1}) of SRS in the topsoil were higher than those of DRS under WW ($p < 0.001$) (Fig. 40a). Under WD, the SRS also absorbed more water than the DRS between 0 and 2 cm ($p < 0.05$), but in the subsoil DRS absorbed much more water than SRS ($p < 0.001$) (Fig. 40b). However, in monoculture under WW, DRS transpired significantly more than SRS (Fig. 38) and differences appeared in the topsoil ($p<0.05$) (Fig. 40c) while under WD, with more equivalent transpiration, DRS absorbed more water than SRS in the subsoil ($p < 0.05$) (Fig. 40d). In addition to this relative difference between SRS and DRS, it was found that both genotypes in mixture under WD reduced their water extraction from the topsoil compared to monoculture (-1.2% cm^{-1} on average for layers 0 to 7 cm; at these depths, water x plant: $p < 0.001$). In contrast, both increased their fRWU from the subsoil layers in mixture (+0.5% cm^{-1} for layers 69 to 80 cm; at these depths, water x plant: $p<0.001$) (Fig. 39b). However, this was reversed under WW, with both SRS and DRS in mixture extracting more water from the surface than the same genotypes in monoculture (+2.0% cm^{-1} from 2 to 7 cm depth) (Fig. 39a).

The amplitude of root water uptake plasticity in response to water deficit differed for each plant modality (Fig. 41). By calculating the difference between the fRWU profiles under WD and those under WW, it can be observed that SRS exhibited a significantly higher level of contribution in the initial 30 cm of soil in order to cope with water deficiency. This result was less pronounced for DRS in subsoil, but it greatly increased the amplitude of the fRWU's shift toward subsoil (i.e., its "natural niche") in response to water deficit. In the context of mixture, both DRS and SRS exhibited comparable WW-WD plasticity profiles for fRWU, which resulted in a decrease in their contribution in the topsoil and an increase in the subsoil. However, this effect was more pronounced for DRS than for SRS (Fig. 41).

When the vertical distribution of fRWU (% cm^{-1}) and root biomass density (dDRFW, % cm^{-1}) were compared layer by layer, it was observed that most points were proportional to a 1:1 line (Fig. 42). The mixed linear regression of dDRFW explaining fRWU, taking into account the random effect of depths, shows a conditional R^2 of 0.67. Two main areas were identified where biomass and water uptake values were found to be non-proportional. Firstly, in the topsoil (0-4 cm), root biomass densities were found to be almost twice as high as their respective water uptake fractions.

Secondly, in the subsoil, between 76 and 78 cm deep, the fRWUs were much higher than their corresponding root biomasses. Furthermore, it was observed that for the SRS under WD at 4-7 cm, the fRWUs exhibited higher values in comparison to the dDRFWs (Fig. 42).

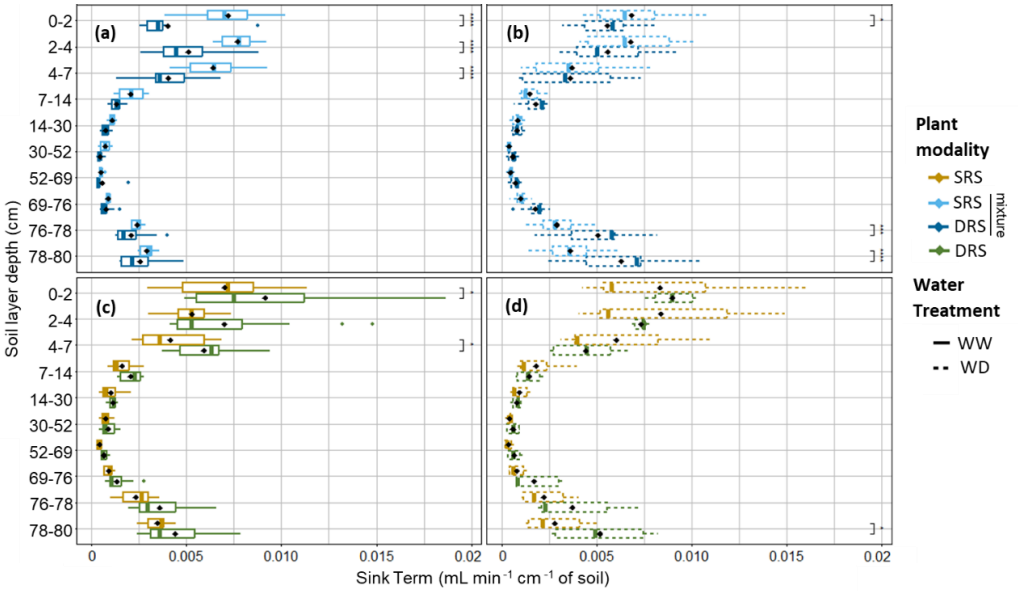

Fig. 40 Distributions of the Sink Term (mL min^{-1} cm^{-1}) estimated between 39 and 42 DaS, for the four plant modalities (DRS in monoculture, dark green; DRS in mixture, dark blue; SRS in mixture, light blue; SRS in monoculture, orange), across ten soil layers (0-2; 2-4; 4-7; 7-14; 14-30; 30-52; 52-69; 69-76; 76-78; 78-80 cm) under well-watered conditions (WW, lines, panels a and c) and water deficit (WD, dots, panels b and d) (n=7-12).

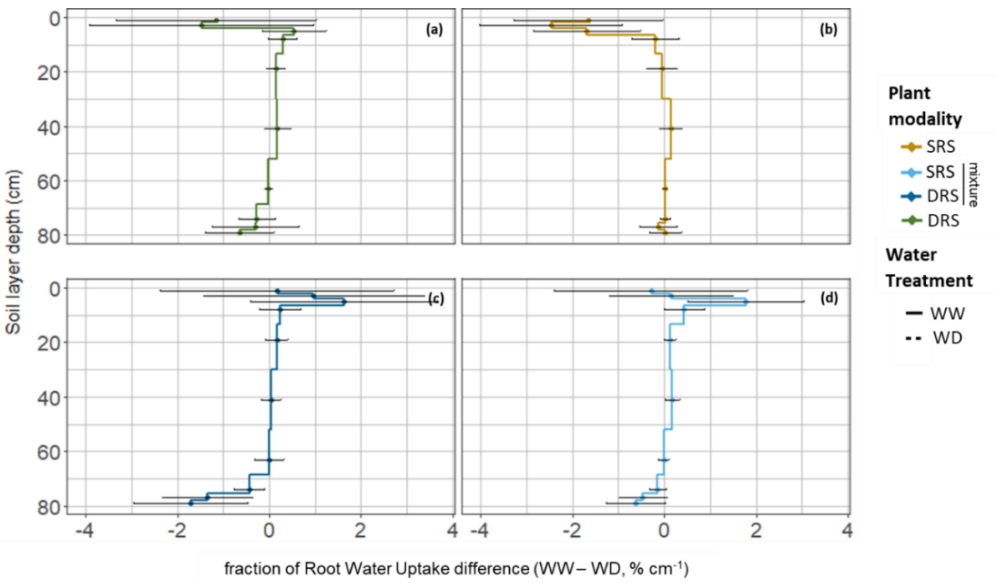

Fig. 41 Differences of fraction of the Root Water Uptake (fRWU, % cm^{-1}) estimated between 39 and 42 DaS between water deficit (WD) and well-watered (WW) conditions for the four plant modalities (DRS in monoculture, dark green, panel a; SRS in monoculture, orange, panel b, DRS in mixture, dark blue, panel c; SRS in mixture, light blue, panel d), across ten soil layers (0-2; 2-4; 4-7; 7-14; 14-30; 30-52; 52-69; 69-76; 76-78; 78-80 cm). Standard deviations are indicated by black bars (n=3).

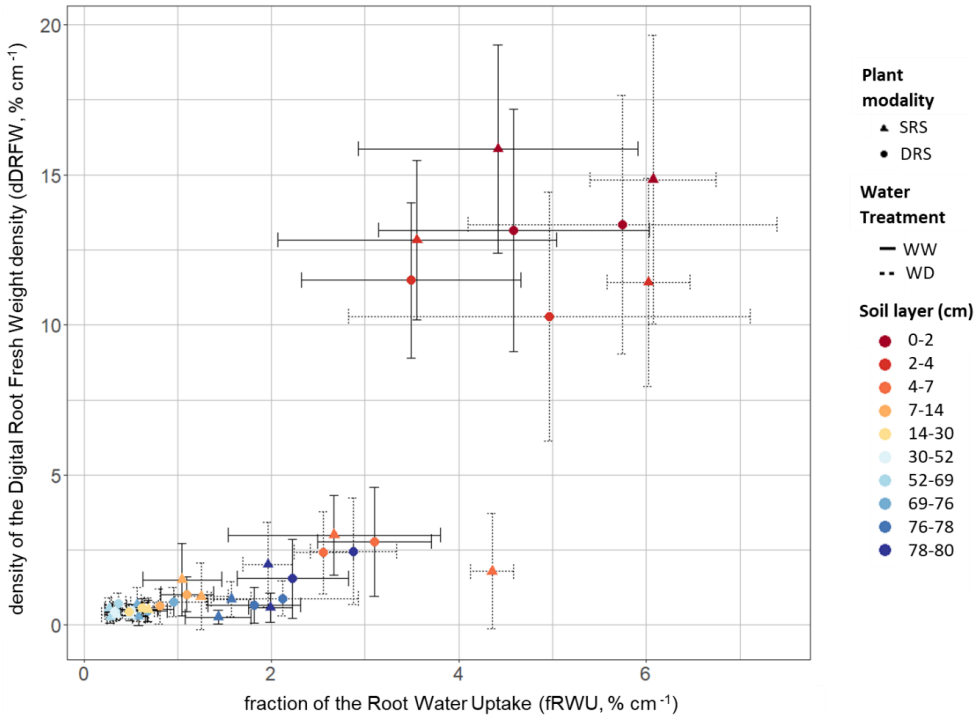

Fig. 42 Density of the Digital Root Fresh Weight (dDRFW, % cm^{-1}, measured at 43 DaS) over the fraction of Root Water Uptake (fRWU, % cm^{-1}, estimated between 39 and 42 DaS). The points represent the average value of two plant modalities (DRS in monoculture, circle shape; SRS in monoculture, triangle shape), across ten soil layers (0-2; 2-4; 4-7; 7-14; 14-30; 30-52; 52-69; 69-76; 76-78; 78-80 cm) under well-watered conditions (WW, lines) and water deficit (WD, dots). Black bars indicate standard deviations.

4. Discussion

4.1. Root traits and water uptake

We corroborated the first hypothesis, namely that the SRS genotype in monoculture extracts more water in the topsoil layers than the DRS genotype in monoculture, and the converse was observed in the subsoil layers, especially under chronical water deficit conditions (Fig. 39; 40). The soil pF profiles and LWP at this booting stage are consistent with this, showing significant differences between genotypes, reflecting contrasting histories of root water (Fig. 35; 36; 37). Previous modeling studies have shown that root ideotype water uptake profiles can be partially explained by root biomass and morphology distributions (Fort et al., 2017; McMurtrie et al., 2012; Bramley et al., 2009). This was observed in our experimental study as the distribution of root biomass, fine root surface and root tip density exhibited higher values in the topsoil for SRS and in the subsoil for DRS (Fig. 28; 29; 30; 31; 32). Lattacher et al. (2025b) also observed in the same experiment, following a ^{13}C-CO_2 labelling, a trend towards an increased $\delta^{13}C$ signal in the subsoil roots for MIX and DRS compared to SRS in both water treatments, thus confirming the contrasting depth-related root activities exhibited by these genotypes.

While the root biomass density profile (dDRFW, % cm^{-1}) can explain most (67%) of the variability in fRWU distribution (% cm^{-1}) for both genotypes in monoculture, this relation was not constant at all depths - water uptake by root biomass units was lower in the topsoil and higher in the subsoil (Fig. 42). This result reflect the dominant hydraulic role of the structural root fraction in determining bulk water transport, while the residual 33% unexplained variance may partly correspond to fine-root-mediated uptake processes occurring below the MRI detection threshold (~300 µm, corresponding to the voxel resolution of the 4.7 T imaging system used in this study). Moreover, physiological processes such as suberization, cambial growth and root hair loss may affect the water uptake properties of the oldest roots in the topsoil, as such alterations have been reported in wheat and other Poaceae during earlier stages of development (Guhr et al., 2025; Kreszies et al., 2019; Schneider et al., 2020; Terletskaya et al., 2020).

It was noteworthy that, while the disparity in basal root angles between the two genotypes – the initial selection criterion – proved significant in the early stages of development (Rambla et al., 2022), in our experiment at booting stage these differences were only marginal and no longer significant (Fig. 29). This highlights the fact that the early characterization of root traits was not necessarily a good indicator for later stages. Therefore, it was imperative to validate these root traits results at the different studied stages of development (Comas et al., 2013).

We acknowledge that our experimental system standardized soil and climate conditions, which are more heterogeneous in agricultural fields. However, we believe

this simplification was necessary in order to observe specific plant responses to water treatments and a first step to prove the concept. Our conditions were based on a typical temperate climate in Western Europe, comparing average (WW) or dry (WD) spring conditions. We used soil from the same pedoclimatic ensemble, compressed to an average bulk density observed in the field (Weihermüller et al., 2007). We simulated rainfall using surface irrigation and modulated light intensity sinusoidally to reproduce average daily sunlight variations. Additionally, we induced a temperature gradient between the light-exposed topsoil and the insulated subsoil, similar to what was found in field conditions (Wang et al., 2025). These efforts enabled us to obtain root distribution patterns similar to those observed in field conditions in the same loamy soil or in other studies, consistently higher in the topsoil than the subsoil (Nguyen et al., 2024; Svoboda et al., 2020; Zhao et al., 2023). However, the depth of our soil column (80 cm) may have caused root accumulation, concentrating processes that typically span tens of centimeters into the final few centimeters (Fig. 30).

Another experimental design element that may have influenced the comparison between genotypes is the method of water application. In our experiment, the soil surface was irrigated, periodically rewetting the topsoil layers (neglecting the few mL added at five different depths for the water stable isotopic labelling). This occurred more frequently under WW than WD, but was present in both. This surface irrigation regime could have created a structural advantage for SRS, whose root system is preferentially distributed in the topsoil layers most directly recharged by each irrigation event. Conversely, DRS roots, which were relatively more developed in the subsoil, benefited from water percolating downward through the soil profile with a time lag and at a lower water potential than the freshly wetted surface. Under field conditions, precipitation and irrigation originate at the surface. However, the greater lateral heterogeneity of field rainfall and the preferential flow pathways created by macropores partly compensate for the vertical asymmetry by delivering water to greater depths more rapidly than in a uniformly packed column (Beven and Germann, 2013). The systematic rewetting of the topsoil by surface irrigation may have contributed to SRS's better drought resistance observed in our study. This occurred independently of any intrinsic trait advantage by ensuring the preferred rooting niche of SRS remained at a less negative water potential than DRS throughout the experiment. This interpretation is consistent with the finding that topsoil pF values decreased more for SRS than for DRS under WW and that SRS had a higher topsoil fine root surface area (Fig. 32; 35).

4.2. Genotypes strategies facing water deficit

In the present study, we observed that the average fRWU and root biomass for all plant modalities in the subsoil under WD increased. This strategy was more pronounced for DRS than SRS in monoculture, reflecting their natural niche preferences (Fig. 30). However, in the topsoil under WD, where water availability has been shown to decrease significantly (from pF 2.5 to 4), the fRWU increased on

average. This increase was driven by maintained high contributions from DRS in monoculture and an increase in SRS in monoculture, with no significant change in root biomass (Fig. 35). This finding aligned with the extant literature, which also indicated that several grassland and crop species facing a water deficit showed a preference for maintaining or even increasing root water uptake from the topsoil, despite its lower soil water availability (Deseano Diaz et al., 2023; Prechsl et al., 2015; Angeletti et al., 2022). This finding subsequently invalidate the second hypothesis, which postulated that water resource availability may predict root water uptake, as proposed by (Kulmatiski et al., 2017). Thus to correctly estimate root water uptake, we showed that it was essential to consider both the environmental factors, such as soil water availability, and plant individual root traits, including distribution of root biomass and morphology (Delval et al., 2024; Müllers et al., 2023; Rickard et al., 2025).

Furthermore, the root water uptake strategy in response to water deficit was not uniform, but rather contingent on the genotype-specific root traits and those of the neighboring plant. The water niches differences could be partially attributable to the distribution of fine root surface area (less than 250 μm), which was more abundant in the topsoil of the SRS than the DRS under WD (Fig. 32). This root trait may have resulted, for SRS under WD, in better root hydraulic conductance and greater root exudation in this soil layer, enhancing the soil's hydro-physical properties in the rhizosphere (Bramley et al., 2009; Doussan et al., 2024; Le Gall et al., 2024; McDougall and Rovira, 1970). In addition, arbuscular mycorrhizal fungi (AMF), which have been shown to be able to improve RWU, have been found to be more prevalent in the topsoil of SRS monoculture, and conversely in the DRS monoculture subsoil (Lattacher et al., 2025c; Zaman et al., 2024).

Most articles on root traits suggest that deep roots improve the plant's resistance to drought (Bagale et al., 2025; Kou et al., 2022; Odone et al., 2024; Shoaib et al., 2022; Uga et al., 2013). However, this was not what we observed in our study. Although the root traits and RWU of DRS were oriented toward the subsoil, where water was more accessible, SRS oriented toward topsoil resisted better to water deficit, as evidenced for DRS by the higher reduction in the number of tillers and total leaf area from 35 days after sowing, i.e., nearly a week before the booting stage studied (Fig. 33). Similar evidences have been demonstrated for trees (*Juglans regia*) and perennials (*Cichorium intybus L.*) that increasing the proportion of deep root water uptake facing water deficit does not guarantee greater water deficit resistance (Rasmussen et al., 2020; Sun et al., 2011). To the best of our knowledge, this was the first demonstration of this phenomenon for the wheat. This observation could be explained by aboveground traits such as higher stomatal density for DRS than SRS, resulting in a reduce drought tolerance (Hasanuzzaman et al., 2023; Robertson et al., 2023)(Table S1). The deep-rooting genotype may have also incurred a higher metabolic cost and a greater investment in photoassimilates than SRS to maintain deep root activity,

leading to reduced shoot growth or limited stomatal regulation in response to prolonged water deficit (B. Li et al., 2022; Tardieu, 2012).

4.3. A niche complementarity in the wheat genotype mixture?

The third hypothesis of our study focused on the conservation of contrasted root water uptake distribution of the two genotypes in the mixture, allowing for "hydrological niche segregation" (Zhao et al., 2024). In the mixture, the two genotypes exhibited distinct fRWU profiles corresponding to their respective preferred niches, a particularly significant characteristic under water-deficient conditions (Fig. 39 and 41). Lattacher et al. (2025b) used an independent method involving ^{15}N labeling to demonstrate that the SRS genotype in monoculture extracted more nitrogen (enabled by the root water uptake, which contains nutrients) from the topsoil than the DRS, with a more pronounced effect in mixtures under water deficit conditions (Gorska et al., 2008; Plett et al., 2020). These observations supports the view that slight variations in root biomass distribution between two root systems developed in the same soil profile (Fig. 30) can have a significant impact on water uptake patterns (Fig. 39; Kulmatiski et al., 2020). The maintenance, or even increase, of these contrasting nutrient and water uptake patterns by the genotypes allowed better spatial distribution of access to these resources under water deficit in the mixtures, which can partly explain the high or higher yield and protein quality in such condition (Vidal et al., 2020a; Kong et al., 2023a; Stefan et al., 2025b).

Furthermore, it was observed that, in addition to niche complementarity in terms of access to water and nutrients, the SRS and DRS mixtures were associated with an increase in fRWU towards the subsoil layers and a decrease in the topsoil layer in situations of water deficit (Fig. 39 and 41) compared to the monocultures. In addition, a significantly higher number of seminal roots was observed in the mixture than in the two monocultures, regardless of water treatment (Fig. 28). According to Lynch (2022), this high number of taproots could have be linked to increased foraging in the topsoil, leading to increased competition at the surface and forcing a shift to deeper horizons. However, no significant faster diminution of water availability in the topsoil of the MIX treatment compared to the two monocultures was observed before the end of the elongation phase and until the beginning of the stem elongation phase (35DaS) (Fig. 25), which could have forced them to increase their contributions from the subsoil layers. Therefore, surface competition at early vegetative stages between individual plants would not be sufficient to fully explain the process of niche displacement towards the subsoil in mixture.

The emerging niche-shift in mixture towards subsoil layers would be therefore the result of the interaction of the two genotypes, compared to their behavior in monoculture. To our knowledge, this was the first documented instance of this phenomenon being observed among genotypes of the same species, specifically

Triticum aestivum L. But this emerging pattern of water uptake niche-shift toward subsoil layers has been observed between different tree species (Demir et al., 2024), grassland species (Guderle et al., 2018) and crop species (Schmutz and Schöb, 2023) compared to monocultures. In order to understand this phenomenon, the sole perspective of higher topsoil competition between individuals faced with the scarcity of the same resource to exploit (Tragedy of the Commons) during the early stages of surface development was not sufficient. (Montazeaud et al., 2025a) showed that wheat variety mixtures actually reduced root competition for water and nitrogen between individuals during the early stages of development. Indeed, our study did not observe any greater initial depletion of soil water in mixed crops compared to monocultures, indicating that there was no early increase in water extraction competition.

We therefore propose that mechanisms enabling recognition of whether another individual belongs to the same genotype may have been at work through chemical communication between roots, leading to changes in their individual physiology and function (e.g., number of shoots and primary roots, and deeper water uptake). In our study, this communication could have been mediated by soluble pathways, as demonstrated by Ghatak et al. (2025) for several dozen wheat genotypes. Each genotype exudes a distinct metabolome, capable of inducing a specific physiological response in neighboring plants of a different genotype (e.g., allelopathy or allelobiosis; Mathieu et al. (2025)). During the four days of fRWU measurement, if this communication existed, it could only have been maintained underground in a mixture, as each individual was isolated in two gas exchange chambers independent of each other.

A further structural observation in the context of niche complementarity was the significantly lower root tip density (RTD) recorded in the mixture treatment compared to the two monocultures, regardless of water treatment (Fig. 31). Root tips are primary sites of root elongation, water and nutrient absorption, and exudate release (Kuzyakov and Razavi, 2019); therefore, their reduction in the mixture is significant. Two non-exclusive interpretations may explain this pattern. First, chemical root-to-root communication between the two genotypes may partially suppress individual root foraging. This is consistent with reduced topsoil water competition observed in the mixture and with Montazeaud et al.'s (2025b) findings on reduced root competition in wheat variety mixtures. In this case, the reduced RTD may reflect an adaptive reduction of competitive root proliferation in favor of a more spatially partitioned, resource-efficient root architecture. In this interpretation, each genotype invests less in producing new root tips in zones occupied by neighbors, redirecting growth toward preferred niche depths. This hypothesis is consistent with the observations on the carbon exudation in this same experiment that were constantly lower in mixture than in monocultures reported by Adrian Lattacher et al (2025b). Second, the lower RTD in the mixture could partly reflect a methodological artifact of the MRI-based analysis. Root tips with a diameter below the 300 µm detection threshold are not captured by NMRooting. If the mixture stimulates the production of finer-diameter lateral roots at

the expense of thicker primary root tips, these would be invisible in the MRI scan, yet visible in the WinRHIZO analysis after the destructive sampling. Indeed we observed (Fig. 32) significantly higher fine root surface area per unit depth in the subsoil for MIX under WW but not under WD, which can then also be consistent with this second interpretation.

In the context of water deficit, no substantial disparities in total transpiration were observed among the various modalities (WD-DRS: 2349 ± 148 mL; WD-SRS: 2517 ± 375 mL; WD-MIX: 2451 ± 155 mL per plant; NS, Fig 28). Under these conditions, the three modalities displayed similar diurnal transpiration curves, with a single midday peak reaching approximately 0.08–0.10 mL min^{-1} and a significant reduction relative to WW (water: $p<0.05$, Fig. 38). This suggests that under chronic water deficit, fRWU niche complementarity in the mixture thus operated primarily through spatial partitioning of a shared resource, consistent with the theoretical expectation that complementarity does not necessarily entail an increase in per-capita demand (Loreau and Hector, 2001). However, under higher water availability conditions, a distinctly divergent pattern became evident. The mixture exhibited a substantially higher water demand per plant than either DRS and SRS in monoculture (resp. +38% and 27%, NS, Fig. 28). This difference was also visually apparent in the diurnal transpiration curves, where the MIX consistently exceeded both monocultures during the daytime peak, reaching approximately 0.15 mL min^{-1} against 0.10 mL min^{-1} for the monocultures (Fig. 38). This increase in total water consumption in the mixture under non-limiting conditions is consistent with the higher root crown number discuss above suggesting that the two genotypes in mixture developed a larger and more active root system than either genotype alone, rather than only partitioning the same resource pool differently.

This higher transpiration in MIX-WW, without a proportional increase in biomass production, resulted in a lower WUE recorded (resp. 21% and 25%, NS, Fig 28). This finding suggests that the mixture effect under well-watered conditions is not solely a niche-complementarity phenomenon but also involves an additive increase in total water use. The contrast with the water-deficit response, where total transpiration converged across modalities, points to a resource-availability dependence of the mixture mechanism. In scenarios of scarcity, spatial niche partitioning dominates, while enhanced collective resource capture emerges under conditions of abundance.

The plasticity of the water uptake profile by roots was therefore not only determined by the root traits of the genotype and the characteristics of soil water availability (Fromm, 2019), but also by the interaction with the root traits of neighboring plants, i.e., in this case, the cultivation practice of wheat in mixture or monoculture. This implies that when selecting wheat varieties for mixed cropping, characteristics can be selected not only in single-species trials but also in functionally complementary combinations. Genotype-specific root traits, such as the number of seminal roots or

fine root surface area rather than root angle insertion, could be used in experimental and modeling approaches to design mixtures of root ideotypes that improve water use efficiency and yield stability compared to monocultures. However, we highlighted too that breeding deep-rooted systems does not guarantee better drought resistance and may even be disadvantageous, as in our case. To improve the plant's water deficit resistance, breeding efforts should consider both root and shoot traits. Thus, we call on the scientific community and breeding programs to provide increasingly comprehensive descriptions of crop root traits to enable the study, improvement, and use of lines that maintain or enhance beneficial plastic responses to climate change and ensure better yields through crop mixture systems.

5. Conclusion

This study demonstrates that mixing wheat genotypes with contrasting root traits (deep- and shallow-rooting) leads to complementary root water uptake strategies, particularly under water deficit. Using stable isotope tracing (δ^2H and $\delta^{18}O$) and high-resolution root imaging, we quantified distinct vertical RWU patterns: the shallow-rooting genotype (SRS) absorbed significantly more water from the top 7 cm of soil, while the deep-rooting genotype (DRS) showed greater uptake in deeper soil layers (69 – 80 cm), especially when water was limited.

In mixtures, these uptake patterns were preserved, with RWU shifting toward deeper layers under drought—by approximately 0.5% cm^{-1}—while decreasing in the topsoil. The number of crown roots was also higher in mixtures compared to monocultures, suggesting enhanced soil exploration despite similar total root biomass. To our knowledge, this was the first time that hydrological niche segregation and shift towards subsoil has been observed between genotypes of the same species. Furthermore, these findings suggest that contrasting wheat root trait mixture may enhance access to deeper water sources and root water uptake complementarity during periods of water deficit at this critical growth stage, which could potentially lead to an increase in yield.

This study highlights how fine-scale monitoring of root water uptake can reveal the benefits of intra-specific diversity for improving water use in cropping systems. However, it also demonstrates that high-resolution root trait data alone are insufficient to predict RWU distribution under heterogeneous matric potential conditions, emphasizing the need for direct or indirect RWU measurements through, for instance, stable isotope labelling experiments. However, the effect of water deficit on intraspecific root interaction during plant diurnal cycles, which allows potential hydraulic lifting to be observed, remains to be studied. In order to corroborate the outcomes of this controlled condition experiment comparing two wheat species with contrasting root systems, we recommended to pursue the research in real-world conditions and to increase the number of compared genotypes per root type (shallow/deep roots). Finally, the results of this study support the strategic design of genotype mixtures as a practical approach to enhance resilience to drought, offering potential benefits for yield stability and resource efficiency under climate change conditions.

Chapter 4

Dynamics of root and aboveground traits in wheat genotype mixture leading to higher yield under field conditions

This chapter presents the field-scale counterpart of the controlled column experiment (Chapter 3), conducted at the TERENO Selhausen platform (Jülich, Germany) during the 2022–2023 growing season. The specific objective was to evaluate whether the root trait contrasts between UQR12 (SRS) and UQR15 (DRS), and their non-additive effects in Mixture documented under controlled conditions, are expressed and carry agronomic consequences under field pedoclimatic variability. The root trait contrast between the two genotypes was less pronounced in the field, with some architectural differences attenuated or reversed by population-level interactions and seasonal climate variability. Despite this and as expected, mixture plots outperformed both monocultures in yield under water-limited conditions, and SRS maintained a relatively higher aboveground physiological resistance during the spring drought — consistent with the shallow water access advantage documented in Chapter 3. These findings confirm that functional complementarity between the two genotypes produces measurable agronomic effects even when the underlying root architectural mechanisms are only partially preserved at field scale. A complementary article addressing microbiological aspects, nitrogen dynamics, and rhizosphere exudation is currently in preparation (Adrian et al.).

1. Introduction

To test the correspondence root trait – function and their possible complementarity for two wheat genotypes growing in mixture facing water deficit conditions, we conducted in a controlled environment, that was published in two articles (Lattacher et al., 2025b; Le Gall et al., 2025). The study examined two wheat varieties, SRS (shallow root system) and DRS (deep root system), with contrasting root traits at key stages of booting development. The results showed that the combination of these root traits resulted in corresponding combinations in water and nitrogen uptake, as well as in the distribution of carbon in organs and soil exudates. Additionally, the niche resource uptake complementarity of the two genotypes increased in mixture, particularly enhancing the uptake of accessible deep water and paving the way for better adaptation. Furthermore, (Lattacher et al., 2024) identified differences in root systems and microbial activity among various cultivars at four successive vegetative development stages, underscoring the significance of underground interactions in ensuring crop resilience.

However, this study was 1) limited to the key booting stage and 2) conducted under controlled conditions to mitigate climatic and soil variability significantly and test the proof of concept. Therefore, to test the transferability of our conclusions to field conditions, we conducted another, complementary experiment in the same loamy-clay Luvisol agricultural soil and with the same two genotypes using a mini-rhizotron device installed at depths of up to 120 cm. In the spring of 2023, eighteen microplots (3 x 2.5 m) were sown and managed using conventionally practices according to three cultivation methods: a monoculture of a deep-rooted wheat (DRS), a monoculture of a shallow-rooted one (SRS), and the equal mixture of the two cultivars. We tested the following three hypotheses: first, the root characteristics of the DRS and SRS cultivars selected in the laboratory for their root characteristics persist despite greater climatic and soil variability. Second, the superior resistance to water deficit of the SRS cultivar, as described under controlled conditions during the booting stage, enables this genotype to achieve higher yields in the event of water deficit. Third, the additive effects of mixing the two genotypes result in similar or higher yields in the event of water deficit.

2. Materials and methods

2.1. Pedoclimatic conditions, agricultural practices and experimental design

The experiment was conducted at the Mini-Rhizotron facility in Selhausen, North Rhine-Westphalia, Germany (50°52′09″N, 6°27′01″E), which is part of the TERENO (Terrestrial Environmental Observatories) Eifel/Lower Rhine Observatory.

The eighteen soil plots (3 x 2.5 m) consist of a silty-clay Luvisol with an average bulk density of 1.4 and an organic carbon content of 1.1% in the top 30 cm and 0.4% in the lower layers, as measured on site on April 29, 2020 (Fig. 43a, b). The average particle size distribution was measured as follows: 12% between 2 and 0.063 mm, 66% between 0.063 and 0.002 mm, and 22% < 0.002 mm (Fig. 43c).

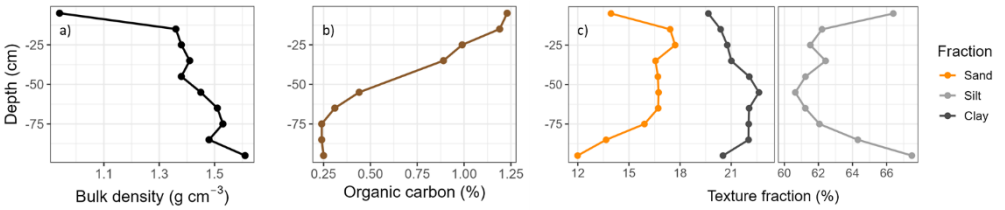

Fig. 43 Vertical distribution from 0 to 95 cm depth of the (a) bulk density (g cm^{-3}); (b) organic carbon content (%) ; (c) soil texture fractions showing sand (orange), silt (gray), and clay (dark gray) distribution.

The Selhausen test site has been the subject of numerous studies employing geophysical measurement techniques (Bauer et al., 2021; Weihermüller et al., 2007). Nine of the plots are situated above a mini-rhizotron facility (described in Nguyen et al. (2024)) to observe the root system in situ at depths of 10, 20, 40, 60, 80, and 120 centimeters (Fig. 44).

The experimental plots were seeded on March 20, 2023, at a density of 300 seeds per square meter, following mechanical weeding and superficial seedbed preparation using a rake and a hoe. These plots were then subjected to three distinct cultivation modalities: The first treatment consisted of a "pure crop" of the deep-rooted UQR15 wheat cultivar ("D"). The second treatment consisted of a "pure crop" of the shallow-rooted UQR12 wheat cultivar ("S"). The third treatment consisted of a 50%-50% mixture of the UQR12 and UQR15 wheat cultivars grown together ("M").

Fig. 44 Location of the destructive sampling on the plots (DRS in dark green, MIX in blue, SRS in orange) at the Elongation and Grain filling stage (aboveground biomass and belowground soil core) and the measure the compound of the yield at the harvesting time. The minirhizotron tubings are represented by dotted white lines. Drone picture credit Jordan Bates, 10/07/2023.

Conventional fertilizer was applied thrice: The initial application of nitrogen was 60 kilograms per hectare on April 19, coinciding with the three-leaf stage of plant development. This was followed by a second application of 80 kilograms per hectare on May 22, which occurred during the tillering stage. The third and final application of nitrogen was 40 kilograms per hectare on June 23, timing with the grain-filling stage. The plots were not irrigated. The experimental plots were sown on March 20, 2023, at a density of 300 seeds/m² after mechanical weeding, with three crop modalities. The experiment consisted of three distinct crop types: 1) a "pure crop" of the deep-rooted UQR15 wheat cultivar (DRS), 2) a "pure crop" of the shallow-rooted UQR12 wheat cultivar (SRS), and 3) a 50%-50% mixture of UQR12 and UQR15 wheat cultivars grown together (MIX).

Manual weeding was performed during the tillering stage to prevent competition from other weeds. No growth regulators were applied. Conventional fertilizer was applied thrice: the initial application of nitrogen was 60 kilograms per hectare on April 19, coinciding with the three-leaves stage of plant development. This was followed by a second application of 80 kilograms per hectare on May 22, which occurred during the tillering stage. The third and final application of nitrogen was 40 kilograms per hectare on June 23, timing with the grain-filling stage. The plots were not irrigated.

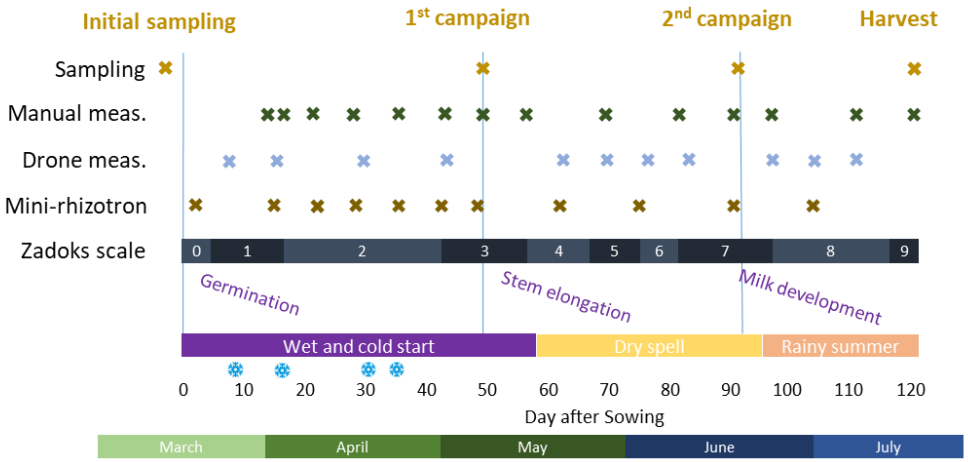

Fig. 45 Chronogram of the experiment with the labeling and destructive sampling campaigns, the manual, drone and mini-rhizotron measurements, the daily rain precipitation amount, the freezing days, the three main climatic periods and the plant stages. On the Zadoks scale, the numbers corresponds to: 0-Germinations; 1-Seedling growth; 2-Tillering; 3-Stem elongation; 4-Booting; 5-Ear emergence; 6-Flowering (anthesis); 7-Milk development; 8-Doughy development; 9-Ripening

The prevailing climate conditions (Fig. 45) consisted of:

1) 0 to 55 Days after Sowing (DaS): the initial phase of the plant growth was marked by a wet (119 millimeters of precipitation over a span of 60 days) and cold (average temperature of 10°C) start during the winter months, with freezing temperatures recorded till end of April (at 36 DaS, Tillering stage). This period persisted until the onset of the early spring season, extending from the initial stages of seed germination to the subsequent phases of tillering and stem elongation.

2) 55 to 92 DaS: a period of aridity lasting 30 days was observed during the spring season. This period commenced from the stage of ear emergence and continued until the onset of flowering, as well as the initial stage of grain filling. the average daily temperature increased from 10 to 23°C, with a total of 1 mm of precipitation over 30 days.

3) 99 to 118 DaS: the summer of 2023 was marked by an abundance of precipitation. An extrem rain event (26-mm precipitation) happened at 94 days after sowing (DaS) in mid-June, subsequently followed by sporadic rainfall that persisted throughout the culminating grain-filling stages until the harvest on July 18, 2023, at 119 DaS. The mean temperature was 20°C, and the plants received a total of 46 millimeters of precipitation in less than a month.

2.2. Soil and plant measurements

Plots 1, 4, and 7 were equipped with soil water potential (MPa) and temperature (°C) sensors (Teros 21, Meter, Munich, Germany), but also with water content sensors (Meter, Munich, Germany) at the depths of 10, 20, 40, 60, 80, and 120 centimeters (Fig. 44).

Soil was sampled on three occasions: once before sowing on March 7, 2023; once during stem elongation on May 10, 50 DaS; and once at milk stage development on June 19, 89 DaS. For each sampling date, we extracted 100 cm soil cores with a 50 mm diameter in plots 10 to 18 (Fig. 43) using a Wacker system. Then, we used a 32-mm-diameter drilling tube to sample a soil core from 100 to 150 cm in depth. The soil core was subdivided into six 10-cm layers at depths of 10, 20, 40, 60, 80, and 120 cm. The aboveground parts of the plants were also sampled from a 40 x 40 cm surface area to determine fresh and dry biomass.

On July 19, the plots were harvested. Three subplots (40 cm x 40 cm) were harvested in each plot to measure aboveground plant and ear dry biomass, ear density, dry grain weight per soil surface, dry grain weight per ear, and average grain weight. The grains were milled into powder to analyze their carbon and nitrogen content.

2.3. Aboveground plant measurements

In each of the 18 plots, four plants were annotated and monitored for growth measurements. In the pure crop, four plants were annotated, of which two were designated as DRS and two as SRS. In the mixture (MIX), two plants per plots were labelled as DRS and two as SRS, on which manual measurements were taken on a weekly basis until the elongation stage and subsequently every two weeks until harvest. Non-destructive measurements were obtained, including the average leaf chlorophyll content, as determined by the SPAD 502, the number of tillers per plant, the total number of green and yellow leaves per plant, the blade leaf width and length (facilitating the calculation of green leaf area per tiller and plant), and the plant height. Furthermore, the average fresh and dry biomass of three individual plants per plot was measured, and the reproductive organs were measured separately when present. The leaf water potential was measured on a single plant per plot at this time scale using a pressure chamber, following the recommended practices of Rodriguez-Dominguez et al. (2022) in the late morning.

Concurrent with these manual measurements, a UAS-based multi-sensor platform was deployed on a biweekly basis in the morning on the days designated for data collection. The platform consisted of a Matrice 600 Pro hexacopter (DJI, France) carrying three co-registered sensors: a RedEdge-M multispectral camera (Micasense, USA) providing reflectance data in five spectral bands (blue, green, red, red-edge, and near-infrared), a thermal infrared (TIR) camera for canopy surface temperature

estimation, and a YellowScan Surveyor LiDAR sensor (YellowScan, France) for structural characterization. The multispectral and thermal sensors were flown at 100 m altitude and the LiDAR at 50 m altitude above ground level, following the protocol described in Bates et al. (2025).

From the LiDAR point cloud, canopy height (CH) was derived as the difference between the digital surface model and the digital terrain model, and multi-layer gap fraction (GF) was computed at multiple height thresholds (10, 20, and 30 cm above ground) to characterize the vertical distribution of canopy elements across growth stages. From the multispectral imagery, the normalized difference vegetation index (NDVI) and green area index (GAI) were extracted at plot scale after radiometric calibration using a reference panel. Canopy surface temperature derived from TIR data served as a proxy for stomatal conductance and canopy water status, particularly during the drought period.

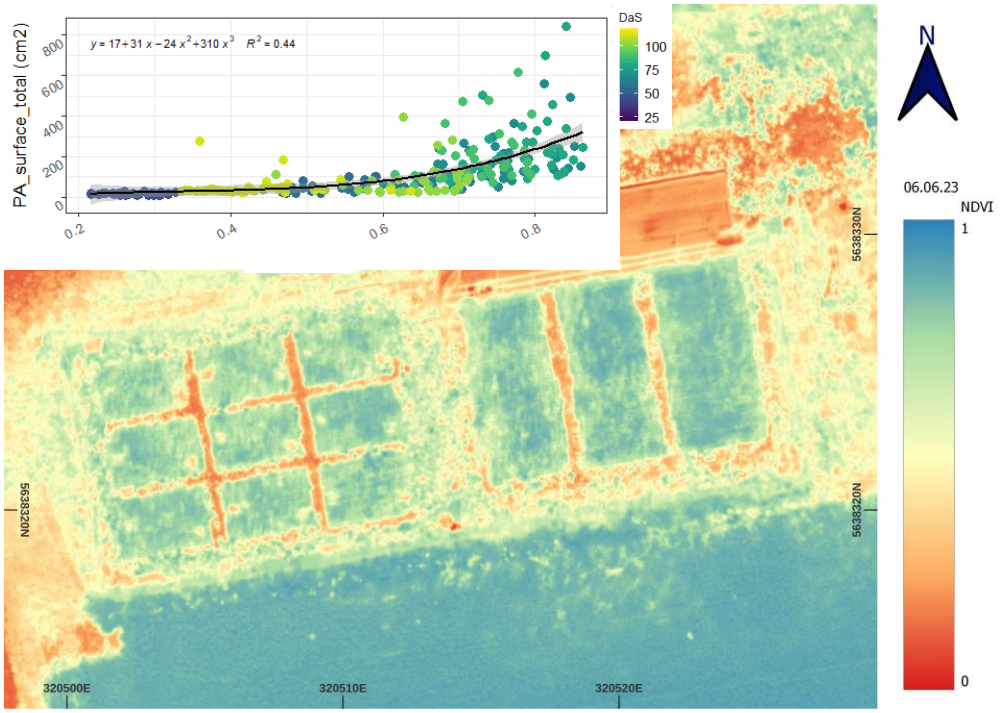

Fig 46 NDVI picture taken by drone on June 6, 2023, 77 DaS (end of the flowering stage). We see the heterogeneity inside each plot. On the plot, we see the photosynthetically active surface (green leaf surface) over the NDVI values, along the growing season. The data come from 36 plants measured manually and their NDVI corresponding pixels, over the growing season.

2.4. Mini-rhizotron measurements

The mini-rhizotron facility at the Selhausen field enabled the repeated in situ imaging of root systems in accordance with the established protocols that had been implemented for several years prior to the commencement of the experiment (Nguyen et al., 2024). Images were obtained on a weekly basis during the initial vegetative stages of development and subsequently at two- to three-week intervals. A total of twenty images were captured for each tube at 160-degree intervals, resulting in forty images per tube. Each plant modality was encompassed by three rows of tubes at six depths.

The analysis pipeline incorporated a convolutional neural network (CNN) to facilitate the segmentation of roots within the images. A subset of the images was manually annotated to create a balanced training set encompassing various depths, soil types, dates, and root levels. This set was utilized for the training of a CNN model employing RootPainter software, that was then implemented in batch processing mode to automatically differentiate between root pixels and the soil background in all images. Subsequently, the images were converted into binary masks (roots = foreground; soil = background) to facilitate robust feature extraction. The RhizoVision Explorer software utilized a skeletonization process to analyze the extracted root structures, thereby deriving quantitative metrics. This module automated several steps, including artifact filtering, segmentation, hole filling, and removing non-root fragments, with a particular focus on total root length per root diameter slice. The analysis pipeline utilized in this study is analogous to one previously published by (Bauer et al., 2022a)

2.5. Statistics and Data Representation

The statistical analyses were executed in R (Version 4.2.0; R Core Team 2020). The assumptions of normality and homoscedasticity of the model residuals were evaluated using QQ plots and Levene tests (Fox et al., 2001). In instances where residuals exhibited substantial deviations from these assumptions, logarithmic or square-root transformations were implemented to stabilize variance and enhance the quality of residual distributions. The significance of the observed differences was assessed using a linear mixed-effects model, which was implemented through the lme function from the nlme package (Pinheiro and Bates, 2000). Genotype, depth, and water regime were considered as fixed effects, while columns and runs were treated as random effects. We used the following symbols to indicate statistical significance: " ": $p > 0.05$; "*": $p <= 0.05$; "**": $p <= 0.01$; "***": $p <= 0.001$; "****": $p <= 0.0001$. The comparison among treatments were carried out via the emmeans test adjusted with the bonferroni method with the package stat_pwc {ggpubr}.

3. Results

3.1. Plant aboveground measurements

Leaf water potential (Ψleaf, in bar, Fig. 47a) at noon progressively declined from ~3–5 bar at 40 DaS to 15–20 bar by 100 DaS, with the steepest decrease occurring during the flowering-to-grain-filling period (40–100 DaS). All cultivars reached severe drought stress levels (>15 bar) by late grain filling, approaching the permanent wilting point, with no significant differences between them (NS).

The water content of the plants (percent mass, Fig. 47b) remained approximately 80 percent during the wet, cold start. Subsequently, a steady decrease was observed, commencing from 60 to 105 days after sowing (DaS), culminating in 50% for the three planting methods. Ultimately, the percentage reached approximately 10% at the conclusion of ripening (date: $p < 0.0001$). On several dates, the DRS was found to be drier than the SRS (plant x date: $p < 0.01$), particularly at the end of grain filling and ripening (between DRS and SRS at 111 and 119 DaS: $p < 0.01$).

The plant dry biomass (g) exhibited exponential growth during the initial two periods, reaching a maximum of 92 DaS (Fig. 47c). The DRS exhibited a mean value that was higher than the SRS (5.1 and 3.8 g, respectively; $p < 0.05$). The dry plant biomass exhibited a decline for DRS and MIX, while maintaining relative stability for SRS until harvest.

The variation in leaf surface temperature (LST_var, °C, Fig. 47d) was defined as the difference between the mean plant cover temperature and the specific plot temperature of the leaf surface, normalized by the mean temperature. The mean value for the three plant modalities was nearly zero in the initial period. During the second period, a significant gradient manifested, with negative values for DRS denoting a cooler leaf surface compared to MIX and SRS displaying a higher relative leaf surface temperature. From 29 to 71 days after sowing (DaS), LST_var was successively and significantly higher ($p < 0.05$) for SRS than for DRS. In the third period, no significant differences were observed between the modalities.

The green leaf area (PGA, cm^2, Fig. 47e) exhibited a tenfold increase from 36 DaS to 71 DaS. During the second period characterized by the dry spell, PGA growth exhibited a higher level of expression for DRS in comparison to SRS ($p < 0.01$ from 57 to 84 DaS between the two genotypes). However, the PGA decreased steadily for DRS from 71 to 111 DaS, and more rapidly than for SRS and MIX. The discrepancy in PGA gradually diminished and then reversed at 99 DaS; in this instance, SRS was considerably higher than DRS ($p < 0.05$). The MIX PGA demonstrated a comparable tendency to the SRS throughout the season. It demonstrated superior resilience during the period of grain filling and maturation, exhibiting higher PGA values (NS) at 111 DaS when compared to DRS.

Canopy height exhibited an initial increase, followed by a sixfold increase during the subsequent dry period, which corresponded to the early stages of reproduction. Subsequently, it remained constant during the final period (Fig. 47f). The growth rate and stature of DRS monocultures surpassed those of SRS and MIX monocultures (plant x date: $p<0.0001$). Furthermore, DRS genotypes in mixtures exhibited slower growth rates and shorter lengths than those in monoculture.

The number of shoots (Fig. 47g) was low for all treatments, likely due to late frosts and soil moisture close to saturation from regular, heavy rainfall during the early stages of development. Initially, the DRS mixture produced a greater number of tillers than the monoculture at 43 DaS ($p < 0.05$), as did the SRS ($p < 0.1$). During the dry period from 60 days after sowing (DaS) onwards, all modalities exhibited a loss of tillers. Preliminary findings indicate that the initial higher tiller emission resulted in a greater number of fertile shoots (dotted line from 90 DaS) of SRS in mixed planting relative to monoculture ($p < 0.05$). This phenomenon was also observed in the DRS (NS) case.

The higher number of tillers per plant for the two genotypes up to 60 DaS resulted in a higher number of green leaves per plant after this date (Fig. 47h). This number underwent a decrease, returning to averages comparable to those of the corresponding genotypes in monoculture by 80 DaS.

While the mixture produced a greater number of shoots and leaves, there was an average decrease in leaf length of one to two centimeters for both varieties (Fig. 47i) (NS). Beginning at 80 DaS, there was a precipitous decline in average leaf length, with a decrease of 5 centimeters. This decline can be attributed to a higher rate of desiccation compared to regrowth. Following the precipitation at 94 DaS, there was an observed increase in the mean leaf length of 3 centimeters across all plant types. This phenomenon can be attributed to the proliferation of green leaves that survived the rainfall.

With regard to the average chlorophyll content of the plants' leaves, no significant behavioral differences were observed between the treatments over time (Fig. 47j). However, a general trend with two peaks in SPAD values was observed at 45 and 85 days after sowing (DaS) after the two fertilizations. Following the precipitation at 94 DaS, an increase in chlorophyll content was observed, attributable to the release of nitrogen in progressively arid soil, which exhibited diminished accessibility for assimilation.

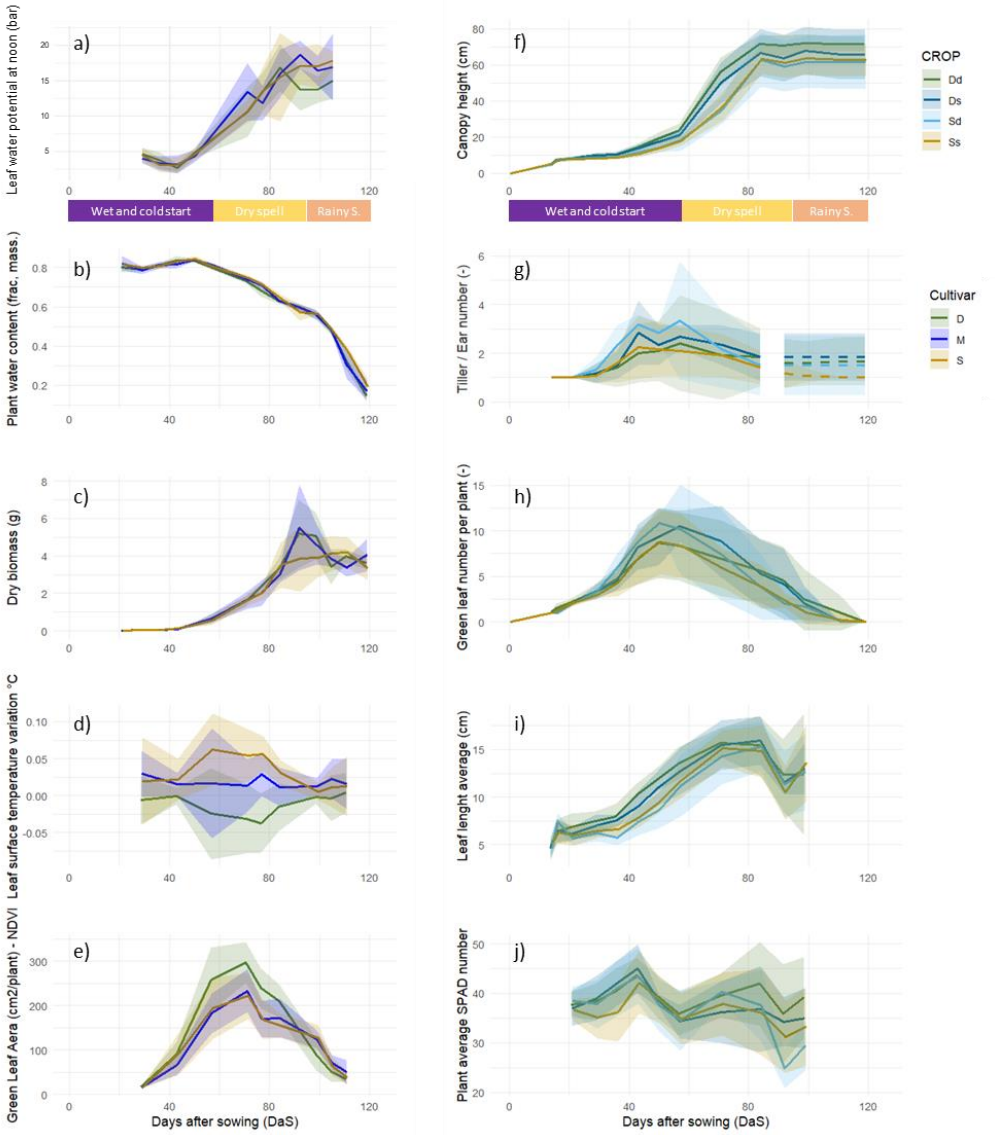

Fig. 47. (a–e) Foliar water potential at noon (bar), plant water content (frac.), dry biomass (g), leaf surface temperature relative variation (°C), and green leaf area (cm²/plant, calculated from NDVI data). (f–j) Canopy height (cm), number of tillers/ears, number of green leaves, leaf length (cm), and average SPAD index per plant. Climatic phases: wet/cold start (purple, 0–40 DaS), drought period with high evaporative demand (yellow, 40–100 DaS, peak stress ~92 DaS), return of precipitation (orange, >100 DaS). Flowering occurs between 75 and 80 DaS. Colors: DRS monoculture (green), MIX (blue, with dark blue for DRS components and light blue for SRS components), SRS monoculture (orange). Shading zone = ±1 standard deviation.

3.2. Roots development

The length density of flat roots (cm/cm², pRLD) greater than 300 μm in the main root structure has been shown to indicate normal growth in spring wheat (Sharma and Ghildyal (1987); Fig. 48). The roots attained a depth of 20 centimeters within a 16-day period. Subsequently, the team observed the attainment of the remaining soil depths of the mini-rhizotron at a rate of approximately 3 centimeters per day.

The root density dynamics exhibited a substantial dependence on both depth and the developmental stage (depth x date: $p < 0.0001$). Initially, root density was higher at the surface (0.25 cm/cm² at 16 DaS) and gradually increased in all soil layers (Fig. 48j–o). However, the average pRLD stagnated or decreased between days 22 and 36 after sowing (DaS) due to successive frosts (nights of days 15–18 and 25–26 DaS) and intense, regular rainfall. Subsequently, the pRLD exhibited an increase at depths of 10 and 20 centimeters for all plant modalities at 51 days after sowing (DaS) and reached a maximum at 65 DaS.

Subsequent to the initial 65 DaS, during the second period (termed the "dry period"), root densities at depths of 40, 60, and 80 centimeters (cm) exhibited higher values in comparison to surface densities (Fig. 48j–o). Subsequent to this, root density at the surface diminished as water availability diminished. At 105 days after the cessation of extreme rainfall, root density at the surface exhibited a renewed increase, reaching levels comparable to those observed during flowering one month prior.

The three plant types exhibited significant structural differences in their roots ($p < 0.001$) and different vertical root distributions (plane x depth: 0.053). An initial trend was observed during the first 51 days: SRS demonstrated a consistently higher pRLD compared to DRS at 40 and 60 cm on days 22, 29, and 36 ($p > 0.05$) (Fig. 48a–c). In the top 10-centimeter layer of soil, SRS was consistently higher than DRS, though not significantly so. However, this trend was not observed in the second phase, which occurred between flowering and the final stages of grain maturation. In the subsoil (at depths of 80 and 120 centimeters), the DRS exhibited a higher mean value compared to the SRS, beginning on average 77 days after sowing (DaS).

Furthermore, the pRLD of MIX was not consistently intermediate between SRS and DRS, particularly at 20 cm. In this case, the mean MIX value was consistently higher than the SRS and DRS values, with a considerable margin in some instances. For instance, on days 22, 29, 36, 51, and 77 DaS, the pRLD of MIX was found to be significantly higher than that of SRS and DRS ($p > 0.05$) (Fig. 48k). During the flowering stage (77 DaS) and the milk stage (90 DaS), the propensity for the pRLD of MIX to exceed that of SRS and DRS was also observed at depths of 60 and 80 centimeters.

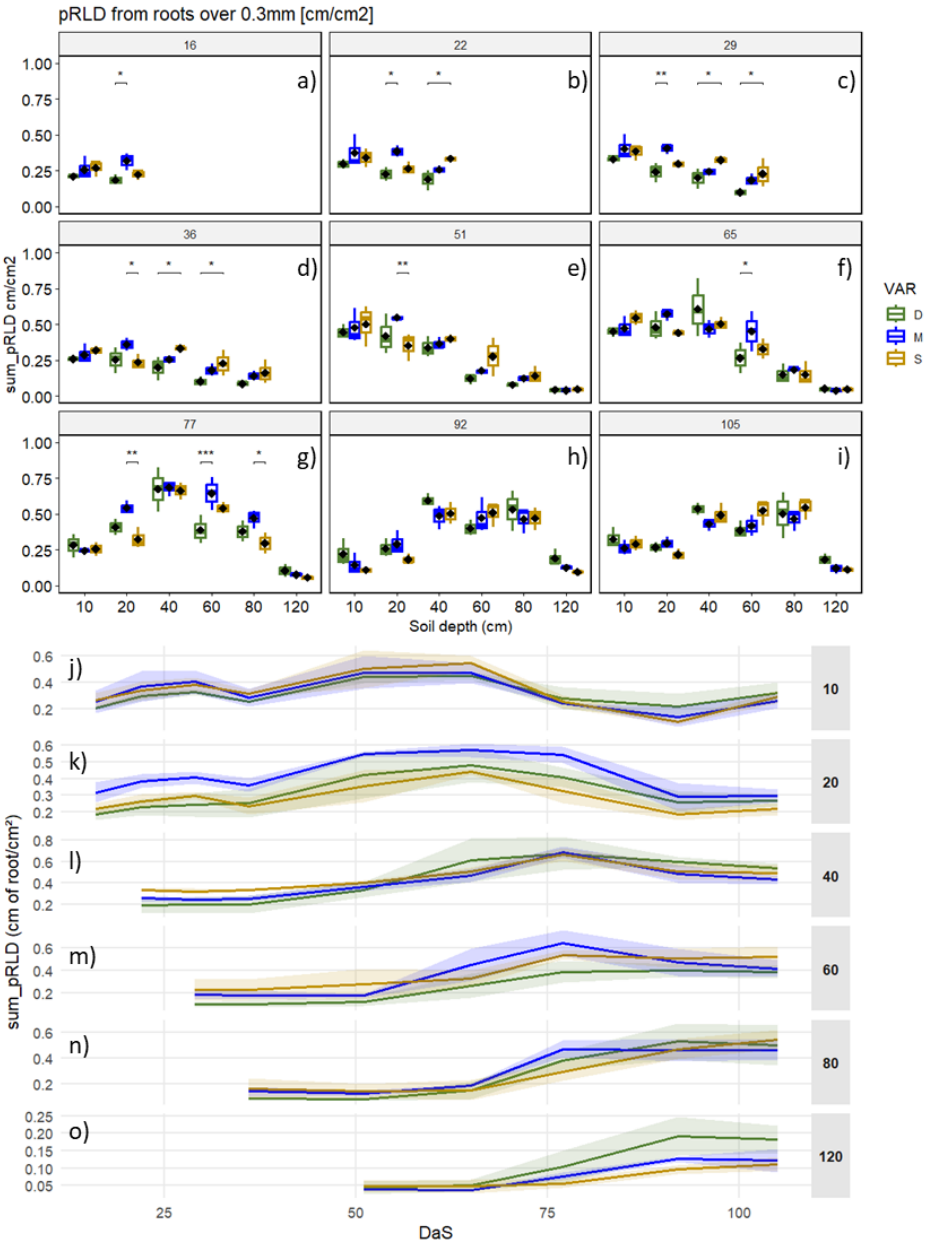

Fig. 48 Distribution of the plant root length density (pRLD, cm root per cm2 of soil) per soil depth (10 to 120cm) from 16 DaS (panel a) to 105 (panel i) for root diameters above 300 µm. The evolution of the average (solid line) and the standard deviation (transparent envelope) from 16 to 105 DaS is displayed layer per layer pane j) to o).

3.3. Soil water status

Soil moisture content, expressed as a percentage of volume by weight (Fig. 49a), exhibited variability throughout the season and at varying depths within the soil profile. The maximum average was recorded in the subsoil layers, reaching 40%, while the minimum average was 15% in the topsoil, which was attained following the return of intense rainfall at the onset of the third period (94 DaS).

During the initial wet and cold period, the layers beneath 20 centimeters of soil exhibited minimal alterations, with no substantial disparities observed among the various plant types. However, at a depth of 20 centimeters, the DRS exhibited accelerated desiccation. In the two uppermost layers, soil water content (SWC) exhibited an increase on specific dates due to intense precipitation episodes, which occurred at 7, 10, 30, and 50 days after sowing (DaS). The interval between days 10 and 30 demonstrated the most substantial decrease in water content, with a reduction exceeding 5%, a phenomenon attributable to increased root water uptake activity. Subsequently, a period of stagnation ensued from 30 to 50 DaS, characterized by a 28% SWC and minimal fluctuations in water content. At these depths, the SWC reached one of the highest soil water contents of the entire season, averaging 35% (Fig. 49a).

During the subsequent drought period, which occurred between 60 and 94 days after sowing (DaS), the soil water content (SWC) exhibited a significant decrease at all depths and for all plant types (period x plant x depth: $p < 0.05$). The decline in SWC was more pronounced for SRS and MIX than for DRS at 40, 60, and 80 centimeters, while the reverse was observed at 20 centimeters. These disparities were especially pronounced during the pivotal flowering stage (plant × depth: $p < 0.05$; Fig. 49b). The observed disparities resulted in MIX and SRS experiencing a 20 mm greater decrease in soil water reserves than DRS ($p < 0.01$, Fig. 49c).

The third period was characterized by a sudden 3% increase in topsoil (10 cm) water content, which was observed across all plant types. Subsequent to this augmentation in water supply, the soil water content curves attained stability across the majority of depths. For DRS, an increase in SWC was also observed from 110 DaS onwards, indicating that water absorption was lower than the amount replenished by precipitation. Conversely, SWC exhibited a decline for SRS at 80 and 120 centimeters from 100 days of sowing (DaS) until harvest (Fig. 49b). This finding suggests that, at these depths, the genotype persisted in extracting water at a rate that exceeded the rate of precipitation replenishment.

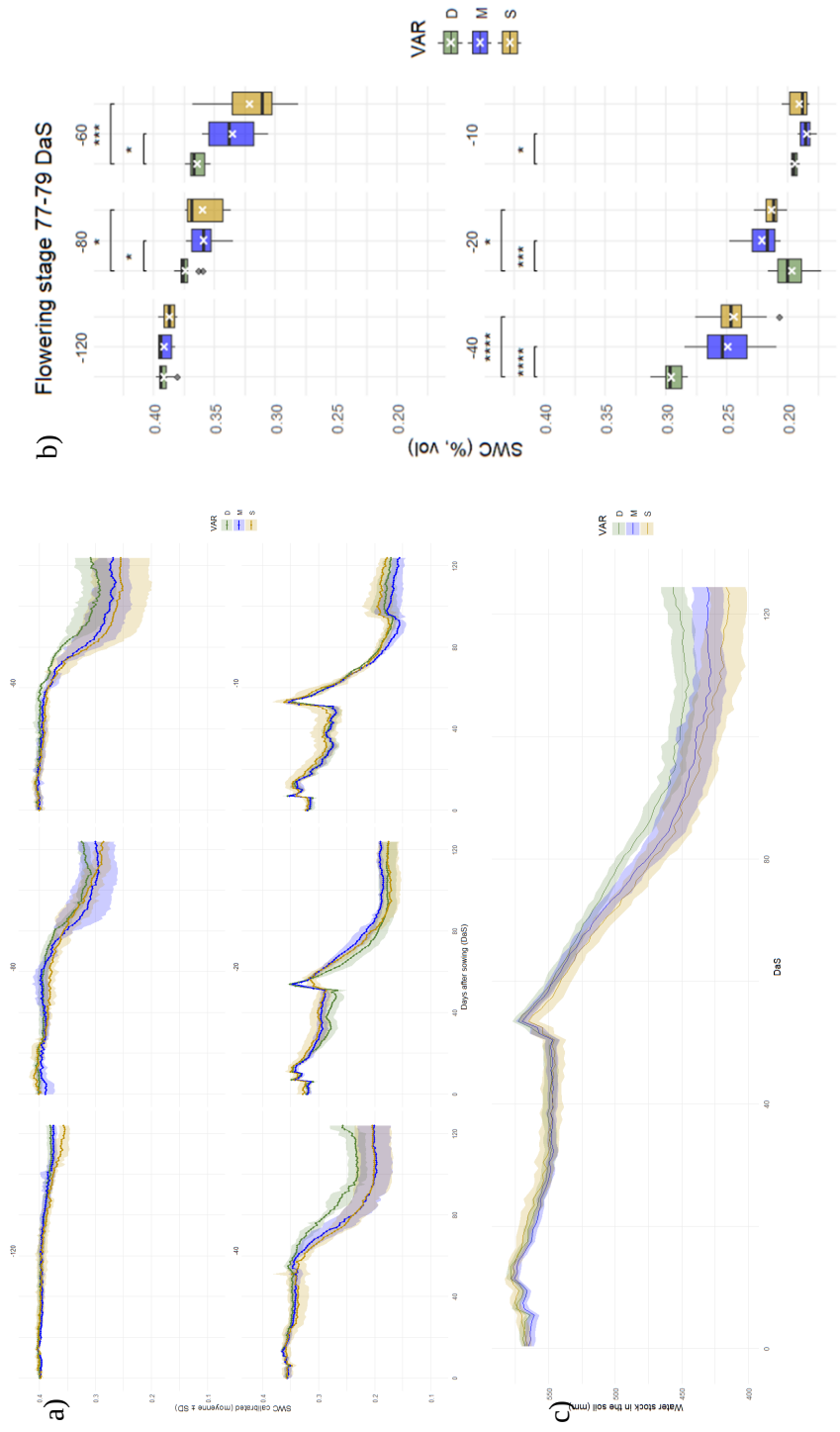

Fig. 49. a) Evolution of the daily soil water content at the 6 soil depth during the growing season from 0 to 120 DaS, b) Soil Water Content (SWC, %, vol.) distribution among the plant modalities at the flowering stage between 77 and 79 DaS at 120, 80, 60, 40, 20 and 10 cm soil depth c) Water stock evolution in the soil during the growing season from 0 to 120 DaS. DRS was in green, MIX in blue and SRS in orange.

During the growth stage, daily soil water loss exhibited a strong and positive correlation with root density growth (date: $p < 0.0001$, Fig. 50). The relationship between pRLD and SWC daily variation was also significantly influenced by the stage of development (date: $p < 0.05$). While the linear regression of the two variables for DRS demonstrates a greater intensity of root extraction per unit of root density ($y=85x$, $R^2=0.72$) in comparison to MIX ($y=80x$, $R^2=77$) and SRS ($y=74x$, $R^2=77$), this discrepancy between varieties was not statistically significant (Fig. 50).

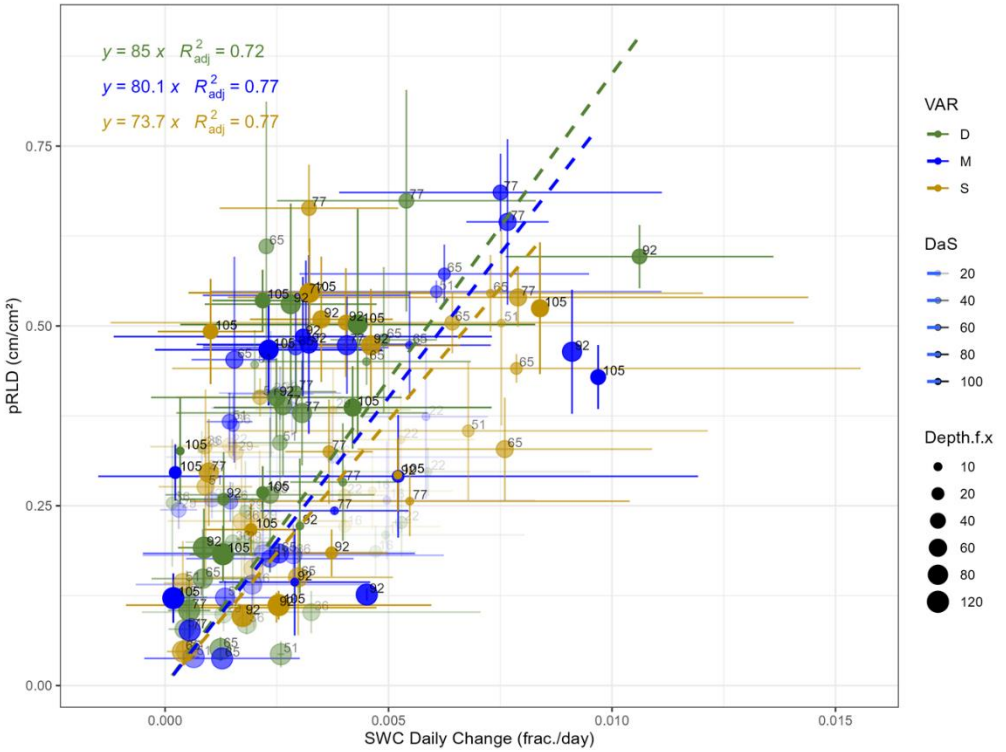

Fig. 50 Plane root length density (pRLD, cm cm^{-2}) over the daily absolute difference of SWC (volumetric fraction) recorded on the same dates (16, 22, 29, 36, 51, 65, 77, 92 and 105 DaS). The points represent the average value and the bars the standard deviations of three plant modalities (DRS in monoculture, dark green; MIX, blue; SRS in monoculture, orange), across six soil depths (10, 20, 40, 60, 80, 120 cm). Dashed lines represent the linear regression for each plant modality.

All three cultivars exhibited a bell-shaped relationship between soil water content and projected root length density (Fig. 51), with a pronounced optimum between SWC = 0.25–0.30 cm³/cm³ (mean pRLD ~0.50–0.65 cm/cm²). Before and beyond this threshold, pRLD declined sharply reaching minimal values (~0.20 cm/cm²) at SWC values of both 0.18 and 0.38. Although the relationship between projected root length

density (pRLD) and soil water content (SWC) was statistically equivalent across all three wheat cultivars (plant: NS, Fig 51), the MIX cultivar deviated from the arithmetic mean of its parental genotypes (expected: slope = (9.37 + 12.26)/2 = 10.8; observed: slope = 12.05), suggesting a possible non-additive or transgressive response at intermediate water availabilities.

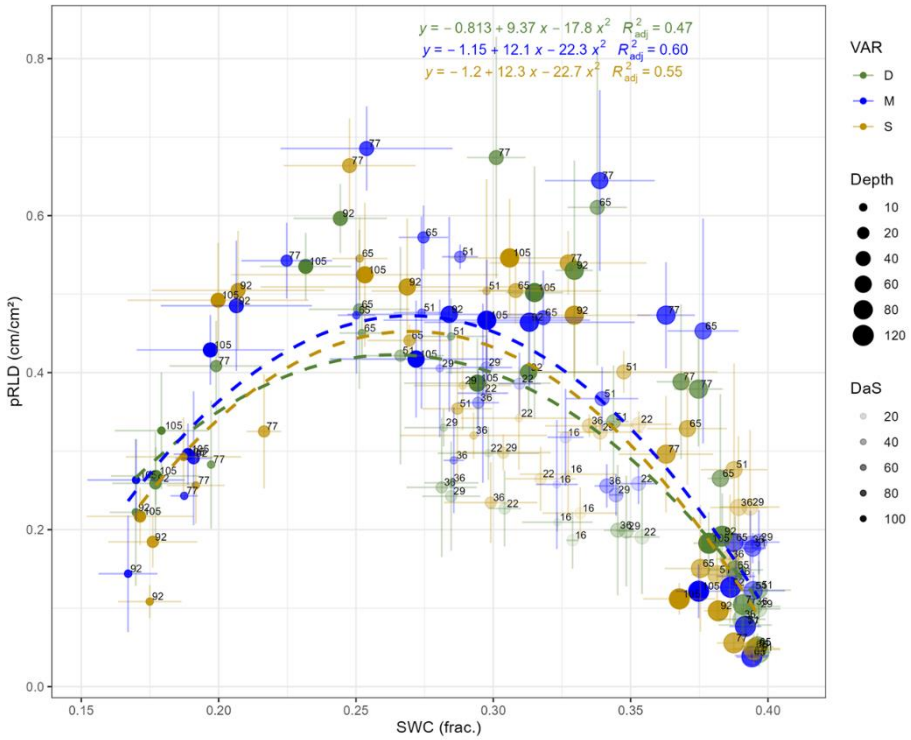

Fig. 51 Plan root length density (pRLD, cm cm^{-2}) as a function of soil water content (SWC, volumetric fraction) recorded at the same dates (16, 22, 29, 36, 51, 65, 77, 92 and 105 DaS). Points represent mean values and bars indicate standard deviations for three plant modalities (DRS in monoculture, in dark green; MIX, in blue; SRS in monoculture, in orange) across six soil depths (10, 20, 40, 60, 80 and 120 cm), with point size increasing with DaS (from 20 to 100 DaS). Dashed curves represent second-order polynomial regressions fitted for each plant modality.

3.4. Yield and biomass

At harvest time, the dry biomass production revealed a relative advantage for SRS over DRS monocultures (+23% in grain; +20% in ears; and only +7% in total aboveground plant; Fig. 52a–c). Although DRS produced marginally higher fertile ear density (466 vs. 435 ears/m²; NS, Fig. 52d), this yield (grain biomass) differential was driven primarily by grain number per ear, where SRS exceeded DRS by 33% ($p < 0.01$; Fig. 52e). The grain filling remained comparable between monocultures (4.12 ± 0.08 g/100 grains for both genotypes; Fig. 52f).

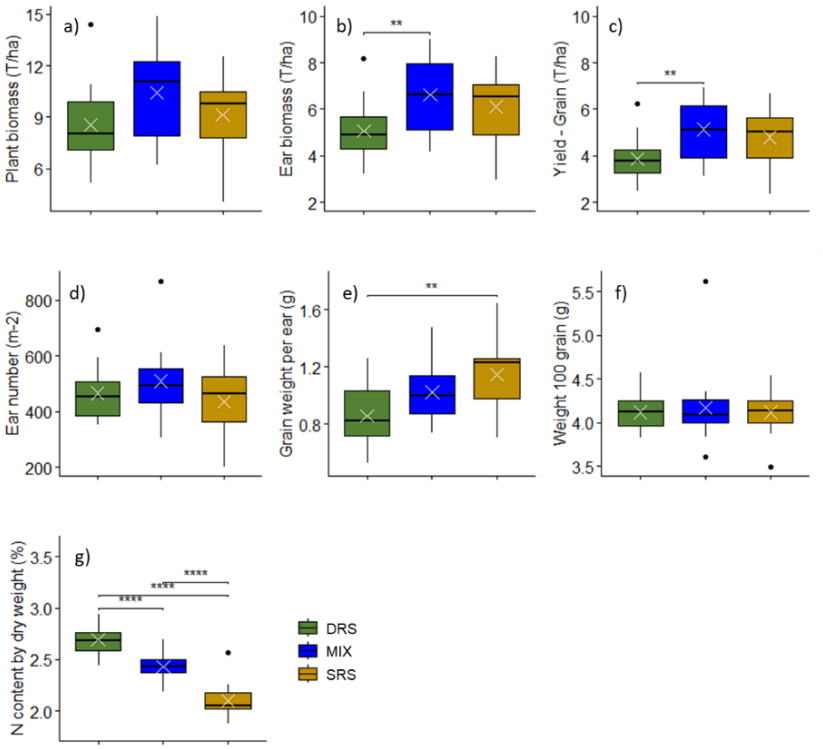

Fig. 52 The ear (a), aboveground plant organs (b) and grain (yield) (c) biomass after the harvest, as well the ear density per soil surface (d), the grain weight per ear (e), the weight of 100 grains (f) and the nitrogen content (g), for the three plant modalities DRS (dark green), MIX (blue) and SRS (orange), evaluated over a surface of 40cmx40cm. (n = 18)

Contrary to the monoculture pattern, MIX demonstrated transgressive performance, exceeding both parental monocultures, with total plant biomass (10.4 t/ha) and grain yield (5.1 t/ha), significantly surpassing DRS ($p < 0.01$; Fig. 52a–c). The yields of DRS, SRS, and MIX (3.9, 4.8, and 5.1 t/ha, respectively) result in a Land Equivalent Ratio (LER, introduced by Mead and Willey, 1980) of 1.19, meaning that for our experiment, the land use was 19% more efficient in mixture than in a monoculture. In the yield compounds, the MIX fertile ear density in particular was 9% and 17% higher

than DRS and SRS, respectively (NS; Fig. 52d), while grain number per ear remained intermediate between monocultures values and grain filling was statistically equivalent to monocultures (only +1% increase; NS; Fig. 52e–f).

With respect to grain quality, DRS exhibited significantly higher nitrogen content than SRS ($p < 0.001$; Fig. 52g), reflecting higher protein accumulation. The MIX grain composition was intermediate, overlapping the range of parental monocultures but closer to the DRS phenotype for nitrogen content (Fig. 2g–h).

4. Discussion

4.1. Genotype specific spatial niche occupation dynamic and water use

In this study, the first hypothesis concerning the conservation of root traits oriented towards topsoil for SRS and subsoil for DRS was not fully validated. SRS exhibited faster root development in the first soil layers than DRS, while DRS demonstrated in later development stages denser root growth in the subsoil (80 and 120cm). However, these differences were negligible and largely non-significant (Fig. 48).

Contrary to the expectations or observations recorded in controlled conditions (Le Gall et al., 2025), the DRS resulted in faster water content reduction in the topsoil (at 20 cm soil depth) during the second period (drought) when compared to the SRS plots (Fig. 50). Conversely, the SRS led to more rapid water content reduction in the deeper soil layers than the DRS plots.

Weather conditions (frost, repeated heavy rainfall) during the early vegetative stages led to a stabilization or even a regression of both pRLD and water content reduction that can be attributed to root, particularly visible in the topsoil for both varieties around 30 DaS. Root traits must be interpreted in their temporal context, as early thermal and hydric stresses altered the following plant plasticity, as observed, for example, in the very low tillering rate (and therefore the number of adventive root emissions) compared to normal conditions or to the same genotypes under optimal conditions (Le Gall et al., 2025).

In addition to the daily and seasonal variability in meteorological conditions compared to controlled conditions, the variability in soil was greater in the field than in controlled conditions, particularly with regard to vertical gradients in soil composition from the surface to greater depths. Gradients in soil bulk density, temperature, nutrients and organic matter affect root architecture by modulating root penetration capacity, root internal cell activity, root promotion and impacting the diversity and abundance microbial communities involved in soil-root interactions (Carvalho et al., 2024; Dini-Andreote et al., 2025; Lattacher et al., 2024; Wang, 2025).

Another factor that may have led to differences between our climate chamber and field results was the intensity of plant-plant interactions. Under controlled conditions, the planting density was 200 plants per m², whereas in the field, it was 300 plants per m² (Le Gall et al., 2025). Second, plant-plant interactions were limited to two individuals in a single soil column in the climate chamber. In the field, however, each plant interacted with potentially 150 other wheat individuals considering an average root spread over a radius of 20cm (Weaver, 1926). The diversity of individuals involved in root-to-root communication can elicit different responses than when exposed to a single other individual, in a so called “population effect” whereby responses to a single neighbor differ qualitatively from responses to a plant community (Semchenko et al., 2014; Yang et al., 2015).

These results underscore the significance of phenotyping roots under field conditions and at various stages of development to ensure that, the traits of genotypes of interest correspond to the targeted environmental variability. Although root phenotyping and experiments in controlled environments are essential for the temporal and spatial detail of the data collection, as well as the higher diversity of available instruments and methods, they cannot replace field trials with greater pedoclimatic and biological variability. Consequently, when developing ideotypes within plant selection schemes, it may be advantageous to prioritize not only the selection of genotypes for "average" traits but also for their capacity to exhibit resistance and dynamic resilience to rapid environmental fluctuations.

4.2. Resource allocation strategies and adaptation to seasonal climate variability

With regard to vegetative traits, in contrast to belowground traits, the DRS in monoculture exhibited a faster rate of spatial occupation of the aerial space than the SRS. This phenomenon was evident in the faster and higher growth of canopy height, blade leaf size and therefore leaf area (Fig. 47e). Consequently, there was a 25% increase in average aboveground dry biomass for DRS in comparison to SRS at 90 DaS (Fig. 47c). The leaf surface's functions in terms of transpiration may have differed as well. DRS showed lower average leaf temperatures in the middle of the day than SRS (NS) (Fig. 47d).

Consequently, the two genotypes showed two different strategies for allocating resources to develop water uptake and transpiration structures. The SRS initially prioritized developing the root system, while the DRS prioritized developing aboveground structures. These physiological differences were most pronounced during the vegetative period and early reproductive stages. Subsequent to flowering, the SRS aboveground traits demonstrated a gradual convergence with the DRS, and vice versa for underground structures, to the extent that the pRLD of the DRS was in the subsoil (120 cm) compared to the SRS (Fig. 48).

After faced with a one month chronic water deficit over the keys stages of ear ovule development to flowering, the aerial structures of the DRS proved to be less resistant than those of the SRS. These results are consistent with the replicated controlled experiment conducted at the booting stage (20 days before flowering in the field), which demonstrated that these same SRS genotypes exhibited superior water deficit resistance compared to DRS (Le Gall et al., 2025). Here the DRS dried out and lost leaf area more quickly than SRS in the late grain filling stages, reducing the reproductive stages duration (Fig. 47e). While this was not enough to affect significantly the grain filling, the number of fertile flowers per ear, led to significant differences between the SRS and DRS (Fig. 52c). Thus, the tension between allocating above-ground resources for carbon assimilation by above-ground structures and allocating underground resources for water and nutrient assimilation by roots may have caused the DRS to allocate fewer resources to reproduction than the SRS.

In the framework of this experiment alternating severe thermal and water events during a complete spring wheat growing season, the strategy of SRS, prioritizing first the investment in belowground organs, proved to be the most suitable in terms of physiological resistance to water deficit. Thus, rather than just root depth during the water deficit period, the relative dynamics of root-to-shoot development during vegetative establishment of the individuals, with an initial relative priority given to roots, appears to be an important trait for drought adaptation. This finding was consistent with the conclusions of recent literature reviews, which described an adaptive advantage to water deficit for a higher root-to-shoot investment (Eziz et al., 2017; Shoaib et al., 2022; Xu et al., 2025). The adaptive advantage ultimately resulted in a 23% increase in yield for SRS compared to DRS.

4.3. Non-additive effects of the wheat genotype mixture for better yield

Our second hypothesis was that mixing two varieties produces non-additive effects (synergy, niche complementarity, etc.) leading to yields similar to or higher than those obtained in monoculture under stress conditions.

We can confirm this hypothesis by observing higher wheat yields in the mixture than in the two monocultures. This was due, in particular, to the mixture having a 9% and 17% higher density of fertile ears than the DRS and SRS monocultures, respectively, resulting in more leaves production and fertile tillers, in particular for SRS (+60%) and for DRS (+ 14%) genotypes growing in mixture than in monoculture. Such emerging pattern in mixture was also observed in other recent studies (Kong et al., 2023a; Stefan et al., 2025a). This may also have led to increased adventitious root emission from the tillers, resulting in greater root density at a depth of 20 cm (Fig. 48k).

This overproduction of shoots for both varieties in the mixture, as well as the slower growth in canopy height for the SRS compared to monoculture, may have been induced by a complementary strategy of space occupation and resource exploitation. At the first development stage, SRS in mixture was more aggressive in developing its root system in the topsoil and was able to benefit from 50% of the surrounding individuals being less competitive in their root development strategy, as reported under controlled conditions by Montazeaud et al. (2025). This in turn may have forced the DRS genotype to decrease its investment in canopy height in mixture, lower than in monoculture (Fig. 45f). This reallocation is consistent with the well-established negative relationship between plant height and harvest index in wheat: taller stems represent an increased vegetative carbon sink that competes with ear development for assimilates, while reduced stem elongation has been shown to improve dry matter partitioning towards reproductive organs and increase yield under water-limited conditions (Shaheen et al., 2025). The mixture-induced moderation of DRS canopy height may thus reflect a shift in resource allocation from stem elongation to tiller and ear production, consistent with the higher fertile ear density observed in the mixture. Furthermore, it was possible that chemical signaling between genetically distinct neighbors (shown to modify root allocation and shoot development in response to non-self root exudates) may have contributed to the over-tillering response observed in the mixture (Biedrzycki et al., 2010).

Root system architecture, quantified here by the minirhizotron plane root length density (pRLD), may have played a role leading to these aboveground non transgressive effects. The root profile exhibits a typically plastic response to soil water availability, with peak proliferation occurring under optimal water conditions (SWC = 0.25–0.30 cm^3/cm^3). This pattern reflects a compensatory allocation strategy: when water is neither scarce nor in excess, plants maximize their root investment to enhance water and nutrient uptake; conversely, both water deficit and waterlogging inhibit root growth through distinct physiological constraints (Duan et al., 2010; Jones et al., 2025; Spollen and Sharp, 1991). Thus, the pRLD–SWC relationship observed in field conditions demonstrated how a key structural trait responds dynamically to fluctuations in resource availability, maintaining a functional balance across heterogeneous soil profiles (Fig. 51).

In examining the plant modalities' responses to this trait-environment relationship, we observed a trend toward transgression for the MIX (NS) mixture, which exhibited a modal maximum root density of 0.47 cm cm^{-2}, compared to 0.45 cm cm^{-2} for the SRS and 0.42 cm cm^{-2} for the DRS, suggesting that physiological integration within the mixture could rise emerging root allocation strategies.

This trend could be explained in part by the observations at a depth of 20 cm of the mixture exhibited a root density throughout the growing season that exceeded the

arithmetic mean of the two monocultures for the same soil water content (SWC), indicating a non-additive root effect ($p < 0.05$). This positive transgression was also observable at the flowering stage at 60 cm (compared to the DRS; $p < 0.001$) and at 80 cm (compared to the SRS; $p < 0.05$).

Two mechanisms may provide a theoretical basis for theses phenomenon: The initial observation indicates an increase in the number of primary roots in the mixture (see Chapter 3), which mechanically increases root density at all depths. Secondly, plasticity in root proliferation is induced by the recognition of neighbors of a different genotype, which is consistent with the results of Montazeaud et al. (2025) on the reduction of root competition in wheat mixtures and according to Mathieu et al. (2024), demonstrating the specific effect of metabolite cocktails on the wheat root phenotypes when combined with a mixture.

It is important to note here a critical methodological issue with the minirhizotron that could have affected the root distribution under dry soil conditions for all plant modalities. On the one hand, the clay particles in our soil can shrink away from the surface and detach the roots from contact with the transparent tube, thereby altering the camera's focus that was on the tube surface. On the other hand, as the soil dries out, it lightens in color, making the soil-root contrast more difficult to segment for the CNN. To address this, our segmentation model was trained on images covering all stages of root development and soil conditions; however, these are potential biases that should be noted.

Our study also showed that the amount of water extracted by the roots was not directly proportional to yield levels. Starting from the second drought period, we observed that SRS extracted in absolute more water from the soil profile than MIX, and even more than DRS. Although the DRS extracted relatively less water and had the lowest yield, higher C and N rates (and therefore higher concentrations) were observed for the DRS than for the SRS. The greater water deficit experienced by the DRS compared to the SRS may have led to a nutrient concentration in the reproductive organs without increasing grain yield levels. In contrast, MIX, which had intermediate C and N concentrations between SRS and DRS, had a higher grain yield than SRS despite extracting less water. The greater water use efficiency with which this wheat mixture use water for grain production underscores the importance of resource allocation strategies described above. As Messina et al. (2021) point out, in addition to improving ideotypes characterized by aboveground, reproductive, and root traits, breeding programs should consider these non-additive effects of genetically diverse populations.

In terms of grain maturity, the DRS genotype demonstrated a more rapid response to water stress compared to the SRS genotype, resulting in a three days earlier grain

maturity by several days. Nonetheless, this negligible discrepancy did not negate the potential for a combined harvest from an agronomic perspective.

5. Conclusions

This study highlights the complex interactions between wheat genotypes and environmental variability, demonstrating that both temporal and spatial variability shape root and shoot development. The SRS and DRS genotypes exhibited contrasting strategies for resource allocation: SRS prioritized early root investment, enhancing resilience to water deficit and achieving higher yield under alternating drought and heat stresses, while DRS allocated more resources to aboveground growth initially, which improved early vegetative biomass but reduced reproductive success under prolonged stress. These findings underscore the importance of considering not only static root and shoot traits but also their dynamic plasticity across developmental stages and in response to fluctuating environmental conditions.

The results also confirm that genotype mixtures can produce non-additive effects that enhance overall performance under different abiotic stress. The mixture outperformed the monocultures in yield, not necessarily through greater water uptake but via improved resource-use efficiency, complementarity in root development, reduced canopy high and mitigated early competition among genotypes. This demonstrates that strategic combinations of genotypes can take advantage of differences in root and shoot allocation to buffer environmental stresses and optimize resource utilization at the population level.

These findings have important implications for crop selection and management. Rather than targeting "average" trait values, we should also consider the ability of genotypes to express complementary strategies. Integrating knowledge about root plasticity at different developmental stages and about the distribution patterns and effectiveness of mixtures can improve ideotype design and the design of mixtures themselves. This can increase wheat productivity resilience to climate variability enhanced with climate change.

Chapter 5

General discussion and future prospects

1. General discussion

1.1. Originality and complementarity of the methods

The application of water stable isotope tracing (δ^2H / $\delta^{18}O$) to root water uptake estimation at the individual plant level has well-established precedents in ecohydrology. This precedent extends from the pioneering destructive approaches of (Dawson and Ehleringer, 1991) to continuous in situ monitoring frameworks developed across multiple research groups (Deseano Diaz et al., 2023; Kübert et al., 2023; Kühnhammer et al., 2020; Rothfuss et al., 2013; Volkmann et al., 2016). However, all published implementations of this approach — whether destructive or continuous — have been conducted on single-plant systems, where the entire root system of one individual occupies the monitored soil volume. The extension of isotopic monitoring to two genotypes cultivated concurrently in the same soil profile represents a methodological advancement: by physically splitting the aerial compartment into two independent flushing circuits, each connected to its own laser spectrometer inlet, the transpiration fluxes of the two plants can be measured separately. This allowed their individual δTr values — and by extension their fractional root water uptake (fRWU) profiles — to be computed independently and simultaneously. To the best of our knowledge, no prior study had simultaneously estimated the individual fractional root water uptake profiles of two genotypes of the same species grown in a shared soil volume.

The experimental design developed in this thesis combines three interdependent aspects:

1) a multi-depth isotopic labeling strategy to decouple the soil water $\delta^{18}O$ and δ^2H profiles. The strategy was designed to generate a monotonic gradient for one isotope and a V-shaped gradient for the other. The result of this strategy was that soil water sources at different depths occupied distinct positions in the two-dimensional isotopic space. This was achieved so that these sources did not align along the Global Meteoric Water Line (Craig, 1961; Deseano Diaz et al., 2023). This decorrelation substantially reduces the uncertainty of fractional source estimates by the SIAR Bayesian mixing model (Parnell et al., 2010), which incorporates root biomass distribution derived from MRI as informative priors;

2) a split-chamber transpiration system was designed and validated, enabling independent continuous monitoring of the vapor flux of each plant through separate gas-tight enclosures connected to a Picarro laser spectrometer. This engineering development had no precedent in the ecohydrological literature (Dubbert et al., 2019; Kühnhammer et al., 2020). The technical challenges encountered during the development process were documented and can now serve as methodological contributions.

3) a non-destructive three-dimensional monitoring system for root architecture based on magnetic resonance imaging (MRI). The scope of application has been extended beyond its use previously described in the literature to account for larger soil volumes (over 7.5 L at 800 mm in height and 110 mm in internal diameter) and, for the first time, two root systems growing within the same soil volume (Gruwel, 2014; Pflugfelder et al., 2022b, 2017; Stingaciu et al., 2013; van Dusschoten et al., 2016). This facilitated the repeated, in situ mapping of the three-dimensional root architecture, as well as the distribution of biomass with respect to depth, for two genotypes growing simultaneously within the same soil profile.

A central and original contribution of this thesis lied in coupling, within a single experimental system, methods that each provide complementary information on root system structure and function — none of which, taken alone, would have resolved the questions addressed here. Magnetic resonance imaging (MRI) facilitated non-destructive three-dimensional mapping of root architecture at a vertical resolution of 7 millimeters, capturing primary root and crown root structures exceeding 350 micrometers in diameter. This approach provided the biomass and root tip density distributions across depth horizons to better discuss the SIAR fRWU estimations profiles derived from water stable isotope analysis, without prior information's following the recommendations of Rothfuss and Javaux (2017). In parallel, the destructive WinRHIZO analysis at harvest provided total root length, and specific root surface per diameter class, specific root length.

In field conditions (see Chapter 4), mini-rhizotron imaging provided non-destructive monitoring of root length density dynamics at six depth intervals across the full growing season. This method captured temporal patterns of root growth and senescence that are inaccessible to single-date destructive sampling (Bauer et al., 2022b). UAS-mounted multispectral imaging provided canopy-scale estimates of green area index, NDVI, and fractional radiation interception at weekly resolution, thereby enabling the establishment of a link between root dynamics and canopy performance at the plot scale.

Collectively, these methods established a multi-scale characterization framework from the root segment (MRI, WinRHIZO) to the individual plant (fRWU, manual aboveground traits recording) and the plot (mini-rhizotron, UAS).

In addition, the use of water stable isotopes unfold plant water uptake patterns but requires the assumption of steady-state transpiration to be met and is limited in vertical resolution by the dimensions and positioning of the gas-permeable membranes. Mini-rhizotron imaging was a great indicator of the timing of root development across the season, although it yields only relative root length densities.

At the canopy scale, UAS-derived indicators — including LiDAR-based plant height, multispectral LAI from NDVI, and thermal leaf surface temperature — extended this framework to the plot level, bridging individual plant measurements and

genotype-scale functional differences. Their convergence with ground-truth manual measurements validated the upscaling approach, while leaf surface temperature in particular provided a non-destructive canopy-scale proxy for genotype-specific hydraulic strategies during the spring drought. However, the discrete nature of UAS acquisitions — conducted at one to two week intervals and at a fixed time of day — limits the interpretation of thermal and spectral signals, given that stomatal conductance, canopy temperature, and radiation interception vary substantially across the diurnal cycle and in response to rapid meteorological fluctuations.

The integration of these methods within a two complementary experimental frameworks was mandatory to address our scientific questions.

1.2. Limitations

The greater ecological realism of the field setting came with methodological trade-offs: the root length densities measured in the minirhizotron were relative estimation rather than absolute RLD values as the six discrete measurement points were located along a 120-centimeter profile, and as the pictures were taken over a cylindrical surface area rather than within a soil volume. This was in contrast to destructive measurements using WinRhizo scanning or soil column MRI measurements, which were able to display root traits a soil volume. Additionally, the soil water dynamics monitored with TDR and Teros21 sensors considered both precipitation, water transfer between soil horizons and evapotranspiration fluxes as the absence of individual isotopic tracking prevented any direct estimation of fRWU.

Another source of discrepancy between the column experiment and field conditions concerns sowing density. The two column sizes used in this experiment correspond to sowing densities of approximately 400 plants m^{-2} (8 cm diameter, 50 cm^2 cross-section) and 200 plants m^{-2} (11 cm diameter, 100 cm^2), both of which fall within the agronomic range recommended for spring wheat in Central Europe (200–350 wheat grains sown m^{-2}). However, field sowing densities are deliberately set above the target plant density to account for germination failures, seedling emergence losses, and early mortality due to frost, pest or pathogen pressure (Peltonen-Sainio et al., 2009). In the column experiment, pre-germinated seedlings were individually selected and transferred, effectively guaranteeing a 100% establishment rate with no loss, and the two least vigorous seedlings per column were subsequently removed to standardize the plant number to two. The population density in the columns is therefore more homogeneous and less representative of the inter-plant variability that characterizes a field stand, where the irregular distribution of establishment failures creates micro-patches of reduced local competition that can substantially modify individual plant tillering and root foraging behavior.

Beyond the choice of measurement methods, a more fundamental limitation of this thesis concerns the choice of biological model. We used two quasi-isogenic spring wheat lines (UQR12 and UQR15) with contrasting root architectures, whereas—as

noted in Chapter 1—winter wheat is much more widely cultivated than spring wheat at Central European latitudes and is generally better adapted to the region's climatic risks (e.g., late spring frosts, early spring drought).

The selection of these spring genotypes was informed by two interwoven methodological constraints. Firstly, the central scientific question necessitated a genetic pair that exhibited a robust, reproducible and architecturally well-characterized root contrast (shallow vs. deep root system) while sharing a synchronous phenology, with the objective of disentangling the effects of root strategy from those of developmental asynchrony. UQR12 and UQR15 are full sister lines, having been derived from the same biparental cross with the recurrent parent Borlaug100. The lines in question have been characterized in the literature for their contrasting seminal root angles (Rambla et al., 2022), thus rendering them the most suitable pair available at the time of the experimental design. Conversely, the controlled column experiment necessitated a relatively brief growth cycle to facilitate its replication within the time constraints imposed by the thesis, with a duration of approximately 45 days from sowing to the booting stage. This approach was rendered impractical when working with winter genotypes, which require a vernalization step of several weeks at low temperature.

Consequently, the present thesis should be regarded as a proof-of-concept demonstration rather than as a direct test of winter-wheat behavior under field-relevant drought scenarios. The mechanisms documented here — root-trait-driven niche segregation, non-additive uptake patterns in mixture, mixture-induced tillering plasticity — are mechanistically generic and are therefore expected to operate similarly in winter cultivars expressing comparable root-architectural diversity.

1.3. From controlled conditions to field variability

As delineated in Chapter 2, the biological and technical underpinnings of the thesis were established. The comparative phenotypic screening of commercial varieties (Treblir®/Milaneco®) and near-isogenic experimental lines (UQR12/UQR15) showed that UQR12 and UQR15 exhibited the most divergent root structural and functional traits at booting stage. A notable finding was the revelation of a limitation to early-stage phenotyping in controlled conditions (Rambla et al., 2023) — which offer the advantage of direct root visualization but constrain growth to a two-dimensional plane and an artificial substrate — compared to later root trait characterization at later development stage. Specifically, the root insertion angle measured at the seedling stage did not persist as a reliable predictor of architectural divergence – even if divergences regarding other traits were displayed later. This observation highlights the potential risk of extrapolating single-stage controlled observations to the entire growth cycle. The subsequent validation of the isotopic labeling protocol and split-chamber transpiration system — which enables continuous, individual-level monitoring of vapor flux but imposes strict constraints

on column geometry, soil volume, and labeling timing — identified the experimental configuration that maximized fRWU estimation quality, at the cost of a soil volume below those experienced by wheat under agronomic reality.

Chapter 3 leveraged the high internal validity of this controlled framework to address the central mechanistic question: does hydrological niche segregation exist between two wheat genotypes with contrasting root architectures, is it modified in mixture, and does water deficit reinforce or attenuate it? The reproducibility and environmental control of the column system were of the essence in this study, as they enabled the attribution of observed fRWU differences to genotypic rather than environmental factors. The findings indicated that niche segregation was not only identifiable but also exhibited reinforcement under conditions of water deficit. Furthermore, the mixture induced a collective downward shift in water uptake that could not be attributed to the root biomass distribution of either genotype alone. This finding would have been unattainable through root architecture measurements alone and necessitated the comprehensive isotopic fRWU estimation pipeline. This finding was consistent with the isotopic evidence for niche restructuring induced by interspecific interactions documented by (Kinzinger et al., 2024) in mixed beech-spruce forests, and with the first systematic evidence for isotope-detectable hydrological complementarity in agricultural intercropping systems (Schmutz and Schöb, 2023). Furthermore, the replicated controlled conditions was possible thanks to homogenized conditions and standardized procedures over the six successive run, thereby enabling statistical analysis and the validation of the concept. However, such set-up did not take into account the natural climate or soil variability present in field conditions.

Therefore, Chapter 4 examined the validity of these conclusions under field conditions at the TERENO Selhausen platform (Germany). The natural variable weather conditions of the 2022–2023 growing season was used as the source of seasonal stress variability, including late spring frost, a month-long drought, and intense rainfall during grain filling. This provided an agronomically realistic but experimentally uncontrolled stress variability. Within the aforementioned constraints, several conclusions from Chapter 3 were corroborated: SRS demonstrated greater drought tolerance in comparison to DRS, despite exhibiting lower transpiration rates and stomatal conductance both in field and controlled conditions, resulting in higher field yields for SRS in comparison to DRS. Furthermore, the mixed-crop plots exhibited superior yields in comparison to both monocultures, particularly due to a higher fertile ear density. This phenomenon can be attributed to the enhanced plasticity of plants to tiller in mixed crops compared to monocultures — a manifestation of context-dependent phenotypic plasticity (Tardieu, 2012). This observation has also been made under controlled conditions, involving also the growth of more adventitious roots in mixed crops, but also in other research projects as mentioned in the discussion of Chapter 4.

2. Conclusion and key messages

The combination of stable isotope labeling of water at several depths and Bayesian modeling makes it possible, for the first time, to estimate non-destructively measure the root water uptake profiles of two genotypes of the same species grown in the same soil. We believe that it is ground for detailed, high-resolution studies of intra-specific interactions related to water.

We showed that the two wheat genotypes with contrasting root architectures keep their preferred root water uptake niches when grown in mixture. Moreover, in mixture, we observed a root water uptake collective shift to deeper soil layers for both genotypes.

We highlighted that root water uptake plasticity was not only determined by the root traits and soil water availability, but also by the interaction with the neighboring plants.

Counterintuitively, the deep-rooted genotype (DRS) did not show better resistance to water deficit than the shallow-rooted genotype (SRS). The strategy of favoring investment in underground organs early in the cycle (SRS) was more effective in maintaining leaf area, fertile tiller number, and yield under water stress, both under controlled conditions and in field plots. This further highlights the importance of topsoil layers in plant adaptation strategies to drought, as previously emphasized by (Deseano Diaz et al., 2023; Prechsl et al., 2015).

The tested genotype mixture produced non-additive positive effects on yield, mainly through an increase in fertile ear density (and therefore their numbers of adventive root) and improved water use efficiency. Other non-additive effect emerged in mixture leading to changes in resources allocation within plant structure, such as the root biomass “overdensity” around 20 cm (both in Chap. 2 and 4), the canopy high reduction (Chap. 4) but also a reduced root exudation amount under water deficit (Lattacher et al., 2025b).

These effects could result from the structural and functional complementarity of root systems, from reduced early competition between genotypes and from the transfer and perception of a complex metabolite cocktail whose composition varies with genotype and whose components differentially contribute to receiver phenotypes, rather than a simple increase in total water uptake or to competition alone.

3. Perspectives

3.1. Technical improvements and simplification of the experimental framework

The experimental setup developed in this thesis — comprising simultaneous split gas-exchange chambers and functional pneumatic piping that enables continuous laser isotope monitoring — constitutes a methodological breakthrough for individual RWU estimation in plant mixtures. However, the complexity of the setup limits throughput and replication capacity. A promising direction for simplification is the development of direct plant water sampling methods that bypass the need for transpiration chambers entirely. For annual plants with hollow or semi-hollow stems (including wheat), direct stem water extraction via in-stem vapor continuous sampling would allow isotopic characterization of xylem water without the engineering constraints associated with gas-tight enclosures, airtight stem seals, and humidity regulation. Such an approach, analogous to methods already validated for woody species (Marshall et al., 2020), would make individual isotopic RWU monitoring accessible to a wider range of experimental contexts and genotypic screening programs. Such a method was developed and studied in parallel of this thesis, and submitted in march 2026 to Hydrology and Earth System Sciences by Rothfuss and colleagues (including Le Gall) with the title "*Online xylem water isotope monitoring and soil water content profiling reveal spatial root water uptake dynamics in sunflower*". The future implementation of such a method for other plant families, as the Poaceaes for example - as they provide more than 50% of the world daily calories, Awika (2011) - would expand its range of application.

Furthermore, infra-daily temporal resolution can be identified as a significant methodological frontier. The present protocol yields a single RWU profile per day, a figure insufficient to capture nocturnal hydraulic redistribution dynamics. The hypothesis that the deep-rooted genotype (UQR15/DRS) redistributes water upward through hydraulic lift during the night – potentially benefiting the neighboring shallow-rooted genotype (UQR12/SRS) – remains untested. Resolving this mechanism would necessitate the undertaking of isotopic measurements at two- to four-hour intervals across the diel cycle. It is technically feasible to achieve this higher temporal resolution within the constraints of the existing split-chamber and laser spectrometry setup. Since soil water isotopic compositions ($\delta^{18}O$ and $\delta^{2}H$) vary at timescales ranging from hours to days rather than minutes, the sampling frequency allocated to soil vapor probes could be reduced relative to that allocated to transpiration flux monitoring. This adjustment would free instrument time for more frequent δ_T acquisitions without compromising the characterization of source water endmembers. A reallocation of measurement frequency between the soil and plant compartments would constitute a protocol adjustment that would be straightforward to implement. This an adjustment would enable diel-cycle resolution of individual fRWU dynamics in future experiments.

A dataset of this nature has been partially collected. It is evident that the transpiration chambers were placed on the replicate plants for a period of just over four consecutive full days. Consequently, the isotopic compositions of the water (δ^2H and $\delta^{18}O$) were measured at three other times of day, which spanned the entire diurnal cycle: early morning, late afternoon, and overnight. However, these were not analyzed in this thesis; rather, they were collected to verify the feasibility of this methodological improvement and to potentially enable future characterization of the temporal dynamics of individual RWU profiles throughout the diurnal cycle. In addition to the datasets that were directly analyzed in this thesis, continuous $\delta^{13}C$ measurements of CO_2 fluxes were also collected in parallel for all modalities and treatments, constituting a dataset available for future characterization of genotype-specific carbon assimilation and respiration dynamics under water deficit.

3.2. Towards more comprehensive semi-mechanistic modeling

Only a small portion of the data accumulated in this thesis — root architecture parameters, biomass distribution by depth, and soil hydraulic properties from DRS genotype only during the experiments developed in the second chapter— has already contributed to the parameterization of the functional-structural plant model CPlantBox (Giraud, Le Gall et al., 2023). This contribution was the preliminary integration of experimental findings into a semi-mechanistic modelling framework. However, the potential for more profound coupling or parametrization remains largely unexplored.

A way forward would be to utilize the complete column and field datasets to model the non-additive effects of intraspecific wheat mixtures, particularly to better understand the mechanism of the collective shift in water uptake depth and the increase in shoot and primary root number documented in Chapters 3 and 4. CPlantBox could be used to test whether these emergent effects are reproducible from root architectural parameters alone, or whether they require the explicit representation of (hydraulic, chemical, or microbial) inter-plant interactions. This approach would facilitate the disentangling of competitive from facilitative mechanisms and the identification of the traits most predictive of non-additive mixture performance. However, beyond water transport, the model does not currently feature a fully developed nitrogen transport module. The development of such a module, when coupled with the existing hydraulic framework, would facilitate the simultaneous simulation of water and nitrogen acquisition strategies in genotype mixtures. This was a critical step given the tight coupling between water and nitrogen uptake through mass flow in the soil solution. Furthermore, the extension of the reproductive phase module of CPlantBox to simulate yield component formation — grain number per spike, grain filling rate, harvest index — would facilitate the closure of the modelling chain from root architecture to final agronomic performance.

Additionally, the rhizosphere model was successfully coupled with the soil-plant-atmosphere model (Giraud et al., 2025; Sırcan et al., 2025). This coupled model could be now used to disentangle the role of root exopolymers — mucilage and other rhizodeposits — in modifying soil hydraulic properties at the root-soil interface in a genotype mixture configuration (Carminati et al., 2016; Doussan et al., 2006, 2024; Le Gall et al., 2021). Integrating this dimension would allow the model to capture genotype-specific differences in rhizosphere hydraulic conductivity that may contribute to the structure-function decoupling documented in Chapter 3.

3.3. Broadening the scope: nitrogen, genotype diversity, and field applicability

While the present thesis focused mainly on the response of intraspecific wheat mixtures to water deficit, it is also important to acknowledge the role of nitrogen nutrition in determining root development, shoot/root growth, and yield. Water and nitrogen acquisition are tightly coupled in the root zone — root foraging strategies that confer a competitive advantage for water uptake under drought may simultaneously alter nitrogen interception, particularly when genotypes with contrasting rooting depths are grown together. Whether the hydrological niche complementarity documented here translates into complementary nitrogen uptake patterns, or whether nitrogen availability modulates the expression of root architectural contrasts and their functional consequences, remains an open question. Field experiments combining contrasting root genotypes with varying nitrogen input levels would be a natural next step, as they would allow assessment of whether the non-additive effects on water use efficiency documented in this thesis are maintained, amplified, or suppressed under nitrogen limitation.

In addition to the two genotype pairs examined in this study, it would be necessary to assess implementation with wheat genotypes from other commercial gene pools that would represent the full range of root functional diversity available in commercial wheat genotypes or even from “older” genotypes (Baca Cabrera et al., 2025), in order to facilitate practical implementation. Key targets include the identification, in available genomic collections, of the root traits most predictive of functional complementarity in mixture—fine root surface area, number of seminal roots, and plasticity of root insertion angle rather than the angle itself—and the assessment of whether mixture ratio (50:50 vs. asymmetric proportions) and sowing density modulate the intensity of non-additive effects.

Under Central European climate scenarios with increasing late-spring drought risk, mixtures offer an insurance strategy: rather than gambling on a single variety's drought tolerance, farmers can blend complementary varieties, reducing yield variance across seasons of variable rainfall. Our results suggest that the combining a shallow- and deep-root system specifically delivers this benefit through improved water-use efficiency and reduced competition intensity.

Beyond the identification of complementary genotypes, understanding why certain genotype combinations generate non-additive effects requires addressing the mechanisms of plant-plant communication at the root level — a question that connects the agronomic context of this thesis to broader evolutionary questions.

3.4. The root trait-function relationship and the plant-plant communication

The relationships between root traits and their associated functions emerge from genetic inheritance expressed under specific environmental conditions. The relationships between root traits and their associated functions are shaped by both the long evolutionary history of plant lineages and, in the case of wheat, more recent domestication. Thus, a study about root traits in German wheat varieties selected over a 100-year period revealed a substantial decrease in the number of root axes and the overall hydraulic conductance of the root system (Baca Cabrera et al., 2025). Analysis of root fossils spanning 300 million years reveals a decline in mean root diameter across major plant lineages (Comas et al., 2013). Meanwhile, contemporary woody species display phylogenetic signals in the correlation between specific root length and specific leaf area, contingent on mycorrhizal type (Suzuki et al., 2026). Furthermore, evidence was presented demonstrating that the chemical composition of root mucilage exhibited a robust phylogenetic signal across eight cultivated angiosperm species, including several Poaceae species, such as wheat (Le Gall et al., 2024). However, its capacity for water retention and its ability to stimulate microbial activity exhibited a divergent pattern, suggesting a dissociation between root trait and associated functions, grounded in the broader root trait literature (Freschet et al., 2021b).

This structure-function decoupling is not confined to the interspecific or phylogenetic scale. At the intraspecific level, Chapters 3 and 4 documented a similar observation: the root traits measured could not fully account for the observed water uptake patterns in either monoculture or mixture. The recurrence of this decoupling — from deep phylogenetic divergences to intraspecific variation within a single cultivated species — suggests that the relationship between root structure and function is inherently context-dependent. Part of this context-dependence may reflect coevolutionary dynamics within plant communities, where the recurring identity of neighbors gradually could have shape root phenotypes through selection (Weiner et al., 2010; Zhu et al., 2019). This co-evolutionary dimension is not only historical: as this thesis demonstrated, the functional expression of root traits and functions in wheat genotypes was actively conditioned by neighboring plants. The collective shift in root water uptake toward deeper layers, the increase in shoot and adventitious root number, and the modification of rhizosphere microbial activity together indicate inter-plant signaling beyond simple competitive displacement, consistent with recent evidence of

chemical communication mediated by rhizosphere metabolite exchanges (Anten and Chen, 2021; Biedrzycki et al., 2010; Mathieu et al., 2025; Semchenko et al., 2014).

Incorporating this signaling dimension into mixture design could open a complementary selection strategy: beyond identifying genotype combinations that maximize resource complementarity through contrasting architectures, breeders could select partners on the basis of the chemical signals they exchange and the phenotypic responses they elicit in neighbors. In this approach each genotype could actively guides the functional trajectory of its companion throughout development.

References

Akanda, S.I., Mundt, C.C., 1997. Effect of two-component cultivar mixtures and yellow rust on yield and yield components of wheat. Plant Pathology 46, 566–580. https://doi.org/10.1046/j.1365-3059.1997.d01-37.x

Albert, C.H., Grassein, F., Schurr, F.M., Vieilledent, G., Violle, C., 2011. When and how should intraspecific variability be considered in trait-based plant ecology? Perspectives in Plant Ecology, Evolution and Systematics 13, 217–225. https://doi.org/10.1016/j.ppees.2011.04.003

Altieri, M.A., Nicholls, C.I., Montalba, R., 2017. Technological Approaches to Sustainable Agriculture at a Crossroads: An Agroecological Perspective. Sustainability 9, 349. https://doi.org/10.3390/su9030349

Angeletti, F.G.S., Mariotti, M., Tozzi, B., Pampana, S., Saia, S., 2022. Herbage and silage quality improved more by mixing hybrid barley and faba bean than by N fertilization or stage of harvest. Agronomy. https://doi.org/10.3390/agronomy12081790

Anten, N.P.R., Chen, B.J.W., 2021. Detect thy family: Mechanisms, ecology and agricultural aspects of kin recognition in plants. Plant, Cell & Environment 44, 1059–1071. https://doi.org/10.1111/pce.14011

Asadullah, Kalhoro, S.A., Farhad, W., Iqbal, A., Sultan, Waheed, A., Rashid, M., Shah, S.R.U., 2024. Exploring the variability of root system architecture under drought stress in heat-tolerant spring-wheat lines. Plant Soil 502, 103–119. https://doi.org/10.1007/s11104-024-06795-4

Awika, J.M., 2011. Major Cereal Grains Production and Use around the World, in: Advances in Cereal Science: Implications to Food Processing and Health Promotion, ACS Symposium Series. American Chemical Society, pp. 1–13. https://doi.org/10.1021/bk-2011-1089.ch001

Baca Cabrera, J.C., Vanderborght, J., Boursiac, Y., Behrend, D., Gaiser, T., Nguyen, T.H., Lobet, G., 2025. Decreased root hydraulic traits in German winter wheat cultivars over 100 years of breeding. Plant Physiol 198, kiaf166. https://doi.org/10.1093/plphys/kiaf166

Bagale, S., Enesi, R.O., Gorim, L.Y., 2025. An overview of root traits and ideotypes for improving crop productivity and addressing agronomic challenges. Rhizosphere 34, 101105. https://doi.org/10.1016/j.rhisph.2025.101105

Barot, S., Allard, V., Cantarel, A., Enjalbert, J., Gauffreteau, A., Goldringer, I., Lata, J.-C., Le Roux, X., Niboyet, A., Porcher, E., 2017. Designing mixtures of varieties for multifunctional agriculture with the help of ecology. A review. Agron. Sustain. Dev. 37, 13. https://doi.org/10.1007/s13593-017-0418-x

Bates, J.S., Montzka, C., Bajracharya, R., Vereecken, H., Jonard, F., 2025. Spatiotemporal Characterization of Wheat Development Using UAV LiDAR Structure–Intensity Fusion with Multispectral and Thermal Data. EGUsphere 1–31. https://doi.org/10.5194/egusphere-2025-5336

Bauer, F.M., Lärm, L., Morandage, S., Lobet, G., Vanderborght, J., Vereecken, H., Schnepf, A., 2022. Development and Validation of a Deep Learning Based Automated Minirhizotron Image Analysis Pipeline. Plant Phenomics 2022, 9758532. https://doi.org/10.34133/2022/9758532

Beven, K., Germann, P., 2013. Macropores and water flow in soils revisited. Water Resources Research 49, 3071–3092. https://doi.org/10.1002/wrcr.20156

Beyer, M., Koeniger, P., Gaj, M., Hamutoko, J.T., Wanke, H., Himmelsbach, T., 2016. A deuterium-based labeling technique for the investigation of rooting depths, water uptake dynamics and unsaturated zone water transport in semiarid environments. Journal of Hydrology 533, 627–643. https://doi.org/10.1016/j.jhydrol.2015.12.037

Biedrzycki, M.L., Jilany, T.A., Dudley, S.A., Bais, H.P., 2010. Root exudates mediate kin recognition in plants. Commun Integr Biol 3, 28–35. https://doi.org/10.4161/cib.3.1.10118

Bilgic, H., Hakki, E.E., Pandey, A., Khan, M.K., Akkaya, M.S., 2016. Ancient DNA from 8400 Year-Old Çatalhöyük Wheat: Implications for the Origin of Neolithic Agriculture. PLOS ONE 11, e0151974. https://doi.org/10.1371/journal.pone.0151974

Bittlingmaier, M., Delgado-Baquerizo, M., Soliveres, S., Freschet, G.T., 2026. Plant Competitive Balance and Intransitivity Shape Ecosystem Multifunctionality in Grasslands Under Drought. Ecology Letters 29, e70354. https://doi.org/10.1111/ele.70354

Blanc, L., Lampurlanés, J., Simon-Miquel, G., Jean-Marius, L., Plaza-Bonilla, D., 2024. Rapeseed-pea intercrop outperforms wheat-legume ones in land-use efficiency in Mediterranean conditions. Field Crops Research 318, 109612. https://doi.org/10.1016/j.fcr.2024.109612

Bongers, F.J., Evers, J.B., Anten, N.P.R., 2025. Plastic responses for intercrop functioning. npj Sustain. Agric. 3, 8. https://doi.org/10.1038/s44264-025-00048-2

Borg, J., Kiær, L.P., Lecarpentier, C., Goldringer, I., Gauffreteau, A., Saint-Jean, S., Barot, S., Enjalbert, J., 2018. Unfolding the potential of wheat cultivar mixtures: A meta-analysis perspective and identification of knowledge gaps. Field Crops Research 221, 298–313. https://doi.org/10.1016/j.fcr.2017.09.006

Bramley, H., Turner, N.C., Turner, D.W., Tyerman, S.D., 2009. Roles of Morphology, Anatomy, and Aquaporins in Determining Contrasting Hydraulic Behavior of Roots. Plant Physiology 150, 348–364. https://doi.org/10.1104/pp.108.134098

Brannan, T., Bickler, C., Hansson, H., Karley, A., Weih, M., Manevska-Tasevska, G., 2023. Overcoming barriers to crop diversification uptake in Europe: A mini review. Frontiers in Sustainable Food Systems 7.

Brooker, R.W., Bennett, A.E., Cong, W.-F., Daniell, T.J., George, T.S., Hallett, P.D., Hawes, C., Iannetta, P.P.M., Jones, H.G., Karley, A.J., Li, L., McKenzie, B.M., Pakeman, R.J., Paterson, E., Schöb, C., Shen, J., Squire, G., Watson, C.A., Zhang, C., Zhang, F., Zhang, J., White, P.J., 2015. Improving intercropping: a synthesis of

research in agronomy, plant physiology and ecology. New Phytologist 206, 107–117. https://doi.org/10.1111/nph.13132

Bruelheide, H., Dengler, J., Purschke, O., Lenoir, J., Jiménez-Alfaro, B., Hennekens, S.M., Botta-Dukát, Z., Chytrý, M., Field, R., Jansen, F., Kattge, J., Pillar, V.D., Schrodt, F., Mahecha, M.D., Peet, R.K., Sandel, B., van Bodegom, P., Altman, J., Alvarez-Dávila, E., Arfin Khan, M.A.S., Attorre, F., Aubin, I., Baraloto, C., Barroso, J.G., Bauters, M., Bergmeier, E., Biurrun, I., Bjorkman, A.D., Blonder, B., Čarni, A., Cayuela, L., Černý, T., Cornelissen, J.H.C., Craven, D., Dainese, M., Derroire, G., De Sanctis, M., Díaz, S., Doležal, J., Farfan-Rios, W., Feldpausch, T.R., Fenton, N.J., Garnier, E., Guerin, G.R., Gutiérrez, A.G., Haider, S., Hattab, T., Henry, G., Hérault, B., Higuchi, P., Hölzel, N., Homeier, J., Jentsch, A., Jürgens, N., Kącki, Z., Karger, D.N., Kessler, M., Kleyer, M., Knollová, I., Korolyuk, A.Y., Kühn, I., Laughlin, D.C., Lens, F., Loos, J., Louault, F., Lyubenova, M.I., Malhi, Y., Marcenò, C., Mencuccini, M., Müller, J.V., Munzinger, J., Myers-Smith, I.H., Neill, D.A., Niinemets, Ü., Orwin, K.H., Ozinga, W.A., Penuelas, J., Pérez-Haase, A., Petřík, P., Phillips, O.L., Pärtel, M., Reich, P.B., Römermann, C., Rodrigues, A.V., Sabatini, F.M., Sardans, J., Schmidt, M., Seidler, G., Silva Espejo, J.E., Silveira, M., Smyth, A., Sporbert, M., Svenning, J.-C., Tang, Z., Thomas, R., Tsiripidis, I., Vassilev, K., Violle, C., Virtanen, R., Weiher, E., Welk, E., Wesche, K., Winter, M., Wirth, C., Jandt, U., 2018. Global trait–environment relationships of plant communities. Nat Ecol Evol 2, 1906–1917. https://doi.org/10.1038/s41559-018-0699-8

Bybee-Finley, K.A., Ryan, M.R., 2018. Advancing Intercropping Research and Practices in Industrialized Agricultural Landscapes. Agriculture 8, 80. https://doi.org/10.3390/agriculture8060080

Calleja-Cabrera, J., Boter, M., Oñate-Sánchez, L., Pernas, M., 2020. Root Growth Adaptation to Climate Change in Crops. Front Plant Sci 11, 544. https://doi.org/10.3389/fpls.2020.00544

Carminati, A., Javaux, M., 2020. Soil Rather Than Xylem Vulnerability Controls Stomatal Response to Drought. Trends in Plant Science 25, 868–880. https://doi.org/10.1016/j.tplants.2020.04.003

Carminati, A., Zarebanadkouki, M., Kroener, E., Ahmed, M.A., Holz, M., 2016. Biophysical rhizosphere processes affecting root water uptake. Ann Bot 118, 561–571. https://doi.org/10.1093/aob/mcw113

Carvalho, J.I., Carayugan, M.B., Tran, L.T.N., Hernandez, J.O., Youn, W.B., An, J.Y., Park, B.B., 2024. Variation in Root Biomass and Distribution Based on the Topography, Soil Properties, and Tree Influence Index: The Case of Mt. Duryun in Republic of Korea. Plants 13, 1340. https://doi.org/10.3390/plants13101340

Ceperley, N., Gimeno, T.E., Jacobs, S.R., Beyer, M., Dubbert, M., Fischer, B., Geris, J., Holko, L., Kübert, A., Le Gall, S., Lehmann, M.M., Llorens, P., Millar, C., Penna, D., Prieto, I., Radolinski, J., Scandellari, F., Stockinger, M., Stumpp, C., Tetzlaff, D., van Meerveld, I., Werner, C., Yildiz, O., Zuecco, G., Barbeta, A., Orlowski, N., Rothfuss, Y., 2024. Toward a common methodological framework for

the sampling, extraction, and isotopic analysis of water in the Critical Zone to study vegetation water use. WIREs Water 11, e1727. https://doi.org/10.1002/wat2.1727

Chabert, S., Eeraerts, M., DeVetter, L.W., Borghi, M., Mallinger, R.E., 2024. Intraspecific crop diversity for enhanced crop pollination success. A review. Agron. Sustain. Dev. 44, 50. https://doi.org/10.1007/s13593-024-00984-2

Chamberlain, C.J., Cook, B.I., Morales-Castilla, I., Wolkovich, E.M., 2021. Climate change reshapes the drivers of false spring risk across European trees. New Phytologist 229, 323–334. https://doi.org/10.1111/nph.16851

Chanda, S.V., Singh, Y.D., 2002. Estimation of leaf area in wheat using linear measurements. Plant Breeding and Seed Science 46, 75–79.

Charmet, G., 2011. Wheat domestication: Lessons for the future. Comptes Rendus. Biologies 334, 212–220. https://doi.org/10.1016/j.crvi.2010.12.013

Chen, H., Nguyen, K., Iqbal, M., Beres, B.L., Hucl, P.J., Spaner, D., 2020. The performance of spring wheat cultivar mixtures under conventional and organic management in Western Canada. Agrosystems, Geosciences & Environment 3, e20003. https://doi.org/10.1002/agg2.20003

Chen, S., Long, L., Sun, X., Parsons, D., Zhou, Z., 2025. Responsive root traits and mitigating strategies for wheat production under single or combined abiotic stress. European Journal of Agronomy 162, 127393. https://doi.org/10.1016/j.eja.2024.127393

Chung, Y.A., 2023. The temporal and spatial dimensions of plant–soil feedbacks. New Phytologist 237, 2012–2019. https://doi.org/10.1111/nph.18719

Colagè, I., d'Errico, F., 2025. An empirically-based scenario for the evolution of cultural transmission in the human lineage during the last 3.3 million years. PLOS ONE 20, e0325059. https://doi.org/10.1371/journal.pone.0325059

Comas, L., Becker, S., Cruz, V.M.V., Byrne, P.F., Dierig, D.A., 2013. Root traits contributing to plant productivity under drought. Front. Plant Sci. 4. https://doi.org/10.3389/fpls.2013.00442

Copernicus Climate Change Service (C3S), 2025. European State of the Climate 2024. Copernicus Climate Change Service (C3S). https://doi.org/10.24381/14J9-S541

Craig, Harmon, 1961. Standard for Reporting Concentrations of Deuterium and Oxygen-18 in Natural Waters. Science 133, 1833–1834. https://doi.org/10.1126/science.133.3467.1833

Craig, H., 1961. Isotopic Variations in Meteoric Waters. Science 133, 1702–1703. https://doi.org/10.1126/science.133.3465.1702

Dawson, T.E., Ehleringer, J.R., 1991. Streamside trees that do not use stream water. Nature 350, 335–337. https://doi.org/10.1038/350335a0

Delval, L., Vanderborght, J., Javaux, M., 2024. Combination of plant and soil water potential monitoring and modelling demonstrates soil-root hydraulic disconnection during drought. Plant Soil. https://doi.org/10.1007/s11104-024-07062-2

Demir, G., Guswa, A.J., Filipzik, J., Metzger, J.C., Römermann, C., Hildebrandt, A., 2024. Root water uptake patterns are controlled by tree species interactions and

soil water variability. Hydrology and Earth System Sciences 28, 1441–1461. https://doi.org/10.5194/hess-28-1441-2024

Deseano Diaz, P.A., van Dusschoten, D., Kübert, A., Brüggemann, N., Javaux, M., Merz, S., Vanderborght, J., Vereecken, H., Dubbert, M., Rothfuss, Y., 2023. Response of a grassland species to dry environmental conditions from water stable isotopic monitoring: no evident shift in root water uptake to wetter soil layers. Plant Soil 482, 491–512. https://doi.org/10.1007/s11104-022-05703-y

Dini-Andreote, F., Wells, D.M., Atkinson, J.A., Atkinson, B.S., Finkel, O.M., Castrillo, G., 2025. Microbial drivers of root plasticity. New Phytologist 248, 52–67. https://doi.org/10.1111/nph.70371

Donald, C.M., 1968. The breeding of crop ideotypes. Euphytica 17, 385–403. https://doi.org/10.1007/BF00056241

Doussan, C., Gall, S.L., Ruy, S., Bérard, A., 2024. Utiliser les racines pour moduler les impacts des déficits en eau et améliorer la gestion de l'eau dans les agrosystèmes. Sciences Eaux & Territoires 8144–8144. https://doi.org/10.20870/Revue-SET.2024.45.8144

Doussan, C., Pierret, A., Garrigues, E., Pagès, L., 2006. Water Uptake by Plant Roots: II – Modelling of Water Transfer in the Soil Root-system with Explicit Account of Flow within the Root System – Comparison with Experiments. Plant Soil 283, 99–117. https://doi.org/10.1007/s11104-004-7904-z

Duan, Y., Zhang, W., Li, B., Wang, Y., Li, K., Sodmergen, Han, C., Zhang, Y., Li, X., 2010. An endoplasmic reticulum response pathway mediates programmed cell death of root tip induced by water stress in Arabidopsis. New Phytologist 186, 681–695. https://doi.org/10.1111/j.1469-8137.2010.03207.x

Dubbert, M., Cuntz, M., Piayda, A., Werner, C., 2014. Oxygen isotope signatures of transpired water vapor: the role of isotopic non-steady-state transpiration under natural conditions. New Phytologist 203, 1242–1252. https://doi.org/10.1111/nph.12878

Dubin, H.J., Wolfe, M.S., 1994. Comparative behavior of three wheat cultivars and their mixture in India, Nepal and Pakistan. Field Crops Research 39, 71–83. https://doi.org/10.1016/0378-4290(94)90010-8

Duchene, O., Celette, F., Barreiro, A., Dimitrova Mårtensson, L.-M., Freschet, G.T., David, C., 2020. Introducing Perennial Grain in Grain Crops Rotation: The Role of Rooting Pattern in Soil Quality Management. Agronomy 10, 1254. https://doi.org/10.3390/agronomy10091254

Duchene, O., Vian, J.-F., Celette, F., 2017. Intercropping with legume for agroecological cropping systems: Complementarity and facilitation processes and the importance of soil microorganisms. A review. Agriculture, Ecosystems & Environment 240, 148–161. https://doi.org/10.1016/j.agee.2017.02.019

Durodola, O.S., Rothfuss, Y., Hawes, C., Smith, J., Valentine, T.A., Geris, J., 2025. Stable water isotopes reveal modification of cereal water uptake strategies in agricultural co-cropping systems. Agriculture, Ecosystems & Environment 381, 109439. https://doi.org/10.1016/j.agee.2024.109439

El Hassouni, K., Alahmad, S., Belkadi, B., Filali-Maltouf, A., Hickey, L.T., Bassi, F.M., 2018. Root System Architecture and Its Association with Yield under Different Water Regimes in Durum Wheat. Crop Science 58, 2331–2346. https://doi.org/10.2135/cropsci2018.01.0076

Engbersen, N., Brooker, R.W., Stefan, L., Studer, B., Schöb, C., 2021. Temporal Differentiation of Resource Capture and Biomass Accumulation as a Driver of Yield Increase in Intercropping. Front Plant Sci 12, 668803. https://doi.org/10.3389/fpls.2021.668803

Essell, H., Krusic, P.J., Esper, J., Wagner, S., Braconnot, P., Jungclaus, J., Muschitiello, F., Oppenheimer, C., Büntgen, U., 2023. A frequency-optimised temperature record for the Holocene. Environ. Res. Lett. 18, 114022. https://doi.org/10.1088/1748-9326/ad0065

Eziz, A., Yan, Z., Tian, D., Han, W., Tang, Z., Fang, J., 2017. Drought effect on plant biomass allocation: A meta-analysis. Ecology and Evolution 7, 11002–11010. https://doi.org/10.1002/ece3.3630

Fang, L., Struik, P.C., Girousse, C., Yin, X., Martre, P., 2024. Source–sink relationships during grain filling in wheat in response to various temperature, water deficit, and nitrogen deficit regimes. J Exp Bot 75, 6563–6578. https://doi.org/10.1093/jxb/erae310

Feng, S., Gu, S., Zhang, H., Wang, D., 2017. Root vertical distribution is important to improve water use efficiency and grain yield of wheat. Field Crops Research 214, 131–141. https://doi.org/10.1016/j.fcr.2017.08.007

Feng, Z., Liang, Q., Yao, Q., Bai, Y., Zhu, H., 2024. The role of the rhizobiome recruited by root exudates in plant disease resistance: current status and future directions. Environmental Microbiome 19, 91. https://doi.org/10.1186/s40793-024-00638-6

Fischer, R.A., 1985. Number of kernels in wheat crops and the influence of solar radiation and temperature. The Journal of Agricultural Science 105, 447–461. https://doi.org/10.1017/S0021859600056495

Fletcher, A., Ogden, G., Sharma, D., 2019. Mixing it up – wheat cultivar mixtures can increase yield and buffer the risk of flowering too early or too late. European Journal of Agronomy 103, 90–97. https://doi.org/10.1016/j.eja.2018.12.001

Fort, F., Volaire, F., Guilioni, L., Barkaoui, K., Navas, M.-L., Roumet, C., 2017. Root traits are related to plant water-use among rangeland Mediterranean species. Functional Ecology 31, 1700–1709. https://doi.org/10.1111/1365-2435.12888

Freschet, G.T., Pagès, L., Iversen, C.M., Comas, L.H., Rewald, B., Roumet, C., Klimešová, J., Zadworny, M., Poorter, H., Postma, J.A., Adams, T.S., Bagniewska-Zadworna, A., Bengough, A.G., Blancaflor, E.B., Brunner, I., Cornelissen, J.H.C., Garnier, E., Gessler, A., Hobbie, S.E., Meier, I.C., Mommer, L., Picon-Cochard, C., Rose, L., Ryser, P., Scherer-Lorenzen, M., Soudzilovskaia, N.A., Stokes, A., Sun, T., Valverde-Barrantes, O.J., Weemstra, M., Weigelt, A., Wurzburger, N., York, L.M., Batterman, S.A., Gomes de Moraes, M., Janeček, Š., Lambers, H., Salmon, V., Tharayil, N., McCormack, M.L., 2021a. A starting guide to root ecology:

strengthening ecological concepts and standardising root classification, sampling, processing and trait measurements. New Phytologist 232, 973–1122. https://doi.org/10.1111/nph.17572

Freschet, G.T., Roumet, C., Comas, L.H., Weemstra, M., Bengough, A.G., Rewald, B., Bardgett, R.D., De Deyn, G.B., Johnson, D., Klimešová, J., Lukac, M., McCormack, M.L., Meier, I.C., Pagès, L., Poorter, H., Prieto, I., Wurzburger, N., Zadworny, M., Bagniewska-Zadworna, A., Blancaflor, E.B., Brunner, I., Gessler, A., Hobbie, S.E., Iversen, C.M., Mommer, L., Picon-Cochard, C., Postma, J.A., Rose, L., Ryser, P., Scherer-Lorenzen, M., Soudzilovskaia, N.A., Sun, T., Valverde-Barrantes, O.J., Weigelt, A., York, L.M., Stokes, A., 2021b. Root traits as drivers of plant and ecosystem functioning: current understanding, pitfalls and future research needs. New Phytol 232, 1123–1158. https://doi.org/10.1111/nph.17072

Fromm, H., 2019. Root Plasticity in the Pursuit of Water. Plants (Basel) 8, 236. https://doi.org/10.3390/plants8070236

Gaba, S., Lescourret, F., Boudsocq, S., Enjalbert, J., Hinsinger, P., Journet, E.-P., Navas, M.-L., Wery, J., Louarn, G., Malézieux, E., Pelzer, E., Prudent, M., Ozier-Lafontaine, H., 2015. Multiple cropping systems as drivers for providing multiple ecosystem services: from concepts to design. Agron. Sustain. Dev. 35, 607–623. https://doi.org/10.1007/s13593-014-0272-z

Gawinowski, M., Enjalbert, J., Cournède, P.-H., Flutre, T., 2024. Contrasted reaction norms of wheat yield in pure vs mixed stands explained by tillering plasticities and shade avoidance. Field Crops Research 310, 109368. https://doi.org/10.1016/j.fcr.2024.109368

Ghatak, A., Kanellopoulos, A.E., López-Hidalgo, C., Malits, A., Meng, Y., Schindler, F., Zhang, S., Li, J., Waldherr, S., Ribeiro, H., Kerou, M., Hodgskiss, L.H., Dreer, M., Mir, R.R., Sharma, S., Bachmann, G., Karpouzas, D.G., Schleper, C., Papadopoulou, E.S., Chaturvedi, P., Weckwerth, W., 2025. Natural variation of the wheat root exudate metabolome and its influence on biological nitrification inhibition activity. Plant Biotechnol J 23, 4755–4772. https://doi.org/10.1111/pbi.70248

Giraud, M., Gall, S.L., Harings, M., Javaux, M., Leitner, D., Meunier, F., Rothfuss, Y., van Dusschoten, D., Vanderborght, J., Vereecken, H., Lobet, G., Schnepf, A., 2023. CPlantBox: a fully coupled modelling platform for the water and carbon fluxes in the soil–plant–atmosphere continuum. in silico Plants 5, diad009. https://doi.org/10.1093/insilicoplants/diad009

Giraud, M., Sırcan, A.K., Streck, T., Leitner, D., Lobet, G., Pagel, H., Schnepf, A., 2026. In silico analysis of carbon and water dynamics in the rhizosphere under drought conditions. SOIL 12, 371–419. https://doi.org/10.5194/soil-12-371-2026

Giraud, M., Sırcan, A.K., Streck, T., Leitner, D., Lobet, G., Pagel, H., Schnepf, A., 2025. In silico analysis of carbon stabilisation by plant and soil microbes for different weather scenarios. EGUsphere 1–76. https://doi.org/10.5194/egusphere-2025-572

Giunta, F., Cadeddu, F., Mureddu, F., Virdis, A., Motzo, R., 2020. Triticale cultivar mixtures: Productivity, resource use and resource use efficiency in a Mediterranean

environment. European Journal of Agronomy 115, 126019. https://doi.org/10.1016/j.eja.2020.126019

Gonfiantini, R., 1978. Standards for stable isotope measurements in natural compounds. Nature 271, 534–536. https://doi.org/10.1038/271534a0

Gorska, A., Ye, Q., Holbrook, N.M., Zwieniecki, M.A., 2008. Nitrate control of root hydraulic properties in plants: translating local information to whole plant response. Plant Physiol 148, 1159–1167. https://doi.org/10.1104/pp.108.122499

Groman-Yaroslavski, I., Weiss, E., Nadel, D., 2016. Composite Sickles and Cereal Harvesting Methods at 23,000-Years-Old Ohalo II, Israel. PLOS ONE 11, e0167151. https://doi.org/10.1371/journal.pone.0167151

Gruwel, M.L.H., 2014. In Situ Magnetic Resonance Imaging of Plant Roots. Vadose Zone Journal 13, vzj2013.08.0158. https://doi.org/10.2136/vzj2013.08.0158

Guderle, M., Bachmann, D., Milcu, A., Gockele, A., Bechmann, M., Fischer, C., Roscher, C., Landais, D., Ravel, O., Devidal, S., Roy, J., Gessler, A., Buchmann, N., Weigelt, A., Hildebrandt, A., 2018. Dynamic niche partitioning in root water uptake facilitates efficient water use in more diverse grassland plant communities. Functional Ecology 32, 214–227. https://doi.org/10.1111/1365-2435.12948

Guhr, T., Song, Z., Andersen, A.G., de la Cruz Jiménez, J., Pedersen, O., 2025. Root morphology and anatomy respond similarly to drought and flooding in two wheat cultivars. Ann Bot mcaf152. https://doi.org/10.1093/aob/mcaf152

Guo, X., Svane, S.F., Fuchtbauer, W.S., Andersen, J.R., Jensen, J., Thorup-Kristensen, K., 2020. Genomic prediction of yield and root development in wheat under changing water availability. Plant Methods 16. https://doi.org/10.1186/s13007-020-00634-0

Hafeez, A., Ali, S., Javed, M.A., Iqbal, R., Khan, M.N., ÇIĞ, F., Sabagh, A.E., Abujamel, T., Harakeh, S., Ercisli, S., Ali, B., 2024. Breeding for water-use efficiency in wheat: progress, challenges and prospects. Mol Biol Rep 51, 429. https://doi.org/10.1007/s11033-024-09345-4

Harmand, S., Lewis, J.E., Feibel, C.S., Lepre, C.J., Prat, S., Lenoble, A., Boës, X., Quinn, R.L., Brenet, M., Arroyo, A., Taylor, N., Clément, S., Daver, G., Brugal, J.-P., Leakey, L., Mortlock, R.A., Wright, J.D., Lokorodi, S., Kirwa, C., Kent, D.V., Roche, H., 2015. 3.3-million-year-old stone tools from Lomekwi 3, West Turkana, Kenya. Nature 521, 310–315. https://doi.org/10.1038/nature14464

Hasanuzzaman, M., Zhou, M., Shabala, S., Hasanuzzaman, M., Zhou, M., Shabala, S., 2023. How Does Stomatal Density and Residual Transpiration Contribute to Osmotic Stress Tolerance? Plants 12. https://doi.org/10.3390/plants12030494

Haslinger, K., Mayer, K., 2023. Early spring droughts in Central Europe: Indications for atmospheric and oceanic drivers. Atmospheric Science Letters 24, e1136. https://doi.org/10.1002/asl.1136

Hawes, C., Iannetta, P.P.M., Squire, G.R., 2021. Agroecological practices for whole-system sustainability. CABI Reviews 2021. https://doi.org/10.1079/PAVSNNR202116005

Henrich, J., 2004. Demography and Cultural Evolution: How Adaptive Cultural Processes can Produce Maladaptive Losses: The Tasmanian Case. American Antiquity 69, 197–214. https://doi.org/10.2307/4128416

Holz, M., Zarebanadkouki, M., Benard, P., Hoffmann, M., Dubbert, M., 2024a. Root and rhizosphere traits for enhanced water and nutrients uptake efficiency in dynamic environments. Front. Plant Sci. 15. https://doi.org/10.3389/fpls.2024.1383373

Holz, M., Zarebanadkouki, M., Benard, P., Hoffmann, M., Dubbert, M., 2024b. Root and rhizosphere traits for enhanced water and nutrients uptake efficiency in dynamic environments. Front. Plant Sci. 15. https://doi.org/10.3389/fpls.2024.1383373

Homulle, Z., George, T.S., Karley, A.J., 2022. Root traits with team benefits: understanding belowground interactions in intercropping systems. Plant Soil 471, 1–26. https://doi.org/10.1007/s11104-021-05165-8

Huang, S., Gill, S., Ramzan, M., Ahmad, M.Z., Danish, S., Huang, P., Al Obaid, S., Alharbi, S.A., 2023. Uncovering the impact of AM fungi on wheat nutrient uptake, ion homeostasis, oxidative stress, and antioxidant defense under salinity stress. Sci Rep 13, 8249. https://doi.org/10.1038/s41598-023-35148-x

Huang, Y., Zhang, N., 2025. A century of winter wheat breeding decreases root hydraulic traits. Plant Physiol 198, kiaf235. https://doi.org/10.1093/plphys/kiaf235

Hublin, J.-J., Ben-Ncer, A., Bailey, S.E., Freidline, S.E., Neubauer, S., Skinner, M.M., Bergmann, I., Le Cabec, A., Benazzi, S., Harvati, K., Gunz, P., 2017. New fossils from Jebel Irhoud, Morocco and the pan-African origin of Homo sapiens. Nature 546, 289–292. https://doi.org/10.1038/nature22336

Ionita, M., Nagavciuc, V., Kumar, R., Rakovec, O., 2020. On the curious case of the recent decade, mid-spring precipitation deficit in central Europe. npj Clim Atmos Sci 3, 49. https://doi.org/10.1038/s41612-020-00153-8

Jones, D.H., Kajala, K., Kawa, D., Lopez-Valdivia, I., Kreszies, T., Schneider, H.M., 2025. The root cortex of the Poaceae: a diverse, dynamic, and dispensable tissue. Plant Soil 514, 1627–1662. https://doi.org/10.1007/s11104-025-07498-0

Jung, V., Violle, C., Mondy, C., Hoffmann, L., Muller, S., 2010. Intraspecific variability and trait-based community assembly. Journal of Ecology 98, 1134–1140. https://doi.org/10.1111/j.1365-2745.2010.01687.x

Kabukcu, C., Asouti, E., Pöllath, N., Peters, J., Karul, N., 2021. Pathways to plant domestication in Southeast Anatolia based on new data from aceramic Neolithic Gusir Höyük. Sci Rep 11, 2112. https://doi.org/10.1038/s41598-021-81757-9

Kaisermann, A., de Vries, F.T., Griffiths, R.I., Bardgett, R.D., 2017. Legacy effects of drought on plant–soil feedbacks and plant–plant interactions. New Phytologist 215, 1413–1424. https://doi.org/10.1111/nph.14661

Kaloterakis, N., Rashtbari, M., Reichel, R., Razavi, B.S., Brüggemann, N., 2025. Compost Application Compensates Yield Loss in a Successive Winter Wheat Rotation: Evidence From a Multiple Isotope Labelling Study. Journal of Sustainable Agriculture and Environment 4, e70079. https://doi.org/10.1002/sae2.70079

Kiær, L.P., Skovgaard, I.M., Østergård, H., 2009. Grain yield increase in cereal variety mixtures: A meta-analysis of field trials. Field Crops Research 114, 361–373. https://doi.org/10.1016/j.fcr.2009.09.006

Kinzinger, L., Mach, J., Haberstroh, S., Schindler, Z., Frey, J., Dubbert, M., Seeger, S., Seifert, T., Weiler, M., Orlowski, N., Werner, C., 2024. Interaction between beech and spruce trees in temperate forests affects water use, root water uptake pattern and canopy structure. Tree Physiol 44, tpad144. https://doi.org/10.1093/treephys/tpad144

Koeniger, P., Marshall, J.D., Link, T., Mulch, A., 2011. An inexpensive, fast, and reliable method for vacuum extraction of soil and plant water for stable isotope analyses by mass spectrometry. Rapid Communications in Mass Spectrometry 25, 3041–3048. https://doi.org/10.1002/rcm.5198

Kong, X., Li, L., Peng, P., Zhang, K., Hu, Z., Wang, X., Zhao, G., 2023. Wheat cultivar mixtures increase grain yield under varied climate conditions. Basic and Applied Ecology 69, 13–25. https://doi.org/10.1016/j.baae.2023.03.007

Kou, X., Han, W., Kang, J., 2022. Responses of root system architecture to water stress at multiple levels: A meta-analysis of trials under controlled conditions. Front Plant Sci 13, 1085409. https://doi.org/10.3389/fpls.2022.1085409

Kreszies, T., Shellakkutti, N., Osthoff, A., Yu, P., Baldauf, J.A., Zeisler-Diehl, V.V., Ranathunge, K., Hochholdinger, F., Schreiber, L., 2019. Osmotic stress enhances suberization of apoplastic barriers in barley seminal roots: analysis of chemical, transcriptomic and physiological responses. New Phytologist 221, 180–194. https://doi.org/10.1111/nph.15351

Kristoffersen, R., Jørgensen, L.N., Eriksen, L.B., Nielsen, G.C., Kiær, L.P., 2020. Control of Septoria tritici blotch by winter wheat cultivar mixtures: Meta-analysis of 19 years of cultivar trials. Field Crops Research 249. https://doi.org/10.1016/j.fcr.2019.107696

Kübert, A., Dubbert, M., Bamberger, I., Kühnhammer, K., Beyer, M., van Haren, J., Bailey, K., Hu, J., Meredith, L.K., Nemiah Ladd, S., Werner, C., 2023. Tracing plant source water dynamics during drought by continuous transpiration measurements: An in-situ stable isotope approach. Plant, Cell & Environment 46, 133–149. https://doi.org/10.1111/pce.14475

Kübert, A., Paulus, S., Dahlmann, A., Werner, C., Rothfuss, Y., Orlowski, N., Dubbert, M., 2020. Water Stable Isotopes in Ecohydrological Field Research: Comparison Between In Situ and Destructive Monitoring Methods to Determine Soil Water Isotopic Signatures. Front. Plant Sci. 11. https://doi.org/10.3389/fpls.2020.00387

Kühnhammer K, Dahlmann A, Iraheta A, et al., 2022. Continuous in situ measurements of water stable isotopes in soils, tree trunk and root xylem: Field approval. Rapid Communications in Mass Spectrometry 36, e9371. https://doi.org/10.1002/rcm.9371

Kühnhammer, K., Kübert, A., Brüggemann, N., Diaz, P.D., Dusschoten, D. van, Javaux, M., Merz, S., Vereecken, H., Dubbert, M., Rothfuss, Y., 2020. Investigating

the root plasticity response of Centaurea jacea to soil water availability changes from isotopic analysis. New Phytologist 226, 98–110. https://doi.org/10.1111/nph.16352

Kulmatiski, A., Adler, P.B., Stark, J.M., Tredennick, A.T., 2017. Water and nitrogen uptake are better associated with resource availability than root biomass. Ecosphere 8, e01738. https://doi.org/10.1002/ecs2.1738

Kulmatiski, A., Beard, K.H., Holdrege, M.C., February, E.C., 2020. Small differences in root distributions allow resource niche partitioning. Ecology and Evolution 10, 9776–9787. https://doi.org/10.1002/ece3.6612

Kuzyakov, Y., Razavi, B.S., 2019. Rhizosphere size and shape: Temporal dynamics and spatial stationarity. Soil Biology and Biochemistry 135, 343–360. https://doi.org/10.1016/j.soilbio.2019.05.011

Lamichhane, J.R., 2021. Rising risks of late-spring frosts in a changing climate. Nat. Clim. Chang. 11, 554–555. https://doi.org/10.1038/s41558-021-01090-x

Lamichhane, J.R., Arseniuk, E., Boonekamp, P., Czembor, J., Decroocq, V., Enjalbert, J., Finckh, M.R., Korbin, M., Koppel, M., Kudsk, P., Mesterhazy, A., Sosnowska, D., Zimnoch-Guzowska, E., Messéan, A., 2018. Advocating a need for suitable breeding approaches to boost integrated pest management: a European perspective. Pest Management Science 74, 1219–1227. https://doi.org/10.1002/ps.4818

Lattacher, A., Gall, S.L., Rothfuss, Y., Gao, C., Harings, M., Pagel, H., Giraud, M., Alahmad, S., Hickey, L.T., Kandeler, E., Poll, C., 2024. Rooting for microbes: Impact of root architecture on the microbial community and function in top- and subsoil. https://doi.org/10.21203/rs.3.rs-4545243/v1

Lattacher, A., Le Gall, S., Rothfuss, Y., Gao, C., Harings, M., Pagel, H., Giraud, M., Alahmad, S., Hickey, L.T., Kandeler, E., Poll, C., 2025a. Rooting for microbes: impact of root architecture on the microbial community and function in top- and subsoil. Plant Soil. https://doi.org/10.1007/s11104-024-07181-w

Lattacher, A., Le Gall, S., Rothfuss, Y., Harings, M., Armbruster, W., van Dusschoten, D., Pflugfelder, D., Alahmad, S., Hickey, L.T., Kandeler, E., Poll, C., 2025b. Combining spring wheat genotypes with contrasting root architectures modifies plant–microbe interactions under different water regimes. Plant Soil. https://doi.org/10.1007/s11104-025-07759-y

Le Gall, S., Bérard, A., Page, D., Lanoe, L., Bertin, N., Doussan, C., 2021. Increased exopolysaccharide production and microbial activity affect soil water retention and field performance of tomato under water deficit. Rhizosphere 19, 100408. https://doi.org/10.1016/j.rhisph.2021.100408

Le Gall, S., Dusschoten, D. van, Lattacher, A., Giraud, M., Harings, M., Diaz, P.D., Pflugfelder, D., Alahmad, S., Hickey, L., Sircan, A., Kandeler, E., Lobet, G., Schnepf, A., Pagel, H., Poll, C., Vereecken, H., Javaux, M., Rothfuss, Y., 2025. Combining spring wheat genotypes with contrasting root architectures for a better use of water resources in soil? Evidence from column-scale water stable isotopic experiments. https://doi.org/10.21203/rs.3.rs-7411150/v1

Le Gall, S., Lapie, C., Cajot, F., Doussan, C., Corridor, L., Bérard, A., 2024. Chemical diversity of crop root mucilages: Implications for their maximal water content and decomposition. Rhizosphere 29, 100858. https://doi.org/10.1016/j.rhisph.2024.100858

Le Gall, S., van Dusschoten, D., Lattacher, A., Giraud, M., Harings, M., Diaz, P.D., Pflugfelder, D., Alahmad, S., Hickey, L., Sircan, A., Kandeler, E., Lobet, G., Schnepf, A., Pagel, H., Poll, C., Vereecken, H., Javaux, M., Rothfuss, Y., 2026. Combining spring wheat genotypes with contrasting root traits for a better use of water resources in soil? Evidence from column-scale water stable isotopic experiments. Plant Soil. https://doi.org/10.1007/s11104-026-08386-x

Li, B., Zhang, X., Morita, S., Sekiya, N., Araki, H., Gu, H., Han, J., Lu, Y., Liu, X., 2022. Are crop deep roots always beneficial for combating drought: A review of root structure and function, regulation and phenotyping. Agricultural Water Management 271, 107781. https://doi.org/10.1016/j.agwat.2022.107781

Li, H., Li, L., Liu, N., Chen, S., Shao, L., Sekiya, N., Zhang, X., 2022. Root efficiency and water use regulation relating to rooting depth of winter wheat. Agricultural Water Management 269, 107710. https://doi.org/10.1016/j.agwat.2022.107710

Litrico, I., Violle, C., 2015. Diversity in Plant Breeding: A New Conceptual Framework. Trends in Plant Science 20, 604–613. https://doi.org/10.1016/j.tplants.2015.07.007

Liu, L., Wang, J., Rosenberg, D., Zhao, H., Lengyel, G., Nadel, D., 2018. Fermented beverage and food storage in 13,000 y-old stone mortars at Raqefet Cave, Israel: Investigating Natufian ritual feasting. Journal of Archaeological Science: Reports 21, 783–793. https://doi.org/10.1016/j.jasrep.2018.08.008

Lopez, G., Hadir, S., Mouratidis, S.D., Shuva, M.A., Hüging, H., Bauke, S.L., Gaiser, T., Schaaf, G., Seidel, S.J., 2025. Winter wheat shoot and root phenotypic plasticity under fertilized and nutrient-deficient field conditions. European Journal of Agronomy 168, 127634. https://doi.org/10.1016/j.eja.2025.127634

Marshall, J.D., Cuntz, M., Beyer, M., Dubbert, M., Kuehnhammer, K., 2020. Borehole Equilibration: Testing a New Method to Monitor the Isotopic Composition of Tree Xylem Water in situ. Front. Plant Sci. 11. https://doi.org/10.3389/fpls.2020.00358

Martani, E., Ferrarini, A., Amaducci, S., 2022. Reversion of Perennial Biomass Crops to Conserve C and N: A Meta-Analysis. Agronomy 12, 232. https://doi.org/10.3390/agronomy12020232

Mason, C.M., Goolsby, E.W., Davis, K.E., Bullock, D.V., Donovan, L.A., 2017. Importance of whole-plant biomass allocation and reproductive timing to habitat differentiation across the North American sunflowers. Ann Bot 119, 1131–1142. https://doi.org/10.1093/aob/mcx002

Mathieu, L., Ballini, E., Morel, J.-B., Méteignier, L.-V., 2024. The root of plant-plant interactions: Belowground special cocktails. Current Opinion in Plant Biology 80, 102547. https://doi.org/10.1016/j.pbi.2024.102547

Mathieu, L., Chloup, A., Marty, S., Savajols, J., Rouveyrol, C., Valls, J., Pétriacq, P., Morel, J.-B., Méteignier, L.V., Ballini, E., 2025. Early root-root interactions weaken foliar defense responses against Septoria tritici blotch in a durum wheat varietal mixture. https://doi.org/10.1101/2025.07.30.667709

Matthus, E., Zwetsloot, M., Delory, B.M., Hennecke, J., Andraczek, K., Henning, T., Mommer, L., Weigelt, A., Bergmann, J., 2025. Revisiting the root economics space—its applications, extensions and nuances advance our understanding of fine-root functioning. Plant Soil 514, 1–27. https://doi.org/10.1007/s11104-025-07379-6

McAlvay, A.C., DiPaola, A., D'Andrea, A.C., Ruelle, M.L., Mosulishvili, M., Halstead, P., Power, A.G., 2022. Cereal species mixtures: an ancient practice with potential for climate resilience. A review. Agron. Sustain. Dev. 42, 100. https://doi.org/10.1007/s13593-022-00832-1

McDougall, B.M., Rovira, A.D., 1970. Sites of Exudation of 14c-Labelled Compounds from Wheat Roots. New Phytologist 69, 999–1003. https://doi.org/10.1111/j.1469-8137.1970.tb02479.x

McMurtrie, R.E., Iversen, C.M., Dewar, R.C., Medlyn, B.E., Näsholm, T., Pepper, D.A., Norby, R.J., 2012. Plant root distributions and nitrogen uptake predicted by a hypothesis of optimal root foraging. Ecology and Evolution 2, 1235–1250. https://doi.org/10.1002/ece3.266

Mead, R., Willey, R.W., 1980. The Concept of a 'Land Equivalent Ratio' and Advantages in Yields from Intercropping. Experimental Agriculture 16, 217–228. https://doi.org/10.1017/S0014479700010978

Messéan, A., Viguier, L., Paresys, L., Aubertot, J.-N., Canali, S., Iannetta, P., Justes, E., Karley, A., Keillor, B., Kemper, L., Muel, F., Pancino, B., Stilmant, D., Watson, C., Willer, H., Zornoza, R., 2021. ENABLING CROP DIVERSIFICATION TO SUPPORT TRANSITIONS TOWARD MORE SUSTAINABLE EUROPEAN AGRIFOOD SYSTEMS. Front. Agr. Sci. Eng. 8, 474–480. https://doi.org/10.15302/J-FASE-2021406

Messina, C., McDonald, D., Poffenbarger, H., Clark, R., Salinas, A., Fang, Y., Gho, C., Tang, T., Graham, G., Hammer, G.L., Cooper, M., 2021. Reproductive resilience but not root architecture underpins yield improvement under drought in maize. J Exp Bot 72, 5235–5245. https://doi.org/10.1093/jxb/erab231

Mettauer, R., Thoumazeau, A., Le Gall, S., Soiron, A., Rakotondrazafy, N., Bérard, A., Brauman, A., Mézière, D., 2023. Soil health in temperate agroforestry: influence of tree species and position in the field. Archives of Agronomy and Soil Science 69, 1781–1800. https://doi.org/10.1080/03650340.2022.2116013

Migliano, A.B., Vinicius, L., 2021. The origins of human cumulative culture: from the foraging niche to collective intelligence. Philos Trans R Soc Lond B Biol Sci 377, 20200317. https://doi.org/10.1098/rstb.2020.0317

Mille, B., Fraj, M.B., Monod, H., de Vallavieille-Pope, C., 2006. Assessing Four-Way Mixtures of Winter Wheat Cultivars from the Performances of their Two-Way and Individual Components. Eur J Plant Pathol 114, 163–173. https://doi.org/10.1007/s10658-005-4036-0

Montazeaud, G., Roumet, P., Lamboeuf, M., Jeudy, C., Ecarnot, M., Malicet-Chebbah, L., Salon, C., Fréville, H., 2025. Mixing varieties mitigates early root competition in wheat under water and nutrient limitation. J Exp Bot 76, 4171–4184. https://doi.org/10.1093/jxb/eraf163

Moore, J.W., Semmens, B.X., 2008. Incorporating uncertainty and prior information into stable isotope mixing models. Ecology Letters 11, 470–480. https://doi.org/10.1111/j.1461-0248.2008.01163.x

Moreau, P., Ruiz, L., Raimbault, T., Vertès, F., Cordier, M.O., Gascuel-Odoux, C., Masson, V., Salmon-Monviola, J., Durand, P., 2012. Modeling the potential benefits of catch-crop introduction in fodder crop rotations in a Western Europe landscape. Science of The Total Environment 437, 276–284. https://doi.org/10.1016/j.scitotenv.2012.07.091

Müllers, Y., Postma, J.A., Poorter, H., van Dusschoten, D., 2023. Deep-water uptake under drought improved due to locally increased root conductivity in maize, but not in faba bean. Plant, Cell & Environment 46, 2046–2060. https://doi.org/10.1111/pce.14587

Mussi, M., Skinner, M.M., Melis, R.T., Panera, J., Rubio-Jara, S., Davies, T.W., Geraads, D., Bocherens, H., Briatico, G., Le Cabec, A., Hublin, J.-J., Gidna, A., Bonnefille, R., Di Bianco, L., Méndez-Quintas, E., 2023. Early Homo erectus lived at high altitudes and produced both Oldowan and Acheulean tools. Science 382, 713–718. https://doi.org/10.1126/science.add9115

Nakhforoosh, A., Grausgruber, H., Kaul, H.-P., Bodner, G., 2014. Wheat root diversity and root functional characterization. Plant Soil 380, 211–229. https://doi.org/10.1007/s11104-014-2082-0

Nerlich, K., Graeff-Hönninger, S., Claupein, W., 2013. Agroforestry in Europe: a review of the disappearance of traditional systems and development of modern agroforestry practices, with emphasis on experiences in Germany. Agroforest Syst 87, 475–492. https://doi.org/10.1007/s10457-012-9560-2

Nguyen, T.H., Lopez, G., Seidel, S.J., Lärm, L., Bauer, F.M., Klotzsche, A., Schnepf, A., Gaiser, T., Hüging, H., Ewert, F., 2024. Multi-year aboveground data of minirhizotron facilities in Selhausen. Sci Data 11, 674. https://doi.org/10.1038/s41597-024-03535-2

Ober, E.S., Alahmad, S., Cockram, J., Forestan, C., Hickey, L.T., Kant, J., Maccaferri, M., Marr, E., Milner, M., Pinto, F., Rambla, C., Reynolds, M., Salvi, S., Sciara, G., Snowdon, R.J., Thomelin, P., Tuberosa, R., Uauy, C., Voss-Fels, K.P., Wallington, E., Watt, M., 2021. Wheat root systems as a breeding target for climate resilience. Theor Appl Genet 134, 1645–1662. https://doi.org/10.1007/s00122-021-03819-w

Odone, A., Popovic, O., Thorup-Kristensen, K., 2024. Deep roots: implications for nitrogen uptake and drought tolerance among winter wheat cultivars. Plant Soil 500, 13–32. https://doi.org/10.1007/s11104-023-06255-5

Orellana-Torrejon, C., Vidal, T., Boixel, A.-L., Gélisse, S., Saint-Jean, S., Suffert, F., 2022. Annual dynamics of Zymoseptoria tritici populations in wheat cultivar

mixtures: A compromise between the efficacy and durability of a recently broken-down resistance gene? Plant Pathology 71, 289–303. https://doi.org/10.1111/ppa.13458

Orlowski, N., Frede, H.-G., Brüggemann, N., Breuer, L., 2013. Validation and application of a cryogenic vacuum extraction system for soil and plant water extraction for isotope analysis. Journal of Sensors and Sensor Systems 2, 179–193. https://doi.org/10.5194/jsss-2-179-2013

Ortiz, R., Sayre, K.D., Govaerts, B., Gupta, R., Subbarao, G.V., Ban, T., Hodson, D., Dixon, J.M., Iván Ortiz-Monasterio, J., Reynolds, M., 2008. Climate change: Can wheat beat the heat? Agriculture, Ecosystems & Environment, International Agricultural Research and Climate Change: A Focus on Tropical Systems 126, 46–58. https://doi.org/10.1016/j.agee.2008.01.019

Parnell, A.C., Inger, R., Bearhop, S., Jackson, A.L., 2010. Source Partitioning Using Stable Isotopes: Coping with Too Much Variation. PLOS ONE 5, e9672. https://doi.org/10.1371/journal.pone.0009672

Pathoumthong, P., Zhang, Z., Roy, S.J., El Habti, A., 2023. Rapid non-destructive method to phenotype stomatal traits. Plant Methods 19, 36. https://doi.org/10.1186/s13007-023-01016-y

Peltonen-Sainio, P., Jauhiainen, L., Laurila, I.P., 2009. Cereal yield trends in northern European conditions: Changes in yield potential and its realisation. Field Crops Research 110, 85–90. https://doi.org/10.1016/j.fcr.2008.07.007

Perrone, R., Rolland, B., Mabire, C., Enjalbert, J., Borg, J., et al., 2017. Evolution of adoption of variety mixtures and low-input multi-resistant bread wheat varieties since two decades in France. IDEEV day, Gif-sur-Yvette.

Pflugfelder, D., Kochs, J., Koller, R., Jahnke, S., Mohl, C., Pariyar, S., Fassbender, H., Nagel, K.A., Watt, M., van Dusschoten, D., 2022. The root system architecture of wheat establishing in soil is associated with varying elongation rates of seminal roots: quantification using 4D magnetic resonance imaging. J Exp Bot 73, 2050–2060. https://doi.org/10.1093/jxb/erab551

Pflugfelder, D., Metzner, R., van Dusschoten, D., Reichel, R., Jahnke, S., Koller, R., 2017. Non-invasive imaging of plant roots in different soils using magnetic resonance imaging (MRI). Plant Methods 13, 102. https://doi.org/10.1186/s13007-017-0252-9

Phillips, D.L., Gregg, J.W., 2003. Source partitioning using stable isotopes: coping with too many sources. Oecologia 136, 261–269. https://doi.org/10.1007/s00442-003-1218-3

Pinheiro, J.C., Bates, D.M. (Eds.), 2000. Linear Mixed-Effects Models: Basic Concepts and Examples, in: Mixed-Effects Models in S and S-PLUS. Springer, New York, NY, pp. 3–56. https://doi.org/10.1007/0-387-22747-4_1

Plett, D.C., Ranathunge, K., Melino, V.J., Kuya, N., Uga, Y., Kronzucker, H.J., 2020. The intersection of nitrogen nutrition and water use in plants: new paths toward improved crop productivity. J Exp Bot 71, 4452–4468. https://doi.org/10.1093/jxb/eraa049

Poorter, H., B Hler, J., van Dusschoten, D., Climent, J., Postma, J.A., 2012. Pot size matters: a meta-analysis of the effects of rooting volume on plant growth. Funct Plant Biol 39, 839–850. https://doi.org/10.1071/FP12049

Prado, K., Holland, B.L., McSpadden Gardener, B., Lundquist, P.K., Santiago, J.P., VanBuren, R., Rhee, S.Y., 2025. Building climate-resilient crops: genetic, environmental, and technological strategies for heat and drought stress tolerance. J Exp Bot 76, 4395–4413. https://doi.org/10.1093/jxb/eraf111

Prechsl, U.E., Burri, S., Gilgen, A.K., Kahmen, A., Buchmann, N., 2015. No shift to a deeper water uptake depth in response to summer drought of two lowland and sub-alpine C3-grasslands in Switzerland. Oecologia 177, 97–111. https://doi.org/10.1007/s00442-014-3092-6

Rambla, C., Kang, Y., Ober, E., Hickey, L., Alahmad, S., Voss-Fels, K., Watt, M., Wasson, A., Dinglasan, E., Meer, S., 2023. Easy-to-build rhizobox method to support wheat root research and breeding for future production systems. https://doi.org/10.21203/rs.3.rs-2464820/v1

Rambla, C., Van Der Meer, S., Voss-Fels, K.P., Makhoul, M., Obermeier, C., Snowdon, R., Ober, E.S., Watt, M., Alahmad, S., Hickey, L.T., 2022. A toolkit to rapidly modify root systems through single plant selection. Plant Methods 18, 2. https://doi.org/10.1186/s13007-021-00834-2

Rasmussen, C.R., Thorup-Kristensen, K., Dresbøll, D.B., 2020. Uptake of subsoil water below 2 m fails to alleviate drought response in deep-rooted Chicory (Cichorium intybus L.). Plant Soil 446, 275–290. https://doi.org/10.1007/s11104-019-04349-7

Ren, P., Li, P., Zhou, X., Liu, Z., Tang, J., Zhang, C., Zou, Z., Li, T., Peng, C., 2024. Shifts in Plant Phenology Significantly Affect the Carbon Allocation in Different Plant Organs. Ecol Lett 27, e70024. https://doi.org/10.1111/ele.70024

Rezaei, E.E., Webber, H., Asseng, S., Boote, K., Durand, J.L., Ewert, F., Martre, P., MacCarthy, D.S., 2023. Climate change impacts on crop yields. Nat Rev Earth Environ 4, 831–846. https://doi.org/10.1038/s43017-023-00491-0

Rickard, W., Hossain, I., Zhang, X., Cooper, H.V., Mooney, S.J., Hawkesford, M.J., Whalley, W.R., 2025. Field plants strategically regulate water uptake from different soil depths by spatiotemporally adjusting their radial root hydraulic conductivity. New Phytologist n/a. https://doi.org/10.1111/nph.70013

Riehl, S., Karakaya, D., Zeidi, M., Conard, N.J., 2024. Contextualizing wild cereal harvesting at Middle Palaeolithic Ghar-e Boof in the southern Zagros. Sci Rep 14, 18748. https://doi.org/10.1038/s41598-024-69056-5

Rios-Garaizar, J., López-Bultó, O., Iriarte, E., Pérez-Garrido, C., Piqué, R., Aranburu, A., Iriarte-Chiapusso, M.J., Ortega-Cordellat, I., Bourguignon, L., Garate, D., Libano, I., 2018. A Middle Palaeolithic wooden digging stick from Aranbaltza III, Spain. PLOS ONE 13, e0195044. https://doi.org/10.1371/journal.pone.0195044

Robertson, B.C., Han, Y., Li, C., Robertson, B.C., Han, Y., Li, C., 2023. A Comparison of Different Stomatal Density Phenotypes of Hordeum vulgare under

Varied Watering Regimes Reveals Superior Genotypes with Enhanced Drought Tolerance. Plants 12. https://doi.org/10.3390/plants12152840

Rodriguez-Dominguez, C.M., Forner, A., Martorell, S., Choat, B., Lopez, R., Peters, J.M.R., Pfautsch, S., Mayr, S., Carins-Murphy, M.R., McAdam, S.A.M., Richardson, F., Diaz-Espejo, A., Hernandez-Santana, V., Menezes-Silva, P.E., Torres-Ruiz, J.M., Batz, T.A., Sack, L., 2022. Leaf water potential measurements using the pressure chamber: Synthetic testing of assumptions towards best practices for precision and accuracy. Plant, Cell & Environment 45, 2037–2061. https://doi.org/10.1111/pce.14330

Rothfuss, Y., Javaux, M., 2017. Reviews and syntheses: Isotopic approaches to quantify root water uptake: a review and comparison of methods. Biogeosciences 14, 2199–2224. https://doi.org/10.5194/bg-14-2199-2017

Rothfuss, Y., Le Gall, S., Brüggemann, N., Jahan, S., Javaux, M., Klaus, J., Vereecken, H., van Dusschoten, D., 2026. Online xylem water isotope monitoring and soil water content profiling reveal spatial root water uptake dynamics in sunflower. EGUsphere 1–30. https://doi.org/10.5194/egusphere-2026-1518

Rothfuss, Y., Vereecken, H., Brüggemann, N., 2013. Monitoring water stable isotopic composition in soils using gas-permeable tubing and infrared laser absorption spectroscopy. Water Resources Research 49, 3747–3755. https://doi.org/10.1002/wrcr.20311

Sarandon, S.J., Sarandon, R., 1995. Mixture of Cultivars: Pilot Field Trial of an Ecological Alternative to Improve Production or Quality of Wheat (Triticum aestivum). Journal of Applied Ecology 32, 288–294. https://doi.org/10.2307/2405096

Scheifes, D.J.P., te Beest, M., Olde Venterink, H., Jansen, A., Kinsbergen, D.T.P., Wassen, M.J., 2024. The plant root economics space in relation to nutrient limitation in Eurasian herbaceous plant communities. Ecology Letters 27, e14402. https://doi.org/10.1111/ele.14402

Schenk, H.J., Jackson, R.B., 2002. Rooting depths, lateral root spreads and below-ground/above-ground allometries of plants in water-limited ecosystems. Journal of Ecology 90, 480–494. https://doi.org/10.1046/j.1365-2745.2002.00682.x

Schmid, B., Hector, A., Saha, P., Loreau, M., 2008. Biodiversity effects and transgressive overyielding. J Plant Ecol 1, 95–102. https://doi.org/10.1093/jpe/rtn011

Schmidt, M., Felsche, E., 2024. The effect of climate change on crop yield anomaly in Europe. Climate Resilience and Sustainability 3, e61. https://doi.org/10.1002/cli2.61

Schmidt, M.V., Zhao, Y., Hinterberger, V., Martinez, S.L.Z., Maurer, A., Reif, J.C., El Hanafi, S., 2026. Wheat variety mixtures enhance yield stability and result in pronounced overyielding for certain line combinations. European Journal of Agronomy 172, 127886. https://doi.org/10.1016/j.eja.2025.127886

Schmutz, A., Schöb, C., 2023. Crops grown in mixtures show niche partitioning in spatial water uptake. Journal of Ecology 111, 1151–1165. https://doi.org/10.1111/1365-2745.14088

Schneider, H.M., Postma, J.A., Kochs, J., Pflugfelder, D., Lynch, J.P., van Dusschoten, D., 2020. Spatio-Temporal Variation in Water Uptake in Seminal and Nodal Root Systems of Barley Plants Grown in Soil. Front. Plant Sci. 11. https://doi.org/10.3389/fpls.2020.01247

Schöb, C., Engbersen, N., López-Angulo, J., Schmutz, A., Stefan, L., 2023. Crop Diversity Experiment: towards a mechanistic understanding of the benefits of species diversity in annual crop systems. Journal of Plant Ecology rtad016. https://doi.org/10.1093/jpe/rtad016

Semchenko, M., Saar, S., Lepik, A., 2014. Plant root exudates mediate neighbour recognition and trigger complex behavioural changes. New Phytol 204, 631–637. https://doi.org/10.1111/nph.12930

Senapati, N., Stratonovitch, P., Paul, M.J., Semenov, M.A., 2019. Drought tolerance during reproductive development is important for increasing wheat yield potential under climate change in Europe. J Exp Bot 70, 2549–2560. https://doi.org/10.1093/jxb/ery226

Shaheen, A., Li, Z., Yang, Y., Xie, J., Zhu, L., Li, C., Nie, F., Wang, M., Wang, Y., Rasheed, A., Li, H., Zhou, Y., Song, C.-P., 2025. Genetic regulation of wheat plant architecture and future prospects for its improvement. New Crops 2, 100048. https://doi.org/10.1016/j.ncrops.2024.100048

Sharma, R.B., Ghildyal, B.P., 1987. Elongation Rate of Wheat Root Axes. journal of agronomy and crop science 159.

Sharma, R.C., Dubin, H.J., 1996. Effect of wheat cultivar mixtures on spot blotch (Bipolaris sorokiniana) and grain yield. Field Crops Research 48, 95–101. https://doi.org/10.1016/S0378-4290(96)01031-3

Sharma, S., Kumar, T., Foulkes, M.J., Orford, S., Singh, A.M., Wingen, L.U., Karnam, V., Nair, L.S., Mandal, P.K., Griffiths, S., Hawkesford, M.J., Shewry, P.R., Bentley, A.R., Pandey, R., 2023. Nitrogen uptake and remobilization from pre- and post-anthesis stages contribute towards grain yield and grain protein concentration in wheat grown in limited nitrogen conditions. CABI Agric Biosci 4, 12. https://doi.org/10.1186/s43170-023-00153-7

Shazadi, K., Christopher, J.T., Chenu, K., 2024. Does late water deficit induce root growth or senescence in wheat? Front. Plant Sci. 15. https://doi.org/10.3389/fpls.2024.1351436

Shoaib, M., Banerjee, B.P., Hayden, M., Kant, S., 2022. Roots' Drought Adaptive Traits in Crop Improvement. Plants (Basel) 11, 2256. https://doi.org/10.3390/plants11172256

Siddiqui, Md.N., Ambaw, A.M., Shrestha, A., Pandey, K., Teferi, T.J., Gabi, M.T., Duarte-Delgado, D., Léon, J., Ballvora, A., 2025. Natural genetic variation in nodal root growth angle and anatomy underlies drought tolerance in bread wheat. Environmental and Experimental Botany 237, 106220. https://doi.org/10.1016/j.envexpbot.2025.106220

Silva, J.V., Rijk, B., Berghuijs, H.N.C., de Wit, A.J.W., Reidsma, P., van Ittersum, M.K., 2026. Agronomic management drives the wheat yield plateau in high-yielding

environments of northwest Europe. Nat Food 7, 45–54. https://doi.org/10.1038/s43016-025-01286-w

Sırcan, A.K., Streck, T., Schnepf, A., Giraud, M., Lattacher, A., Kandeler, E., Poll, C., Pagel, H., 2025. Trait-based modeling of microbial interactions and carbon turnover in the rhizosphere. Soil Biology and Biochemistry 202, 109698. https://doi.org/10.1016/j.soilbio.2024.109698

Slafer, G.A., Savin, R., Sadras, V.O., 2014. Coarse and fine regulation of wheat yield components in response to genotype and environment. Field Crops Research 157, 71–83. https://doi.org/10.1016/j.fcr.2013.12.004

Spohn, M., Kuzyakov, Y., 2014. Spatial and temporal dynamics of hotspots of enzyme activity in soil as affected by living and dead roots—a soil zymography analysis. Plant Soil 379, 67–77. https://doi.org/10.1007/s11104-014-2041-9

Spollen, W.G., Sharp, R.E., 1991. Spatial Distribution of Turgor and Root Growth at Low Water Potentials. Plant Physiol 96, 438–443. https://doi.org/10.1104/pp.96.2.438

Sprenger, M., Leistert, H., Gimbel, K., Weiler, M., 2016. Illuminating hydrological processes at the soil-vegetation-atmosphere interface with water stable isotopes. Reviews of Geophysics 54, 674–704. https://doi.org/10.1002/2015RG000515

Stefan, L., Colbach, N., Fossati, D., Strebel, S., Levy Häner, L., 2025a. Plasticity in ear density drives complementarity effects and yield benefits in wheat variety mixtures. Agron. Sustain. Dev. 45, 55. https://doi.org/10.1007/s13593-025-01051-0

Stefan, L., Fossati, D., Camp, K.-H., Pellet, D., Foiada, F., Levy, L., 2024. Asynchrony is more important than genetic distance in driving yield stability in wheat variety mixtures. Crop Science 64, 455–469. https://doi.org/10.1002/csc2.21151

Stefan, L., Strebel, S., Camp, K.-H., Christinat, S., Fossati, D., Städeli, C., Levy Häner, L., 2025b. Multi-trait assessment of wheat variety mixtures performance and stability: Mixtures for the win! European Journal of Agronomy 164, 127504. https://doi.org/10.1016/j.eja.2024.127504

Stingaciu, L., Schulz, H., Pohlmeier, A., Behnke, S., Zilken, H., Javaux, M., Vereecken, H., 2013. In Situ Root System Architecture Extraction from Magnetic Resonance Imaging for Water Uptake Modeling. Vadose Zone Journal 12, vzj2012.0019. https://doi.org/10.2136/vzj2012.0019

Stirling, S.A., Guercio, A.M., Patrick, R.M., Huang, X.-Q., Bergman, M.E., Dwivedi, V., Kortbeek, R.W.J., Liu, Y.-K., Sun, F., Tao, W.A., Li, Y., Boachon, B., Shabek, N., Dudareva, N., 2024. Volatile communication in plants relies on a KAI2-mediated signaling pathway. Science 383, 1318–1325. https://doi.org/10.1126/science.adl4685

Sun, S.-J., Meng, P., Zhang, J.-S., Wan, X., 2011. Variation in soil water uptake and its effect on plant water status in Juglans regia L. during dry and wet seasons. Tree Physiology 31, 1378–1389. https://doi.org/10.1093/treephys/tpr116

Suzuki, K.C., Kajino, H., Hirokawa, S., Tomimatsu, H., Kadowaki, K., Hikosaka, K., 2026. The coordination between root and leaf functional traits across 33 woody

plant species shifts between mycorrhizal types. Tree Physiol 46, tpaf151. https://doi.org/10.1093/treephys/tpaf151

Svoboda, P., Kurešová, G., Raimanová, I., Kunzová, E., Haberle, J., 2020. The Effect of Different Fertilization Treatments on Wheat Root Depth and Length Density Distribution in a Long-Term Experiment. Agronomy 10, 1355. https://doi.org/10.3390/agronomy10091355

Tardieu, F., 2012. Any trait or trait-related allele can confer drought tolerance: just design the right drought scenario. Journal of Experimental Botany 63, 25–31. https://doi.org/10.1093/jxb/err269

Terletskaya, N.V., Lee, T.E., Altayeva, N.A., Kudrina, N.O., Blavachinskaya, I.V., Erezhetova, U., 2020. Some Mechanisms Modulating the Root Growth of Various Wheat Species under Osmotic-Stress Conditions. Plants 9, 1545. https://doi.org/10.3390/plants9111545

Uga, Y., Sugimoto, K., Ogawa, S., Rane, J., Ishitani, M., Hara, N., Kitomi, Y., Inukai, Y., Ono, K., Kanno, N., Inoue, H., Takehisa, H., Motoyama, R., Nagamura, Y., Wu, J., Matsumoto, T., Takai, T., Okuno, K., Yano, M., 2013. Control of root system architecture by DEEPER ROOTING 1 increases rice yield under drought conditions. Nat Genet 45, 1097–1102. https://doi.org/10.1038/ng.2725

van der Wiel, K., Batelaan, T.J., Wanders, N., 2023. Large increases of multi-year droughts in north-western Europe in a warmer climate. Clim Dyn 60, 1781–1800. https://doi.org/10.1007/s00382-022-06373-3

van Dusschoten, D., Metzner, R., Kochs, J., Postma, J.A., Pflugfelder, D., Bühler, J., Schurr, U., Jahnke, S., 2016. Quantitative 3D Analysis of Plant Roots Growing in Soil Using Magnetic Resonance Imaging. Plant Physiology 170, 1176–1188. https://doi.org/10.1104/pp.15.01388

Vance, E.D., Brookes, P.C., Jenkinson, D.S., 1987. An extraction method for measuring soil microbial biomass C. Soil Biology and Biochemistry 19, 703–707. https://doi.org/10.1016/0038-0717(87)90052-6

Vanneste, T., Govaert, S., De Kesel, W., Van Den Berge, S., Vangansbeke, P., Meeussen, C., Brunet, J., Cousins, S.A.O., Decocq, G., Diekmann, M., Graae, B.J., Hedwall, P.-O., Heinken, T., Helsen, K., Kapás, R.E., Lenoir, J., Liira, J., Lindmo, S., Litza, K., Naaf, T., Orczewska, A., Plue, J., Wulf, M., Verheyen, K., De Frenne, P., 2020. Plant diversity in hedgerows and road verges across Europe. Journal of Applied Ecology 57, 1244–1257. https://doi.org/10.1111/1365-2664.13620

Vestergaard, N.F., Jørgensen, L.N., 2024. Variety mixtures of winter wheat: a general status and national case study. J Plant Dis Prot 131, 1127–1136. https://doi.org/10.1007/s41348-023-00856-z

Vidal, T., Saint-Jean, S., Lusley, P., Leconte, M., Ben Krima, S., Boixel, A., Wheatamix Consortium, Vallavieille-Pope, C., 2020a. Cultivar mixture effects on disease and yield remain despite diversity in wheat height and earliness. Plant Pathol 69, 1148–1160. https://doi.org/10.1111/ppa.13200

Vidal, T., Saint-Jean, S., Lusley, P., Leconte, M., Ben Krima, S., Boixel, A.-L., Consortium, W., de Vallavieille-Pope, C., 2020b. Cultivar mixture effects on disease

and yield remain despite diversity in wheat height and earliness. Plant Pathology 69, 1148–1160. https://doi.org/10.1111/ppa.13200

Vincent-Caboud, L., Casagrande, M., David, C., Ryan, M.R., Silva, E.M., Peigne, J., 2019. Using mulch from cover crops to facilitate organic no-till soybean and maize production. A review. Agron. Sustain. Dev. 39, 45. https://doi.org/10.1007/s13593-019-0590-2

Volkmann, T.H.M., Kühnhammer, K., Herbstritt, B., Gessler, A., Weiler, M., 2016. A method for in situ monitoring of the isotope composition of tree xylem water using laser spectroscopy. Plant, Cell & Environment 39, 2055–2063. https://doi.org/10.1111/pce.12725

Wan, C., Dang, P., Gao, L., Wang, J., Tao, J., Qin, X., Feng, B., Gao, J., 2022. How Does the Environment Affect Wheat Yield and Protein Content Response to Drought? A Meta-Analysis. Front. Plant Sci. 13. https://doi.org/10.3389/fpls.2022.896985

Wang, D., 2025. Root-Soil Interactions Affecting Maize Growth. Molecular Soil Biology 16.

Wang, T.-C., Moritz, A., Mabrouk, M., Villar Alegría, E., Arinalp, B., Ganji, E., Förter, L., Wittkop, B., Herzog, E., Snowdon, R.J., Stahl, A., Chen, T.-W., 2026. Plasticity of source-sink dynamics contributes to wheat yield stability. Nat Commun 17, 3781. https://doi.org/10.1038/s41467-026-72330-x

Wang, Y., Wu, J., Zhang, J., Guan, T., Wang, G., Jin, J., Wang, Z., 2025. Depth distributions of soil temperature: Seasonal sensitivity and simulation across dryness/wetness conditions. Agricultural Water Management 316, 109571. https://doi.org/10.1016/j.agwat.2025.109571

Wang, Y., Zhang, Y., Ji, W., Yu, P., Wang, B., Li, J., Han, M., Xu, X., Wang, Z., 2016. Cultivar Mixture Cropping Increased Water Use Efficiency in Winter Wheat under Limited Irrigation Conditions. PLOS ONE 11, e0158439. https://doi.org/10.1371/journal.pone.0158439

Wang, Zhili, Yung, W.-S., Gao, Y., Huang, C., Zhao, X., Chen, Y., Li, M.-W., Lam, H.-M., 2024. From phenotyping to genetic mapping: identifying water-stress adaptations in legume root traits. BMC Plant Biol 24, 749. https://doi.org/10.1186/s12870-024-05477-8

Wang, Ziqian, Zhang, B., Li, J., Lian, S., Zhang, J., Shi, S., 2024. Effects of Deficit-Regulated Irrigation on Root-Growth Dynamics and Water-Use Efficiency of Winter Wheat in a Semi-Arid Area. Water 16, 2678. https://doi.org/10.3390/w16182678

Wasson, A.P., Richards, R.A., Chatrath, R., Misra, S.C., Prasad, S.V.S., Rebetzke, G.J., Kirkegaard, J.A., Christopher, J., Watt, M., 2012. Traits and selection strategies to improve root systems and water uptake in water-limited wheat crops. Journal of Experimental Botany 63, 3485–3498. https://doi.org/10.1093/jxb/ers111

Weaver, J.E., 1926. Root Development of Field Crops: Chapter V. McGRAW-HILL BOOK COMPANY, INC., Lincoln, Nebraska.

Weigel, R., Werner, A., Würzberg, L., Zembold, K., Angulo, K., Bach, W., Hémonnet-Dal, C., Nähring, T., Hiebenga, M., Muffler, L., 2025. Root and shoot traits of two common herbs respond differently to drought and fertilization in a

multifactorial global change experiment. Plant Soil 514, 2975–2990. https://doi.org/10.1007/s11104-025-07560-x

Weihermüller, L., Huisman, J.A., Lambot, S., Herbst, M., Vereecken, H., 2007. Mapping the spatial variation of soil water content at the field scale with different ground penetrating radar techniques. Journal of Hydrology 340, 205–216. https://doi.org/10.1016/j.jhydrol.2007.04.013

Weiner, J., Andersen, S.B., Wille, W.K.-M., Griepentrog, H.W., Olsen, J.M., 2010. Evolutionary Agroecology: the potential for cooperative, high density, weed-suppressing cereals. Evolutionary Applications 3, 473–479. https://doi.org/10.1111/j.1752-4571.2010.00144.x

Wezel, A., Casagrande, M., Celette, F., Vian, J.-F., Ferrer, A., Peigné, J., 2014. Agroecological practices for sustainable agriculture. A review. Agron. Sustain. Dev. 34, 1–20. https://doi.org/10.1007/s13593-013-0180-7

White, R.G., Kirkegaard, J.A., 2010. The distribution and abundance of wheat roots in a dense, structured subsoil--implications for water uptake. Plant Cell Environ 33, 133–148. https://doi.org/10.1111/j.1365-3040.2009.02059.x

Wilcox, J., Makowski, D., 2014. A meta-analysis of the predicted effects of climate change on wheat yields using simulation studies. Field Crops Research 156, 180–190. https://doi.org/10.1016/j.fcr.2013.11.008

Wu, W., Wang, Y., Wang, L., Xu, H., Zörb, C., Geilfus, C.-M., Xue, C., Sun, Z., Ma, W., 2022. Booting stage is the key timing for split nitrogen application in improving grain yield and quality of wheat – A global meta-analysis. Field Crops Research 287, 108665. https://doi.org/10.1016/j.fcr.2022.108665

Wu, Y., Ma, Q., Liu, Y., Wang, Z., 2026. Enhancing water use efficiency and crop production through shallow- and deep-rooted crop strip intercropping in semi-arid regions. Soil and Tillage Research 258, 107043. https://doi.org/10.1016/j.still.2025.107043

Würschum, T., Langer, S.M., Longin, C.F.H., Tucker, M.R., Leiser, W.L., 2017. A modern Green Revolution gene for reduced height in wheat. The Plant Journal 92, 892–903. https://doi.org/10.1111/tpj.13726

Xu, C., Tao, H., Tian, B., Gao, Y., Ren, J., Wang, P., 2016. Limited-irrigation improves water use efficiency and soil reservoir capacity through regulating root and canopy growth of winter wheat. Field Crops Research 196, 268–275. https://doi.org/10.1016/j.fcr.2016.07.009

Xu, J., Lowe, C., Hernandez-Leon, S.G., Dreisigacker, S., Reynolds, M.P., Valenzuela-Soto, E.M., Paul, M.J., Heuer, S., 2022. The Effects of Brief Heat During Early Booting on Reproductive, Developmental, and Chlorophyll Physiological Performance in Common Wheat (Triticum aestivum L.). Front Plant Sci 13, 886541. https://doi.org/10.3389/fpls.2022.886541

Xu, W., Zhang, W., Yu, Y., Sun, W., Yu, L., Shang, D., Xue, C., Zhang, Q., 2025. Response of crop photosynthetic product allocation under different water supply conditions: A global synthetic analysis. Field Crops Research 333, 110104. https://doi.org/10.1016/j.fcr.2025.110104

Yang, L., Callaway, R.M., Atwater, D.Z., 2015. Root contact responses and the positive relationship between intraspecific diversity and ecosystem productivity. AoB Plants 7, plv053. https://doi.org/10.1093/aobpla/plv053

Zadoks, J.C., Chang, T.T., Konzak, C.F., 1974. A decimal code for the growth stages of cereals. Weed Research 14, 415–421. https://doi.org/10.1111/j.1365-3180.1974.tb01084.x

Zaman, F., Hassan, M.U., Khattak, W.A., Ali, A., Awad, M.F., Chen, F.-S., 2024. The pivotal role of arbuscular mycorrhizal fungi in enhancing plant biomass and nutrient availability under drought stress conditions: A global meta-analysis. Science of The Total Environment 955, 176960. https://doi.org/10.1016/j.scitotenv.2024.176960

Zhang, Y., Wu, X., Wang, X., Dai, M., Peng, Y., 2025. Crop root system architecture in drought response. Journal of Genetics and Genomics 52, 4–13. https://doi.org/10.1016/j.jgg.2024.05.001

Zhao, D.-Y., Zhang, X.-L., Zhao, W.-F., Zhao, S.-P., Liu, G.-L., Siddique, K.H.M., 2023. Root Distribution, Agronomic Performance, and Phosphorus Utilization in Wheat as Mediated by Phosphorus Placement under Rainfed Coastal Saline Conditions. Agronomy 13, 2700. https://doi.org/10.3390/agronomy13112700

Zhao, Y., Wang, L., Chun, K.P., Ziegler, A.D., Evaristo, J., 2024. Dynamic hydrological niche segregation: How plants compete for water in a semi-arid ecosystem. Journal of Hydrology 630, 130677. https://doi.org/10.1016/j.jhydrol.2024.130677

Zheng, L., Barry, K.E., Guerrero-Ramírez, N.R., Craven, D., Reich, P.B., Verheyen, K., Scherer-Lorenzen, M., Eisenhauer, N., Barsoum, N., Bauhus, J., Bruelheide, H., Cavender-Bares, J., Dolezal, J., Auge, H., Fagundes, M.V., Ferlian, O., Fiedler, S., Forrester, D.I., Ganade, G., Gebauer, T., Haase, J., Hajek, P., Hector, A., Hérault, B., Hölscher, D., Hulvey, K.B., Irawan, B., Jactel, H., Koricheva, J., Kreft, H., Lanta, V., Leps, J., Mereu, S., Messier, C., Montagnini, F., Mörsdorf, M., Müller, S., Muys, B., Nock, C.A., Paquette, A., Parker, W.C., Parker, J.D., Parrotta, J.A., Paterno, G.B., Perring, M.P., Piotto, D., Wayne Polley, H., Ponette, Q., Potvin, C., Quosh, J., Rewald, B., Godbold, D.L., van Ruijven, J., Standish, R.J., Stefanski, A., Sundawati, L., Urgoiti, J., Williams, L.J., Wilsey, B.J., Yang, B., Zhang, L., Zhao, Z., Yang, Y., Sandén, H., Ebeling, A., Schmid, B., Fischer, M., Kotowska, M.M., Palmborg, C., Tilman, D., Yan, E., Hautier, Y., 2024. Effects of plant diversity on productivity strengthen over time due to trait-dependent shifts in species overyielding. Nat Commun 15, 2078. https://doi.org/10.1038/s41467-024-46355-z

Zhou, X., Zhang, J., Shi, J., Khashi u Rahman, M., Liu, H., Wei, Z., Wu, F., Dini-Andreote, F., 2024. Volatile-mediated interspecific plant interaction promotes root colonization by beneficial bacteria via induced shifts in root exudation. Microbiome 12, 207. https://doi.org/10.1186/s40168-024-01914-w

Zhu, Y.-H., Weiner, J., Yu, M.-X., Li, F.-M., 2019. Evolutionary agroecology: Trends in root architecture during wheat breeding. Evolutionary Applications 12, 733–743. https://doi.org/10.1111/eva.12749

Zohner, C.M., Mo, L., Renner, S.S., Svenning, J.-C., Vitasse, Y., Benito, B.M., Ordonez, A., Baumgarten, F., Bastin, J.-F., Sebald, V., Reich, P.B., Liang, J., Nabuurs, G.-J., de-Miguel, S., Alberti, G., Antón-Fernández, C., Balazy, R., Brändli, U.-B., Chen, H.Y.H., Chisholm, C., Cienciala, E., Dayanandan, S., Fayle, T.M., Frizzera, L., Gianelle, D., Jagodzinski, A.M., Jaroszewicz, B., Jucker, T., Kepfer-Rojas, S., Khan, M.L., Kim, H.S., Korjus, H., Johannsen, V.K., Laarmann, D., Lang, M., Zawila-Niedzwiecki, T., Niklaus, P.A., Paquette, A., Pretzsch, H., Saikia, P., Schall, P., Šebeň, V., Svoboda, M., Tikhonova, E., Viana, H., Zhang, C., Zhao, X., Crowther, T.W., 2020. Late-spring frost risk between 1959 and 2017 decreased in North America but increased in Europe and Asia. Proceedings of the National Academy of Sciences 117, 12192–12200. https://doi.org/10.1073/pnas.1920816117

Zoomash, n.d. Selhausen Annual Weather Averages [WWW Document]. World® Weather Online. URL https://www.worldweatheronline.com/selhausen-weather-averages/nordrhein-westfalen/de.aspx (accessed 3.10.25).